SKELETAL EFFECTS OF BISPHOSPHONATE TREATMENT AND JUMPING RESISTANCE EXERCISE ON ADULT RATS EXPOSED TO SIMULATED MICROGRAVITY

A Dissertation

by

SCOTT EDWARD LENFEST

Submitted to the Office of Graduate and Professional Studies of
Texas A&M University
in partial fulfillment of the requirements for the degree of

DOCTOR OF PHILOSOPHY

Chair of Committee,	Harry Hogan
Committee Members,	Susan Bloomfield
	Sevan Goenezen
	Bruce Tai
Head of Department,	Andreas Polycarpou

May 2020

Major Subject: Mechanical Engineering

ABSTRACT

The purpose of our study was to investigate the effects of a single period of bisphosphonate (BP) treatment on bone loss resulting from multiple periods of simulated microgravity. We hypothesized that the protective effects of BP treatment would extend through two periods of hindlimb unloading (HU) and an intervening recovery period, and that the BP zoledronate (ZOL) would outperform the BP alendronate (ALN) at preserving bone strength and quality due to ZOL's higher binding affinity and anti-resorptive potency. Male Sprague-Dawley rats (6-months-old) were given either a single injection of ZOL (HU+ZOL), ALN injections three times per week for 5 weeks (HU+ALN), or assigned to aging control (AC) or HU control (HU) groups. HU groups were then exposed to 28 days of HU, followed by 56 days of recovery and a second 28-day HU period. The first and second HU periods resulted in significant declines in total (-5.05%, -0.25%) and cancellous (-18.4%, -9.98%) volumetric bone mineral density (vBMD) at the proximal tibia metaphysis (PTM). BP treatment protected (ALN) or overprotected (ZOL) against losses in bone density and microarchitecture.

Additionally, we aimed to develop a model of voluntary jumping exercise (VJE) that employs positive reinforcement-based training and validate its efficacy as a countermeasure to simulated microgravity. We hypothesized that VJE pre-treatment would effectively preserve bone strength and quality during a subsequent HU period, but that these beneficial effects would not extend to the recovery period following unloading. Male Sprague-Dawley rats (6-months-old) performed VJE for 4 weeks

(HU+VJE) and were subsequently exposed to 28 days of HU, followed by 56 days of recovery. HU+VJE had significantly higher total vBMD at the PTM (+8.95%), distal femur metaphysis (+7.57%), and femoral neck (+6.03%) compared to AC at the end of the exercise period. VJE pre-treatment also prevented losses in bone strength and quality measures due to HU and promoted recovery at certain bone sites. These results indicate that BP treatment may be a successful countermeasure against spaceflight bone loss, and that positive reinforcement-based VJE pre-treatment is a useful model of rodent exercise and an effective countermeasure against HU-induced bone loss.

DEDICATION

To Grampy, who taught me to dream

and

To Jay, who inspired me to grow.

ACKNOWLEDGEMENTS

This project could not have been completed without the support of my many mentors, colleagues, friends, and family.

I would like to thank my committee chair, Dr. Harry Hogan, for mentoring me from my time as head teaching assistant in the mechanical engineering undergraduate seminar, to the very last word written in this dissertation. I would like to thank Dr. Susan Bloomfield for introducing me to bone biology in 2013, for the many pieces of advice and feedback over the years, and for sitting on my committee. Additional thinks go to Dr. Sevan Goenezen and Dr. Bruce Tai for sitting on my committee and helping guide me through the process of earning my Ph.D.

Thanks to my many colleagues who were always willing, if not eager, to help when I needed it. Thanks to members of the Bone Biomechanics Lab, including Dr. Jess Brezicha, Jon Paul Elizondo, Jennifer Kosniewski, Jeremy Black, and Dr. Ray Boudreaux. Thanks also to members of the Bone Biology lab, including Dr. Corinne Metzger, Dr. Rihana Bokhari, and Dr. Heather Allaway. Thanks to all of you for making the daily grind bearable. Thanks to the many undergraduate students who helped me with every facet of this project, from countless hours of animal work to mechanical testing.

Thanks to my brother, Justin Lenfest, who never fails to make me laugh, and who is always willing to listen. Thanks to Chris and Laurie Looper, for supporting me, for caring, and for being the best in-laws I could hope for. Thanks to my parents, Michael

and Gina Lenfest, for supporting me in every way imaginable, for teaching me, and for loving me unconditionally.

And finally, I would like to express my deep gratitude to my wife, Dr. Amelia Looper. Without her unfailing support, I could not have made it through these long years of study and research. Additionally, I had the extreme pleasure or working directly with Dr. Looper to design the Voluntary Jumping Exercise protocol. Her knowledge of animal behavior modification and training was instrumental, and I never could have attempted this without her expert consultation during the conception and implementation of the protocol. From showing us how to build food reward interest in the animals, to advising me on training method adjustments, to teaching undergraduate students proper positive reinforcement training procedures, Amelia consistently leant a hand and was always an absolute delight to work with. Thank you, for everything.

CONTRIBUTORS AND FUNDING SOURCES

Contributors

This work was supervised by a dissertation committee consisting of Professor Harry Hogan [advisor] and Professor Sevan Goenezen and Professor Bruce Tai of the Department of Mechanical Engineering and Professor Susan Bloomfield of the Department of Kinesiology.

The histomorphometry data analyzed for Chapter 3 and Chapter 4 were provided by Dr. Corinne Metzger, formerly of the Department of Kinesiology. The μCT data analyzed for Chapter 3 and Chapter 4 were provided by Dr. Matt Allen of the Department of Anatomy & Cell Biology at the Indiana University School of Medicine. Dr. Matt Allen also donated the alendronate and zoledronate.

All other work conducted for the dissertation was completed by the student independently.

Funding Sources

Graduate study was supported in part by the National Space Biomedical Research Institute under Grant Number NCC9-58 (Space Life Science Pre-Doctoral Mentored Training Program).

This work was also made possible in part by NASA under Grant Number NNX13AQ87G and by NASA Space Biology under Grant Number NNX13AM43G. Its contents are solely the responsibility of the authors and do not necessarily represent the official views of NASA or NASA Space Biology.

TABLE OF CONTENTS

Page

LIST OF FIGURES

Page

LIST OF TABLES

Page

1. INTRODUCTION

In addition to its well known structural functions of support and protection, bone also contributes to body movement, mineral homeostasis, hematopoiesis, and endocrine regulation. Because of its rigidity and strength, bone is able to give shape to the human body and protect major organs from damage; the hard skull protects the brain and the rib cage protects the heart and lungs housed in the thoracic cavity. Long bones function as attachment points and levers for muscles, facilitating complex motion. Bone also serves as a reservoir for calcium, which is vital to many bodily functions such as muscle contraction and the transmission of nerve signals. Red blood cells are produced in bone marrow, and the secretion of fibroblast growth factor 23 (FGF-23) and osteocalcin contribute to phosphate and energy metabolism, respectively, throughout the body (Burr and Allen, 2014).

1.1. Bone Structure and Composition

Bone is a dynamic, composite material in which organic and inorganic elements intermingle to create a strong, rigid material that remains flexible and adaptable to functional necessities. 65% of bone by mass is mineral, 25% is organic components, and 10% is water. 90% of the organic makeup of bone tissue is Type 1 collagen fibers, and the remaining 10% is various cellular and extracellular non-collagenous proteins. Collagen fibrils are cross-linked together to form large arrays of parallel fibers. Mineral hydroxyapatite crystals are located in the pores between parallel collagen fibrils and the holes between the fibril ends. These crystals are attached to the collagen by hydrogen bonds and water. The collagen and water contribute elasticity to bone tissue, while the

mineral component contributes stiffness. The collagen fibers and bonded mineral plates combine to form sheets that are typically oriented in the primary direction of experienced stresses (Burr and Allen, 2014). This direction varies by bone site, but the collagen-mineral sheets are typically organized longitudinally in response to tensile stress, and transversely in response to compressive stress (Fratzl, 2008).

There are two main types of bone organization. Periods of change such as rapid growth or fracture result in hasty and haphazard bone formation that leads to highly disorganized bone tissue. This rapidly mineralized and poorly organized bone is referred to as woven bone. Woven bone only exists in circumstances that require a significant increase in bone mass over a short period of time, and over time woven bone will undergo remodeling into the primary form of bone found in the body, lamellar bone. In lamellar bone, the collagen-mineral sheets are organized in larger sheets, or lamellae (Burr and Allen, 2014).

On a macro-level, bone can be divided into two different compartments, cortical (compact) bone and cancellous (spongy, trabecular) bone. Cortical bone is stronger and denser than cancellous bone, with only 3% - 5% porosity. Cortical bone is the more prominent of the two bone types, making up 80% of the adult skeleton (Cowin, 2001), and is found mainly in the shaft (diaphysis) of long bones (e.g. femur, tibia, radius, humerus) and short bones (e.g. carpals, tarsals) that make up the extremities, as well as the flat bones (e.g. skull, ribs). A thin shell of cortical bone also surrounds irregular bones (e.g. vertebrae, pelvis) and the ends (metaphysis) of long bones. The lamellar bone that makes up cortical bone is organized into structures called osteons that typically consist of fewer than 10 lamellae organized concentrically around vascular channels called Haversian canals.

Osteons typically have diameters from 50 μm to 100 μm, and their outer edges, called cement lines, are very important in preventing and deflecting crack growth. Osteon geometry allows for efficient blood perfusion throughout bone tissue with a minimal number of blood vessels (Burr and Allen, 2014).

Cancellous bone is found in long bone metaphyses and the main body of vertebrae and other irregular bones. Cancellous bone consists of a highly interconnected network of approximately 200 μm thick bone rods and plates (called trabeculae) that comprise only 25% - 30% of the cancellous tissue volume. The remainder of the volume consists of marrow space, where hematopoiesis takes place. Cancellous bone geometry reduces the total weight of bone while efficiently transmitting stresses to the surrounding cortical shell (Burr and Allen, 2014). Instead of osteons, cancellous bone is made up of numerous parallel lamellae with no blood vessel infiltration. This lack of blood vessel infiltration dictates the 200 μm trabeculae thickness (Currey, 2006). Trabeculae are generally plate-like, as opposed to rod-like, in healthy humans, as plates provide more resistance to bending forces in the load-bearing direction. In mixed cortical and cancellous bone sites, such as long bone metaphyses and vertebrae, the cortical shell contributes to increased bone strength while the cancellous interior contributes to increased energy absorption (Burr and Allen, 2014).

1.2. Bone Adaptation and the Mechanostat

Bone is a dynamic tissue, constantly being renewed and changed over the lifetime of an organism. As bone grows older, it becomes increasingly mineralized. Bone that is too highly mineralized can be brittle, which increases the risk of crack propagation and fracture. Microscopic damage that occurs in the course of daily activities generally releases

energy and helps prevent serious cracks and fracture. However, if enough of this damage is allowed to build up over time, the stiffness and strength of the bone tissue can eventually be reduced. In the year following a hip fracture, patients older than 50 suffer 8% - 36% excess mortality and 60% do not fully regain their pre-fracture level of independence (Abrahamsen et al., 2009, Cosman et al., 2014). Therefore, maintaining bone mass and quality is very important, especially in at-risk populations such as the elderly and osteoporosis patients. The body, therefore, must have a mechanism for repairing and renewing old bone. This process is called bone remodeling.

Remodeling involves specialized bone cells working in sequence to first resorb old bone and then form new bone matrix that becomes mineralized over time. Osteoclasts are multi-nucleated cells responsible for bone resorption, or the removal of old bone. After resorption, teams of osteoblasts produce osteoid (unmineralized organic bone matrix) in the osteoclast resorption sites. The primary mineralization process, responsible for 70% of the final mineral content, takes place over the first two to three weeks after osteoid formation. During secondary mineralization, the mineral crystals slowly grow and mature to a physiological limit, which can take anywhere from several months to a year (Burr and Allen, 2014).

During bone formation, some osteoblasts are trapped in osteoid and become osteocytes. Osteocytes comprise 90% of all bone cells and are regularly distributed throughout the mineralized bone matrix. One of the main functions of osteocytes is monitoring and sensing their environments, and then signaling to other cells to coordinate remodeling and other functions. Osteocytes have numerous dendritic processes extending from their cell bodies that create a network with other osteocytes throughout the bone

matrix. Osteocytes sense mechanical loading through cell body deformation and fluid shifts caused by bone tissue deformation. In response to these mechanical stimuli, as well as other hormonal stimuli, osteocytes coordinate osteoclast and osteoblast activity through the production and secretion of factors including osteoprotegerin (OPG), receptor activator of nuclear factor kappa-B ligand (RANKL), and sclerostin, all of which are important in biochemical pathways that regulate osteoblast and osteoclast differentiation and activity (Burr and Allen, 2014).

In cortical bone, remodeling occurs in five stages, with a full cycle usually having a 4 – 6 month duration. The activation stage involves the recruitment of osteoclast precursors to the remodeling site, followed by their differentiation into mature osteoclasts. In the resorption stage, bone lining cells retract from the bone surface, allowing osteoclasts to attach and dissolve bone mineral. Collagen fragments are released as a consequence of osteoclast activity, and can be measured in the blood and urine as biomarkers of bone resorption. The third stage, reversal, occurs when osteoclasts cease resorption and osteoblasts begin formation. In the formation stage, osteoblasts lay down osteoid. When formation is completed osteoblasts die through apoptosis, become osteocytes, or become bone lining cells. The final stage is quiescence, in which osteoblast and osteoclast activity drops to nothing, and the bone matrix is mineralized over time. The majority of bone surfaces throughout the body are in a quiescent state at any point in time (Burr and Allen, 2014).

Bone remodeling is not nearly so organized in cancellous bone. Osteoclasts respond to trabecular damage, changes to the mechanical environment, and systemic calcium homeostasis needs by forming Howship's lacunae, small 40 μm - 60 μm deep

resorption regions. Osteoblasts eventually lay down new bone in these lacunae, as long as the trabecula is not completely severed. When resorption is elevated above normal levels, such as in osteoporosis patients or disuse, Howship's lacunae can be located too closely, and end up penetrating through trabeculae. Osteoblasts then have no ability to replace the lost trabeculae in the same location (Bartel et al., 2006).

Bone resorption and formation are coupled in remodeling, but are rarely balanced, especially in cortical bone. Bone remodeling has a slight negative balance in healthy individuals, mainly due to new Haversian canals formed along with each new osteon. This slight negative balance leads to the bone loss often observed in humans beginning in middle age. Disease states such as postmenopausal osteoporosis exacerbate this problem and cause a significantly negative bone remodeling balance that results in rapid bone loss (Burr and Allen, 2014).

In contrast to bone remodeling, the process by which decoupled formation or resorption leads to bone growth or shape change is called bone modeling. As the human body changes size and shape during development, the bones also must change shape or orientation in order to maximize bone strength and function. Bone modeling takes care of these needs and therefore occurs most during development, though it does take place in skeletally mature individuals at a low rate.

A holistic understanding of all these processes and cell activities that maintain and regulate bone quality leads to an understanding of bone as a living and highly adaptable tissue. One of the most important and relevant adaptations bone tissue makes is to its mechanical environment. Julius Wolff was the first person to describe these adaptations after he and his contemporaries noticed the trabeculae of cancellous bone arranged in

directions that made structural and engineering sense (Wolff, 1892). Wolff codified these observations as Wolff's Law, which can be paraphrased as the shape and geometry of bone is dictated by the stresses it experiences. This idea was modernized and taken further by Harold Frost, who proposed a negative feedback system model for bone adaptation, using a thermostat analogy (Frost, 1964).

Much as a thermostat turns on when it senses temperature above or below a predetermined level, bone remodeling turns on when strains above or below a set point occur. Frost's model, which he named the mechanostat, defines four levels of mechanical loading at which various adaptive processes occur. When mechanical loading is within normal ranges, bone maintenance occurs through standard bone remodeling that replaces old bone tissue. This is the level at which bone normally operates. When strain and strain rates are increased above normal, bone tissue deforms and fluid within the bone is forced into new locations. Osteocytes sense the deformation of their cell walls and the fluid flow that occurs. Osteocytes then signal to osteoclasts and osteoblasts, resulting in decreased bone resorption and increased bone formation. Net bone formation takes place in the directions that will most strengthen the bone in response to this new mechanical loading. This effect can be harnessed through resistive exercise, which has been demonstrated with head-down bed rest (HDBR) subjects (Shackelford et al., 2004) and NASA astronauts (Leblanc et al., 2013, Smith et al., 2012).

When the mechanical load is high enough to cause damage or fracture, net bone formation is dramatically increased. At this level, disorganized woven bone can be formed to rapidly increase bone mass, and then remodeled into a more organized geometry after the damage is stabilized. Conversely, when mechanical loading is reduced, osteoclast

activity and bone resorption increase, while simultaneously osteoblast activity and bone formation decrease. This leads to net bone resorption and an eventual decrease in bone density and strength. This level of mechanical loading can be caused by disuse and results from studies involving spinal cord injury patients, HDBR subjects, and NASA crewmembers all support this trend (Garland et al., 1992, Lang et al., 2004, LeBlanc et al., 2007, Zerwekh et al., 1998).

1.3. Spaceflight and Bone

Astronauts undergo significant bone loss at weight-bearing sites during spaceflight. On 4-6 month missions to the International Space Station (ISS), astronauts can lose up to 1.5% of integral bone mineral density per month in the hip, which is roughly 10 times greater than the bone loss rate in postmenopausal Caucasian women, the population most at-risk for osteoporosis (Carpenter et al., 2010, Cauley et al., 2005, Lang et al., 2004, Lang et al., 2006, LeBlanc et al., 2000). A study by Keyak et al. (2009) demonstrated that these losses in bone mineral density suffered by astronauts translate into significant reductions in mechanical strength of the proximal femur. Finite element analysis (FEA) based on QCT images obtained before and after 4.3 to 6.5 month spaceflight missions showed that 13 astronauts experienced up to 5% loss in femoral strength per month. Additionally, the average amount of FEA estimated femoral strength loss under normal stance loading was almost half the average lifetime stance strength loss experienced by Caucasian women (Keyak et al., 2009). Although it is likely that several mechanisms contribute to spaceflight induced bone loss, a significant contributor is reduced mechanical force on the lower limbs and vertebral column as a result of the lack of normal weight-bearing while in low Earth orbit (LEO).

Studies of countermeasures to this bone loss have identified several useful methods of promoting bone formation and reducing bone resorption (Cavanagh et al., 2005). Use of the advanced resistive exercise device (ARED) onboard the ISS for 1.5 hours per day, six days per week has helped attenuate or prevent this bone loss in many astronauts. In recent studies where astronauts used the ARED, crewmembers exhibited reduced bone density at weight-bearing and non-weight-bearing sites as a result of 4-6 month missions, and recovery of this bone loss did not occur during the 12 months following return to Earth and normal gravity (Sibonga et al., 2019, Vico et al., 2017). Use of the anti-resorptive bisphosphonate alendronate (ALN) in combination with the ARED and nutritional support virtually eliminated bone density loss at the hip, pelvis, and lumbar spine as assessed by two-dimensional dual-energy x-ray absorptiometry (DXA) methodology (Leblanc et al., 2013, Sibonga et al., 2019, Smith et al., 2015).

Use of bisphosphonates, however, is not standard among astronauts and cosmonauts aboard the ISS. ISS astronauts are also increasingly embarking on repeat spaceflights, which exposes them to multiple bouts of microgravity separated by extended periods of weight-bearing on Earth. It is plausible that the benefits of taking bisphosphonates for one mission could extend to a subsequent mission without need for additional treatment.

Additionally, some of these countermeasures will not be suitable for missions that travel beyond low Earth orbit, such as to the Moon or Mars. The ARED is a large and heavy device that takes up a significant portion of the ISS. Together with the cycle ergometer and treadmill used for aerobic exercise, the exercise equipment onboard the ISS weighs at least 4,000 lbs. and takes up about 850 cubic feet of space. There will not be

room for these devices in any vehicle astronauts will use on an exploration class mission, including the Orion space capsule. Any failure of exercise equipment would deprive astronauts of a bone health countermeasure for the remainder of the probable 1- to 3-year-long mission. Resistive exercise, by its nature, increases the risk of injury, which would not only prevent the astronaut from continuing their necessary exercise, but could also prevent them from performing other mission-critical tasks. Finally, astronaut time is one of the most valuable commodities in any space mission. Including aerobic exercise, astronauts currently exercise about 2.5 hours each day in order to attempt to maintain pre-flight levels of health while on board the ISS. This level of time commitment is not desirable and may not always be feasible on an exploration class mission. Pharmaceutical interventions are therefore of paramount importance to identify and study as adjuncts to exercise regimens for extended LEO, Lunar, and Mars missions.

In this study, we used the *in vivo* rat hindlimb unloading (HU) model to investigate potential countermeasures for use in preventing bone loss due to unloading. This study addresses the ability of anti-catabolic bisphosphonates to reduce or prevent disuse bone loss in two periods of hindlimb unloading separated by 56 days of recovery. This experimental design is meant to mimic a situation where an astronaut flies on multiple missions separated by a year. We also sought to create a novel method of modeling resistance exercise in rats, based on a positive reinforcement training method that elicits a voluntary behavior from the animals.

1.4. Multiple Hindlimb Unloading

The rodent hindlimb unloading (HU) model is a very well established ground-based model of microgravity and fluid shifts that was first described by Morey-Holton and

Globus (Globus and Morey-Holton, 2016, Morey-Holton et al., 2005, Morey-Holton and Globus, 1998, Morey-Holton and Globus, 2002). In this model, rodents are suspended by their tail in order to remove all weight-bearing from the hindlimbs. Rodents have full access to their cage, but their inability to bear weight on their hindlimbs simulates the low-force environment experienced by astronauts in microgravity. Due to the suspension, rodents also experience a 30° head-down tilt which mimics the headward fluid shifts experienced in microgravity. This results in a systemic model of microgravity that has produced similar bone mineral density loss to spaceflight, as well as significant deterioration of the material and structural properties of bone (Bloomfield et al., 2002, Bloomfield et al., 2016).

Surprisingly, only a few studies have looked at multiple HU events separated by recovery, a situation that more astronauts are experiencing as they fly multiple missions aboard the ISS. These studies found that exposing mice to multiple HU events resulted in compounded losses in trabecular microarchitecture at the distal femur (Gupta et al., 2012), but did not increase the total amount of bone loss in the lumbar spine compared with just one exposure (Gupta et al., 2013), and that increased recovery time between exposures did not reduce ultimate bone loss at the distal femur metaphysis (Manske et al., 2015). In contrast, our laboratory previously determined that multiple HU exposures did not exacerbate total bone loss in the proximal tibia metaphysis of rats (Shirazi-Fard et al., 2013a). Our laboratory also studied resistance exercise during the recovery period between two HU periods as a possible countermeasure for reducing bone loss and promoting recovery. We found that recovery of proximal tibia metaphysis cancellous bone was improved through resistance exercise, but no effect on bone loss during subsequent HU

periods was observed (Shirazi-Fard et al., 2014). This dissertation study was designed to further investigate the effects of multiple HU periods on the rat skeletal system, as well as investigate the ability of the benefits of a single anti-catabolic bisphosphonate treatment during an initial HU period to extend to a later HU period and to examine the benefits of exercise training prior to an unloading period as a countermeasure to HU-induced bone loss.

1.5. Skeletal Effects of Bisphosphonates

Bisphosphonate treatment is one of the main tools physicians use in the prevention and treatment of osteopenia and osteoporosis. Bisphosphonates function in an anti-catabolic manner, meaning they reduce the rate of bone resorption. In contrast, anabolic countermeasures, such as exercise, increase the rate of bone formation and the overall bone mass.

After oral or intravenous administration, bisphosphonates are preferentially attracted to bone, where they bind to hydroxyapatite crystals on bone surfaces (Papapoulos, 2008). Osteoclasts release and take up these bisphosphonate molecules during bone resorption. The actual mechanism of reduction of bone resorption depends on which of two categories the bisphosphonate in use belongs to. Clodronate and etidronate do not contain nitrogen and are referred to as non-nitrogenous bisphosphonates. These bisphosphonates are directly toxic to osteoclasts that ingest them, as they form nonhydrolyzable ATP analogs which cannot actually be used as an energy source, which leads to osteoclast apoptosis. Nitrogenous bisphosphonates, such as risedronate (RIS), zoledronate (zoledronic acid, ZOL), alendronate (ALN), pamidronate, and ibandronate, disrupt bone resorption in two ways. Firstly, nitrogenous bisphosphonates stabilize the

hydroxyapatite crystals, making resorption more difficult. Upon ingestion by osteoclasts, nitrogenous bisphosphonates additionally disrupt the cholesterol synthetic pathway through the inhibition of farnesyl pyrophosphate synthase (FPPS), an enzyme required for osteoclast function and maintenance of proper cytoskeleton shape. As a result, nitrogenous bisphosphonates do not necessarily cause osteoclast apoptosis, but merely an inability to resorb bone effectively (Burr and Allen, 2014, Rogers, 2003).

Two metrics important for comparing the efficacy of various bisphosphonates are binding affinity and anti-resorptive potency. A given bisphosphonate's binding affinity describes how likely it is to attach to a bone surface, and how long it will remain attached if undisturbed. Bisphosphonates are generally very stable, and can reattach to bone sites after being released by osteoclasts. This results in extended effects on bone resorption; a single infusion of ZOL has been documented to maintain increased bone density for 5 years in postmenopausal women (Grey et al., 2012). Anti-resorptive potency is a measure of a bisphosphonate's ability to inhibit bone resorption. In nitrogenous bisphosphonates, anti-resorptive potency is a direct reflection of the level of FPPS inhibition, and is consistently higher than in non-nitrogenous bisphosphonates. This explains the preference for nitrogenous bisphosphonates for clinical applications. Comparative studies of bisphosphonates have ranked ZOL as the highest in both binding affinity and anti-resorptive potency, and ALN as near the top in both measures (Russell et al., 2008).

Bisphosphonates' ability to prevent disuse bone loss has been investigated using the rodent HU model as well as HDBR in humans. HDBR is considered the gold standard for simulated microgravity, as it mimics the lack of gravity-induced forces on the body, as well as the fluid shifts experienced in microgravity via the 15° head-down tilt. HDBR

produces bone changes similar in magnitude to those experienced by astronauts during spaceflight (Giangregorio and Blimkie, 2002). Early HDBR experiments conducted in the 1980's first demonstrated the ability of bisphosphonates to reduce or prevent disuse-induced bone loss (Chappard et al., 1989, Vico et al., 1987). Recent studies in male subjects showed that oral doses of ALN given daily during 17 weeks of HDBR resulted in a 2% increase in areal bone mineral density (aBMD) of the femoral neck, as measured by DXA. Control subjects, who did not receive ALN, exhibited a 2% decrease in aBMD at the same bone site (Leblanc et al., 2002). Intravenous administration of the bisphosphonate pamidronate two weeks prior to a 90 day HDBR also prevented aBMD loss in the total proximal femur (Watanabe et al., 2004).

Rodent HU studies have shown that ALN administered during the unloading period is effective at preventing bone loss. An early study of ALN treatment during 9 days of HU significantly reduced bone resorption, prevented the relative loss of skeletal mass, and increased bone mass in the proximal tibia compared to both HU and cage controls (Bikle et al., 1994). This study and many others were performed on skeletally immature rodents, which are a poor model for astronauts who are largely middle-aged or older. Additionally, many previous studies did not report any measurement of mechanical properties (Bikle et al., 1994, Kodama et al., 1997), while a few studies reported three-point bending (Apseloff et al., 1993a, Apseloff et al., 1993b, Lloyd et al., 2008), or femoral neck (FN) testing and distal femur compression (Mosekilde et al., 2000) results.

Almost all of these studies used an HU period of 9 to 14 days (Apseloff et al., 1993a, Kodama et al., 1997, Lloyd et al., 2008) and another immobilized the right leg with an elastic band for 28 days (Mosekilde et al., 2000). Bisphosphonate treatment was given

throughout the HU or immobilization period in three studies (Apseloff et al., 1993b, Kodama et al., 1997, Mosekilde et al., 2000) and ZOL was administered on day 0 by Lloyd et al. (Lloyd et al., 2008). These studies also did not include results detailing changes in bone during a recovery (re-ambulation plus cessation of the drug following disuse) or secondary HU period. We have previously shown that ALN administered during 28 days of HU has very little effect as a countermeasure in cortical bone (Macias et al., 2012), but is partially or fully effective in the cancellous compartment (Swift et al., 2011). We have shown that ZOL given just prior to HU significantly reduces bone degradation due to 28 days of HU, while maintaining bone formation (Boudreaux, 2014).

A single spaceflight study investigating bisphosphonate use has been conducted. Seven astronauts were administered ALN starting three weeks before launch on a 4-6 month ISS mission, in addition to exercising 6 days per week using the ARED and aerobic equipment. Their DXA assessed aBMD at the total hip, femoral trochanter, and lumbar spine was significantly higher compared to a group of 10 astronauts whose only countermeasure was ARED and aerobic exercise during their 4-6 month ISS missions. Additionally, cancellous vBMD assessed by QCT was significantly higher for the ALN-treated group, and ALN treatment significantly reduced urinary calcium during spaceflight (Leblanc et al., 2013, Sibonga et al., 2019). High urinary calcium increases the risk of renal stone formation. Such a medical emergency would result in an immediate mission cancellation and return to Earth from the ISS, and could potentially be catastrophic on an exploration class mission where a rapid return to Earth would not be possible. Based on the sum of collected data, and the fact that zoledronate can significantly inhibit bone resorption for years after a single dose, the most recent meeting of the NASA Bone Research and

Clinical Advisory Panel in October 2016 resulted in an official recommendation that all astronauts participating in missions longer than 6 months receive intravenous infusions of ZOL prior to launch as a protective countermeasure (Sibonga et al., 2017).

We are aware of only one other study that investigated direct head-to-head comparisons of different bisphosphonates for efficacy in preventing disuse bone loss. Mosekilde et al. compared equal doses of ALN and RIS during 28 days of unilateral hindlimb immobilization, and found no difference between the groups treated with the two bisphosphonates, though both were effective at protecting against disuse bone density and strength loss (Mosekilde et al., 2000).

In this dissertation study, rats were treated with ALN or ZOL during the first HU period in a head-to-head comparison. The binding affinity and anti-resorptive potency of ZOL is known to be higher than ALN (Russell et al., 2008), so this study's comparison of ALN and ZOL treatment reflects the degree of difference between the two and the implications for preserving biomechanical competence of the affected bone sites.

1.6. Animal Models of Exercise

Resistance exercise is a well-documented anabolic method of maintaining or increasing bone health in general (Colletti et al., 1989, Daly et al., 2004, Fuchs et al., 2001) and of counteracting disuse bone loss (Allen et al., 2006, Shackelford et al., 2004, Swift et al., 2010b). Exercises with a significant weight-bearing component such as running, weight-lifting, and jumping stimulate the osteocytes in various bone sites and promote bone formation. Although direct gravitational (weight-lifting) and impact (running, jumping) forces applied to the bone during exercise are important, the largest physiological loads and therefore the largest strains are imparted by muscle contractions. These muscle-

mediated forces have the largest impact on the mechanical environment of bone, and muscle mass and strength are therefore highly correlated to bone mass and strength (Turner, 2000). Exercises such as swimming and cycling that do not involve impact forces can still be beneficial to bone through the strengthening of muscle.

The precise amount of mechanical load necessary to promote bone formation is not known, but it is widely acknowledged that a diverse routine of weight-bearing and non-weight-bearing exercise is best for maintaining or improving muscle, bone, and general health. Studies in children participating in exercise programs combining aerobic and resistance exercise demonstrated significantly higher bone mass and density compared to non-exercising controls (Bass et al., 2007, Kohrt et al., 2004, Linden et al., 2006). Similar studies in adults were effective at preventing bone losses, though not necessarily increasing bone mass (Engelke et al., 2006).

Resistance exercise is the most important countermeasure for the prevention of bone loss due to microgravity, and is currently practiced by every crewmember aboard the ISS using the ARED. Astronauts participating in exploration class missions will undoubtedly have some method of exercising. Several prototype designs for use in the Orion space capsule are currently being explored by NASA, and will soon be on board the ISS for preliminary investigations. Clearly, exercise is an important countermeasure to study and include in research using rodent models.

Previous studies have incorporated various rat models of resistance exercise. External loading involves anesthetizing the rats and applying a cyclical axial or bending strain to a bone, often the tibia, via an external device. This treatment resulted in increased osteoblast surface (Boppart et al., 1998) and increased BMD and bone formation in

paralyzed legs (Morse et al., 2014). Our laboratory has previously investigated simulated resistance training (SRT) via electrical muscle stimulation, which resulted in the elimination of disuse related bone and muscle loss, and increased cortical bone formation (Hubal et al., 2005, Macias et al., 2012, Swift et al., 2010b, Swift et al., 2011).

These paradigms, though effective, rely on involuntary loading, and thus the mechanical force environments of the tissues are not necessarily reflective of physiological conditions. Three models of voluntary exercise have been investigated previously. Consecutive jumps from the bottom of a box enclosure 15 inches up to the edge have repeatedly been shown to increase bone formation and reduce bone loss due to HU or ovariectomy (Honda et al., 2008, Ju et al., 2013, Ju et al., 2012, Okubo et al., 2017, Shimano et al., 2018, Umemura et al., 1997, Yanagihara et al., 2016). A second model consists of encouraging rats to repeatedly climb a 1-meter ladder with a 2 centimeter grid at 85º inclination by gently brushing them with a hand when necessary. Rats were first subjected to two weeks of HU, and then performed 4 weeks of ladder exercise, which resulted in increased bone density compared to ambulatory control and recovery without exercise groups, as assessed by DXA (Song et al., 2018).

In the final model, rats alternately pull a low and high lever in a standing and squatting motion. This movement encompasses both concentric and eccentric muscle contractions, and results in a fair approximation of a human squat exercise. This exercise model was first developed when studying protein synthesis and insulin resistance (Farrell et al., 1998, Fluckey et al., 1995, Fluckey et al., 1996, Garner et al., 1991). Positive musculoskeletal effects were later demonstrated with this model (Farrell et al., 1999, Westerlind et al., 1998) and a similar model adapted for use during HU (Fluckey et al.,

2002). With this model, our laboratory has previously shown that resistance exercise results in significantly higher bone formation and volumetric bone mineral density in the cancellous compartment of the proximal tibia (Swift et al., 2010a). We have also shown that resistance exercise performed during the recovery period between two bouts of HU increases the speed of recovery, but does not mitigate bone loss during the subsequent HU period (Shirazi-Fard et al., 2014).

All of these voluntary exercise models were trained through a negative reinforcement shock-avoidance method, with one exception. In this case, positive reinforcement was implemented using direct brain stimulation (Garner et al., 1991), but this method has the potential for serious confounding neurological effects. Negative reinforcement is one of the four quadrants of operant conditioning, which is the process of behavior change in response to consequences. Negative reinforcement occurs when a behavior increases in frequency in response to the removal of an aversive stimulus, such as when a rat learns to pull a lever to avoid an electrical shock. Positive reinforcement occurs when a behavior increases in frequency in response to the addition of a desirable stimulus, such as when a rat learns to pull a lever in order to receive a food reward (Skinner, 1954). Protocols using both quadrants are effective for training animals to perform a specific behavior, but research performed comparing these methods in rats showed that enthusiasm (measured by total number of attempts to pull a lever during a training session) and number of correct lever pulls were significantly higher in animals trained via positive reinforcement (both high and low value food rewards) compared to animals trained via negative reinforcement (shock avoidance) (Lawson and Watson, 1963). Additionally, a study comparing recall training in dogs with an electric shock collar or positive

reinforcement concluded that there was no difference in efficacy of training, but that dogs trained with the electric collars exhibited greater numbers of stress behaviors (panting, yawning, yelping, lower tail carriage) (Cooper et al., 2014).

In this dissertation study, we developed a positive reinforcement model that uses a food reward as a positive reinforcer to operantly condition the rats to perform a jumping exercise. This new voluntary jumping exercise (VJE) protocol has the benefit of eliminating electrical equipment that can be difficult to use and maintain. VJE also potentially reduces extraneous stress in the animals (positive reinforcement), while also maintaining a reasonable training schedule. The efficacy of this new protocol was validated by documenting the effects of VJE pre-treatment on bone loss as a result of HU.

1.7. Bone Densitometry

X-ray emitting devices have long been the main method of non-invasively monitoring bone health. The standard for diagnosis and monitoring of patients with postmenopausal osteoporosis is DXA, which yields a two-dimensional projection of bone mass and areal bone mineral density (aBMD). Briefly, DXA works by passing an x-ray source emitting two energy levels of x-rays over the body. The differential attenuation of these two x-ray energy levels as they pass through the body is measured and used to produce a two-dimensional image of the skeleton and calculate bone characteristics, as well as lean or fat soft tissue body composition, which vary in water content. This two-dimensional representation prevents the separation of the cortical and cancellous bone compartments, which have different metabolic rates and responses to mechanical stimuli. The cancellous compartment has consistently demonstrated greater losses in bone density and strength in both spaceflight (Carpenter et al., 2010, Vico et al., 2000) and rodent

studies (Bloomfield et al., 2002, Shirazi-Fard et al., 2013a, Shirazi-Fard et al., 2013b). Cancellous vBMD in the femoral neck of astronauts suffered the most significant losses, and did not recover after 2.5 – 4 years of normal weight-bearing activity on Earth (Carpenter et al., 2010). Trabecular vBMD has also been most closely correlated with increased hip fracture risk (Bauer et al., 2006, Black et al., 2008, Bousson et al., 2006, Lang et al., 1997).

Changes in the cancellous compartment are very important for predicting changes in bone strength, and these cancellous compartment changes cannot be readily detected through DXA scans. Quantitative computed tomography (QCT), however, can separate the cortical and cancellous compartments. In QCT, an x-ray source with a set scanning thickness is rotated a full 360° about the subject. The scanning thickness of the x-ray source combined with the two-dimensional representation from the 360° scan results in a three-dimensional or volumetric representation of the scanned object. The size of the pixels in the 360° scan plus the length of the scanning thickness result in the voxel resolution, or the size of the volumetric elements used to represent the bone. A detector rotates with the x-ray source and measures the tissue absorption levels, which are translated to linear attenuation coefficients (LACs) for each voxel. The Hounsfield scale is used to standardize LAC values between different QCT machines that have different kilovoltage settings. The ratio of the LAC of a particular voxel to the LAC of water is defined as a Hounsfield unit, which is used to calibrate the machine to produce accurate volumetric bone mineral density (vBMD) values. Hounsfield units are calibrated by scanning a solid hydroxyapatite phantom. Software performs linear regression analysis to determine a relationship between

the mean Hounsfield units produced by the machine and the known vBMD of hydroxyapatite in the phantom.

Though the three-dimensional nature of QCT results is greatly preferable for monitoring cancellous bone loss, QCT does have disadvantages. The scanning time of QCT is much higher than DXA due to the increased resolution and 360° rotations for each scanning thickness slice. More importantly, the average radiation dose from DXA of 10 μSv to 50 μSv is two orders of magnitude lower than the QCT dose of 1 mSv to 6 mSv (Damilakis et al., 2010, Engelke et al., 2008). The excess cancer risk from these densitometry techniques is very small, but for a population made up exclusively of radiation workers such as astronauts, every mSv counts. Despite the recommendations of the NASA Bone Research and Clinical Advisory Panel in 2010 and 2016, astronauts still do not routinely undergo QCT imaging to monitor their cortical and cancellous bone health (Orwoll et al., 2013, Sibonga et al., 2017).

Though QCT can produce a three-dimensional representation of the bone architecture, separate the cancellous and cortical compartments, and produce volumetric bone density measures, it is still limited by voxel resolution. Many QCT machines have a resolution with voxel sizes greater than the average size of trabeculae, which results in the Hounsfield units for the trabeculae voxels reflecting cancellous bone, collagen, and marrow in combination. This may result in the underestimation of bone density, and is referred to as a partial volume effect. The only remedy for partial volume effects is a higher voxel resolution. μCT machines solve this problem with resolutions as low as 1-10 μm (du Plessis et al., 2017, Genant et al., 2008). μCT is considered by many as the best method of investigating *ex vivo* bone microarchitecture in small rodents (Bouxsein et al.,

2010). μCT offers several unique advantages compared to standard histomorphometry, including a larger volume of interest, production of data at multiple bone sites in hours as opposed to weeks or months, and preservation of the sample, which can be subsequently used for mechanical testing at the scanned bone sites. Recently, efforts to monitor bone properties *in vivo* using μCT have been successful, though concerns about anesthesia length and radiation exposure have been raised (Luan et al., 2014).

1.8. Bone Biomechanical Testing

Bone density is not always an accurate predictor of the mechanical properties of bone, and changes to vBMD tend to underpredict changes in mechanical strength, especially in the cancellous region (Shirazi-Fard et al., 2013a, Shirazi-Fard et al., 2014). Because traditional mechanical testing is destructive and cannot be performed on living human subjects, use of an animal model offers a unique opportunity to directly investigate the impacts of microgravity on bone mechanical properties.

Mechanics is the mathematical framework for describing motion resulting from the forces applied to an object. The principles of mechanics are commonly used to solve engineering problems and study changes within systems. Biomechanics is the application of mechanical principles to biological systems. Bone biomechanics encompasses the mechanical behavior of bone as well as how the biological processes of remodeling, growth, disease, etc. affect that mechanical behavior. Biomechanical testing is frequently used in research to assess bone strength and health, test the efficacy of countermeasures and interventions, and estimate fracture risk associated with bone loss.

The relationship between the force applied and the displacement of the bone sample is represented by the force-displacement curve. Important variables dependent on the bone

structure and size can be obtained from this curve. The ultimate force is the maximum force achieved at any point along the curve, and stiffness is the slope of the initial linear region of the force-displacement curve. Extrinsic properties, such as these, represent the structural mechanical properties of the sample, and are obtained directly from the force-displacement curve. Intrinsic properties represent the tissue-level material properties of the sample and are obtained from the stress-strain curve and beam bending theory. The ultimate force (extrinsic) for two bone specemens of different sizes would vary relative to the size difference, but the ultimate stress (intrinsic) would likely be very similar for two bone specimens, regardless of size differences. Engineering stress is defined by:

$$\sigma = \frac{F}{A} \qquad \text{Equation 1.1}$$

where σ is the engineering stress, F is the applied load, and A is the cross-sectional area. Engineering strain is defined by:

$$\epsilon = \frac{\Delta L}{L} \qquad \text{Equation 1.2}$$

where ϵ is the engineering strain, ΔL is the change in sample length, and L is the original length.

These uniaxial representations of stress and strain are only accurate if the assumptions of isotropy, homogeneity, linear elasticity, and uniform cross-section are true for the material being tested. Even though bone tissue is anisotropic, non-homogeneous,

viscoelastic, and usually has an irregular cross-section, the literature has demonstrated that these assumptions are reasonable enough to produce reliable results with this simple stress analysis and this method is considered standard practice for bone biomechanical testing (Burr and Allen, 2014, Cowin, 2001, Turner and Burr, 1993).

. The stress-strain curve (Figure 1.1) can be divided into two regions, elastic and plastic strain. In the elastic strain region, bone deformation is theoretically recoverable and the relationship between stress and strain is linear. Deformation that extends into the plastic strain region is permanent. Crack initiation and propagation begin in the plastic strain region, and eventually lead to fracture. The yield point separates these two regions and the slope of the linear elastic region is the elastic (Young's) modulus. Ultimate stress is the maximum value of stress at any point on the curve. Depending on material properties, fracture can correspond to ultimate stress (brittle fracture) or can occur at higher strains (ductile fracture). Absorbed energy is the area under the stress-strain curve, and corresponds to the material's fracture resistance.

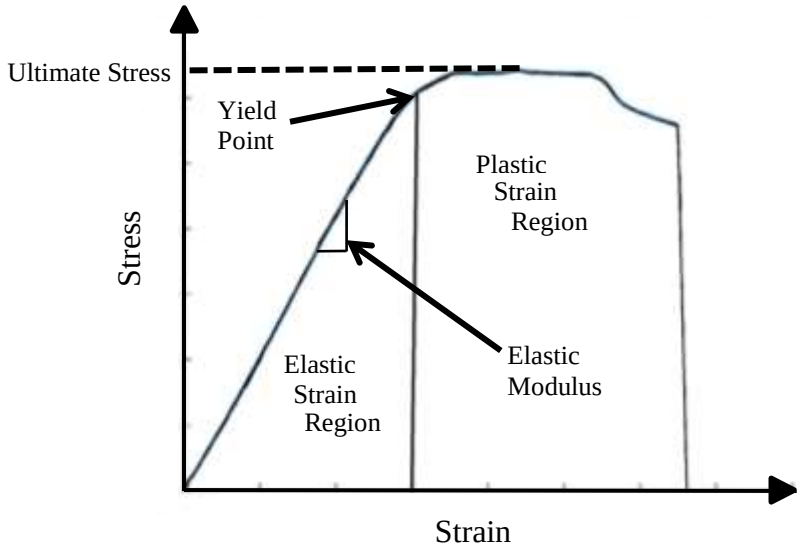

Figure 1.1 Representative Stress-Strain Curve.

Many biomechanical procedures are used to test bone specimens, and one of the most common is three-point bending. In this method, the whole bone rests on two lower support pins and a bending force is applied by an upper loading pin contacting the bone at the center of the span between the lower supports (Figure 1.2). For three-point bending, stress is defined by:

$$\sigma = \frac{FLc}{4I} \qquad \text{Equation 1.3}$$

where F is the applied force, L is the span length between the lower support pins, c is the distance from the neutral axis (estimated as half the vertical diameter of the bone), and I is the cross-sectional moment of inertia. Three-point bending strain is defined by:

$$\epsilon = \frac{12cd}{L^2}$$ Equation 1.4

where d is the displacement. The elastic modulus for three-point bending is defined by:

$$E = \frac{kL^3}{48I}$$ Equation 1.5

where E is the elastic modulus and k is the stiffness. The cross-sectional moment of inertia, I, was obtained from *ex vivo* pQCT in this study.

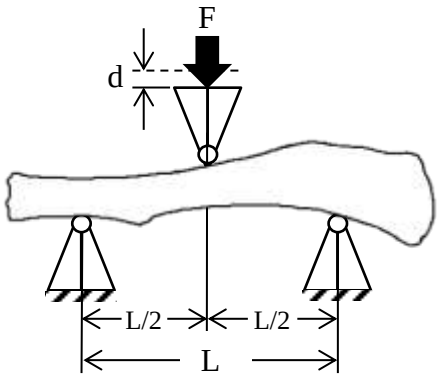

Figure 1.2 Three-Point Bending Experimental Setup.
F is the applied load, d is the bone displacement, L is the span length between the lower supports.

The validity of this three-point bending analysis method relies on four assumptions. First, the sample must have a straight, unstressed, and uniform cross-section along the span length. This assumption is usually violated, as bone specimens rarely have a completely uniform cross-section. The second assumption is that the sample material is linearly elastic, isotropic, and homogenous, which are all violated as discussed previously. The third assumption is that the span length to sample width ratio exceeds 20:1. This assumption is violated for rodent bones, but the use of the longest possible span lengths (typically 15 mm – 20 mm) is adopted to avoid shear stress domination. The final assumption is that deformation due to crushing at the loading and support points does not occur. This assumption is fairly valid assuming loading pins with wide diameters are used. However, even with the 3 mm cylindrical support and loading pins used in this study, some amount of deformation due to shear stress is always unavoidable, and can lead to overestimation of the strain and underestimation of the elastic modulus. Despite these many potentially violated assumptions, this method of stress analysis is considered standard practice for bone three-point bending (Burr and Allen, 2014).

Yield force is one of the commonly reported outcome variables of three-point bending tests for bone. The standard method of 0.2% offset strain is used in uni-axial testing of stell. In this approach, the yield point is estimated by finding the intersection point of a line parallel to the initial slope (linear elastic region) of the stress-strain curve and offset so that it intersects the zero-stress axis at 0.2% of the ultimate strain, and it was validated by loading and unloading steel samples to find the exact point at which all deformation recovered. Because of material and loading differences, this method is not appropriate for three-point bending of bone. The upper and lower surfaces of the bone

cross-section directly below the upper loading arm can deform, resulting in a triangular region of necking that does not affect the force-displacement curve. Therefore, plastic deformation can occur in the linear region of the force-displacement curve. In the data analysis of this study, a secant method for estimating the yield force was used. In this secant method, the yield point is found by extrapolating the user-defined linear slope of the force-displacement curve to zero (k_0), and then finding the point at which a line with a slope 97% the value of the linear region and starting at k_0 intercepts the force-displacement curve. This method results in a value somewhere between a true yield point and a proportional limit, or the point at which a stress-strain curve first deviates from a linear to a non-linear relationship. The secant method arrives at a "yield-like" value using a consistent methodology that has more of a relationship to the physical reality of the behavior of the bone specimen during three-point bending.

Two other mechanical tests were performed in this study. The femoral neck is a mixed bone site containing both cortical and cancellous bone compartments. The femoral neck is very important in humans, as it is the location where most hip fractures occur. In the femoral neck mechanical test, the proximal femur is placed upright in a custom fixture and a cylindrical platen is used to load the femoral head vertically, as seen in Figure 1.3. This test combines normal, bending, and shear loading, and as such only extrinsic properties are reported. Rat femoral necks have a much thicker cortical shell compared to humans, and a significantly lower relative volume of trabecular bone. Because of this, the proximal tibia metaphysis is likely a more relevant site.

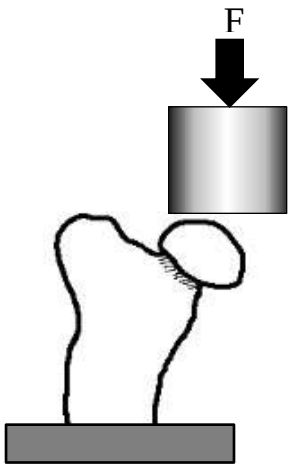

Figure 1.3 Femoral Neck Mechanical Test Experimental Setup.
F is the applied load.

The final mechanical test performed in this study was reduced platen compression (RPC) of the proximal tibia metaphysis. In RPC, a 2 mm section of the proximal tibia metaphysis is obtained and a platen 70% the size of a circle fitting within the endocortical perimeter is used to compress only the cancellous bone. The intrinsic properties are estimated assuming uniaxial compression of an isolated cylindrical specimen (Hogan et al., 2000). Ultimate stress is defined by:

$$\sigma_{ult} = \frac{F_{ult}}{A_p} \qquad \text{Equation 1.6}$$

where σ_{ult} is the ultimate stress, F_{ult} is the ultimate compressive force, and A_p is the platen cross-sectional area. The elastic modulus is defined by:

$$E = \frac{k*h}{A_p} \qquad \text{Equation 1.7}$$

where h is the sample height.

As unloading disproportionately affects the cancellous bone compartment, it is important to evaluate the changes in mechanical properties in the cancellous region. RPC is able to do this by compressing only the cancellous bone while leaving the cortical bone intact. Varying the platen size of the test with the endocortical area of each sample ensures that a consistent proportion of the total cancellous cross-section is tested. Compressing the whole specimen obviously includes the cortical bone, and the cancellous and cortical effects cannot be separated as a result. Cortical bone can carry more than 60% of the load share in vertebral compression tests (Silva et al., 1997). The sensitivity of the test to changes in the cancellous bone is therefore greatly reduced by testing the whole specimen. Previous work has shown that ultimate stress was 60% lower in female rats 3 months after ovariectomy (OVX) compared to sham-OVX rats for RPC tested proximal tibia metaphysis samples, whereas whole proximal tibia metaphysis cross-sections for OVX rats only had 16% lower ultimate stress compared to sham-OVX rats (Hogan et al., 2000).

Completely removing the cortical shell results in samples that are fragile, irregular, and unsuitable for mechanical testing. This is especially true in the tibiae of rats that have undergone HU and lost a significant amount of cancellous bone as a result. The presence of the cortical shell constrains lateral expansion of the cancellous region under compression, and the extent to which this affects RPC results in unknown. However, it may be possible

that the cortical shell would similarly laterally constrain the cancellous bone when responding to applied forces *in vivo*. Additionally, possible local variations in the density and trabecular architecture result in heterogeneous RPC samples. These limitations, however, are outweighed by the increased sensitivity to cancellous bone changes and the built-in simplicity of obtaining intrinsic properties from RPC.

1.9. Study Aims

This dissertation study was conceived with two objectives in mind. The first objective of this study was to investigate the effects of a single period of bisphosphonate administration (ALN and, separately, ZOL) on bone loss suffered due to two bouts of simulated microgravity separated by a period of weight-bearing reambulation. The bisphosphonate was administered for the first HU exposure only, and we compared the effects of the second bout of HU on the bisphosphonate-treated groups to the responses of the untreated group. We also performed a head-to-head comparison of the efficacy of two bisphosphonates, ALN and ZOL. We hypothesized that the benefits to bone strength and quality from bisphosphonate treatment during an initial 28-day HU period would extend throughout the 56-day recovery period and into the second HU period. For the head-to-head comparison of ALN and ZOL, we hypothesized that ZOL would be more effective at preventing the detrimental effects of HU on bone strength and quality due to its higher binding affinity and anti-resorptive potency compared to ALN.

The second objective was to develop a model of voluntary jumping exercise (VJE) that employs positive reinforcement, and validate its efficacy for reducing or preventing disuse-mediated bone loss. We hypothesized that VJE pre-treatment would be effective at preserving bone strength and quality during a subsequent 28 days of unloading, but the

beneficial effects of VJE pre-treatment would not extend to the recovery period following unloading.

Major outcome variables for this study include densitometric and morphologic measures from pQCT scans, extrinsic and intrinsic mechanical measures from mechanical testing of tibia and femur metaphyseal (cancellous) and mid-diaphyseal (cortical) bone regions, and dynamic and static histomorphometric measures of both cortical and cancellous bone regions. Previous studies have shown that 28 days of HU results in losses of bone density and mass similar to the losses experienced by crewmembers on 4-6 month missions in Low-Earth Orbit (LEO) aboard the ISS.

The results of this study provide a more comprehensive understanding of the efficacy of treatment with anti-catabolic pharmaceuticals for mitigating the negative skeletal effects of multiple HU periods, a comparison of two anti-catabolic bisphosphonates in this multiple HU paradigm, and the efficacy of a novel rat model of resistance exercise that uses positive reinforcement-based training procedures for preventing simulated microgravity-induced bone loss.

2. EXPERIMENTAL METHODS

2.1. Animals

Adult male Sprague-Dawley rats (n = 185) were used in these experiments (Envigo, East Millstone, New Jersey, USA). Rats in Experiment 1 were obtained at 5.5 months old, while rats in Experiment 2 were obtained at 4.5 months old. All rats were housed singly in an American Associated for Accreditation of Laboratory Animal Care (AAALAC)-accredited housing facility. They were given ad libitum access to water and food (Teklad 8604, Envigo, East Millstone, New Jersey, USA) and placed on a reverse 12-hour light/dark cycle (dark 10 AM to 10 PM) in a temperature-controlled room (23 ± 2 °C). All rats were given at least two weeks of acclimation before experimental procedures began. Male Sprague-Dawley rats are considered skeletally mature at 6 or 7 months of age. Therefore all experimental interventions began at 6 months. Rats in Experiment 2 were trained starting at 4.5 months so that they were proficient at the behavior when they needed to begin the experiment at 6 months of age. Rats were weighed twice weekly and health checks were performed twice daily by the investigation team and once daily by the housing facility staff. All procedures described in this investigation were reviewed and approved by the Texas A&M University Institutional Animal Care and Use Committee (AUP #'s: 2013-0155, 2013-0164, 2016-0128).

2.2. Experimental Design

This study was divided into two experiments.

2.2.1. Experiment 1

For the first experiment, male 5.5-month-old Sprague-Dawley rats were acclimated for two weeks and then block assigned to baseline control (BC), aging control (AC), hindlimb unloading (HU), alendronate (ALN) treatment plus hindlimb unloading (HU+ALN), and zoledronate (ZOL) treatment plus hindlimb unloading (HU+ZOL) groups by body weight and total volumetric bone mineral density (vBMD) at the proximal tibia metaphysis (PTM). BC animals were euthanized and tissues collected on day 0 (d0), before the start of the first HU period, and served as baseline comparisons for all *ex vivo* analyses. HU, HU+ALN, and HU+ZOL animals were exposed to 28 days of HU, followed by 56 days of recovery, and then a second 28-day HU exposure. Subsets of HU animals were administered ALN (HU+ALN group), ZOL (HU+ZOL group), or no drug (HU group) starting one week before the onset of the first HU period. A visual representation of this experimental design can be seen in Figure 2.1.

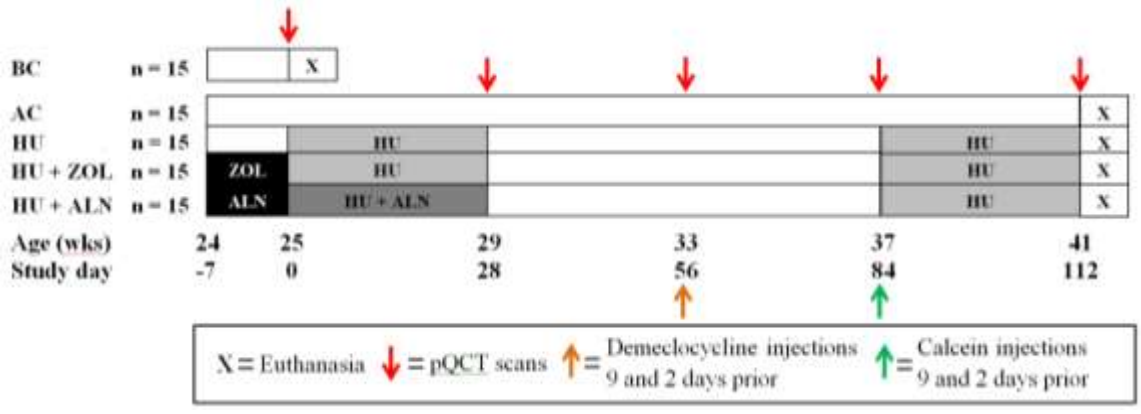

Figure 2.1 Experiment 1 Design.

In vivo longitudinal peripheral quantitative computed tomography (pQCT) scans were conducted at baseline and every 28 days to assess the changes in bone that occurred due to HU and bisphosphonate treatment after the initial period of HU, throughout recovery, and at the end of the second HU period. All other data were limited to a single time point at day 112 (d112) of the study, immediately after the second HU period. Endpoint data were used to determine the extent of persistent bisphosphonate treatment effects on bone through the initial HU period, 56 days of recovery, and the second exposure to HU. This was accomplished by comparing the results of bisphosphonate-treated groups (HU+ALN, HU+ZOL) to the results of HU and AC groups. Twelve animals per group provided adequate statistical power (0.74 – 1.00) to detect key outcome variable changes of 8% in total and cortical vBMD and changes of 15% in cancellous vBMD at the proximal tibia, as measured by pQCT. We have determined population variance ranging from 3% for cortical vBMD and 11% for cancellous vBMD in adult Sprague-Dawley rats for these outcome variables through previous work. Further key outcome variables were produced through biomechanical testing. These outcomes generally have higher variances than densitometric outcomes, thus requiring the increase from twelve to fifteen animals per group.

2.2.2. Experiment 2

For the second experiment, male 4.5-month-old Sprague-Dawley rats were acclimated for 6 weeks. During acclimation, all rats were operantly conditioned in a custom cage to jump onto and off of a 10 inch high platform using 45 mg sucrose pellets (Bio-Serv, Flemington, NJ, USA) as a food reward. Rats were assigned to aging control (AC), HU control (HU) and voluntary jumping exercise (HU+VJE) groups by body weight

and jumping ability. All 110 animals went through the acclimation and operant conditioning phases prior to start of the study (d0), but they did not all learn to perform the jumping behavior at the same rate. Only 35 to 40 of the animals that were assigned to the HU+VJE were fully trained (meaning they could perform 20 jumps up and down from a 10-inch platform in approximately 10 minutes or less) when the exercise phase began (d0). The individuals that were not fully trained merely performed jumps to the best of their ability while we encouraged them to improve and reach the goal of 30 jumps/day on a 10" platform in 10 minutes or less. HU+VJE animals underwent an exercise program of 30 jumps/day, 5 days/week for 28 days. HU+VJE and HU animals were then exposed to 28 days of HU, followed by 56 days of recovery. A visual representation of this experimental design can be seen in Figure 2.2.

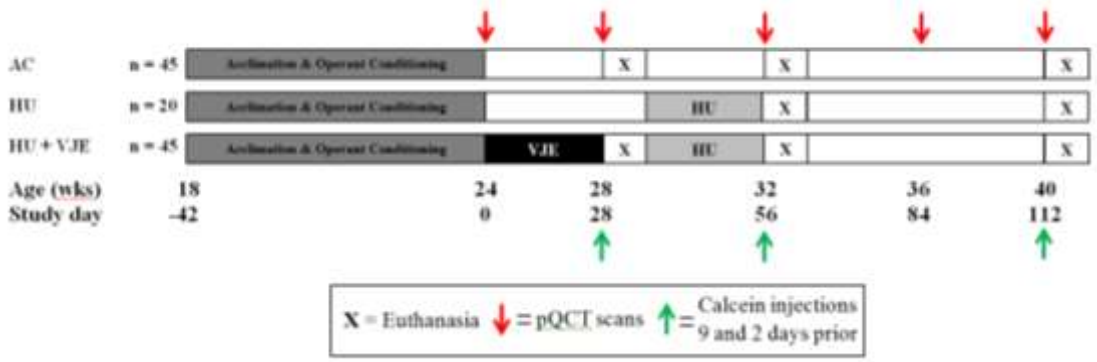

Figure 2.2 Experiment 2 Design.

In vivo longitudinal pQCT scans were made at baseline (after acclimation) and every 28 days to allow assessment of the changes in bone that occurred due to VJE and HU

treatment. A randomly selected subset of 15 animals from the AC and HU+VJE groups were terminated at three time points: day 28 (d28) end of exercise, day 56 (d56) end of HU, and day 112 (d112) end of recovery. A randomly selected subset of 10 animals from the HU group was terminated at d56 and d112. Adequate statistical power (0.74 – 1.00) to detect pQCT key outcome variable changes of 8% in total and cortical vBMD and changes of 15% in cancellous vBMD at the proximal tibia was provided by twelve rats per group. Through previous work, we have determined population variance ranging from 3% for cortical vBMD and 11% for cancellous vBMD in adult Sprague-Dawley rats for these outcome variables. Biomechanical testing produced further key outcome variables. However, biomechanical outcomes have generally higher variances than densitometric outcomes, thus requiring the increase from twelve to fifteen animals per group.

Experiment 2 was part of a larger study investigating the use of anti-catabolic and anabolic pre-treatments as a countermeasure to HU-induced bone quality and strength loss. The AC and HU groups in Experiment 2 were augmented with data from other wings of the study with identical experimental design. These data were used to investigate the effects of pre-treatment VJE on unloading-induced bone loss, and any persistent VJE pre-treatment effects on bone through the HU period and 56 days of recovery. This was accomplished by comparing the results of the HU+VJE group to the results of the HU and AC groups.

2.3. Bisphosphonate Treatment

The two anti-catabolic bisphosphonates used in Experiment 1 (Figure 2.1) of this study are Alendronate (ALN) and Zoledronate (ZOL). ALN (2.4 μg/kg body mass) was administered by subcutaneous injection three times per week for 5 weeks, starting the week

before the initiation of the first HU period and continuing to the end (d28). ZOL (60 μg/kg body mass) was administered in a single subcutaneous injection seven days prior to the initiation of the first HU period. These dosing protocols and concentrations for ALN and ZOL mimic clinical usage in humans for postmenopausal osteoporosis. ALN is given clinically once weekly or daily in tablet form, and ZOL is given once per year as an intravenous infusion.

Previous work in our laboratory has demonstrated that a weekly ALN dose of 30 μg/kg body mass was effective at reducing bone mass and density loss due to HU in skeletally mature male rats (Macias et al., 2012, Swift et al., 2011). The ALN dose in this study (7 μg/kg body mass per week), though lower than most previous studies, is consistent with clinical doses of 70 mg per week, taken orally, for treatment of postmenopausal osteoporosis in humans. The oral dose has an estimated bioavailability of 0.6%, which works out to three doses of 2.4 μg/kg body mass ALN per week, assuming a 60 kg person and 100% bioavailability of the subcutaneous injection (Allen and Burr, 2011).

The ZOL dose of 60 μg/kg body mass is consistent with clinical doses on a mg/kg basis used for the treatment of postmenopausal osteoporosis in humans, 4-5 mg per year (Black et al., 2007). Additionally, previous studies in ovariectomized (OVX, rodent model of postmenopausal osteoporosis) adult female rats demonstrated that both lower (4-20 μg/kg body mass) and higher (100 μg/kg body mass) doses of ZOL were effective at preventing total, cortical, and cancellous volumetric bone mineral density (vBMD) losses at the proximal tibia metaphysis (Gasser et al., 2008). Dr. Matt Allen's laboratory at the Indiana University School of Medicine has demonstrated that this intermediate ZOL dose

prevented increased intracortical remodeling in the mandibles of OVX skeletally mature female mice (Kubek et al., 2010). Previous work in our laboratory has demonstrated that this same ZOL dose is effective at preventing bone density and strength losses in total, cortical, and cancellous regions for skeletally mature male rats subjected to 28 days of HU (Boudreaux, 2014).

2.4. Hindlimb Unloading

HU was used in both Experiments 1 and 2 following a modified version of the method described by Morey-Holton et al. (Morey-Holton et al., 2005, Morey-Holton and Globus, 1998, Morey-Holton and Globus, 2002). In this model, a custom-made harness is used to suspend the animal by the tail in order to remove all weight-bearing from the hindlimbs (Figure 2.3). An approximately 30° head-down tilt is desired, and was achieved by modifying the suspension height. Though the hindlimbs must not be allowed to touch the cage floor, the forelimbs maintain contact and the animal has full access to the cage. All animals were monitored three times daily during HU, with particular attention paid to tail health. Previous studies have shown that 28 days of HU results in losses of bone density and mass similar to losses experienced by crewmembers on 4-6 month missions in Low-Earth Orbit (LEO) aboard the ISS (Allen et al., 2006, Morey-Holton and Globus, 1998).

For Experiment 1 (Figure 2.1), male 6-month-old Sprague-Dawley rats were block assigned to AC and HU groups by body weight and total vBMD. HU animals were exposed to 28 days of HU, followed by 56 days of recovery, and then a second 28-day HU exposure. Subsets of HU animals were administered ALN (HU+ALN), ZOL (HU+ZOL), or no drug (HU). Dosing was administered as described above.

For Experiment 2 (Figure 2.2), male 6-month-old Sprague-Dawley rats were assigned to AC and HU groups by body weight and jumping ability. HU animals were exposed to 28 days of HU, followed by 56 days of recovery, with randomly selected subsets of animals euthanized at the end of the exercise period (d28), at the end of the HU period (d56), and at the end of recovery (d112).

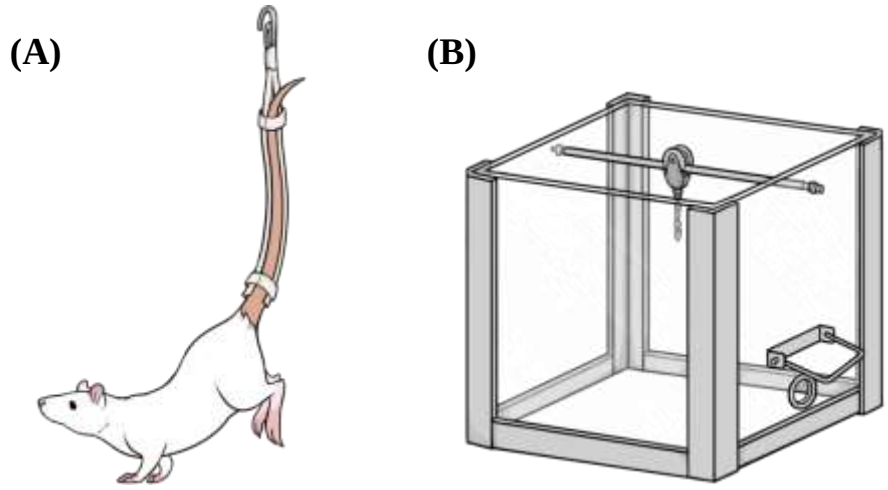

Figure 2.3 Rat Hindlimb Unloading Tail Harness and Cage.
(A) Rat with HU tail harness applied, (B) Rat HU cage, 18" x 18" x 18". Images used with permission from Jenny Kosniewski.

2.5. Operant Conditioning and Voluntary Jumping Exercise

The voluntary jumping exercise (VJE) protocol was used in Experiment 2 (Figure 2.2) only. After the first week of acclimation, rats were food restricted so that their body mass reached 90% of their arrival weight in order to promote interest in the food reward. Between 10 g and 15 g of food was provided to the rats each day during the operant conditioning and exercise periods, with the goal of first reducing their body mass and then maintaining a well-conditioned (3) body condition score. The 45mg sucrose pellet food rewards were first introduced to the rat in their home cage during this period. After a week of acclimation, rats were put in the custom jumping cage (Figure 2.4) with reward pellets scattered in and around the treat receptacle. As the rats became comfortable with the cage, they began eating the pellets around them, which resulted in interaction with the platform and the treat receptacle. Rats remained in the jumping cage either for 8 minutes or until they ascended onto the platform 20 times. At this stage, the platform was set only 4 inches above the cage floor, and the animals could simply step up onto it. At first, any interaction with the platform, including touching it or even looking at it, was marked by an indicator signal in the form of a loud click, followed by the placement of a reward pellet in the treat receptacle. Repetitions of this resulted in increased frequency of this behavior, and led to the rat getting onto the platform. As the reliability and frequency of this behavior increased, the platform height was raised in increments of half an inch to one inch, until the ultimate goal of 10 inches was reached. An individual rat was considered fully trained and prepared to perform VJE when he could perform 20 jumps up and down from a 10 inch platform in approximately 10 minutes or less.

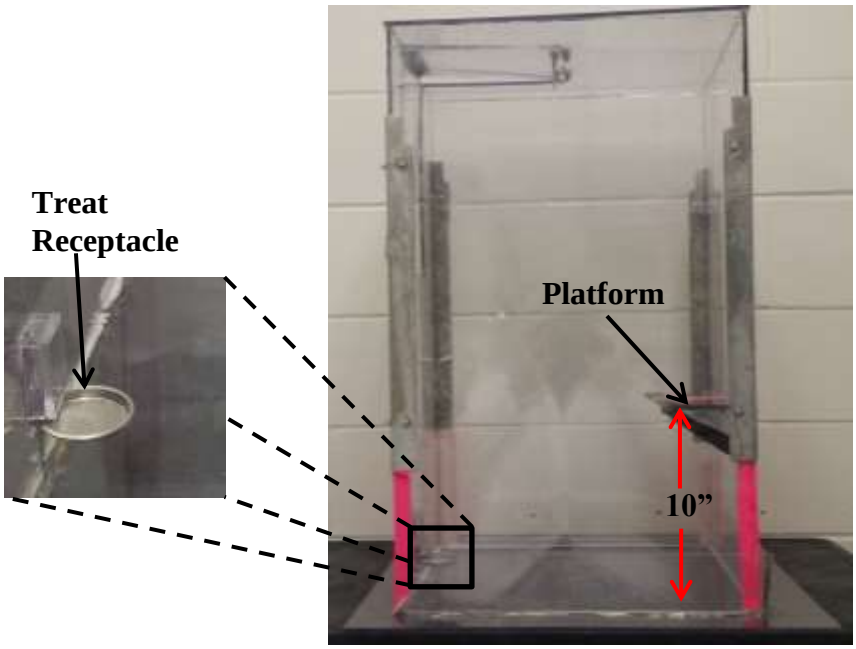

Figure 2.4 Custom Jumping Cage for Operant Conditioning and Voluntary Jumping Exercise. A close-up image of the Treat receptacle can be seen on the left. The platform is set at 10 inches.

2.6. Euthanasia and Tissue Collection

Rats were anesthetized via intraperitoneal injection of ketamine hydrochloride (100 mg/mL, Henry Schein Animal Health, Dublin, OH, USA) and Dexdomitor (dexmeditomidine hydrochloride, 0.5 mg/mL Zoetis, Parsippany, NJ, USA) in a 3 to 2 ratio by volume. They were then euthanized via exsanguination (cardiac puncture) and decapitation at each study endpoint as indicated in Figure 2.1 and 2.2 for Experiments 1 and 2, respectively. The subjects euthanized at the end of an HU period (d28 or d112 for Experiment 1, d56 for Experiment 2) were anesthetized prior to removal from the HU cage to prevent reloading of the hindlimbs. The right and left soleus muscles were excised and wet masses were recorded. The right tibia and femur were cut in half, with both halves of the tibia and the distal half of the femur stored in 10% phosphate-buffered formalin (PBF)

for 24 hours and then switched to 95% ethanol for storage at 4 ºC for subsequent histological analysis. The left tibia, left femur, and proximal half of the right femur were wrapped in gauze and stored in a phosphate-buffered saline (PBS) solution at -20 ºC for subsequent mechanical testing.

2.7. Computed Tomography

2.7.1. Longitudinal *In Vivo* Peripheral Quantitative Computed Tomography

In vivo scans of the left tibia were taken at baseline (d0) and every 28 days (d28, d56, d84, d112) in both Experiments 1 and 2 (Figures 2.1 and 2.2) using a pQCT device (XCT Research M Stratec; Norland Corp., Fort Atkinson, WI) with a voxel size of 100 µm, a scanning beam thickness of 0.5 mm, and a scanning speed of 2.5 mm/s. Animals were anesthetized with isoflurane and placed on a scanning platform with only their left leg extending into the gantry. Transverse cross-sectional scans consisted of four slices (0.5 mm apart) of the proximal tibia metaphysis distal to the growth plate and two slices (1 mm apart) of the tibia diaphysis (TD) at 50% of the tibia length. An image of the scout scan and slice placement for *in vivo* pQCT of the proximal tibia metaphysis and tibia diaphysis can be found in Figure 2.5(A). Scans were analyzed using Stratec software (version 6.00, Norland Corp., Fort Atkinson, WI).

At the proximal tibia metaphysis, the following parameters were used: contour mode 3, peel mode 4, an outer threshold of 450 mg/cm^3 to define the periosteal surface and an inner threshold of 800 mg/cm^3 to define the cancellous compartment. Cortmode 4 with an outer threshold of 450 mg/cm^3 and an inner threshold of -100 mg/cm^3 was used for analysis of the cortical compartment of the proximal tibia metaphysis. Scans at the tibia

diaphysis were analyzed using contour mode 1, peel mode 2, and cortmode 2 with outer and inner thresholds of 650 mg/cm^3.

Outcome variables obtained from the pQCT scans included both densitometric and geometric properties. The densitometric properties are bone mineral content (BMC) and volumetric bone mineral density (vBMD). Figure 2.5(B) and 2.5(C) contain a schematic defining the cortical and cancellous regions of the cross-section. The following more specific outcome variables are reported for densitometric properties: cortical BMC, cancellous BMC, total BMC, cortical vBMD, cancellous vBMD, and total vBMD. For geometric measures, cross-sectional areas are determined in a similar manner as cortical area, cancellous area, and total area. Note that "total" in this context refers to the combined cortical and cancellous regions. Consequently, total BMC, total vBMD, and total area are sometimes referred to as "integral" BMC, vBMD, and area because they represent contributions from both bone compartments. The average cortical thickness was also calculated, assuming a circular cross-section. The average cortical thickness is calculated by:

$$Ct.Th. = \sqrt{\frac{A_{Tot}}{\pi}} - \sqrt{\frac{A_{Canc}}{\pi}} \qquad \text{Equation 2.1}$$

where Ct.Th. is the cortical thickness, A_{Tot} is the total area, and A_{Canc} is the cancellous area. Because the tibia diaphysis contains only cortical bone and a hollow medullary canal (Figure 2.5(D)), the only area parameter reported is the cortical area. The polar area moment of inertia (MOI) and cortical thickness (Equation 2.1) are also reported.

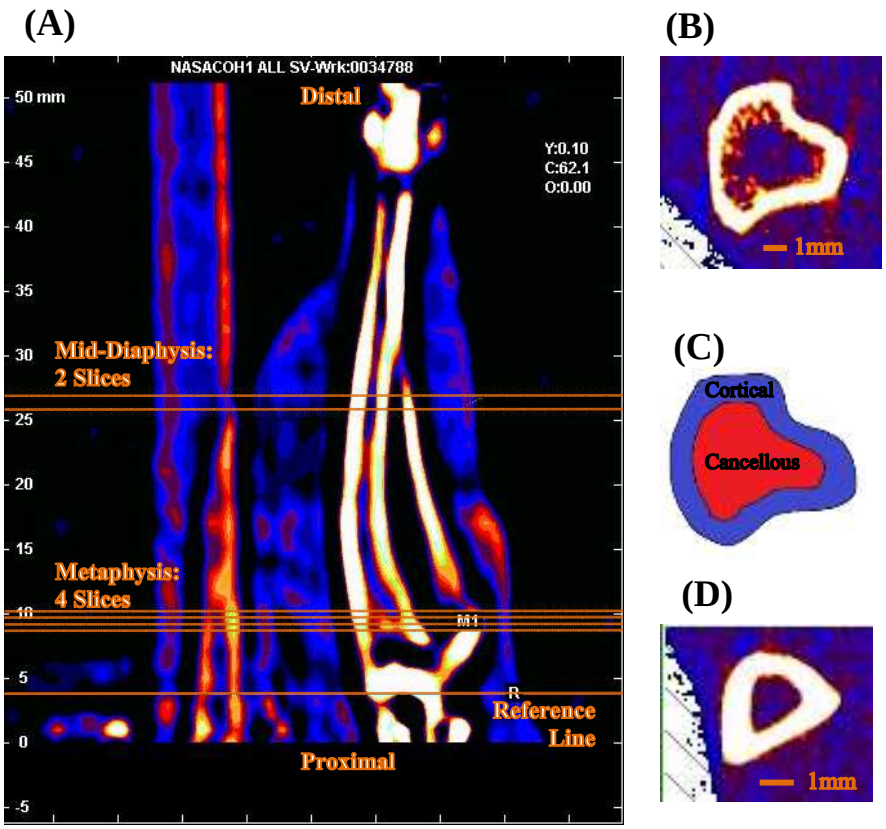

Figure 2.5 Left Tibia *In Vivo* pQCT Scout Scan and Slice Placement.
(A)Scout scan and slice placement. The reference line is placed at the arch of the medial tibia plateau, four proximal tibia metaphysis slices are placed distal to the growth plate, and two tibia diaphysis slices are placed at 50% of the bone length. (B) Sample image of a pQCT slice at the proximal tibia metaphysis. (C) Diagram of bone compartments: cortical (blue), cancellous (red), total (blue + red). (D) Sample image of a pQCT slice at the tibia diaphysis.

2.7.2. *Ex Vivo* Peripheral Quantitative Computed Tomography

Ex Vivo pQCT scans were made of applicable bones at each endpoint in both Experiments 1 and 2 (Figures 2.1 and 2.2). The left proximal tibia metaphysis and tibia diaphysis, left distal femur metaphysis (DFM) and femur diaphysis (FD), and right femoral neck (FN) were scanned *ex vivo* with pQCT using a voxel size of 70 µm, scanning beam thickness of 0.5 mm, and a scanning speed of 2.5 mm/s. Transverse cross-sectional scans of the tibia and femur consisted of four metaphyseal slices, 0.5mm apart and one tibia

diaphysis slice at 50% of bone length. *Ex vivo* tibia and femur scans were analyzed using Stratec software (version 6.00, Norland Corp., Fort Atkinson, WI) at the proximal tibia metaphysis (contour mode 3, peel mode 4, outer threshold 450 mg/cm^3, inner threshold 800 mg/cm^3 and cortmode 4, outer threshold 450 mg/cm^3, inner threshold -100 mg/cm^3) and at the tibia diaphysis (contour mode 1, peel mode 2, cortmode 2, outer and inner thresholds 650 mg/cm^3). Right proximal femora were placed in a custom mold to ensure alignment of the femoral neck with pQCT scanlines, and three slices 0.5mm apart were obtained. Femoral neck scans were analyzed using Stratec software (version 6.00, contour mode 3, peel mode 2, outer threshold 700 mg/cm^3, inner threshold 1200 mg/cm^3). Figure 2.6 displays the scout pQCT scan and the slice placement for the left tibia, Figure 2.7 shows the same for the left femur, and Figure 2.8 the same for the right femoral neck. Outcome variables obtained are total BMC, vBMD (total, cancellous, and cortical), bone area (total and cortical), cortical thickness, and polar area MOI.

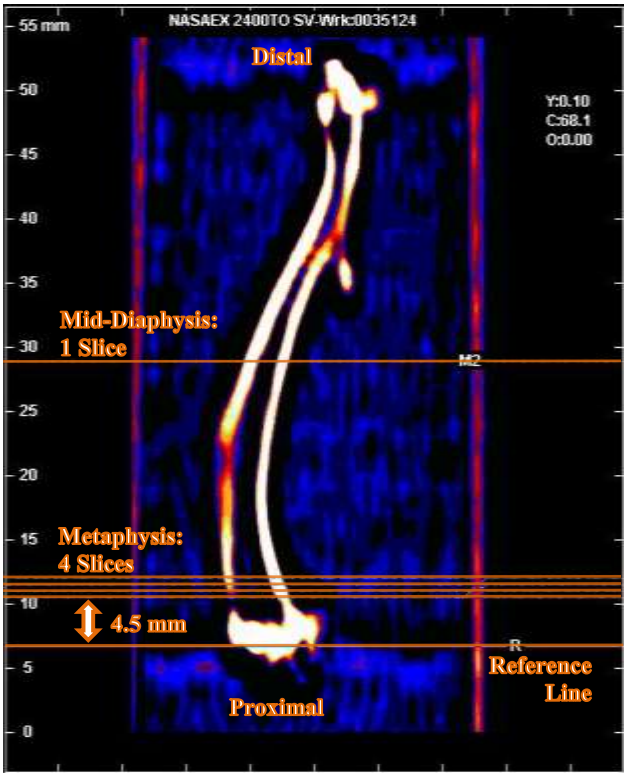

Figure 2.6 Left Tibia *Ex Vivo* pQCT Scout Scan and Slice Placement.
The reference line is placed at the arch of the lateral tibia plateau, four proximal tibia metaphysis slices are placed 4.5 mm distal to the reference line, and one tibia diaphysis slice is placed at 50% of the bone length.

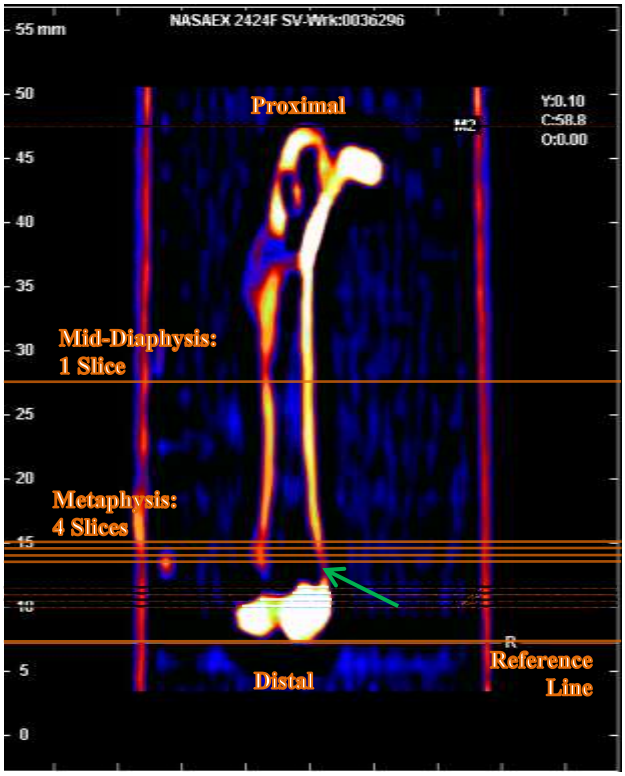

Figure 2.7 Left Femur *Ex Vivo* pQCT Scout Scan and Slice Placement.
The reference line is placed at the proximal tip of the bone, four distal femur metaphysis slices are placed 0.15 mm distal to the thinnest part of the cortical shell (green arrow) near the proximal growth plate, and one femur diaphysis slice is placed at 50% of the bone length.

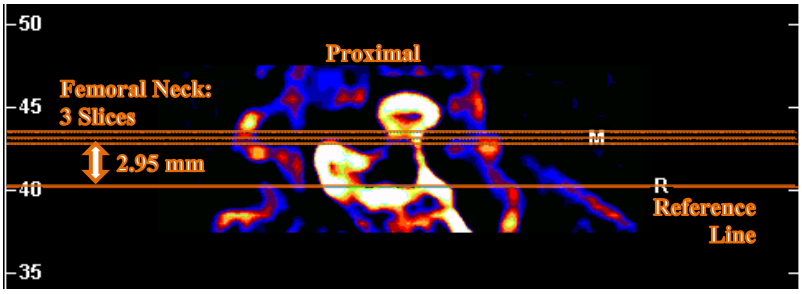

Figure 2.8 Femoral Neck *Ex Vivo* pQCT Scout Scan and Slice Placement.
The reference line is placed on the concave arch of the trochanteric crest, and three femoral neck slices are placed 2.95 mm proximal to the reference line.

2.7.3. *Ex Vivo* Micro-Computed Tomography

Ex vivo scans of the left proximal tibia metaphysis were performed at 12 μm resolution on a μCT device (SkyScan 1172, Bruker, Billerica, MA) by Dr. Matt Allen's laboratory at Indiana University School of Medicine. A 1 mm region of interest located approximately 1 mm distal to the tibial growth plate was selected to assess trabecular microarchitecture while excluding metaphyseal cortical bone. Metaphyseal cortical bone was also assessed separately in Experiment 1, but not in Experiment 2. Key outcome variables are bone volume/tissue volume (BV/TV, %), trabecular thickness (Tb.Th.), trabecular number (Tb.N.), and trabecular separation (Tb.Sp.) for the cancellous compartment, with additional variables for the cortical compartment including cortical thickness, porosity, bone area (total and marrow), and perimeter (endocortical and periosteal).

2.8. Mechanical Testing

2.8.1. Three-point Bending

Cortical bone mechanical properties were measured with 3-point bending tests of the tibia diaphysis and femur diaphysis for both Experiments 1 and 2. Samples were thawed overnight and then the total length, anteroposterior diameter, and mediolateral diameter of each sample was measured at the mid-diaphysis. Samples were then tested using a standard testing machine (Instron 3345, Instron, Norwood, MA) and a 1,000 N load cell. Samples were placed on round steel pin supports with a pin diameter of 3 mm and with spans of 18mm and 15mm for tibiae and femora, respectively. Femora were placed with their anterior side contacting the lower supports, and tibiae with their lateral side contacting the lower supports. The sample was placed so that the upper loading point

was directly over the mid-diaphysis, so that the cross-section tested corresponds to the *ex vivo* pQCT scan data. Starting with an approximately 1 N pre-load to stabilize the specimen, quasi-static loading was applied at the mid-diaphysis at a rate of 2.54mm/min until fracture. Load vs. displacement data were obtained at a sampling rate of 50 Hz and analyzed by Bluehill software (version 2.35.917, Instron, Norwood, MA) and a custom MATLAB tool (The Mathworks, Inc., Natick, MA). Key extrinsic outcome variables are ultimate force, stiffness, yield force, and post-yield displacement, and energy to ultimate force, while key intrinsic outcome variables are ultimate stress and elastic modulus.

2.8.2. Reduced Platen Compression

Cancellous bone mechanical properties were measured by reduced platen compression testing of specimens taken from the proximal tibia metaphysis. 2.0 mm thick samples were cut from the proximal tibia metaphysis starting 0.5 mm distal to the point of the lateral condyle using a Well precision diamond wire saw (Well Diamond Wire Saws, Inc., Norcross, GA). High-resolution photographs were taken of the sample cross-section and edited in Adobe Photoshop (Adobe Systems Incorporated, San Jose, CA) to determine the size of the loading platen, 70% of the diameter of a circle inscribing the endocortical perimeter. Samples were then placed between two platens on a standard testing machine (Instron 3345, Instron, Norwood, MA) using a 100 N load cell. Without pre-loading the specimen, quasi-static loading was applied to the cancellous region of the sample, excluding the cortical shell, at a rate of 0.25mm/min. Figure 2.9 shows a schematic of the RPC specimen location in the proximal tibia metaphysis, platen sizing, and compression testing. Key outcome variables are ultimate stress, elastic modulus, energy to ultimate stress, and strain at ultimate stress.

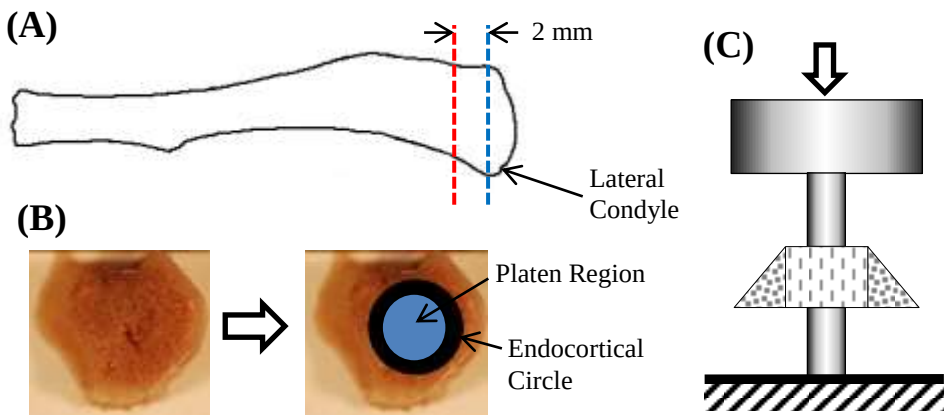

Figure 2.9 Proximal Tibia Metaphysis Reduced Platen Compression Test.
(A) A 2 mm specimen from the proximal tibia metaphysis is obtained. The first cut (blue-dashed line) is placed 0.5 mm distal to the lateral condyle and the second cut (red-dashed line) is placed 2.3 mm distal to the first cut. The extra 0.3 mm accounts for the width of the diamond wire. (B) The proximal tibia metaphysis specimen is photographed and image processing is conducted to find the diameter of the platen region, 70% of the endocortical circle diameter. (C) Diagram of RPC testing setup.

2.8.3. Femoral Neck Mechanical Test

Femoral neck mechanical properties were measured via axial loading in a standard testing machine (Instron 3345, Instron, Norwood, MA) using a 1,000N load cell. The right proximal femur was placed upright in a custom aluminum plate fixture with a 10 mm cylindrical platen serving as the upper loading point. Starting with an approximately 1 N pre-load to stabilize the specimen, quasi-static loading was applied to the femoral head, parallel to the femoral shaft axis at a rate of 2.54 mm/min until fracture. Key outcome variables are ultimate force, stiffness, and energy to ultimate force.

2.9. Histomorphometry

For Experiment 1, rats were administered demeclocycline (15 mg/kg body weight) via intraperitoneal injection nine and two days before the midpoint of recovery (day 56) and received calcein (25 mg/kg body weight) via intraperitoneal injection nine and two

days before the end of recovery (day 84). For Experiment 2, all rats were administered calcein (25 mg/kg body weight) via subcutaneous injection nine and two days before euthanasia. After PBF fixing, the right distal femora and right distal tibiae from Experiment 1, and the right proximal and distal tibiae from Experiment 2 were serially dehydrated and embedded in methyl methacrylate (Aldrich M5, 590-9, St. Louis, MO, USA). Both the proximal tibia and distal femur were cut on a motorized microtome (Leica Biosystems, Wetzlar, Germany) in serial front sections of 8 µm and 4 µm thicknesses at 50% of the metaphysis depth. Von Kossa stain and tetrachrome counterstain was applied to the 4 µm and analyzed with an OsteoMeasure Analysis System v 3.3 (OsteoMetrics, Inc., Atlanta, GA, USA). Key outcome variables are percent bone volume / tissue volume (% BV/TV), trabecular thickness, trabecular separation, trabecular number, relative osteoid surface (OS/BS), and relative osteoclast surface (Oc.S/BS).

For Experiment 1, serial cross sections of the distal tibia midshaft were taken starting 2.5 mm proximal to the tibiofibular junction using an IsoMet Low Speed Saw (Buehler, Lake Bluff, IL). These cross sections and the 8µm sections of the proximal tibia (Experiment 1) and distal femur (Experiment 2) were used for assessing dynamic histomorphometry with the calcein and demeclocycline fluorochrome labels. Figure 2.10 shows a representative image with fluorochrome labels identified by time point. Key outcome variables are mineral apposition rate (MAR, µm/day), mineralizing surface / total bone surface perimeter (MS/BS %), and bone formation rate (BFR, $\mu m^3/\mu m^2$/day). BFR is defined by:

$$BFR = MAR * \frac{MS}{BS}$$ Equation 2.2

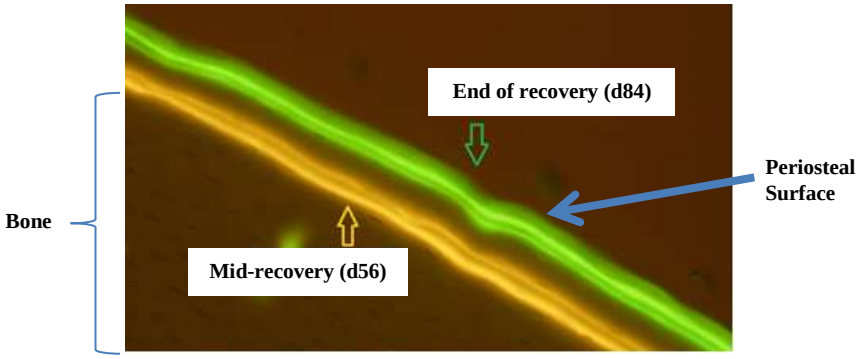

Figure 2.10 Representative Image of Dynamic Histomorphometry Fluorochrome Labels for Exp. 1. Dynamic Cortical Histomorphometry performed at the Tibia Mid-Diaphysis. Demeclocycline (orange double-label) was administered 9 and 2 days before d56, and Calcein (green double-label) was administered 9 and 2 days before d84.

2.10. Statistical Analysis

Data were evaluated for statistical relationships using R (The R Foundation). Outlier analysis was performed for all data using an interquartile range (IQR) method. First the first (Q1) and third (Q3) quartiles are found. Q1 is the middle value of the half of the data set with a value lower than the median; it could be thought of as the "median" of the lower half of the data. Q3, similarly, is the "median" of the upper half of the data (all data with value greater than the median). IQR is found by subtracting Q1 from Q3. The Tukey fences are calculated by adding IQR*1.5 to Q3, and subtracting IQR*1.5 from Q1. Any data point falling outside of these fences is considered an outlier and removed from the data set. This method is less sensitive to skew in the data set than similar methods for

detecting outliers using standard deviation, as extreme outliers increase or decrease the standard deviation to a greater extent compared to the IQR. Outlier analysis was performed prior to evaluating assumptions (normality, homoscedasticity, sphericity) and statistical comparisons.

The normality and homoscedasticity of the data for each outcome were evaluated using the Shapiro-Wilk test and the Brown-Forsythe-Levene test, respectively. For normal and homoscedastic data, the differences among groups were analyzed using a one-factor ANOVA and pairwise comparisons were evaluated using the Tukey-Kramer HSD method when a significant effect was determined. If a significant time effect was determined, pairwise comparisons were evaluated using the Tukey-Kramer HSD method. For non-normal but homoscedastic data, a Kruskal-Wallis rank sum test was used followed by Dunn's test for pairwise comparisons. Normal but heteroscedastic data were assessed using a Welch's ANOVA, followed by a Games-Howell post hoc test if significant. Statistical significance was accepted at $p<0.05$.

Longitudinal pQCT comparisons were evaluated for normality and sphericity using the Shapiro-Wilk test and Mauchly's test, respectively. For normal and homoscedastic data, the differences among groups were analyzed using a repeated measure one-factor ANOVA in order to detect differences over time, and pairwise comparisons were evaluated using the Tukey-Kramer HSD method when a significant effect was determined. For non-normal but spheric data, a Friedmann one-way non-parametric ANOVA was used, followed by a Wilcoxon signed-rank test with Bonferroni correction for pairwise comparisons. Normal but non-spheric were assessed using the Greenhouse-Geisser

correction to the repeated measures ANOVA, followed by the Tukey-Kramer HSD method for pairwise comparisons.

3. EXPERIMENT 1 RESULTS

The figures and tables in this chapter present the data collected in Experiment 1. The vertical axis of each figure displays a unique outcome variable, while the horizontal axis displays the animal groups or the time points for those outcome variables with multiple measures throughout the experiment. The baseline time point and start of the first HU period is defined as day 0 (d0). Subsequent time points occur every 28 days, with day 28 (d28) at the end of the first unloading, day 56 (d56) midway through recovery, day 84 (d84) at the start of the second HU period, and with day 112 (d112) marking the end of the second HU period and the experiment. All *ex vivo* data come from a single time point, day 112 for AC, HU, HU+ALN, and HU+ZOL groups. BC *ex vivo* data were collected at day 0. The decrease in group numbers across the study period occurred due to medical issues during HU (Table 3.1). A lack of significance markers on a graph or table indicates that there were no statistically significant differences found. Full numerical results for all outcome variables from Experiment 1 may be found in Appendix A.

Table 3.1 Number of Specimens Available at Each Time Point for Exp. 1.
(A) Maximum number of specimens for data collected *in vivo*, (B) Maximum number of specimens for data collected *ex vivo*.

(A)

Group	d0	d28	d56	d84	d112
BC	14	-	-	-	-
AC	15	15	14	14	14
HU	15	10	10	10	10
HU+ALN	15	14	14	14	13
HU+ZOL	15	13	13	13	13

(B)

Group	d0	d28	d56	d84	d112
BC	14	-	-	-	-
AC	-	-	-	-	14
HU	-	-	-	-	10
HU+ALN	-	-	-	-	13
HU+ZOL	-	-	-	-	13

3.1. Animals

All animals were weighed twice weekly throughout the study period (Table 3.2). Any animal suffering excessive weight loss, defined as 10% loss in one week or less, would have been removed from the study. No animals were removed from the study due to excessive weight loss. 80% of all rats completed both HU periods successfully. However, two animals in the HU group and two animals each in the HU+ALN and HU+ZOL groups were removed from the study due to tail health issues during unloading. The tail harness can constrict circulation to the tail, and this is the chief medical issue that rats are monitored for during HU.

At day 0, the average body mass was 496.9 ± 38.7 g across all groups with no significant differences among groups. The body mass values at the end of the first HU period (d28) were significantly lower for HU (-9.6%, $p = 0.029$), HU+ALN (-11.3%, p =

0.003), and HU+ZOL (-10.6%, p = 0.005) animals compared to AC animals. In contrast, there were no significant differences in body mass among groups at d56 (p = 0.222), d84 (p = 0.836), or d112 (p = 0.159).

Table 3.2 Body Mass (g) Results for Exp. 1.
Day 28 marks the end of the first HU period and day 112 marks the end of the second HU period.

Group	d0	d28	d56	d84	d112
BC	494.2 ± 46.0	-	-	-	-
AC	498.9 ± 46.1	518.5 ± 48.7	524.6 ± 50.0	524.1 ± 46.8	534.2 ± 48.5
HU	499.4 ± 35.8	469.0 ± 40.4 †	515.1 ± 55.0	533.8 ± 44.1	523.2 ± 41.9
HU+ALN	496.0 ± 30.2	459.9 ± 40.2 †	504.4 ± 37.1	522.2 ± 42.3	509.9 ± 46.8
HU+ZOL	495.9 ± 38.7	463.6 ± 36.7 †	499.6 ± 27.4	518.2 ± 32.4	505.8 ± 23.4

Data presented as mean ± SD.
† indicates significant difference from AC value at same time point, $p < 0.05$.

The soleus is a postural muscle in the lower leg, and changes to its mass are a good indication of the efficacy of HU in achieving consistent non-weight-bearing. Wet mass of the soleus (Figure 3.1) for the AC group was not significantly different from that in the BC group, but soleus wet masses in HU, HU+ALN, and HU+ZOL groups were significantly lower compared to the BC (-51%, -44%, -44% respectively, $p < 0.001$) and AC (-54%, -47%, -47% respectively, $p < 0.001$) groups, confirming the efficacy of unloading in this experiment.

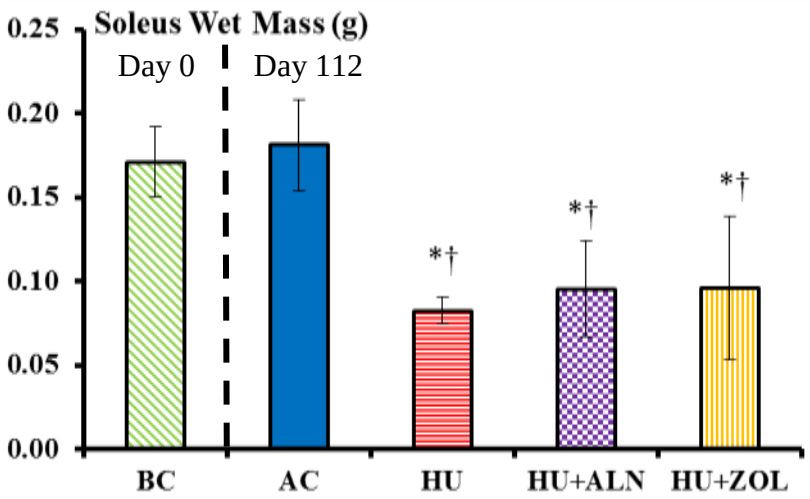

Figure 3.1 *Ex vivo* Soleus Wet Mass for Exp. 1.
Each value represents the averaged mass of the left and right solei together. BC at the start (d0) and other groups at the end (d112) of the experiment.
Data presented as mean ± SD.
* indicates significant difference from BC value, $p < 0.05$.
† indicates significant difference from AC value at d112, $p < 0.05$.

3.2. Computed Tomography

3.2.1. Longitudinal *In Vivo* Peripheral Quantitative Computed Tomography

In order to monitor HU-induced bone changes, *in vivo* pQCT was performed on the left proximal tibia metaphysis (PTM) and tibia mid-diaphysis (TD). Keeping in mind the double-HU design of Experiment 1 (Figure 2.1), "HU-induced changes" can be defined relative to baseline (d0 to d28 and d0 to d112), relative to the start of HU (d0 to d28 and d84 to d112), or relative to the AC group at the end of either HU (d28 and d112). All three types of comparisons have been made, but we have chosen the change from pre- to post-HU (d0 to d28 and d84 to d112) within group as the primary definition of "HU-induced changes", with the other two comparisons serving as secondary reference points.

For determining the effectiveness of the two bisphosphonates, both pre- to post-HU comparisons and between-group comparisons at the end of each HU were considered. Three categories of effectiveness have been defined. “Mitigation” occurs when a bisphosphonate group is significantly higher than HU, but still significantly lower than AC. “Protection” occurs when a bisphosphonate group is significantly higher than HU, but not significantly different from AC (i.e., the same). “Overprotection” occurs when a bisphosphonate group is significantly higher than both the HU and AC groups.

3.2.1.1. Proximal Tibia Metaphysis Densitometry and Geometry

Both HU and bisphosphonate treatment had significant effects on bone density at the proximal tibia metaphysis during the experiment (Figure 3.2). All four groups started with very similar densitometric values. The first HU period resulted in significantly lower values for the HU group in total BMC (-7.0%, $p < 0.001$), total vBMD (-5.0%, $p = 0.007$), and cancellous vBMD (-18%, $p < 0.001$) when comparing pre- (d0) to post-HU (d28). The HU group also exhibited significant pre- (d84) to post-HU (d112) changes in cancellous vBMD (-10%, $p < 0.0001$) for the second HU period. ALN treatment mitigated changes in total vBMD at the end of the first HU period (d28) and was overprotective for cancellous vBMD from midway through recovery (d56) to the end of the second HU (d112). HU+ALN was not significantly different from either the AC or HU groups for total vBMD on d56 or d112, cancellous vBMD on d28, and at all time points for total BMC and cortical BMC. ZOL treatment resulted in potent overprotection from HU-induced bone changes for total BMC, total vBMD, cancellous vBMD, and cortical vBMD at all time points except for cancellous vBMD at d28 and cortical vBMD at d56, where HU+ZOL was merely protective from HU-induced densitometric changes.

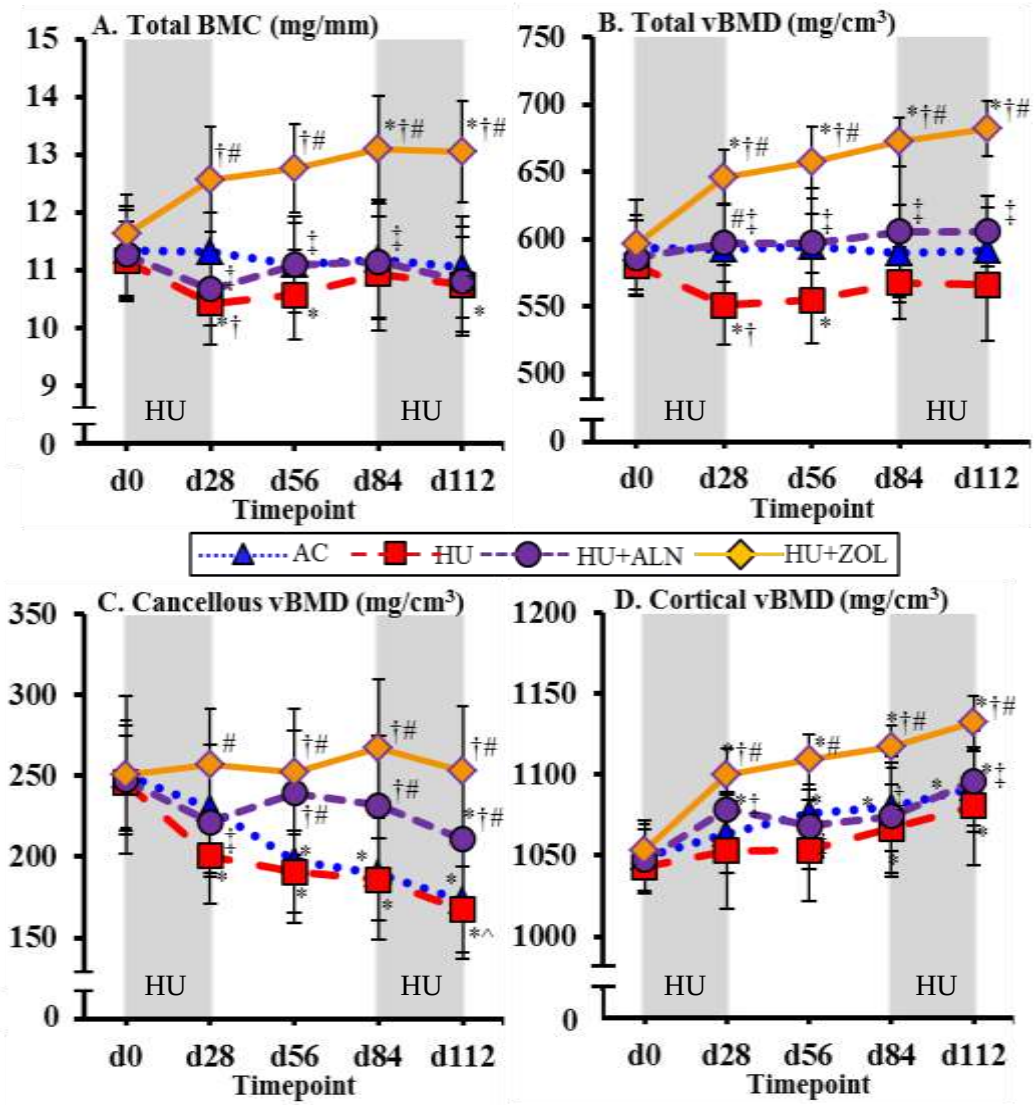

Figure 3.2 *In Vivo* pQCT Densitometric Outcomes at the Proximal Tibia Metaphysis for Exp. 1.
(A) Total BMC, (B) Total vBMD, (C) Cancellous vBMD, (D) Cortical vBMD.
Data presented as mean ± SD.
* indicates significant difference from d0 value, $p < 0.05$.
† indicates significant difference from AC value at same time point, $p < 0.05$.
# indicates significant difference from HU value at same time point, $p < 0.05$.
‡ indicates significant difference from HU+ZOL value at same time point, $p < 0.05$.
^ indicates significant difference from d84 value at d112, $p < 0.05$.

As for geometric outcomes, total bone area was largely unaffected by HU and bisphosphonate treatment throughout the study period (Figure 3.3), with no significant differences in the HU group pre- to post-HU, and no significant differences between the HU+ALN or HU+ZOL groups and either the AC or HU groups. HU caused changes in the cortical thickness pre- (d0) to post-HU (d28) for the HU group (-3.2%, $p = 0.024$). There was no effect of the second HU on cortical thickness. The HU+ALN group cortical thickness was not significantly different from either the AC or HU groups throughout the study, and ZOL treatment overprotected the HU+ZOL group from HU throughout the study.

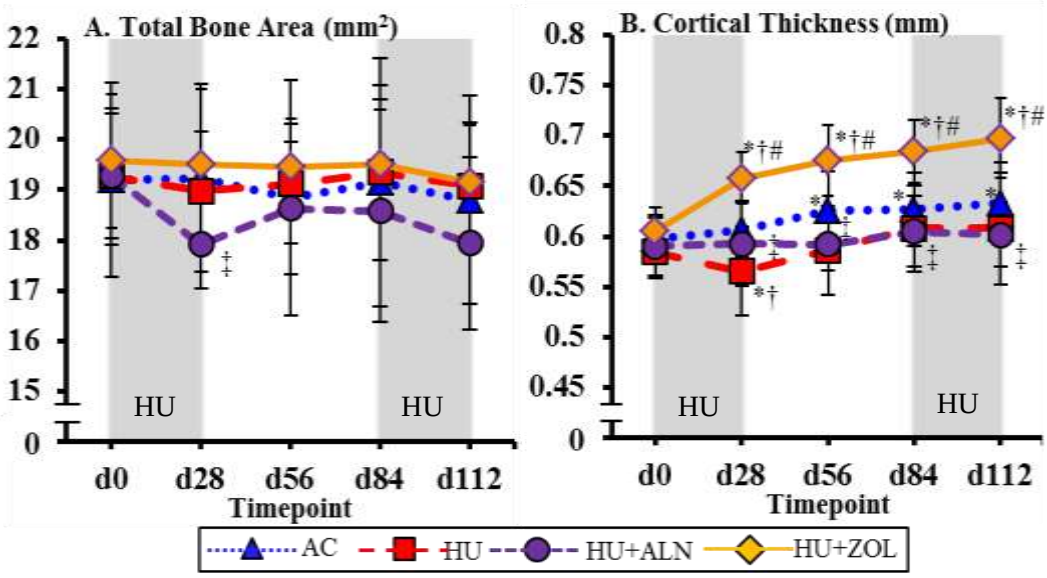

Figure 3.3 *In Vivo* pQCT Geometric Outcomes at the Proximal Tibia Metaphysis for Exp. 1.
(A) Total Bone Area, (B) Cortical Thickness.
Data presented as mean ± SD.
* indicates significant difference from d0 value, $p < 0.05$.
† indicates significant difference from AC value at same time point, $p < 0.05$.
# indicates significant difference from HU value at same time point, $p < 0.05$.
‡ indicates significant difference from HU+ZOL value at same time point, $p < 0.05$.

3.2.1.2. Tibia Mid-Diaphysis Densitometry and Geometry

Tibia diaphysis density and geometry were largely unaffected by both HU and bisphosphonate treatment. Cortical BMC and cortical vBMD gradually increased in all groups over the experimental period (Figure 3.4); these increases were not affected by either HU period or by bisphosphonate treatment. The only exception is a significant difference for cortical vBMD between AC and HU+ALN (-1.0%, $p = 0.024$) on d56. As shown in Figure 3.5, cortical area and cortical thickness also gradually increased in all groups over the study period. HU+ZOL had a significant increase over the second HU period (d84 to d112, +1.8%, $p < 0.001$). Polar area MOI, however, remained constant over the study period for all groups.

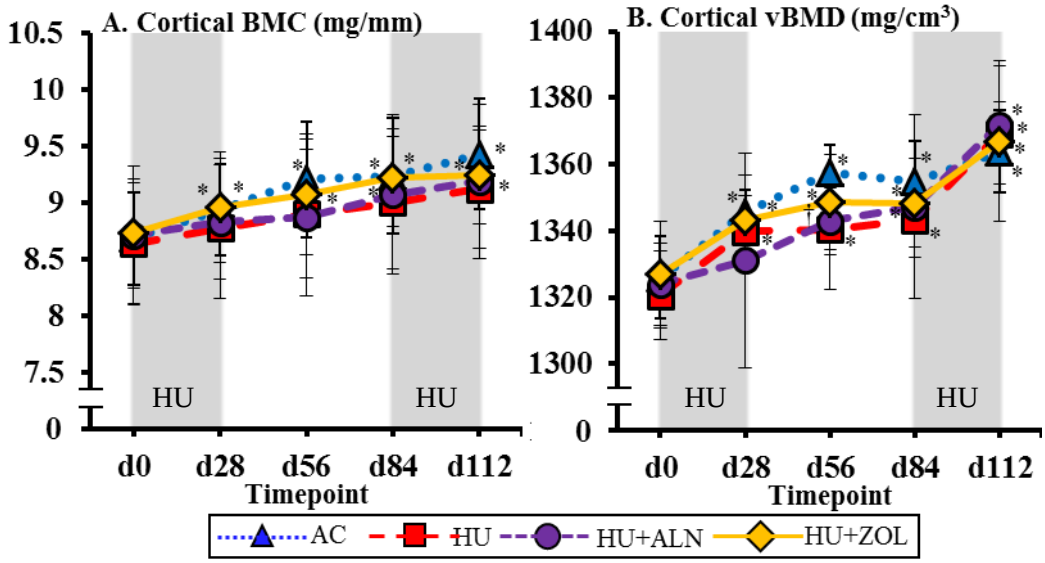

Figure 3.4 *In Vivo* pQCT Densitometric Outcomes at the Tibia Mid-Diaphysis for Exp. 1.
(A) Cortical BMC, (B) Cortical vBMD.
Data presented as mean ± SD.
* indicates significant difference from d0 value, $p < 0.05$.
† indicates significant difference from AC value at same time point, $p < 0.05$.

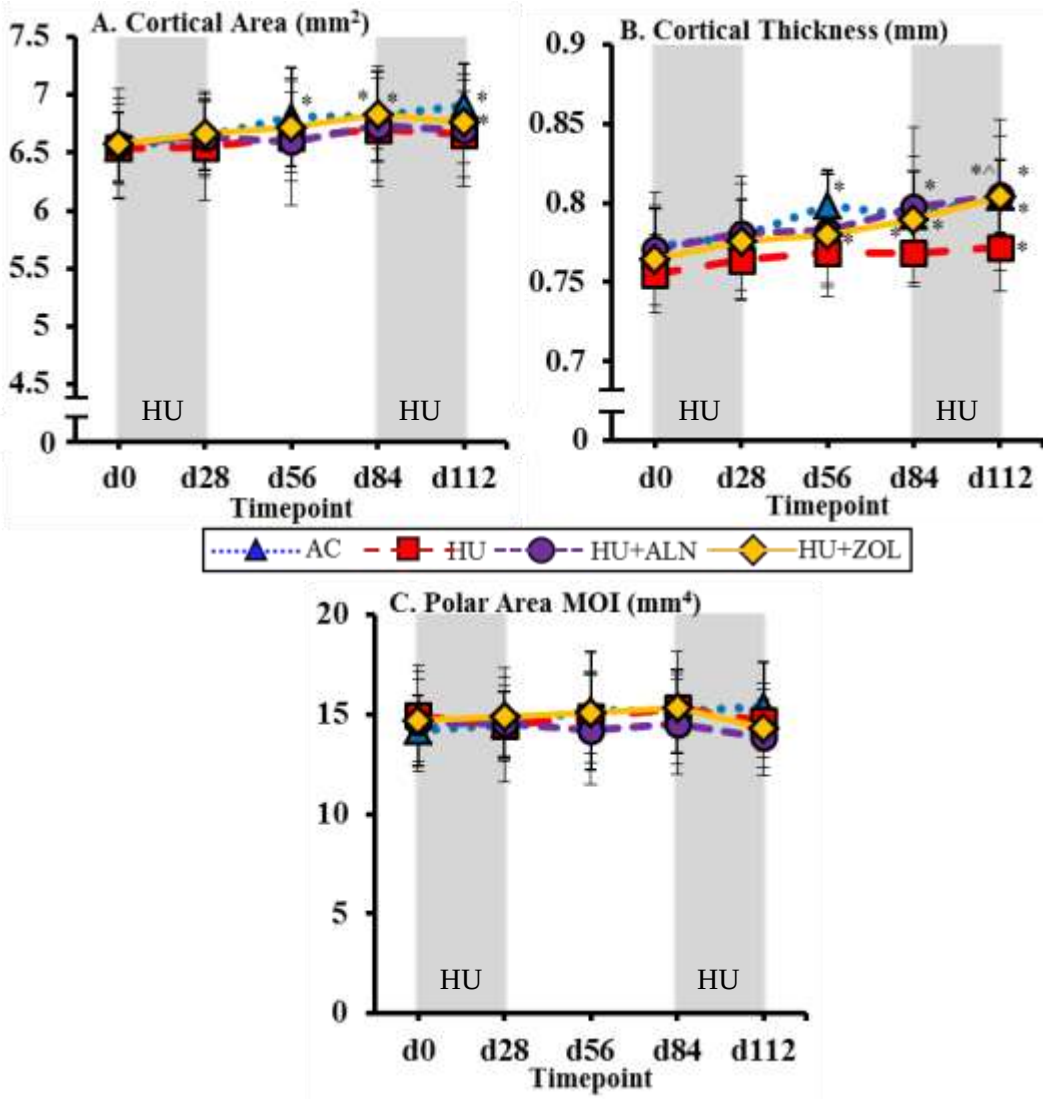

Figure 3.5 *In Vivo* pQCT Geometric Outcomes at the Tibia Mid-Diaphysis for Exp. 1.
(A) Cortical Area, (B) Cortical Thickness, (C) Polar Area MOI.
Data presented as mean ± SD.
* indicates significant difference from d0 value, $p < 0.05$.
† indicates significant difference from AC value at same time point, $p < 0.05$.
^ indicates significant difference from pre- to post-HU value, $p < 0.05$.

3.2.2. *Ex Vivo* Peripheral Quantitative Computed Tomography

In addition to longitudinal *in vivo* surveillance of the left tibia, the left proximal tibia metaphysis and tibia diaphysis, the left distal femur metaphysis (DFM) and femur mid-diaphysis (FD), and the right femoral neck (FN) all underwent *ex vivo* pQCT after euthanasia and tissue collection at d112. The resolution of *ex vivo* pQCT (70 μm) is higher than that for *in vivo* pQCT (100 μm). Therefore, the proximal tibia metaphysis and tibia diaphysis are scanned both *in vivo* and *ex vivo* in order to obtain data consistent with the previous longitudinal scans, and to also obtain the higher resolution *ex vivo* results.

3.2.2.1. Proximal Tibia Metaphysis Densitometry and Geometry

HU-induced changes occurred only in total vBMD, where the HU group (-6.0%, p = 0.005) was significantly lower compared to the AC group (Figure 3.6). ALN treatment resulted in significantly higher cancellous vBMD when comparing HU+ALN (+31%, p = 0.004) rats to HU rats, and ZOL treatment overprotected total vBMD from HU-induced changes and resulted in significantly higher values than observed in all other groups for total BMC, cancellous vBMD, and cortical vBMD.

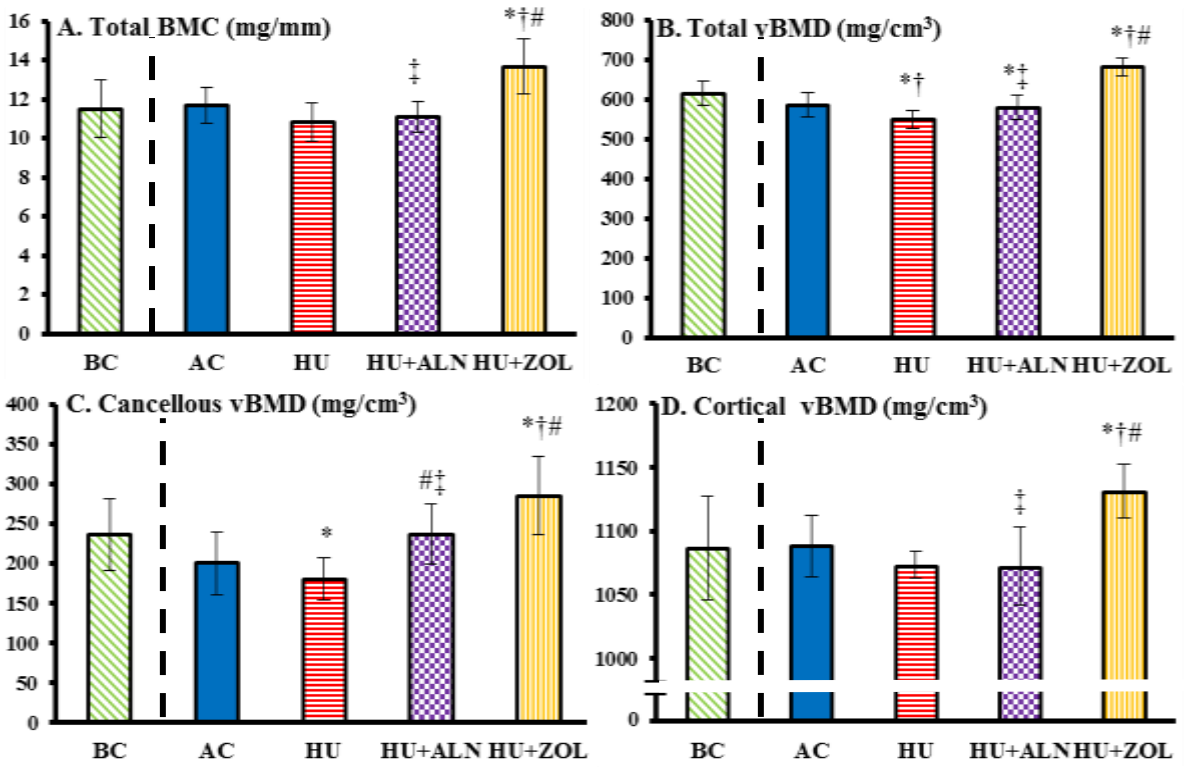

Figure 3.6 *Ex Vivo* pQCT Densitometric Outcomes at the Proximal Tibia Metaphysis for Exp. 1.
(A) Total BMC, (B) Total vBMD, (C) Cancellous vBMD, (D) Cortical vBMD. BC at the start (day 0) and other groups at the end (day 112) of the experiment.
Data presented as mean ± SD.
* indicates significant difference from BC value at d0, $p < 0.05$.
† indicates significant difference from AC value at d112, $p < 0.05$.
# indicates significant difference from HU value at d112, $p < 0.05$.
‡ indicates significant difference from HU+ZOL value at d112, $p < 0.05$.

For geometry measures (Figure 3.7), no significant differences were found between any groups in total bone area. For cortical thickness, however, distinct HU effects were evident, as HU group values were significantly lower (-5.7%, $p = 0.025$) compared to those for the AC group. The negative effects on cortical thickness were not prevented by ALN treatment (-8.4%, $p = 0.004$, compared to the AC group) but ZOL treatment was overprotective compared to AC (+9.9%, $p = 0.017$) and HU (+17%, $p < 0.001$) animals.

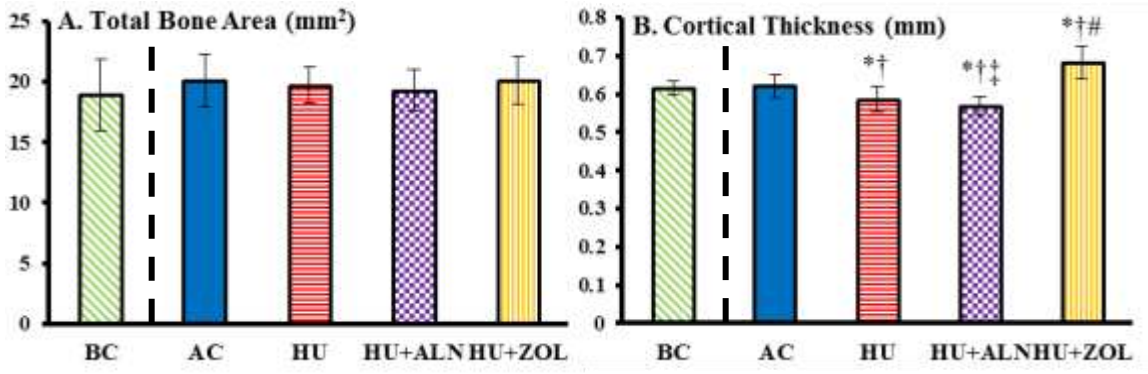

Figure 3.7 *Ex Vivo* pQCT Geometric Outcomes at the Proximal Tibia Metaphysis for Exp. 1.
(A) Total Bone Area, (B) Cortical Thickness. BC at the start (day 0) and other groups at the end (day 112) of the experiment.
Data presented as mean ± SD.
* indicates significant difference from BC value at d0, $p < 0.05$.
† indicates significant difference from AC value at d112, $p < 0.05$.
# indicates significant difference from HU value at d112, $p < 0.05$.
‡ indicates significant difference from HU+ZOL value at d112, $p < 0.05$.

3.2.2.2. Tibia Mid-Diaphysis Densitometry and Geometry

As observed with the *in vivo* pQCT studies, the tibia diaphysis underwent significant increases in both densitometric (reported in Figure 3.8) and geometric (reported in Figure 3.9) outcomes over the course of the experiment in all groups when examined by *ex vivo* pQCT. Additionally, there were no significant effects detected as a result of either HU or bisphosphonate treatment. All experimental groups exhibited significant increases in mean values (versus BC) for cortical BMC, cortical vBMD, cortical area, cortical thickness, and polar area MOI. No further significant differences were observed.

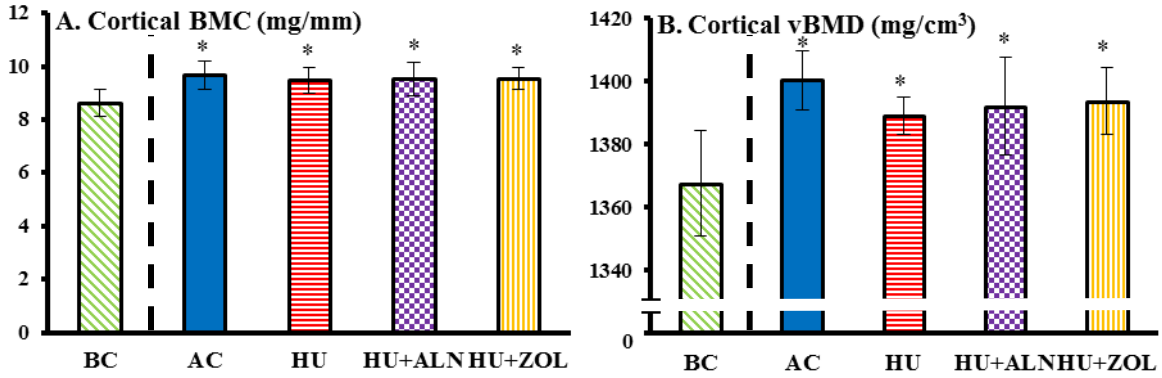

Figure 3.8 *Ex Vivo* pQCT Densitometric Outcomes at the Tibia Mid-Diaphysis for Exp. 1.
(A) Cortical BMC, (B) Cortical vBMD. BC at the start (day 0) and other groups at the end (day 112) of the experiment.
Data presented as mean ± SD.
* indicates significant difference from BC value at d0, $p < 0.05$.

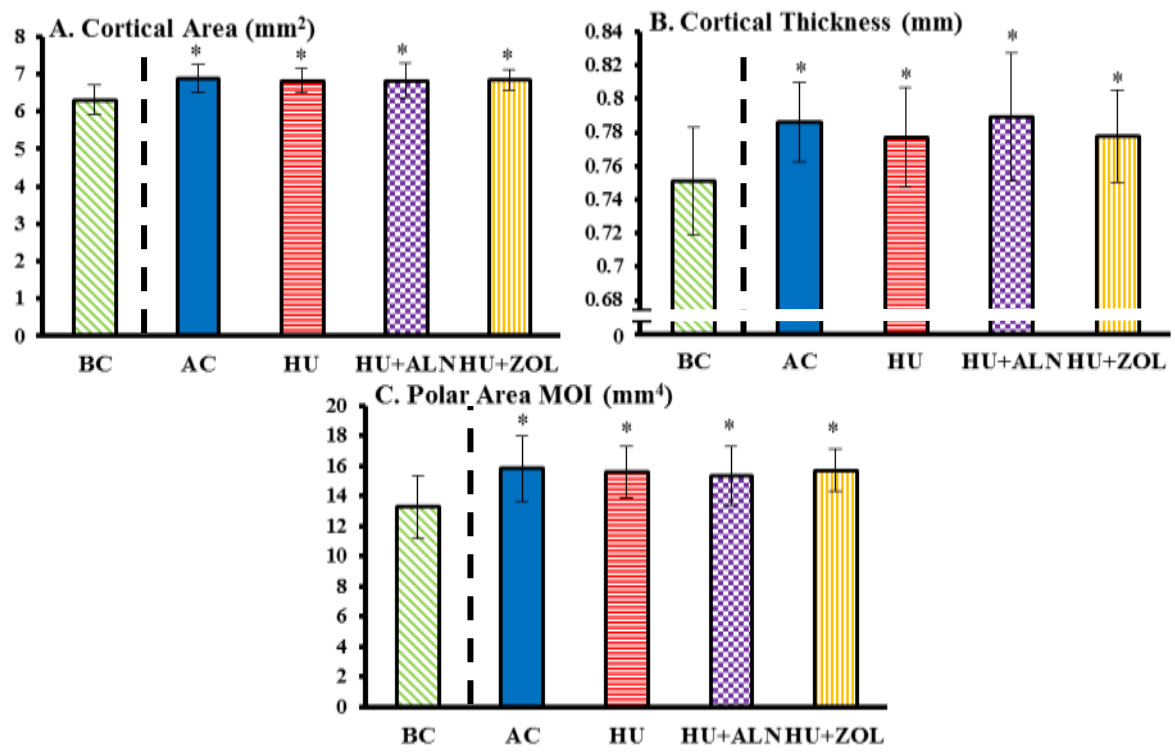

Figure 3.9 *Ex Vivo* pQCT Geometric Outcomes at the Tibia Mid-Diaphysis for Exp. 1.
(A) Cortical Area, (B) Cortical vBMD, (C) Polar Area MOI. BC at the start (day 0) and other groups at the end (day 112) of the experiment.
Data presented as mean ± SD.
* indicates significant difference from BC value at d0, $p < 0.05$.

3.2.2.3. Distal Femur Metaphysis Densitometry and Geometry

No HU-induced changes after the second HU (d112) were observed, as the HU group was not significantly different from the AC group for any of the four densitometric outcome variables (Figure 3.10). Neither was the HU+ALN group significantly different from either the AC or HU groups for the density measures.HU+ZOL animals had significantly higher total BMC and cancellous vBMD compared to both AC (+15%, $p = 0.004$, +31%, $p < 0.001$, respectively) and HU (+28%, $p < 0.001$, +39%, $p < 0.001$, respectively) animals.

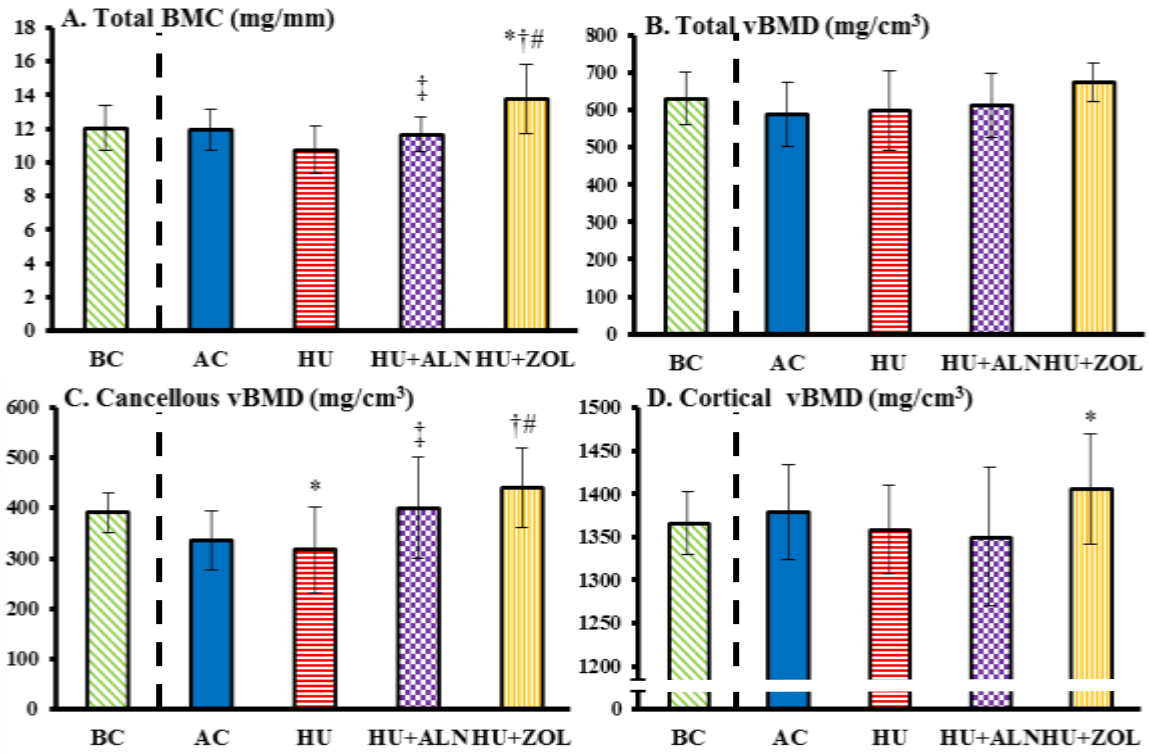

Figure 3.10 *Ex Vivo* pQCT Densitometric Outcomes at the Distal Femur Metaphysis for Exp. 1.
(A) Total BMC, (B) Total vBMD, (C) Cancellous vBMD, (D) Cortical vBMD. BC at the start (day 0) and other groups at the end (day 112) of the experiment. Data presented as mean ± SD.
* indicates significant difference from BC value at d0, $p < 0.05$.
† indicates significant difference from AC value at d112, $p < 0.05$.
# indicates significant difference from HU value at d112, $p < 0.05$.
‡ indicates significant difference from HU+ZOL value at d112, $p < 0.05$.

The geometric results for *ex vivo* pQCT of the distal femur metaphysis, displayed in Figure 3.11, showed no significant differences for any group versus BC or AC values at d112. Neither time nor HU nor bisphosphonate treatment resulted in significant changes in either total bone area or cortical thickness.

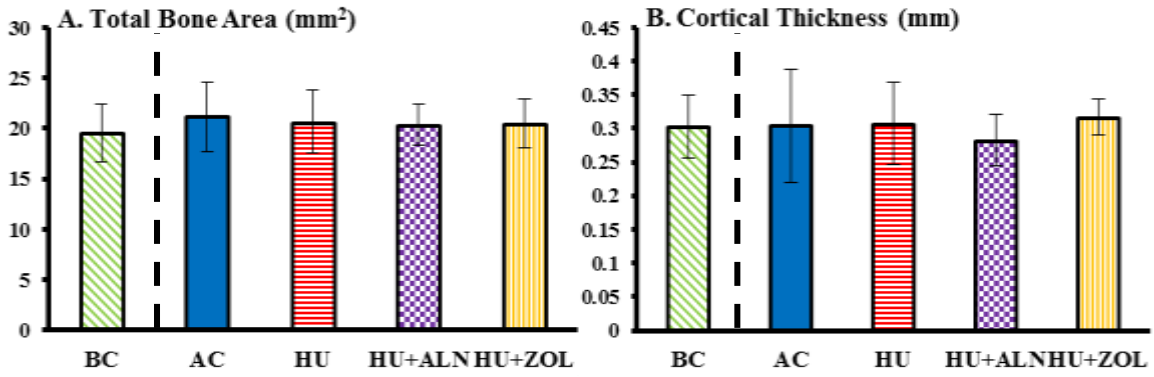

Figure 3.11 *Ex Vivo* pQCT Geometric Outcomes at the Distal Femur Metaphysis for Exp. 1.
(A) Total Bone Area, (B) Cortical Thickness. BC at the start (day 0) and other groups at the end (day 112) of the experiment.
Data presented as mean ± SD.

3.2.2.4. Femur Mid-Diaphysis Densitometry and Geometry

Similar to the tibia diaphysis, all densitometric and geometric outcomes for the femur diaphysis showed a significant increase over the experimental period. It can be seen in Figure 3.12 that all group values were significantly higher compared to those for BC for both cortical BMC and cortical vBMD, and no other significant differences were found. All groups' means were similarly significantly increased when compared to BC for cortical area, cortical thickness, and polar area MOI (Figure 3.13). In addition, the cortical thickness of the HU+ZOL group was significantly higher compared to the AC (+4.7%, p = 0.10), HU (+4.5%, p = 0.025) and HU+ALN (+2.4%, p = 0.026) groups.

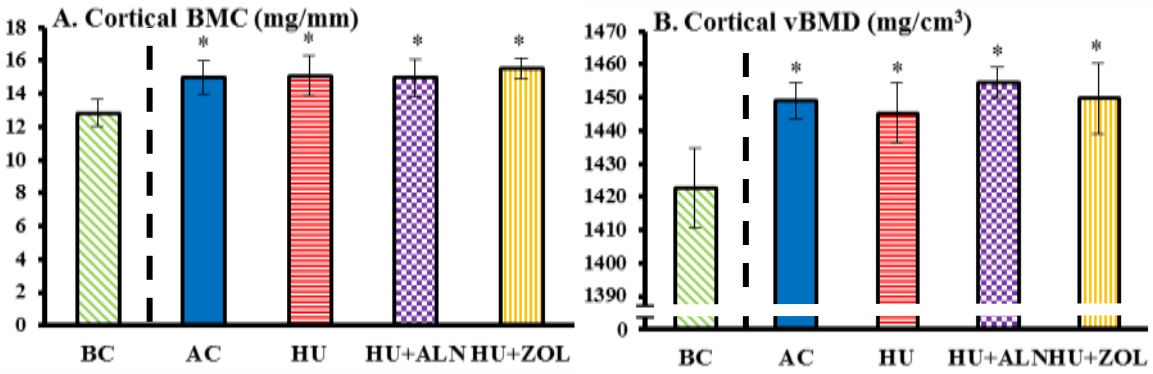

Figure 3.12 *Ex Vivo* pQCT Densitometric Outcomes at the Femur Mid-Diaphysis for Exp. 1.
(A) Cortical BMC, (B) Cortical vBMD. BC at the start (day 0) and other groups at the end (day 112) of the experiment.
Data presented as mean ± SD.
* indicates significant difference from BC value at d0, $p < 0.05$.

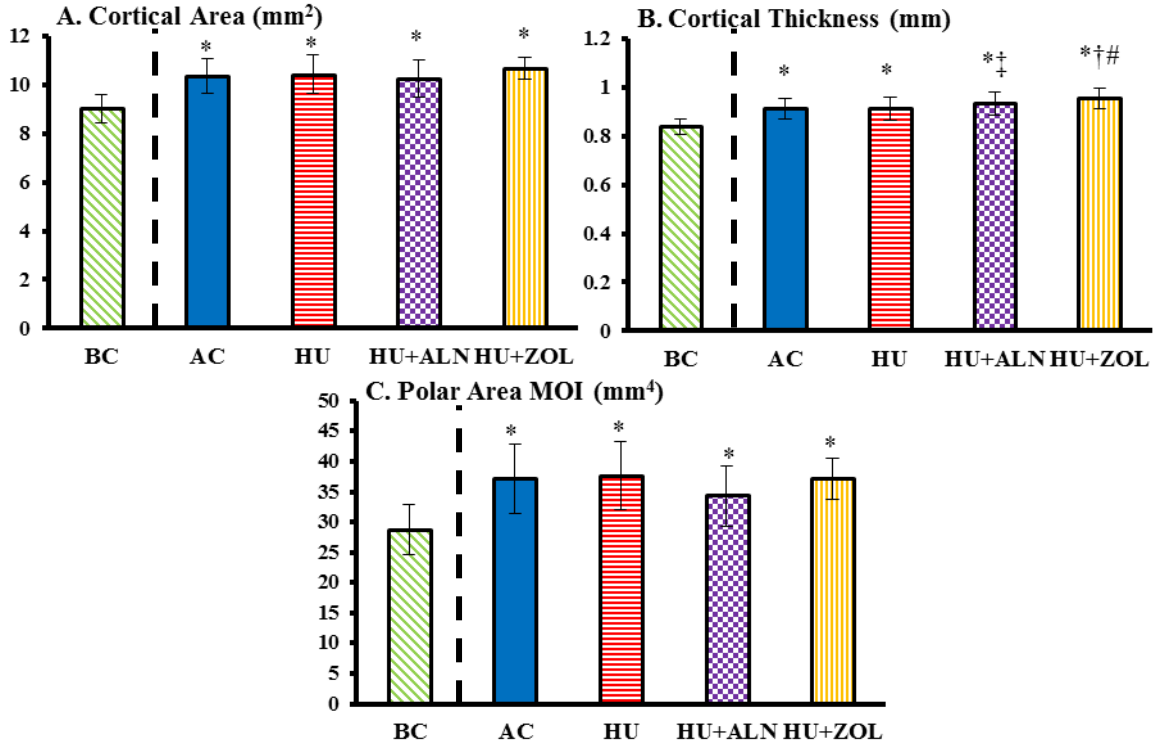

Figure 3.13 *Ex Vivo* pQCT Geometric Outcomes at the Femur Mid-Diaphysis for Exp. 1.
(A) Cortical Area, (B) Cortical Thickness, (C) Polar Area MOI. BC at the start (day 0) and other groups at the end (day 112) of the experiment.
Data presented as mean ± SD.
* indicates significant difference from BC value at d0, $p < 0.05$.
† indicates significant difference from AC value at d112, $p < 0.05$.
# indicates significant difference from HU value at d112, $p < 0.05$.
‡ indicates significant difference from HU+ZOL value at d112, $p < 0.05$.

3.2.2.5. Femoral Neck Densitometry and Geometry

No significant difference between the HU and AC groups were found in the femoral neck *ex vivo* pQCT density results (Figure 3.14), though the average total vBMD and cancellous vBMD for HU rats did trend lower compared to AC rats. ALN and ZOL treatment were protective for cancellous vBMD. ALN treatment resulted in significantly higher cancellous vBMD (+16%, $p = 0.021$) compared to the HU group. ZOL treatment resulted in significantly higher total BMC (+18%, $p < 0.001$) and cancellous vBMD (+23%, $p < 0.001$) when comparing HU+ZOL and HU values.

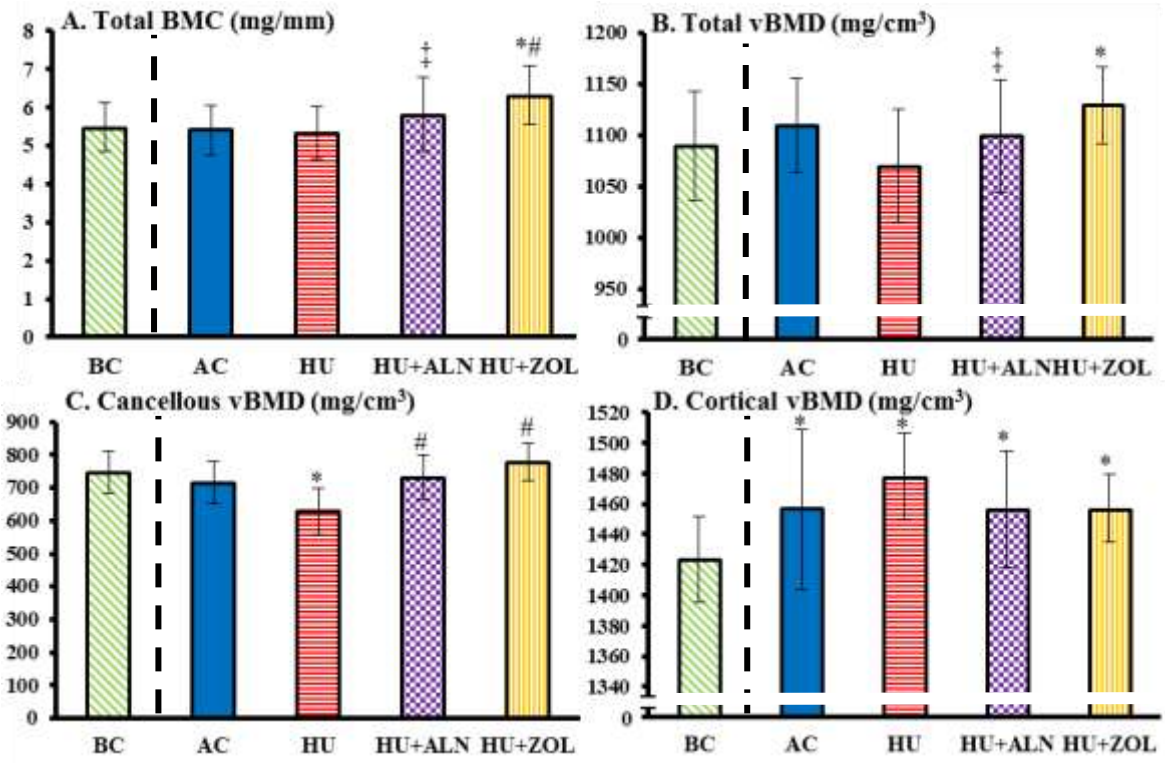

Figure 3.14 *Ex Vivo* pQCT Densitometric Outcomes at the Femoral Neck for Exp. 1.
(A) Total BMC, (B) Total vBMD, (C) Cancellous vBMD, (D) Cortical vBMD. BC at the start (day 0) and other groups at the end (day 112) of the experiment. Data presented as mean ± SD.
* indicates significant difference from BC value at d0, $p < 0.05$.
# indicates significant difference from HU value at d112, $p < 0.05$.
‡ indicates significant difference from HU+ZOL value at d112, $p < 0.05$.

As for geometric outcomes, the HU+ZOL group had significantly higher total bone area (+14%, p = 0.034) and polar area MOI (+23%, p = 0.009) compared to the HU group (Figure 3.15). No other significant differences were detected.

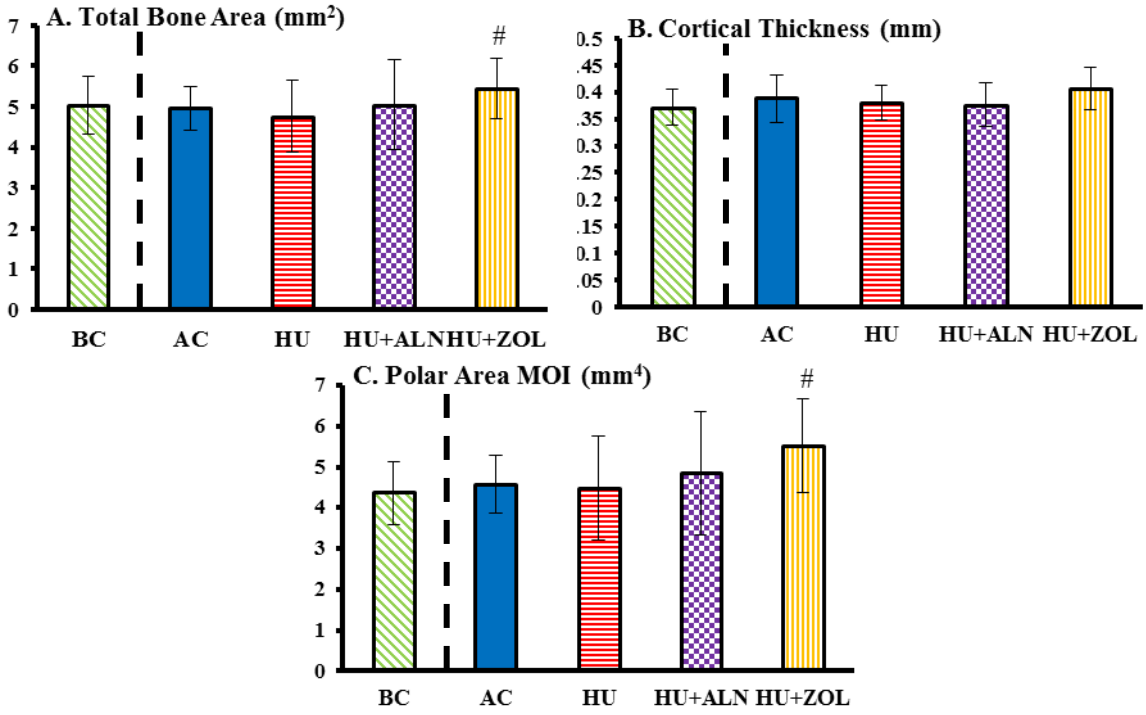

Figure 3.15 *Ex Vivo* pQCT Geometric Outcomes at the Femoral Neck for Exp. 1.
(A) Total Bone Area, (B) Cortical Thickness, (C) Polar Area MOI. BC at the start (day 0) and other groups at the end (day 112) of the experiment.
Data presented as mean ± SD.
# indicates significant difference from HU value at d112, $p < 0.05$.

3.2.3. *Ex Vivo* Micro-Computed Tomography

The cortical and cancellous compartments of the left proximal tibia metaphysis were also examined by μCT after euthanasia and tissue collection at the end of the study (d112).

3.2.3.1. Proximal Tibia Metaphysis Cancellous Densitometry and Geometry

No HU-induced changes in the proximal tibia metaphysis cancellous bone were found at d112 (Figure 3.16). However, both ALN and ZOL treatment resulted in better microarchitecture outcome values. The HU+ALN group had significantly different % BV/TV (+32%, $p = 0.010$), trabecular thickness (-6.7%, $p = 0.007$), trabecular separation (-18%, $p < 0.001$), and trabecular number (+42%, $p < 0.001$) compared to AC and significantly different % BV/TV (+40%, $p = 0.006$), trabecular separation (-13%, $p = 0.023$), and trabecular number (+44%, $p < 0.001$) compared to HU, while the HU+ZOL group had significantly different % BV/TV, trabecular separation, and trabecular number compared to the AC group (+95%, $p < 0.001$, -26%, $p < 0.001$, +87%, $p < 0.001$, respectively) and HU group (+107%, $p < 0.001$, -22%, $p < 0.001$, +89%, $p < 0.001$, respectively).

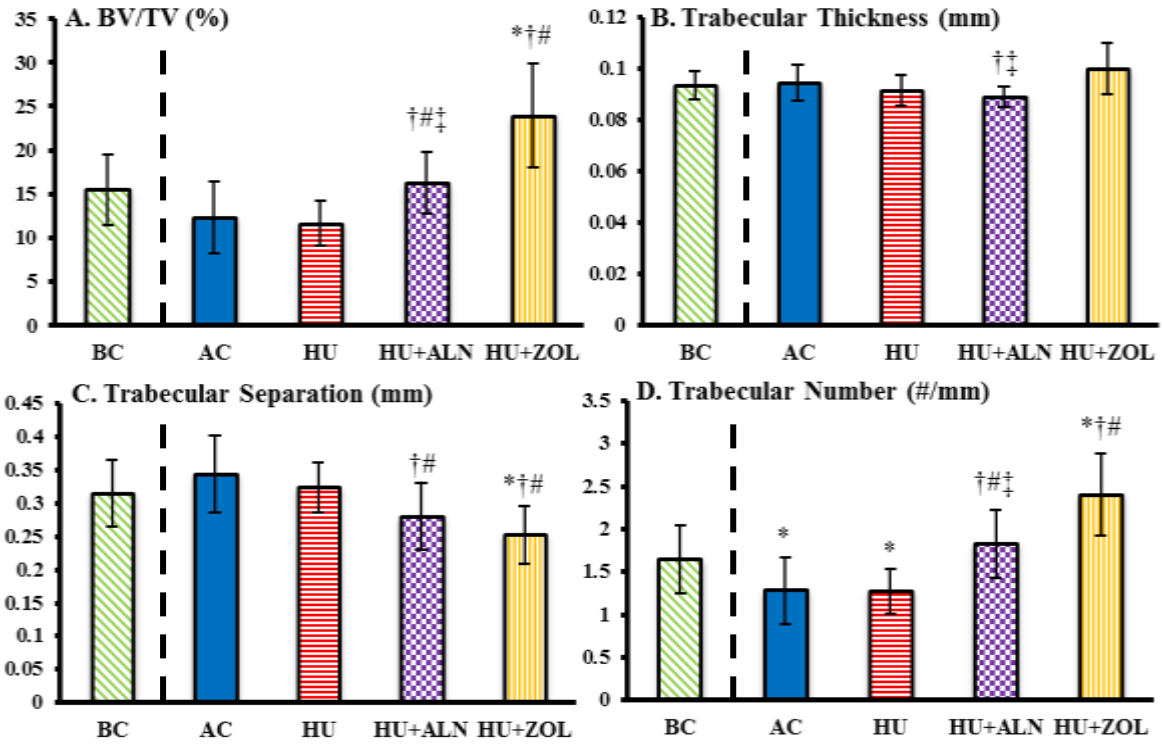

Figure 3.16 *Ex Vivo* µCT Cancellous Outcomes at the Proximal Tibia Metaphysis for Exp. 1.
(A) BV/TV, (B) Trabecular Thickness, (C) Trabecular Separation, (D) Trabecular Number. BC at the start (day 0) and other groups at the end (day 112) of the experiment.
Data presented as mean ± SD.
* indicates significant difference from BC value at d0, $p < 0.05$.
† indicates significant difference from AC value at d112, $p < 0.05$.
# indicates significant difference from HU value at d112, $p < 0.05$.
‡ indicates significant difference from HU+ZOL value at d112, $p < 0.05$.

3.2.3.2. Proximal Tibia Metaphysis Cortical Geometry

There were very few significant differences among groups at d112 in the proximal tibia metaphysis cortical geometry as assessed by µCT (Figure 3.17). The HU group had significantly lower endocortical perimeter (-13%, $p = 0.013$) compared to AC, but the HU+ALN and HU+ZOL groups were not significantly different from either the AC or HU groups. No other significant differences as a result of HU or bisphosphonate treatment were observed.

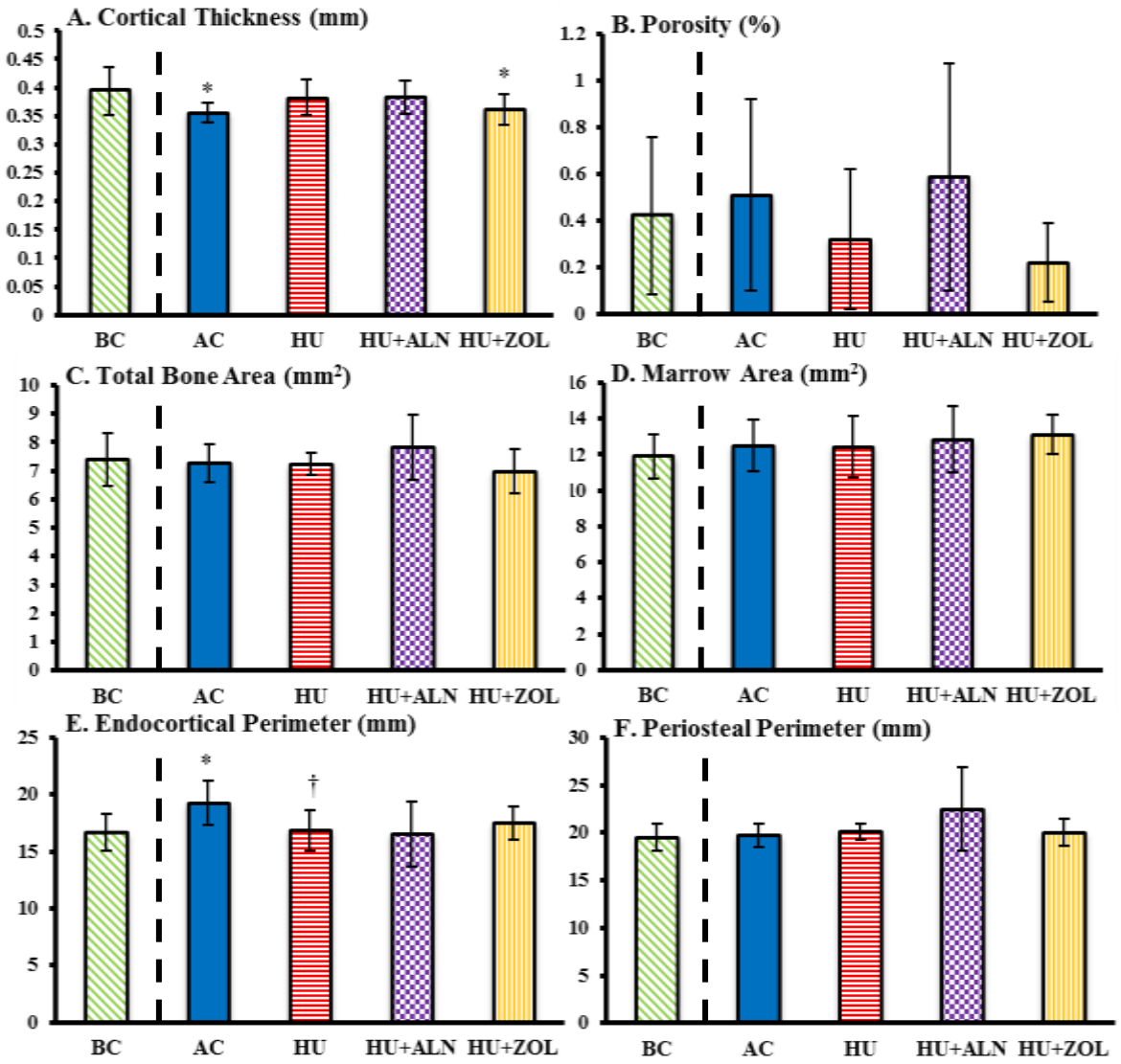

Figure 3.17 *Ex Vivo* µCT Cortical Outcomes at the Proximal Tibia Metaphysis for Exp. 1.
(A) Cortical Thickness, (B) Porosity, (C) Total Bone Area, (D) Marrow Area, (E) Endocortical Perimeter, (F) Periosteal Perimeter. BC at the start (day 0) and other groups at the end (day 112) of the experiment. Data presented as mean ± SD.
* indicates significant difference from BC value at d0, $p < 0.05$.
† indicates significant difference from AC value at d112, $p < 0.05$.

3.3. Mechanical Testing

3.3.1. Tibia Mid-Diaphysis Three-Point Bending

At experiment's end (d112), all four experimental groups had significantly higher stiffness at the tibia diaphysis compared to the BC group (Table 3.3). Otherwise, there were no significant differences observed in extrinsic or intrinsic mechanical properties due to HU, ALN, or ZOL at the tibial mid-shaft.

Table 3.3 Tibia Mid-Diaphysis Three-Point Bending Results for Exp. 1.
BC at the start (day 0) and other groups at the end (day 112) of the experiment.

	BC	AC	HU	HU+ALN	HU+ZOL
Extrinsic Properties					
Stiffness (N/mm)	393.0 ± 44.0	469.0 ± 45.9 *	461.6 ± 40.8 *	439.7 ± 42.3 *	465.4 ± 33.6 *
Ultimate Force (N)	128.4 ± 15.5	135.1 ± 24.2	140.6 ± 16.7	144.7 ± 11.3	147.1 ± 11.1
Yield Force (N)	100.2 ± 9.72	101.2 ± 23.1	103.8 ± 10.2	108.7 ± 14.3	108.1 ± 8.90
Post-Yield Displacement (mm)	0.45 ± 0.22	0.40 ± 0.29	0.31 ± 0.22	0.52 ± 0.17	0.38 ± 0.19
Energy to Ultimate Force (mJ)	36.1 ± 10.5	36.5 ± 18.8	38.5 ± 13.8	45.4 ± 14.1	41.3 ± 11.1
Intrinsic Properties					
Ultimate Stress (MPa)	154.9 ± 30.9	139.2 ± 32.5	151.3 ± 21.6	149.3 ± 25.0	150.4 ± 13.6
Elastic Modulus (GPa)	3.59 ± 0.31	3.62 ± 0.35	3.62 ± 0.31	3.51 ± 0.44	3.61 ± 0.24

Data presented as mean ± SD.
* indicates significant difference from BC value at d0, $p < 0.05$.

3.3.2. Proximal Tibia Metaphysis Reduced Platen Compression

After three-point bending, RPC testing was performed on a section of the left proximal tibia metaphysis. No significant differences were detected in the intrinsic mechanical properties of cancellous bone in the proximal tibia metaphysis (Table 3.4).

Table 3.4 Proximal Tibia Metaphysis Reduced Platen Compression Results for Exp. 1.
BC at the start (day 0) and other groups at the end (day 112) of the experiment.

	BC	AC	HU	HU+ALN	HU+ZOL
Ultimate Stress (MPa)	2.13 ± 2.02	1.21 ± 0.76	0.98 ± 0.50	1.23 ± 0.94	2.40 ± 1.45
Elastic Modulus (MPa)	35.4 ± 28.9	22.0 ± 19.1	21.1 ± 14.0	13.3 ± 5.80	37.9 ± 23.7
Energy to Ultimate Stress (mJ)	1.00 ± 0.83	0.63 ± 0.87	0.65 ± 0.65	0.98 ± 1.20	3.59 ± 4.45
Strain at Ultimate Stress (%)	0.12 ± 0.074	0.18 ± 0.13	0.13 ± 0.093	0.18 ± 0.13	0.21 ± 0.17

Data presented as mean ± SD.

3.3.3. Femur Mid-Diaphysis Three-Point Bending

Three-point bending of the left femur diaphysis was performed at the end of the experiment (Table 3.5). All groups demonstrated significantly higher ultimate force and yield force values compared to those for the BC group. Additionally, HU+ZOL animals had significantly higher stiffness compared to BC animals, and the AC and HU groups both had significantly lower average elastic moduli compared to the BC group. No further significant difference in extrinsic or intrinsic mechanical properties were observed at the femur diaphysis.

Table 3.5 Femur Mid-Diaphysis Three-Point Bending Results for Exp. 1.
BC at the start (day 0) and other groups at the end (day 112) of the experiment.

	BC	AC	HU	HU+ALN	HU+ZOL
Extrinsic Properties					
Stiffness (N/mm)	478.2 ± 57.4	522.4 ± 30.5	515.1 ± 53.5	547.4 ± 52.8	552.9 ± 44.4 *
Ultimate Force (N)	248.2 ± 20.7	289.7 ± 28.0 *	296.0 ± 32.9 *	292.3 ± 26.4 *	305.1 ± 20.7 *
Yield Force (N)	127.8 ± 14.9	155.5 ± 35.5 *	157.5 ± 22.1 *	148.0 ± 13.3 *	148.6 ± 11.7 *
Post-Yield Displacement (mm)	0.61 ± 0.15	0.50 ± 0.13	0.55 ± 0.14	0.61 ± 0.16	0.67 ± 0.22
Energy to Ultimate Force (mJ)	119.2 ± 25.2	128.2 ± 26.6	138.5 ± 16.3	136.7 ± 17.1	142.3 ± 23.6
Intrinsic Properties					
Ultimate Stress (MPa)	127.9 ± 7.64	124.4 ± 14.8	124.4 ± 9.22	132.8 ± 12.0	129.0 ± 12.3
Elastic Modulus (GPa)	1.19 ± 0.19	1.00 ± 0.15 *	0.97 ± 0.14 *	1.13 ± 0.15	1.05 ± 0.09

Data presented as mean ± SD.
* indicates significant difference from BC value at d0, $p < 0.05$.

3.3.4. Femoral Neck Mechanical Test

Femoral neck mechanical testing was performed on specimens collected on d112 to determine extrinsic mechanical properties (Figure 3.18). No significant differences in mechanical properties were observed.

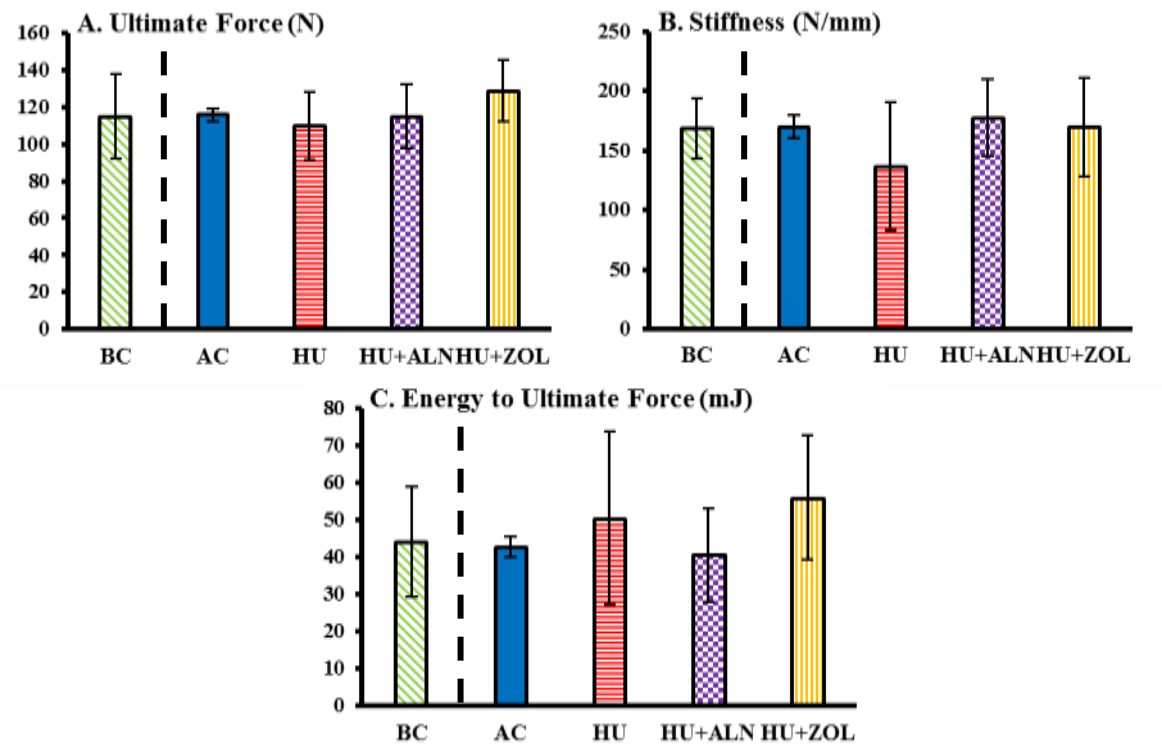

Figure 3.18 *Ex Vivo* Femoral Neck Mechanical Test Results for Exp. 1.
(A) Ultimate Force, (B) Stiffness, (C) Energy to Ultimate Force. BC at the start (day 0) and other groups at the end (day 112) of the experiment.
Data presented as mean ± SD.

3.4. Histomorphometry

3.4.1. Distal Femur Metaphysis Static Cancellous Histomorphometry

Static histomorphometry was performed on the distal femur metaphyses (DFM) collected at the end of the experiment (Figure 3.19). The HU group was not significantly different from the AC group for any of the six outcome variables obtained. However, relative osteoid surface (OS/BS) was 76% lower in HU+ALN animals compared to AC animals ($p = 0.016$) and HU+ZOL animals had 96% and 92% lower relative osteoid surface compared to AC ($p < 0.001$) and HU ($p = 0.041$) animals, respectively. ZOL treatment also resulted in 75% and 76% lower relative osteoclast surface (Oc.S/BS) compared to AC ($p = 0.016$) and HU ($p = 0.010$) rats, respectively. No significant differences in BV/TV, trabecular thickness (Tb.Th.), trabecular separation (Tb.Sp.), or trabecular number (Tb.N.) were observed.

3.4.2. Tibia Mid-Diaphysis Dynamic Cortical Histomorphometry

Dynamic histomorphometry was performed on the fluorochrome labelled cortical bone in the tibia diaphysis at two time points, halfway through recovery (d56) and the end of recovery (d84). A representative image with fluorochrome labels identified by time point was presented previously (Figure 2.10). Demeclocycline (orange label) was given 9 and 2 days before d56, and calcein (green label) was given 9 and 2 days before d84. The HU group had significantly higher MAR (+80%, $p = 0.021$) compared to the AC group at d56, and significantly higher MS/BS (+95%, $p = 0.025$), MAR (+34%, $p = 0.035$), and BFR/BS (+135%, $p = 0.006$) compared to the AC group at d84 (Table 3.6).

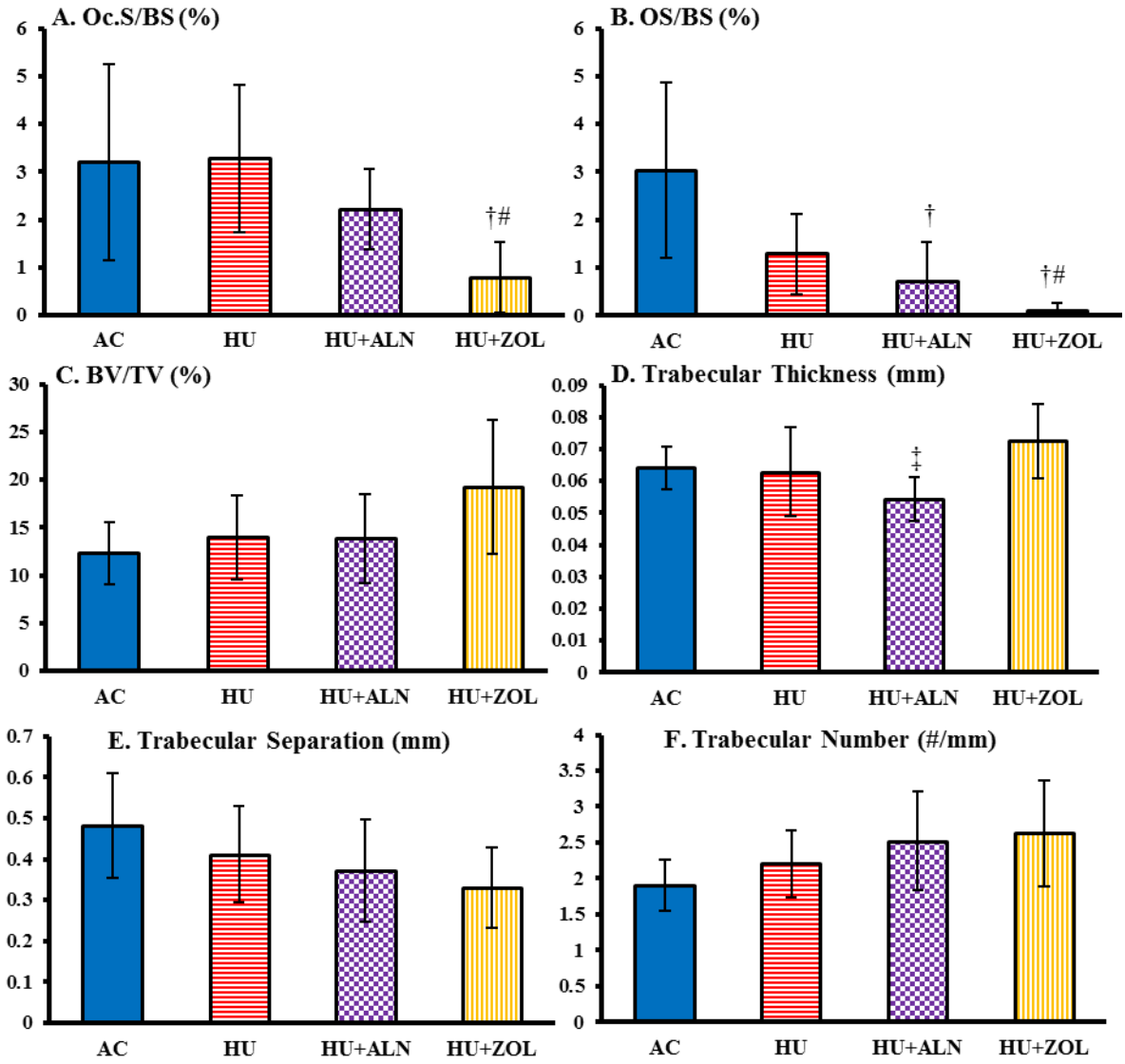

Figure 3.19 Static Histomorphometric Outcomes at the Distal Femur Metaphysis for Exp. 1.
(A) Oc. S./BS, (B) OS/BS, (C) BV/TV, (D) Trabecular Thickness, (E) Trabecular Separation, (F) Trabecular Number.
Data presented as mean ± SD.
† indicates significant difference from AC value at d112, $p < 0.05$.
# indicates significant difference from HU value at d112, $p < 0.05$.
‡ indicates significant difference from HU+ZOL value at d112, $p < 0.05$.

Table 3.6 Tibia Mid-Diaphysis Dynamic Cortical Histomorphometry Results for Exp. 1.

	AC	HU	HU+ALN	HU+ZOL
Mid-Recovery (d56)				
MS/BS (%)	32.8 ± 14.4	50.5 ± 23.8	33.9 ± 16.0	33.1 ± 7.07
MAR (μm/day)	0.59 ± 0.26	1.07 ± 0.39 †	0.79 ± 0.36	0.77 ± 0.16
BFR/BS ($\mu m^3/\mu m^2$/day)	0.21 ± 0.13	0.54 ± 0.34	0.30 ± 0.21	0.26 ± 0.097
End of Recovery (d84)				
MS/BS (%)	29.2 ± 17.8	56.8 ± 12.8 †	45.5 ± 10.2	44.2 ± 10.2
MAR (μm/day)	0.65 ± 0.19	0.87 ± 0.12 †	0.96 ± 0.37	0.73 ± 0.10
BFR/BS ($\mu m^3/\mu m^2$/day)	0.22 ± 0.17	0.51 ± 0.17 †	0.45 ± 0.25	0.33 ± 0.11

Data presented as mean ± SD.
† indicates significant difference from AC at d112, $p < 0.05$.

4. EXPERIMENT 2 RESULTS

The figures and tables in this chapter present the data collected in Experiment 2. The design for Experiment 2 was presented previously in Figure 2.2. The vertical axis of each figure displays a unique outcome variable, while the horizontal axis displays the time points at which measures were taken for those outcome variables. The baseline time point and start of the first HU period is defined as day 0 (d0). Subsequent time points occur every 28 days, with day 28 (d28) at the end of the exercise period, day 56 (d56) at the end of the unloading period and start of recovery, day 84 (d84) midway through recovery, and with day 112 (d112) marking the end of the recovery period and the experiment. All *ex vivo* data comes from three time points, end of exercise (d28), end of HU (d56) and end of recovery (d112). A randomly selected subset of animals from each group was euthanized at the end of the exercise period (d28), end of the HU period (d56), and the end of the recovery period (d112), and the number of specimens available at each time point is shown in Table 4.1. A lack of significance markers on a graph or table indicates that there were no significant differences found. Full numerical results for all outcome variables from Experiment 2 may be found in Appendix B.

Table 4.1 Number of Specimens Available at Each Time Point for Exp. 2.
(A) Maximum number of specimens for data collected *in vivo*, (B) Maximum number of specimens for data collected *ex vivo*.

(A)

Group	d0	d28	d56	d84	d112
AC	63	56	38	22	22
HU	27	27	27	14	14
HU+VJE	45	45	30	15	15

(B)

Group	d0	d28	d56	d84	d112
AC	7	18	16	-	22
HU	-	-	13	-	14
HU+VJE	-	15	15	-	15

4.1. Animals

All animals were weighed twice weekly throughout the study period and the average body masses at each time point are reported in Table 4.2. Any animal suffering excessive weight loss, defined as 10% loss in one week or less, would have been removed from the study. No animals were removed from the study due to excessive weight loss.

At d0, the animals had an average mass of 416.8 ± 57.0 g across all three groups, and the HU+VJE group had significantly lower average body mass compared to both the AC (-13.4% , $p < 0.001$) and HU (-18.4%, $p < 0.001$) groups. The body masses of all three groups displayed an overall increasing trend during the experimental period. The HU group had significantly higher body mass compared to the AC group at d28 (+9.2%, $p = 0.01$). The HU+VJE group actually had significantly lower body mass compared to the HU and AC groups for every remaining time point of the study.

Table 4.2 Body Mass (g) Results for Exp. 2.

Group	d0	d28	d56	d84	d112
AC	430.1 ± 59.4	437.0 ± 65.2	472.7 ± 62.0	489.8 ± 51.4	500.8 ± 52.1
HU	456.7 ± 36.1	477.2 ± 45.6 †	483.4 ± 34.8	512.4 ± 34.3	531.6 ± 44.3
HU+VJE	372.7 ± 31.3 †#	391.4 ± 40.3 †#	432.6 ± 49.7 †#	431.2 ± 35.9 †#	460.2 ± 46.6 †#

Data presented as mean ± SD.
† indicates significant difference from AC value at same time point, $p < 0.05$.
# indicates significant difference from HU value at same time point, $p < 0.05$.

The soleus is a postural muscle in the lower leg, and changes to its mass are a good indication of the efficacy of HU. At d28, HU+VJE had significantly lower soleus wet mass (Figure 4.1) compared to AC (-18.4%, $p = 0.002$). At d56, HU wet mass was significantly lower compared to AC (-44.8%, $p < 0.001$), confirming the efficacy of unloading in this experiment. HU+VJE wet mass was significantly lower compared to both AC (-56.2%, $p < 0.001$) and HU (-20.6%, $p = 0.014$) at d56, and was also significantly lower when compared to HU (-23.4%, $p = 0.005$) at d112. When soleus wet mass was normalized to body mass, the HU (-46.7%) and HU+VJE (-54.0%) groups had significantly lower values compared to AC at d56, further confirming the efficacy of unloading in this experiment, and suggesting that significant differences observed at other time points were due to body mass effects.

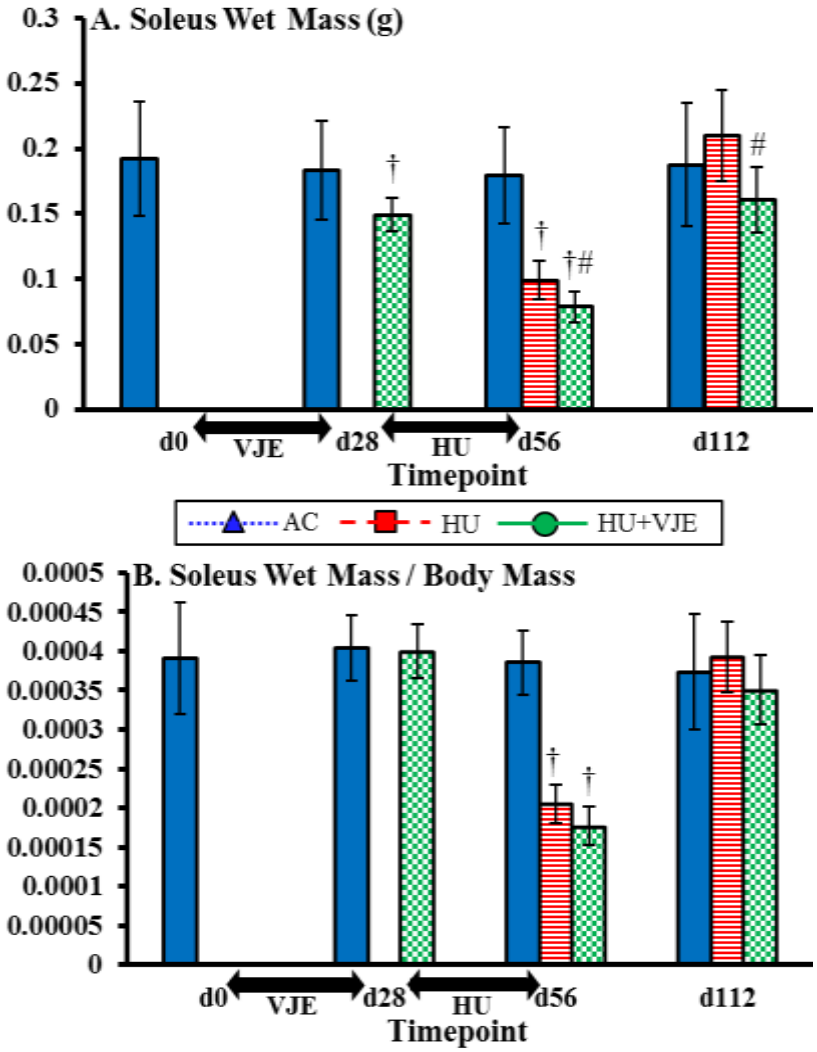

Figure 4.1 *Ex Vivo* Soleus Wet Mass for Exp. 2.
(A) Soleus Wet Mass. Each value represents the averaged mass of the left and right solei together. (B) Soleus Wet Mass normalized to Body Mass. Each value represents the averaged mass of the left and right solei normalized to the body mass at the time of euthanasia.
Data presented as mean ± SD.
† indicates significant difference from AC value at same time point, $p < 0.05$.
# indicates significant difference from HU value at same time point, $p < 0.05$.

4.2. Computed Tomography

4.2.1. Longitudinal *In Vivo* Peripheral Quantitative Computed Tomography

In order to monitor bone structural changes, longitudinal *in vivo* pQCT was performed on the left proximal tibia metaphysis (PTM) and tibia mid-diaphysis (TD). "HU-induced changes" can be defined relative to the start of HU (d28 to d56) or relative to the AC group at the end of HU (d56). Both types of comparisons are important and were considered. For determining the effectiveness of VJE pre-treatment, differences at the end of exercise (d28) and at the end of HU (d56) must be taken into account. A significant difference between the beginning and the end of VJE pre-treatment (d0 to d28) and significant differences from the AC and HU groups at d28 may all be considered "VJE pre-treatment induced changes". At d56, three categories of effectiveness have been defined. "Mitigation" occurs when the HU+VJE group values are significantly higher than those for HU, but significantly lower than those for AC. "Protection" occurs when the HU+VJE group values are significantly higher than those for HU, but not significantly different from those for AC. "Overprotection" occurs when the HU+VJE group values are significantly higher than those for both the HU and AC groups. In the following figures for *in vivo* pQCT, only those subjects euthanized on d112 are included. This allows for the use of a one-way ANOVA with repeated measures for assessing longitudinal changes within groups. Data that includes all subjects can be found in Appendix B.

4.2.1.1. Proximal Tibia Metaphysis Densitometry and Geometry

Both HU and VJE pre-treatment had significant effects on bone density at the proximal tibia metaphysis during the experiment (Figure 4.2). HU+VJE animals started with significantly lower total BMC compared to HU animals(+13.7%, $p = 0.003$). The

effects of unloading were evident in several variables for the HU group. The HU period resulted in significantly lower values for the HU group in total BMC (-9.2%, $p < 0.001$) and cancellous vBMD (-14.7%, $p < 0.012$) when comparing pre- (d28) to post-HU (d56). In addition, the HU group had significantly lower cancellous vBMD compared to the AC group (-16.7%, $p = 0.006$) at d56. The HU group also had significantly higher total BMC compared to AC (+9.8%, $p = 0.009$) at the start of the HU period (d28), but not at the end of HU (d56).

VJE pre-treatment resulted in significantly higher total BMC at d28 compared to d0 (+8.71%, $p < 0.001$), but this did not prevent a significant decrease in total BMC for HU+VJE over the HU period (-6.0%, $p < 0.001$). Total BMC values for HU+VJE was also significantly lower compared to those for AC (-10.6%, $p < 0.001$) at d56, and compared to those for both AC (-7.6%, $p = 0.048$) and HU (-6.5%, $p = 0.016$) at d84. Total vBMD values were significantly higher for HU+VJE animals compared to HU animals (+4.7%, $p = 0.033$) at d28, had a negative trend over the HU period, and were significantly lower compared to AC animals (-4.4%, $p = 0.048$) at d84. Cancellous vBMD values for the HU+VJE group had a positive trend during the exercise period and a negative trend over the HU period, but at the end of the HU period, the HU+VJE group values were significantly higher compared to those for the HU group (+21.2%, $p = 0.005$). VJE pre-treatment was overprotective for cancellous vBMD during recovery (d84 and d112). There were no significant difference between any groups in cortical vBMD values for the first three time points, but HU+VJE animals had significantly lower values at d84 and d112 compared to AC (-3.5%, $p < 0.001$ and -3.04%, $p = 0.003$, respectively) and HU (-3.94%, $p = 0.003$ and -2.56%, $p = 0.028$, respectively) animals.

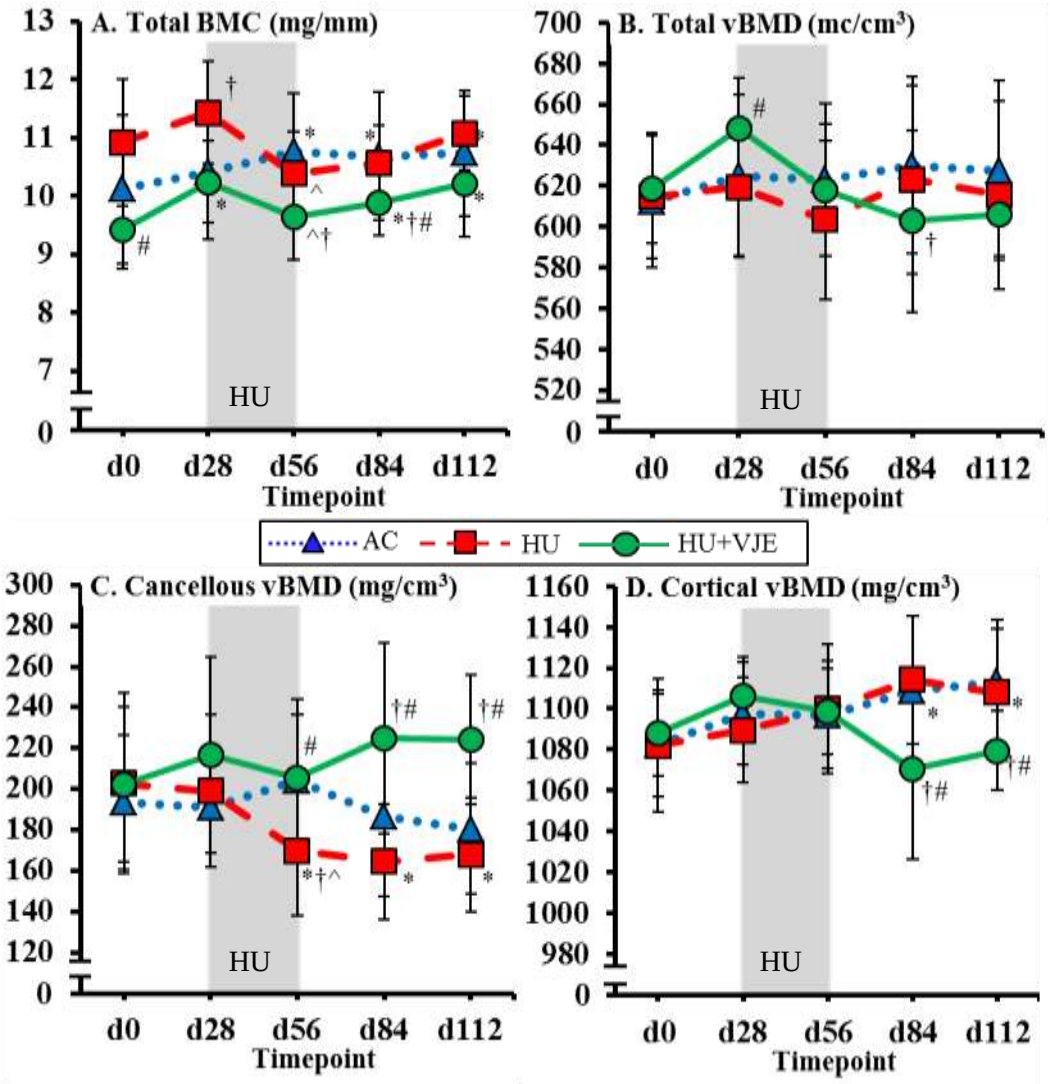

Figure 4.2 *In Vivo* pQCT Densitometric Outcomes at the Proximal Tibia Metaphysis for Exp. 2.
(A) Total BMC, (B) Total vBMD, (C) Cancellous vBMD, (D) Cortical vBMD. Only animals euthanized at d112 included.
Data presented as mean ± SD.
* indicates significant difference from d0 value, $p < 0.05$.
† indicates significant difference from AC value at same time point, $p < 0.05$.
# indicates significant difference from HU value at same time point, $p < 0.05$.
^ indicates significant difference from pre- to post-HU value, $p < 0.05$.

Examining geometric outcomes (Figure 4.3), the HU group had significantly higher total bone area compared to the AC group (+11.0%, $p = 0.006$) at d28, and bone area significantly decreased over the HU period (-6.50%, $p = 0.030$). The HU+VJE group had significantly lower total bone area compared to the HU group at d0 (-14.2%, $p = 0.008$) and d28 (-14.6%, $p < 0.001$), and significantly lower total bone area compared to the AC group at d56 (-9.7%, $p = 0.007$). HU treatment did not result in significant changes in cortical thickness for the HU group, but the HU+VJE group had significantly lower cortical thickness as a result of HU (d56 to d28, -6.34%, $p < 0.001$). HU+VJE animals also had significantly lower cortical thickness compared to AC and HU animals on d56 (-10.5%, $p = 0.054$ and -18.1%, $p < 0.001$, respectively), d84 (-12.2%, $p = 0.031$ and -15.9%, $p < 0.001$, respectively), and d112 (-8.9%, $p = 0.043$ and -17.1%, $p = 0.005$, respectively).

4.2.1.2. Tibia Mid-Diaphysis Densitometry and Geometry

Tibia diaphysis density and geometry were largely unaffected by both VJE pre-treatment and HU. For cortical BMC and cortical vBMD, all groups underwent an increasing trend over the experimental period that was not affected by either HU or VJE pre-treatment (Figure 4.4). Cortical BMC was also significantly lower for the HU+VJE group (-9.2%, $p = 0.025$) compared to the HU group on d0. As shown in Figure 4.5, cortical area, cortical thickness and polar area MOI also demonstrated an increasing trend in all groups over the study period. The HU+VJE group started significantly lower at d0 when compared to the HU group in cortical area (-9.22%, $p = 0.021$) and polar area MOI (-20.3%, $p = 0.037$). Otherwise, there were no notable significant differences observed.

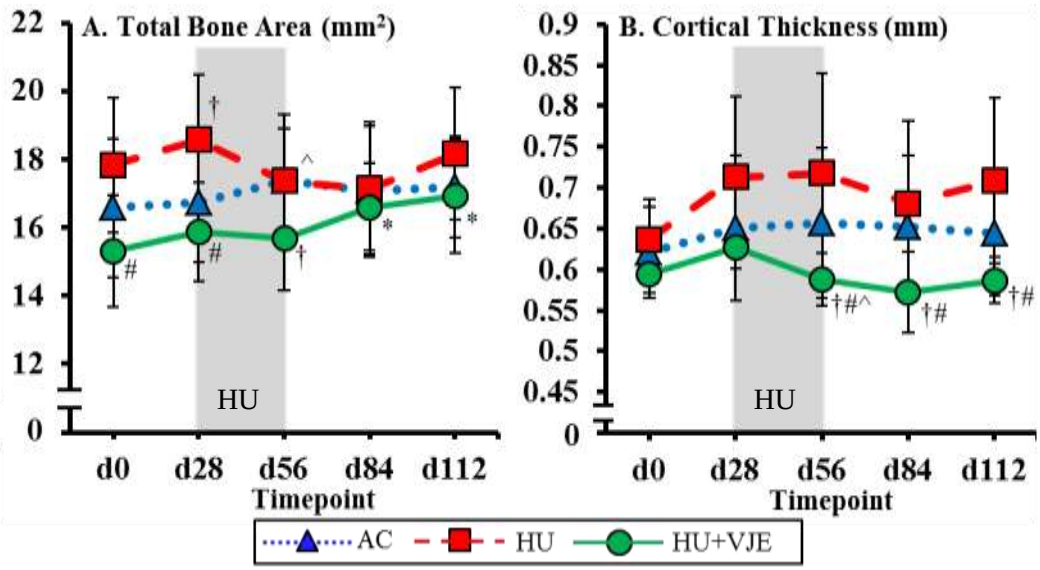

Figure 4.3 *In Vivo* pQCT Geometric Outcomes at the Proximal Tibia Metaphysis for Exp. 2.
(A) Total Bone Area, (B) Cortical Thickness. Only animals euthanized at d112 included.
Data presented as mean ± SD.
* indicates significant difference from d0 value, $p < 0.05$.
† indicates significant difference from AC value at same time point, $p < 0.05$.
# indicates significant difference from HU value at same time point, $p < 0.05$.
^ indicates significant difference from pre- to post-HU value, $p < 0.05$.

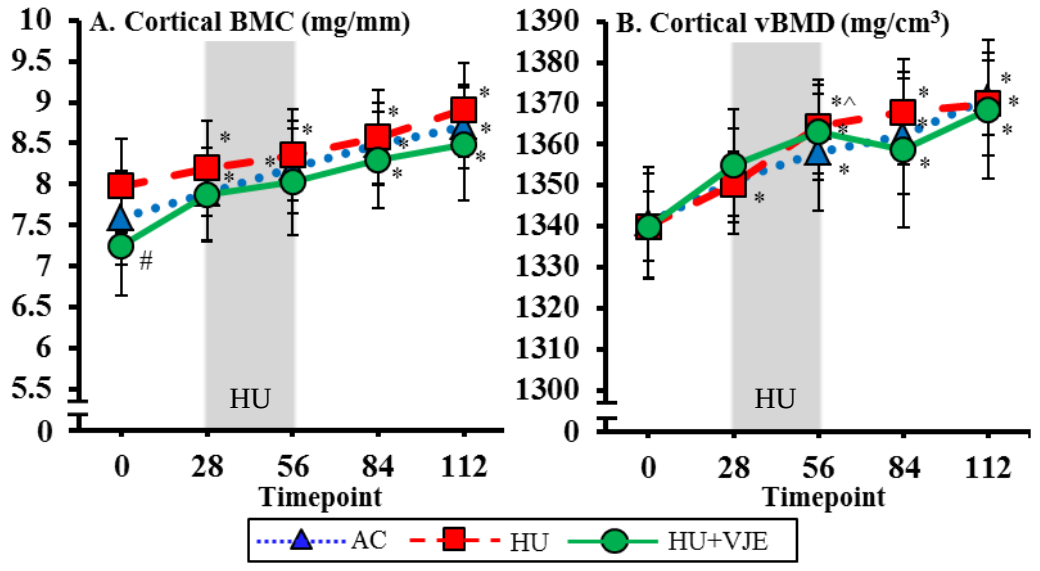

Figure 4.4 *In Vivo* pQCT Densitometric Outcomes at the Tibia Mid-Diaphysis for Exp. 2.
(A) Cortical BMC, (B) Cortical vBMD. Only animals euthanized at d112 included.
Data presented as mean ± SD.
* indicates significant difference from d0 value, $p < 0.05$.
# indicates significant difference from HU value at same time point, $p < 0.05$.
^ indicates significant difference from pre- to post-HU value, $p < 0.05$.

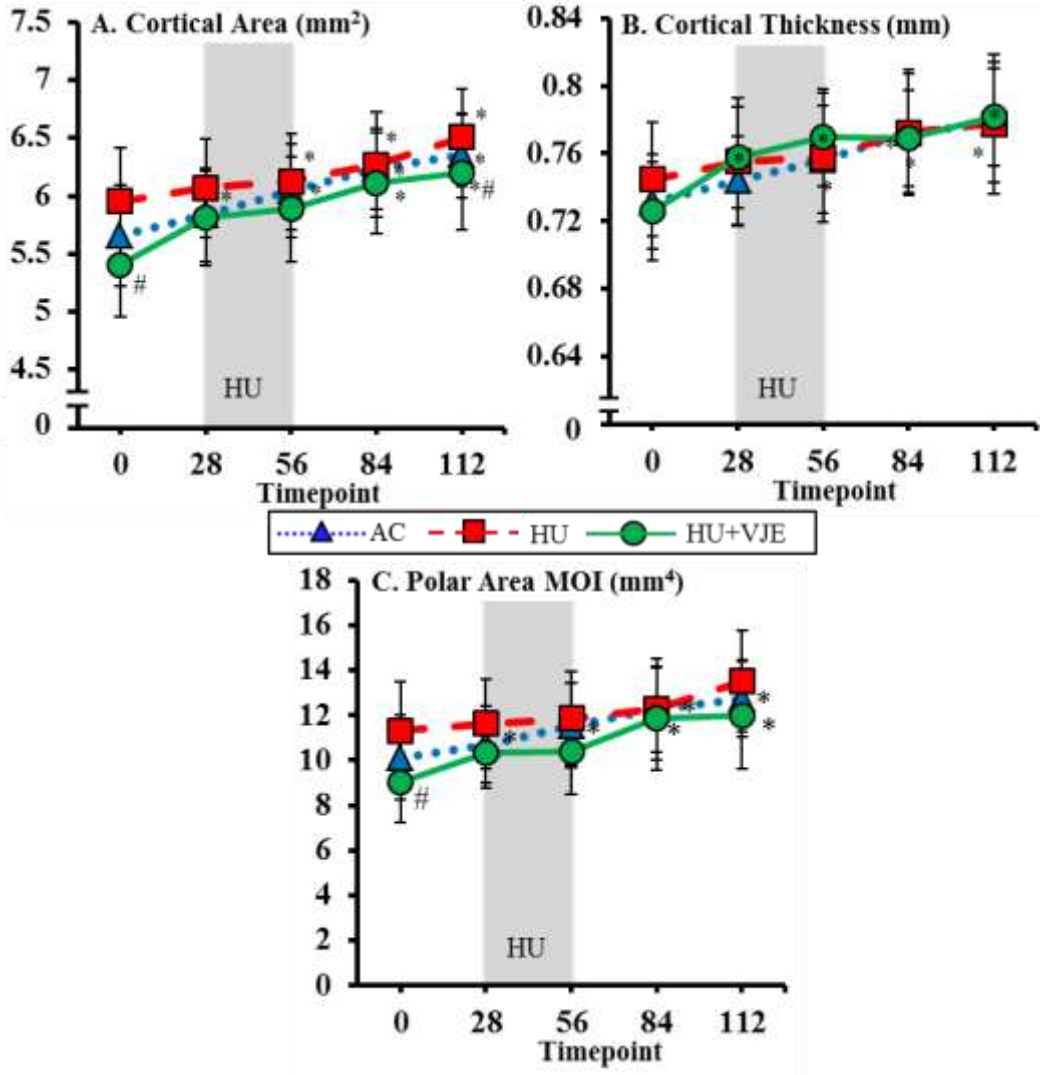

Figure 4.5 *In Vivo* pQCT Geometric Outcomes at the Tibia Mid-Diaphysis for Exp. 2.
(A) Cortical Area, (B) Cortical Thickness, (C) Polar Area MOI. Only animals euthanized at d112 included.
Data presented as mean ± SD.
* indicates significant difference from d0 value, $p < 0.05$.
# indicates significant difference from HU value at same time point, $p < 0.05$.

4.2.2. *Ex Vivo* Peripheral Quantitative Computed Tomography

In addition to longitudinal *in vivo* surveillance of the left tibia, the left proximal tibia metaphysis and tibia diaphysis, the left distal femur metaphysis (DFM) and femur mid-diaphysis (FD), and the right femoral neck (FN) all underwent *ex vivo* pQCT after euthanasia and tissue collection at d28, d56, and d112.

4.2.2.1. Proximal Tibia Metaphysis Densitometry and Geometry

HU-induced changes occurred in total BMC (-11.4%, $p = 0.013$) and total vBMD (-9.2%, $p = 0.001$) at d56 (Figure 4.6). VJE pre-treatment resulted in significantly higher total vBMD (+9.0%, $p < 0.001$) and cortical vBMD (+4.32%, $p = 0.003$) for HU+VJE animals compared to AC animals at d28. VJE pre-treatment also protected total BMC and total vBMD from HU-induced changes and was overprotective for cancellous vBMD at d56. At the end of recovery (d112), the HU+VJE group also had significantly higher total vBMD compared to the AC (+6.6%, $p = 0.003$) and HU (+8.7%, $p < 0.001$) groups, and significantly higher cortical vBMD compared to the HU group (+4.44%, $p < 0.001$). Total BMC, however, was significantly lower for HU+VJE animals compared to HU animals (-9.80%, $p = 0.017$) at d112.

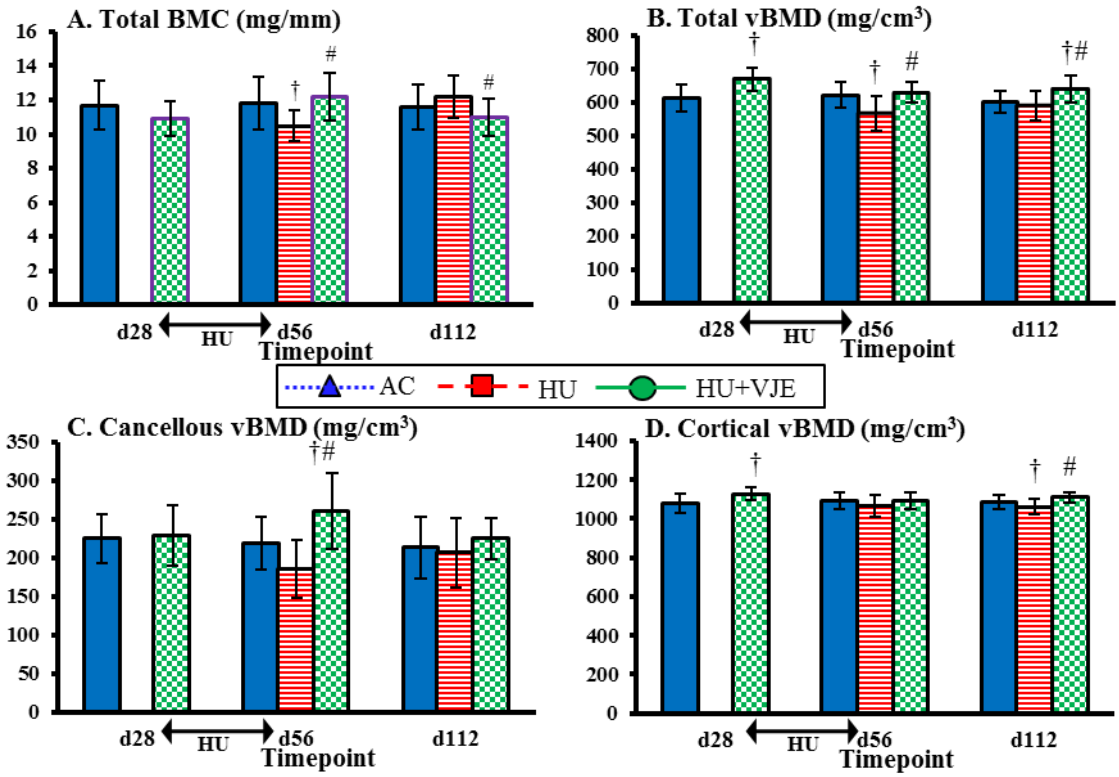

Figure 4.6 *Ex Vivo* pQCT Densitometric Outcomes at the Proximal Tibia Metaphysis for Exp. 2.
(A) Total BMC, (B) Total vBMD, (C) Cancellous vBMD, (D) Cortical vBMD.
Data presented as mean ± SD.
† indicates significant difference from AC value at same time point, $p < 0.05$.
# indicates significant difference from HU value at same time point, $p < 0.05$.

Few significant differences were found in geometric outcomes at the proximal tibia metaphysis from *ex vivo* pQCT scans (Figure 4.7). Total bone area was significantly lower for the HU+VJE group compared to the AC group (-15.0%, $p = 0.003$) at d28, and compared to both the AC (-11.1%, $p = 0.034$) and HU (-17.8%, $p < 0.001$) groups at d112. Cortical thickness underwent HU-induced changes, with HU values lower than AC values (-9.1%, $p < 0.001$) at d56. Values for those rats engaging in VJE pre-treatment were not significantly different from either AC or HU at d56.

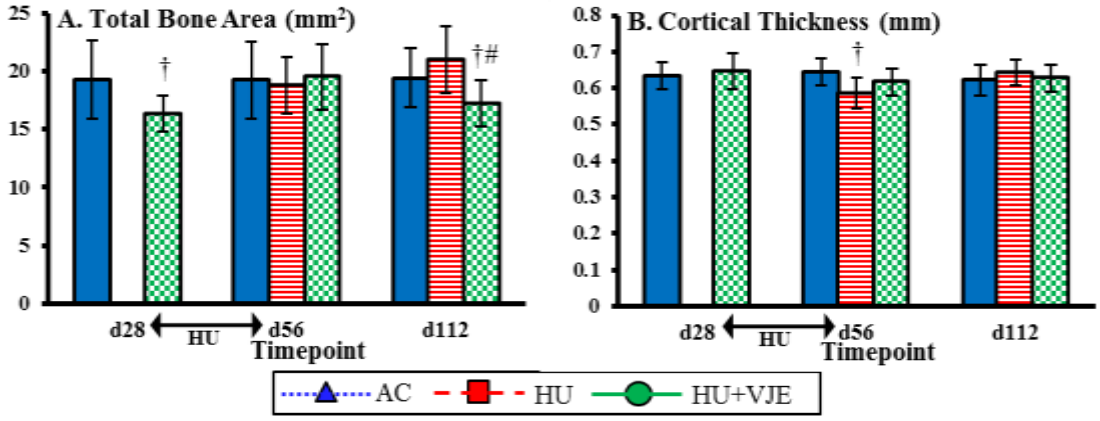

Figure 4.7 *Ex Vivo* pQCT Geometric Outcomes at the Proximal Tibia Metaphysis for Exp. 2.
(A) Total Bone Area, (B) Cortical Thickness.
Data presented as mean ± SD.
† indicates significant difference from AC value at same time point, $p < 0.05$.
# indicates significant difference from HU value at same time point, $p < 0.05$.

4.2.2.2. Tibia Mid-Diaphysis Densitometry and Geometry

As with the *in vivo* pQCT, the tibia diaphysis underwent increasing trends in both densitometric (reported in Figure 4.8) and geometric (reported in Figure 4.9) outcomes over the course of the experiment in all groups when examined by *ex vivo* pQCT. For densitometric outcomes, cortical BMC was significantly higher for HU+VJE animals compared to AC (+11.4%, $p < 0.001$) and HU (+10.0%, $p = 0.002$) animals at d56 and cortical vBMD was significantly higher for HU+VJE rats compared to AC rats (+0.72%, $p = 0.034$) at d28. The HU group had significantly lower cortical vBMD compared to the AC group (-0.694%, $p = 0.037$) at d112. HU+VJE animals also had significantly higher cortical area, cortical thickness, and polar area MOI compared to AC (+11.6%, $p = 0.002$, +7.3%, $p < 0.001$, +23.2%, $p = 0.012$, respectively) and HU (+9.7%, $p = 0.004$, +5.3%, $p = 0.009$, +22.4%, $p = 0.021$, respectively) animals at d56.

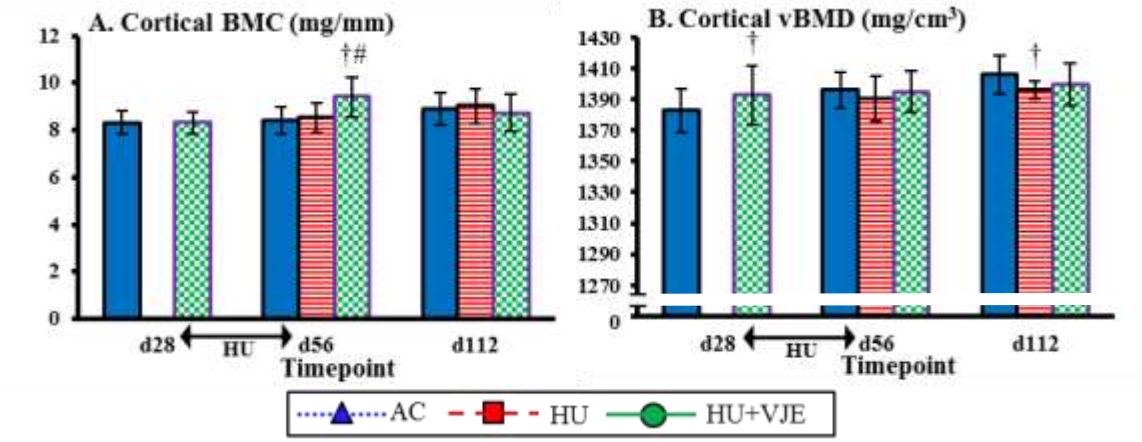

Figure 4.8 *Ex Vivo* pQCT Densitometric Outcomes at the Tibia Mid-Diaphysis for Exp. 2.
(A) Cortical BMC, (B) Cortical vBMD.
Data presented as mean ± SD.
† indicates significant difference from AC value at same time point, $p < 0.05$.
# indicates significant difference from HU value at same time point, $p < 0.05$.

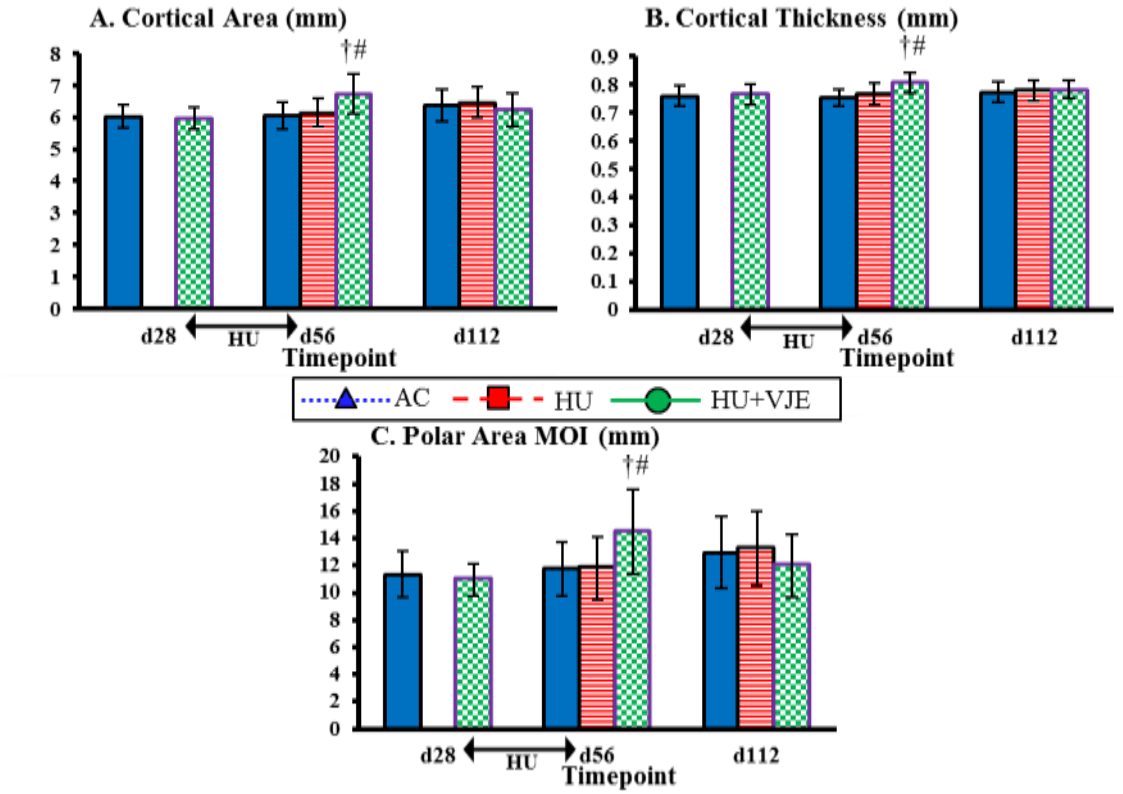

Figure 4.9 *Ex Vivo* pQCT Geometric Outcomes at the Tibia Mid-Diaphysis for Exp. 2.
(A) Cortical Area, (B) Cortical vBMD, (C) Polar Area MOI.
Data presented as mean ± SD.
† indicates significant difference from AC value at same time point, $p < 0.05$.
# indicates significant difference from HU value at same time point, $p < 0.05$.

4.2.2.3. Distal Femur Metaphysis Densitometry and Geometry

HU-induced changes were observed in total BMC (-11.1%, $p = 0.015$) and total vBMD (-12.5%, $p < 0.001$), as the HU group mean value was significantly lower than that for the AC group at d56 for these two outcome variables (Figure 4.10). VJE pre-treatment was protective of total BMC and total vBMD at d56, and overprotective of cancellous vBMD at d56. HU+VJE animals also had significantly higher total vBMD compared to AC animals (+7.6%, $p = 0.002$) at d28 and compared to HU animals (+11.2%, $p = 0.014$) at d112. Additionally, the HU+VJE group had significantly higher cancellous vBMD at d112 compared to both the AC (+14.2%, $p = 0.049$) and HU (+21.3%, $p < 0.001$) groups.

Examining geometric results for *ex vivo* pQCT of the distal femur metaphysis, HU+VJE animals had significantly lower total bone area compared to AC animals (-8.5%, $p < 0.001$) at d28 and compared to HU animals (-12.9%, $p < 0.001$) at d112 (Figure 4.11). Additionally, the HU group had significantly higher total bone area compared to the AC group (+9.4%, $p = 0.023$) at d112. Cortical thickness demonstrated HU-induced changes for the HU group (-11.0%, $p < 0.001$) compared to the AC group at d56, and VJE pre-treatment did not prevent these changes, as the HU+VJE group also had significantly lower cortical thickness compared to the AC group (-5.7%, $p = 0.034$) at d56.

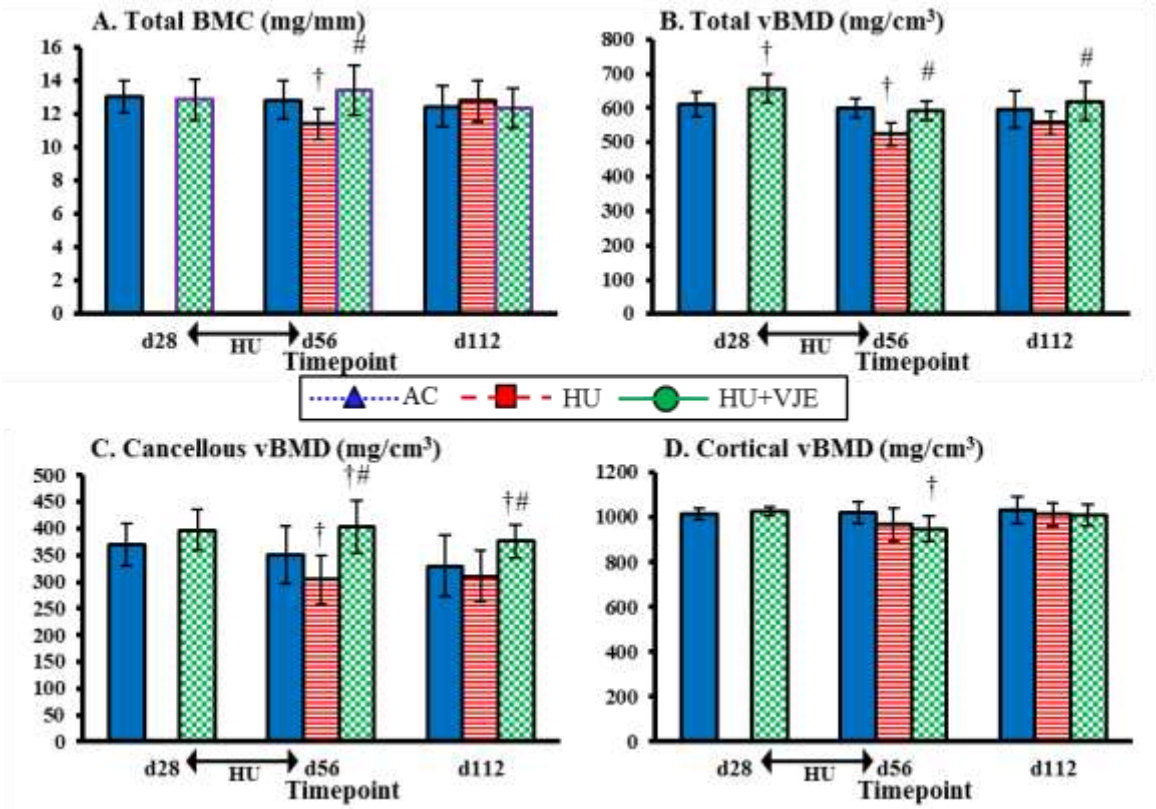

Figure 4.10 *Ex Vivo* pQCT Densitometric Outcomes at the Distal Femur Metaphysis for Exp. 2.
(A) Total BMC, (B) Total vBMD, (C) Cancellous vBMD, (D) Cortical vBMD.
Data presented as mean ± SD.
† indicates significant difference from AC value at same time point, $p < 0.05$.
# indicates significant difference from HU value at same time point, $p < 0.05$.

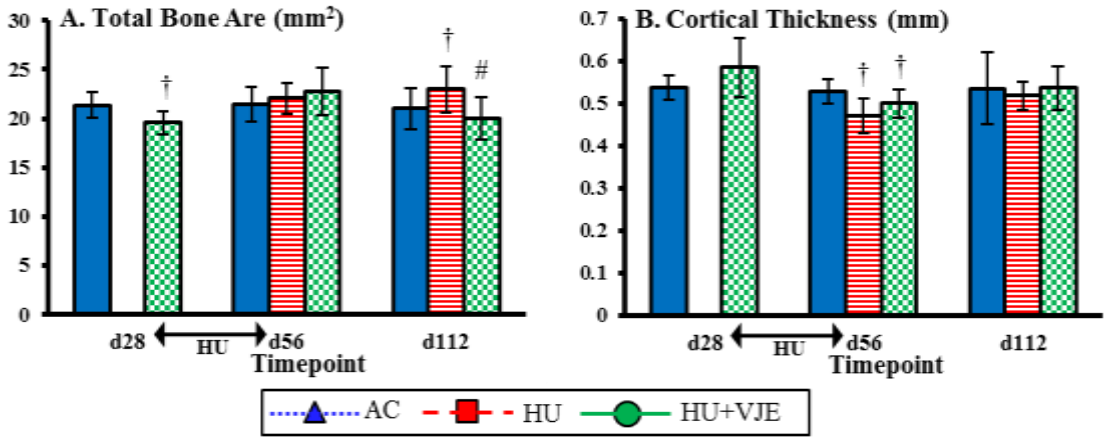

Figure 4.11 *Ex Vivo* pQCT Geometric Outcomes at the Distal Femur Metaphysis for Exp. 2.
(A) Total Bone Area, (B) Cortical Thickness.
Data presented as mean ± SD.
† indicates significant difference from AC value at same time point, $p < 0.05$.
# indicates significant difference from HU value at same time point, $p < 0.05$.

4.2.2.4. Femur Mid-Diaphysis Densitometry and Geometry

No HU-induced changes in densitometric or geometric outcomes were observed in the femur diaphysis. As seen in Figure 4.12, HU+VJE rats had significantly lower cortical BMC at d28 compared to AC rats (-9.9%, $p = 0.001$), and at d112 compared to both AC (-10.1%, $p = 0.018$) and HU (-15.0, $p < 0.001$) rats. Additionally, the HU+VJE group had significantly lower cortical vBMD compared to the AC group (-1.0%, $p < 0.001$) at d28. The geometric results at the femur diaphysis (Figure 4.13) reveal that cortical area, cortical thickness, and polar area MOI all had significantly lower values for the HU+VJE group compared to the AC group (-9.9%, $p < 0.001$, -4.6%, $p = 0.019$, -19.6%, $p < 0.001$, respectively) at d28 and compared to both the AC (-9.6%, $p = 0.02$, -5.7%, $p = 0.004$, -17.0%, $p = 0.010$, respectively) and the HU (-14.9%, $p = 0.001$, -7.6%, $p < 0.001$, -26.8%, $p < 0.001$, respectively) groups at d112.

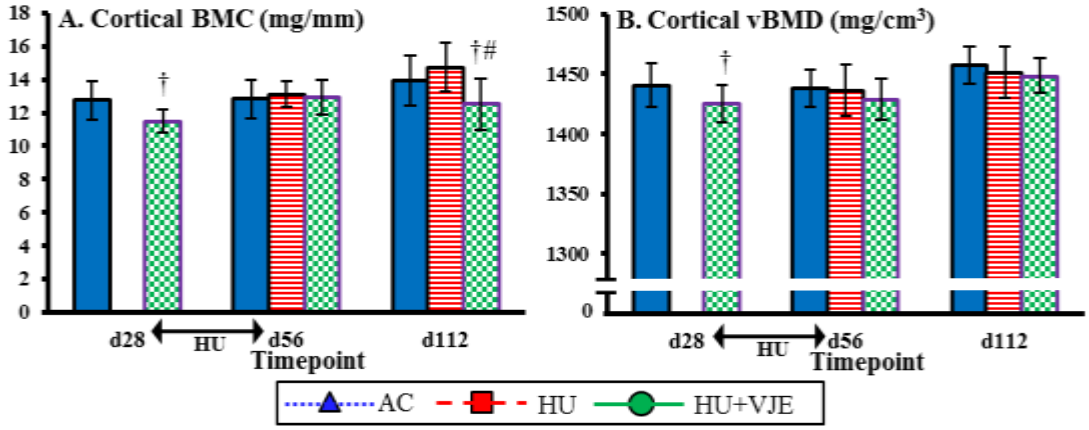

Figure 4.12 *Ex Vivo* pQCT Densitometric Outcomes at the Femur Mid-Diaphysis for Exp. 2.
(A) Cortical BMC, (B) Cortical vBMD.
Data presented as mean ± SD.
† indicates significant difference from AC value at same time point, $p < 0.05$.
# indicates significant difference from HU value at same time point, $p < 0.05$.

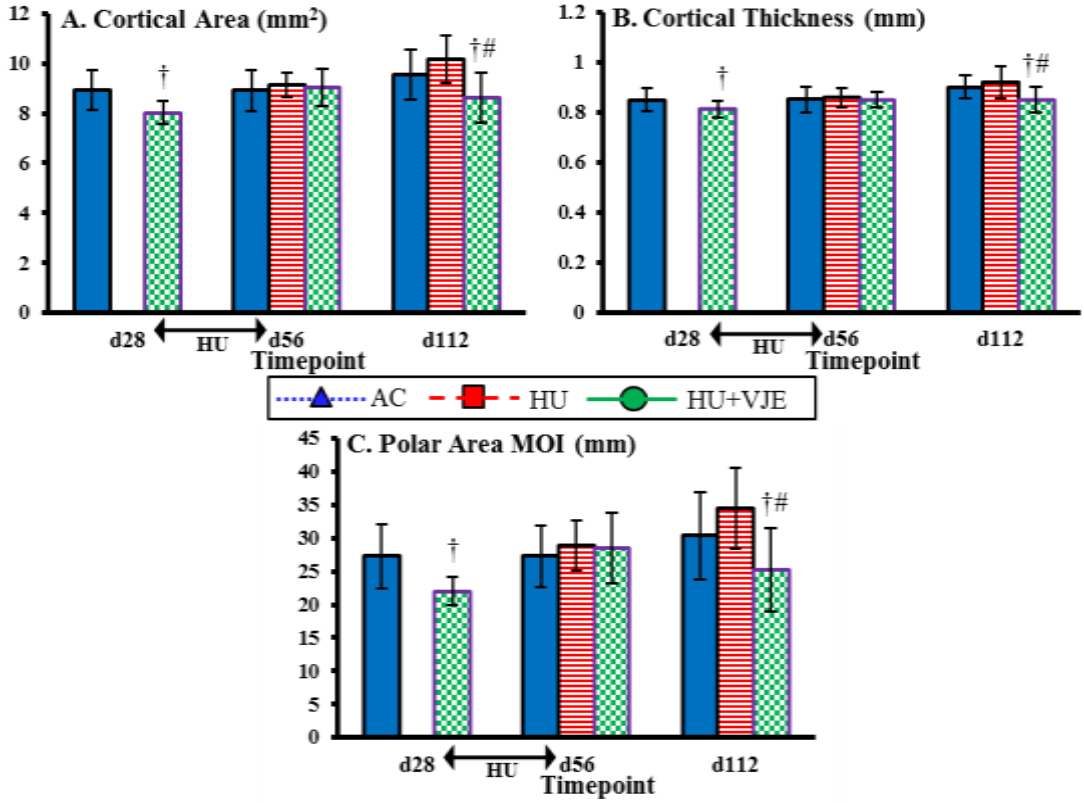

Figure 4.13 *Ex Vivo* pQCT Geometric Outcomes at the Femur Mid-Diaphysis for Exp. 2.
(A) Cortical Area, (B) Cortical Thickness (mm), (C) Polar Area MOI.
Data presented as mean ± SD.
† indicates significant difference from AC value at same time point, $p < 0.05$.
# indicates significant difference from HU value at same time point, $p < 0.05$.

4.2.2.5. Femoral Neck Densitometry and Geometry

HU-induced changes were observed for total vBMD (-7.1%, $p = 0.004$) in the femoral neck (FN) *ex vivo* pQCT densitometric results (Figure 4.14), and VJE pre-treatment protected against these changes. The HU group total vBMD values were significantly lower compared to the AC group (-5.0%, $p = 0.039$) at d112. For total BMC, the HU+VJE group was significantly lower compared to the AC group (-12.6%, $p = 0.006$) at d28 and compared to the HU group (-16.6%, $p = 0.001$) at d112. HU+VJE animals also had significantly higher total vBMD compared to AC animals (+6.0%, $p = 0.003$) at d28 and compared to HU animals (+9.1%, $p < 0.001$) at d112. No significant differences were observed at any time point for cancellous vBMD or cortical vBMD.

As for the geometric outcomes, HU-induced changes were observed for cortical thickness (-11.2%, $p = 0.007$), and VJE pre-treatment protected against these changes (Figure 4.15). Additionally, the HU group means were significantly higher compared to those for the AC group for both total bone area (+15.5%, $p = 0.021$) and polar area MOI (+22.4%, $p = 0.035$) at d112. Mean values for HU+VJE rats were significantly lower compared to those for AC rats (-17.4%, $p = 0.002$) at d28 and HU rats (-23.4%, $p < 0.001$) at d112 for total bone area. For cortical thickness, mean values for HU+VJE rats were significantly higher compared to those for AC (+8.9%, $p = 0.010$) at d28 and those for both AC (+9.9%, $p = 0.015$) and HU (+14.4%, $p = 0.002$) at d112. For polar area MOI, mean values for the HU+VJE group were significantly lower compared to those for AC (-22.0%, $p = 0.004$) at d28 and those for HU (+14.4%, $p < 0.001$) at d112.

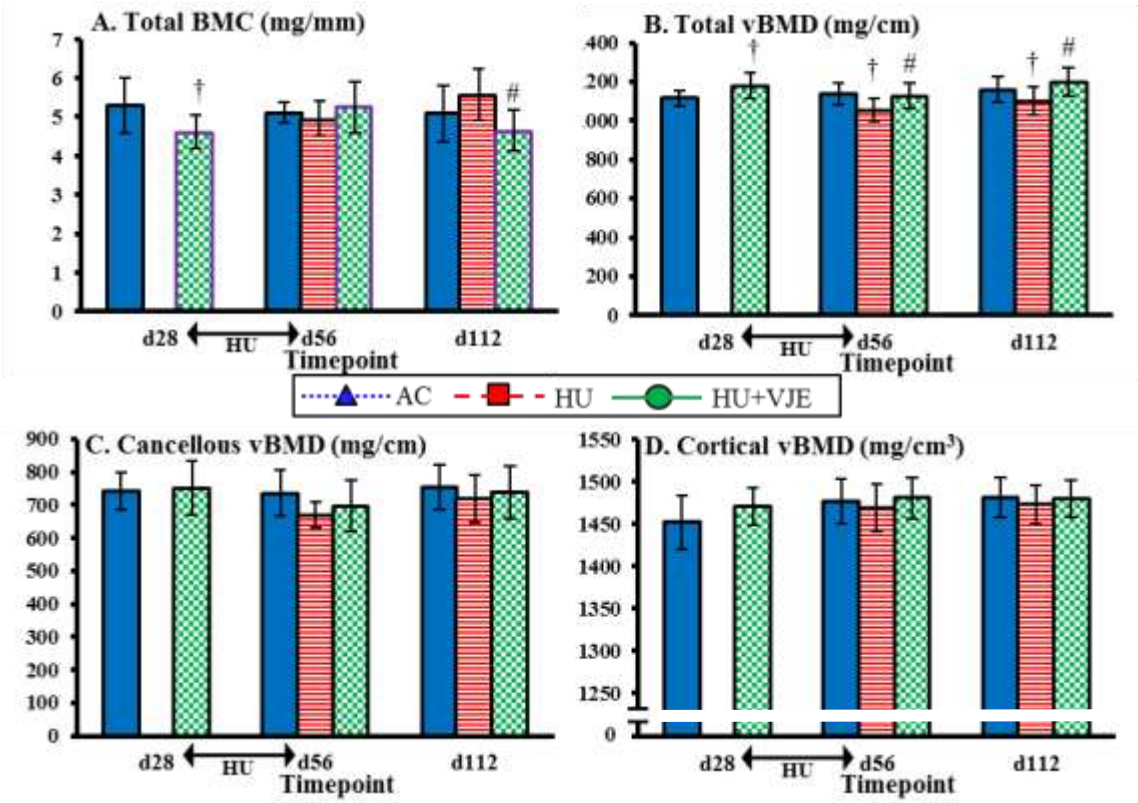

Figure 4.14 *Ex Vivo* pQCT Densitometric Outcomes at the Femoral Neck for Exp. 2.
(A) Total BMC, (B) Total vBMD, (C) Cancellous vBMD, (D) Cortical vBMD.
Data presented as mean ± SD.
† indicates significant difference from AC value at same time point, $p < 0.05$.
# indicates significant difference from HU value at same time point, $p < 0.05$.

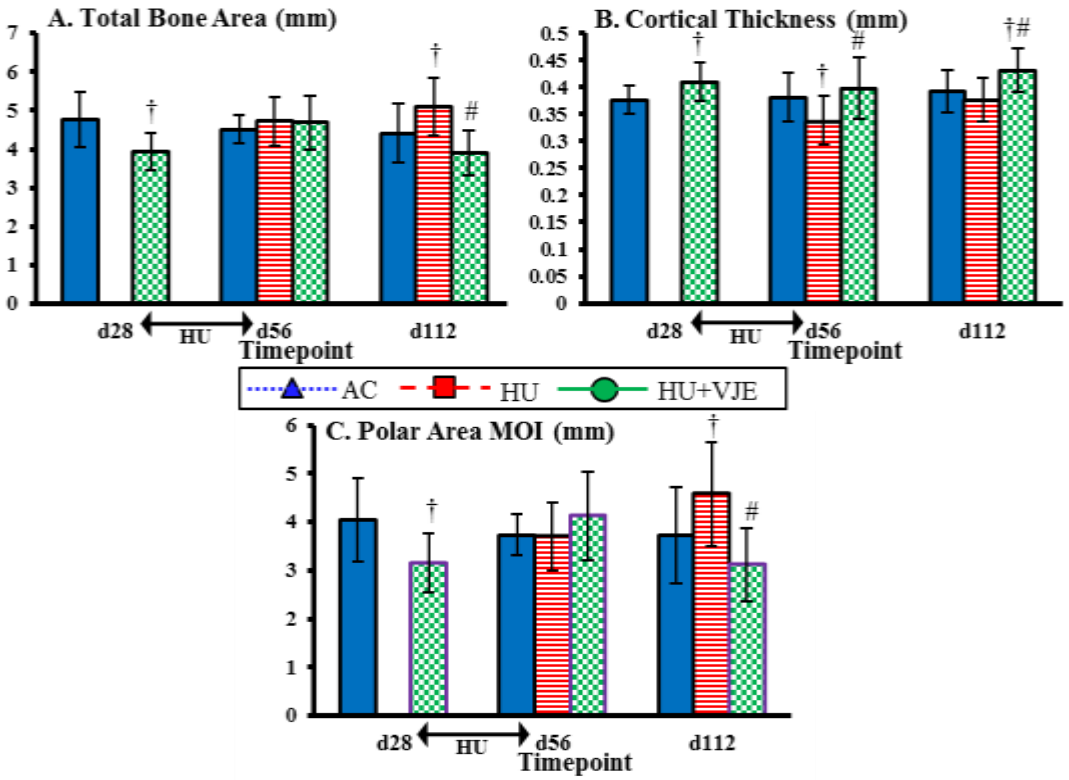

Figure 4.15 *Ex Vivo* pQCT Geometric Outcomes at the Femoral Neck for Exp. 2.
(A) Total Bone Area, (B) Cortical Thickness, (C) Polar Area MOI.
Data presented as mean ± SD.
† indicates significant difference from AC value at same time point, $p < 0.05$.
# indicates significant difference from HU value at same time point, $p < 0.05$.

4.2.3. *Ex Vivo* Micro-Computed Tomography

The cancellous compartment of the left proximal tibia metaphysis was also examined by μCT after euthanasia and tissue collection at d28, d56, and d112.

4.2.3.1. Proximal Tibia Metaphysis Cancellous Densitometry and Geometry

No HU-induced changes in the cancellous compartment were observed (Figure 4.16). However, HU+VJE had significantly higher % BV/TV (+49.2%, $p = 0.042$) and trabecular thickness (+13.6%, $p = 0.009$) compared to AC at d56. Trabecular separation (Tb.Sp.) for HU+VJE was also significantly higher compared to AC (+5.4%, $p = 0.021$) at

d28 and significantly lower compared to AC (-10.8%, p = 0.039) at d56. No significant differences in trabecular number (Tb.N.) were observed at any time point.

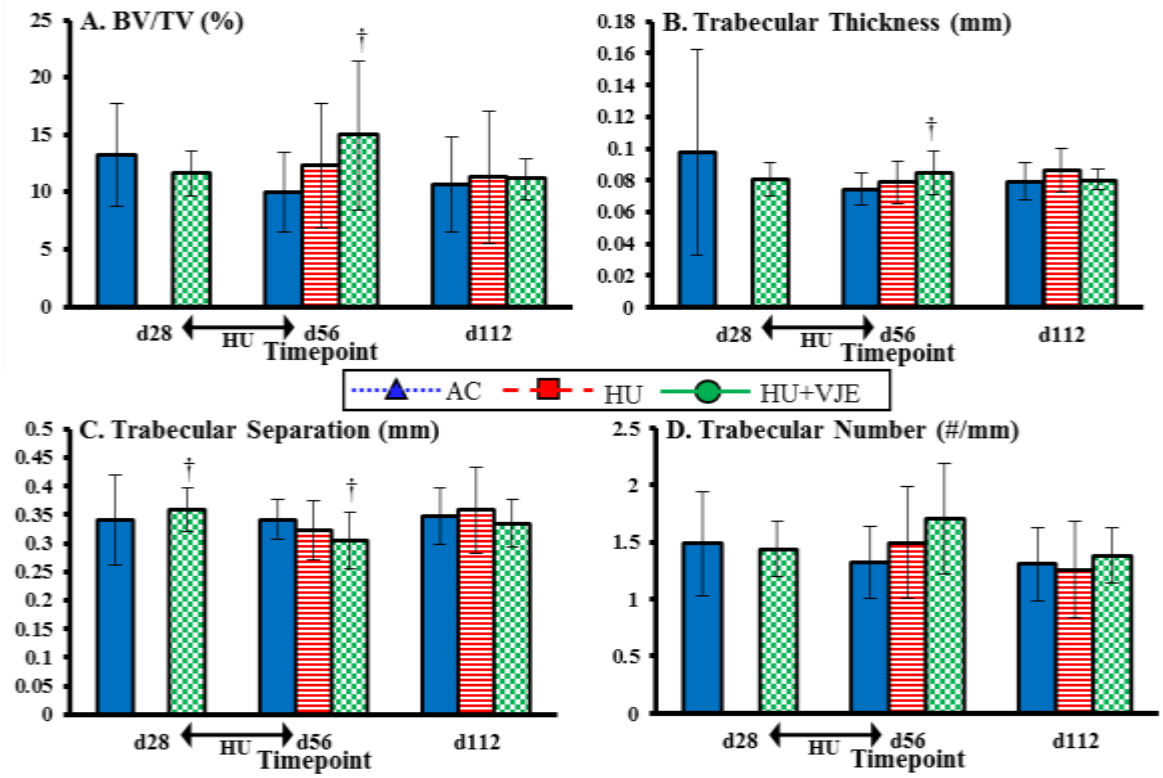

Figure 4.16 *Ex Vivo* µCT Cancellous Outcomes at the Proximal Tibia Metaphysis for Exp. 2.
(A) BV/TV, (B) Trabecular Thickness, (C) Trabecular Separation, (D) Trabecular Number.
Data presented as mean ± SD.
† indicates significant difference from AC value at same time point, $p < 0.05$.

4.3. Mechanical Testing

4.3.1. Tibia Mid-Diaphysis Three-Point Bending

Results of three-point bending at the left tibia diaphysis on d28, d56, and d112 (Table 4.3) reveal that the only significant difference observed due to HU was significantly higher energy to ultimate stress for the HU group compared to the AC group (+18.7%, $p = 0.047$) at d56. HU+VJE rats exhibited significantly higher ultimate force compared to AC rats (+12.0%, $p = 0.043$) at d56 and significantly higher post-yield displacement compared to both AC (+83.0%, $p < 0.001$) and HU (+120%, $p < 0.001$) rats at d112. HU+VJE animals also had significantly lower ultimate stress (-15.0%, $p = 0.014$) and elastic modulus (-17.9%, $p = 0.002$) compared to HU animals at d56.

4.3.2. Proximal Tibia Metaphysis Reduced Platen Compression

After three-point bending, RPC was performed on a section of the left proximal tibia metaphysis and intrinsic mechanical properties are reported in Table 4.4. HU-induced changes were observed in ultimate stress (-61.1%, $p = 0.001$) and energy to ultimate force (-64.5%, $p = 0.010$) for the mean values of HU group compared to those for the AC group. VJE pre-treatment was protective for both of these outcome variables. Additionally, the HU+VJE group had significantly higher elastic modulus compared to the HU group at d56 (+208%, $p < 0.001$) and d112 (+57.8%, $p = 0.039$). HU+VJE animals also had significantly higher ultimate stress compared to AC (+61.0%, $p = 0.013$) and HU (+107%, $p = 0.013$) animals, and significantly higher energy to ultimate force compared to HU animals (+119%, $p = 0.008$) at d112.

Table 4.3 Tibia Diaphysis Three-Point Bending Results for Exp. 2.

	Day	AC	HU	HU+VJE
Extrinsic Properties				
Stiffness (N/mm)	28	354.7 ± 50.4	-	354.0 ± 42.2
	56	352.2 ± 53.5	386.9 ± 44.5	385.3 ± 63.1
	112	387.2 ± 47.3	400.7 ± 32.8	380.8 ± 56.3
Ultimate Force (N)	28	123.0 ± 19.5	-	128.2 ± 16.8
	56	124.9 ± 15.6	138.8 ± 13.5	140.0 ± 20.2 †
	112	126.6 ± 23.5	124.2 ± 20.5	134.3 ± 16.2
Yield Force (N)	28	89.8 ± 13.4	-	96.5 ± 11.8
	56	92.2 ± 17.0	102.4 ± 12.0	102.5 ± 17.0
	112	96.7 ± 12.1	96.9 ± 16.2	103.0 ± 12.6
Post-Yield Displacement (mm)	28	0.43 ± 0.26	-	0.64 ± 0.16 †
	56	0.36 ± 0.19	0.43 ± 0.17	0.53 ± 0.24
	112	0.31 ± 0.21	0.26 ± 0.19	0.57 ± 0.18 †#
Energy to Ultimate Force (mJ)	28	40.8 ± 17.7	-	39.7 ± 8.73
	56	36.3 ± 11.9	43.1 ± 6.18 †	42.5 ± 14.3
	112	33.3 ± 15.0	34.8 ± 17.5	40.6 ± 10.5
Intrinsic Properties				
Ultimate Stress (MPa)	28	142.4 ± 22.5	-	154.4 ± 24.6
	56	140.4 ± 20.2	158.3 ± 23.4	134.5 ± 18.6 #
	112	139.4 ± 29.7	139.0 ± 24.0	152.2 ± 20.2
Elastic Modulus (GPa)	28	3.83 ± 0.50	-	3.94 ± 0.38
	56	3.71 ± 0.67	4.07 ± 0.62	3.34 ± 0.72 #
	112	3.70 ± 0.49	3.77 ± 0.63	3.95 ± 0.32

Data presented as mean ± SD.
† indicates significant difference from AC value at same time point, $p < 0.05$.
# indicates significant difference from HU value at same time point, $p < 0.05$.

Table 4.4 Proximal Tibia Metaphysis Reduced Platen Compression Results for Exp. 2.

	Day	AC	HU	HU+VJE
Ultimate Stress (MPa)	28	1.95 ± 1.14	-	2.83 ± 0.1.70
	56	1.60 ± 0.76	0.62 ± 0.48 †	2.11 ± 0.73 #
	112	1.77 ± 1.27	1.37 ± 1.20	2.85 ± 0.1.60 †#
Elastic Modulus (MPa)	28	30.5 ± 16.4	-	40.0 ± 33.2
	56	28.1 ± 21.6	10.4 ± 6.30	32.0 ± 17.1 #
	112	27.7 ± 23.3	23.3 ± 22.1	36.8 ± 23.6 #
Energy to Ultimate Stress (mJ)	28	1.82 ± 1.77	-	3.00 ± 2.62
	56	1.57 ± 1.01	0.56 ± 0.61 †	1.73 ± 1.05 #
	112	1.43 ±1.11	1.39 ± 1.50	3.05 ± 2.74 #
Strain at Ultimate Stress (%)	28	0.19 ± 0.12	-	0.21 ± 0.12
	56	0.19 ± 0.11	0.18 ± 0.094	0.15 ± 0.10
	112	0.16 ± 0.067	0.18 ± 0.11	0.22 ± 0.13

Data presented as mean ± SD.
† indicates significant difference from AC value at same time point, $p < 0.05$.
# indicates significant difference from HU value at same time point, $p < 0.05$.

4.3.3. Femur Mid-Diaphysis Three-Point Bending

Three-point bending of the left femur diaphysis was performed on femora collected at d28, d56, and d112 (Table 4.5). At the end of the exercise period (d28), HU+VJE animals had significantly lower ultimate force compared to AC animals (-7.9%, $p = 0.021$), and significantly higher yield force compared to AC animals (+8.9%, $p = 0.014$). The HU+VJE group values for ultimate stress were significantly higher compared to those for the AC group (+5.3%, $p = 0.009$) at d28, compared to those for the HU group (+11.0%, $p = 0.038$) at d56, and compared to those for both the AC (+14.1%, $p = 0.037$) and the HU (+16.3%, $p = 0.003$) groups at d112. The elastic modulus values for the HU+VJE group were significantly higher compared to those for the AC group (+19.7%, $p < 0.001$) at d28 and compared to those for both the AC (+29.5%, $p = 0.003$) and the HU (+62.7%, $p < 0.001$) groups at d112, while the elastic modulus values for the HU group were significantly lower compared to those for the AC group (-20.4%, $p = 0.013$) at d112.

Table 4.5 Femur Diaphysis Three-Point Bending Results for Exp. 2.

	Day	AC	HU	HU+VJE
Extrinsic Properties				
Stiffness (N/mm)	28	576.7 ± 93.6	-	559.3 ± 57.0
	56	613.4 ± 91.9	588.6 ± 108.6	593.4 ± 111.8
	112	609.3 ± 135.4	537.4 ± 138.4	659.2 ± 127.7
Ultimate Force (N)	28	261.5 ± 22.9	-	240.8 ± 22.7 †
	56	262.3 ± 27.4	262.7 ± 19.6	275.3 ± 27.1
	112	270.7 ± 41.7	283.6 ± 26.8	269.5 ± 38.2
Yield Force (N)	28	160.0 ± 34.3	-	174.3 ± 14.9 †
	56	164.7 ± 43.7	156.7 ± 29.5	169.1 ± 31.4
	112	186.0 ± 38.4	194.7 ± 61.6	185.3 ± 26.2
Post-Yield Displacement (mm)	28	0.51 ± 0.15	-	0.46 ± 0.09
	56	0.50 ± 0.13	0.49 ± 0.19	0.52 ± 0.13
	112	0.41 ± 0.18	0.44 ± 0.16	0.44 ± 0.07
Energy to Ultimate Force (mJ)	28	125.4 ± 22.7	-	112.5 ± 21.6
	56	123.8 ± 25.8	121.7 ± 38.8	134.7 ± 39.0
	112	128.7 ± 43.8	141.3 ± 27.1	113.7 ± 20.9
Intrinsic Properties				
Ultimate Stress (MPa)	28	144.1 ± 24.8	-	151.7 ± 10.6 †
	56	142.5 ± 17.4	133.3 ± 15.3	148.0 ± 24.0 #
	112	138.3 ± 27.2	135.6 ± 16.1	157.7 ± 10.0 †#
Elastic Modulus (GPa)	28	1.51 ± 0.26	-	1.81 ± 0.24 †
	56	1.63 ± 0.39	1.43 ± 0.28	1.49 ± 0.28
	112	1.46 ± 0.42	1.16 ± 0.35 †	1.89 ± 0.26 †#

Data presented as mean ± SD.
† indicates significant difference from AC value at same time point, $p < 0.05$.
# indicates significant difference from HU value at same time point, $p < 0.05$.

4.3.4. Femoral Neck Mechanical Test

Femoral neck mechanical testing was performed on specimens collected on d28, d56, and d112 (Figure 4.17). HU+VJE rats had significantly higher ultimate force compared to AC rats (+9.0%, p = 0.036) at d28. Stiffness for HU+VJE animals was also significantly higher compared to AC animals at d28 (+30.7%, p = 0.034) and d56 (+29.7%, p = 0.017), but significantly lower compared to HU animal (-20.9%, p = 0.031) at d112. No significant differences were observed at any time point for energy to ultimate force.

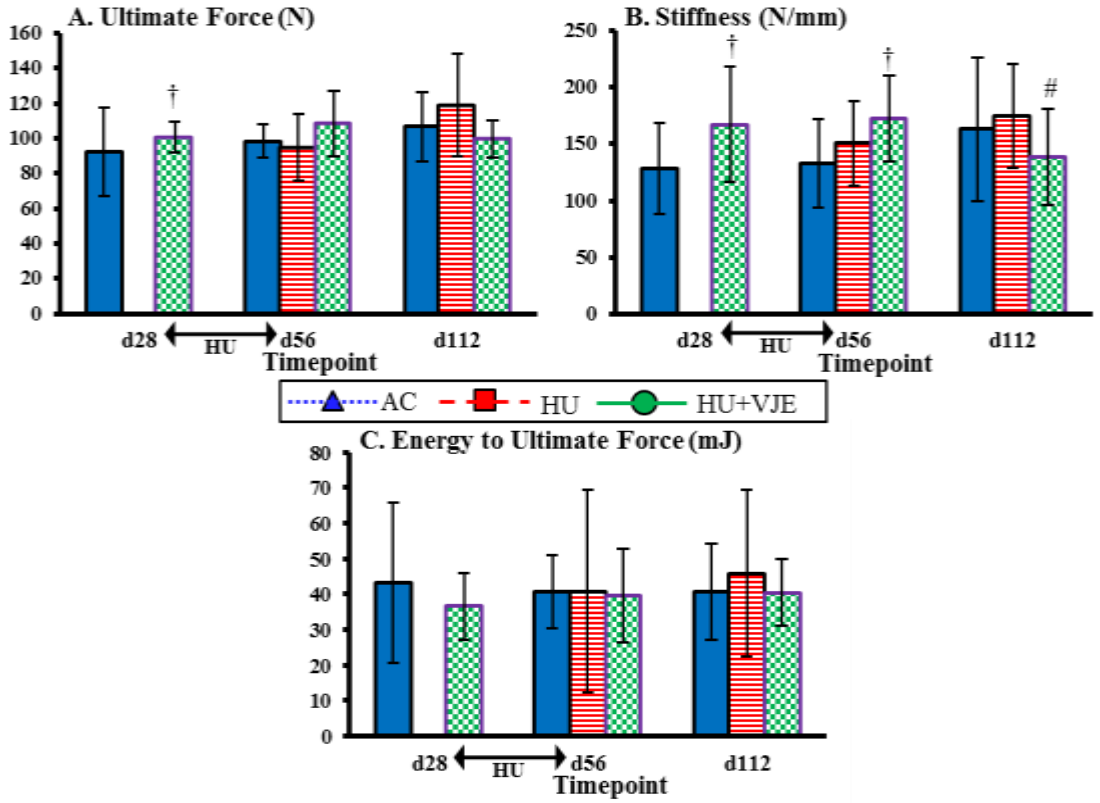

Figure 4.17 *Ex Vivo* Femoral Neck Mechanical Test Outcomes for Exp. 2.
(A) Ultimate Force, (B) Stiffness, (C) Energy to Ultimate Force.
Data presented as mean ± SD.
† indicates significant difference from AC value at same time point, $p < 0.05$.
# indicates significant difference from HU value at same time point, $p < 0.05$.

4.4. Histomorphometry

4.4.1. Proximal Tibia Metaphysis Static Cancellous Histomorphometry

Figure 4.18 displays the results of static histomorphometry performed on four sections of the proximal tibia metaphysis collected at d28, d56, and d112. HU+VJE animals exhibited significantly lower relative osteoclast surface (Oc.S/BS) at d28 compared to AC animals (-56.3%, $p = 0.035$) and at d112 compared to HU animals (-44.4%, $p = 0.014$). For relative osteoid surface (OS/BS), HU+VJE animals had significantly higher values compared to those for AC animals (+166%, $p = 0.017$) at d28, and significantly lower compared to those for both AC (-83.7%, $p < 0.001$) and HU (-73.5%, $p = 0.027$) animals at d56.

4.4.2. Proximal Tibia Metaphysis Dynamic Cancellous Histomorphometry

Dynamic histomorphometry was performed on the cortical bone in the proximal tibia metaphysis at d28, d56, and d112. The HU group had significantly lower MS/BS (-44.8%, $p = 0.018$) compared to the AC group at d56, whereas the HU+VJE group had significantly higher MS/BS (+26.3%, $p = 0.039$) and BFR/BS (37.5%, $p = 0.030$) compared to the AC group at d28 (Table 4.6).

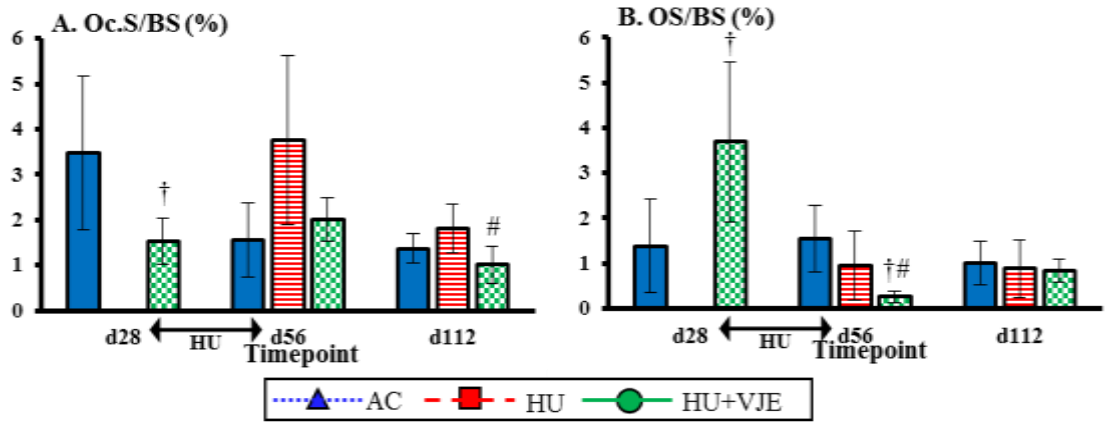

Figure 4.18 Static Histomorphometry Outcomes at the Proximal Tibia Metaphysis for Exp. 2.
(A) Oc.S/BS, (B) OS/BS. † indicates significant difference from AC value at same time point, $p < 0.05$. Data presented as mean ± SD.
# indicates significant difference from HU value at same time point, $p < 0.05$.

Table 4.6 Proximal Tibia Metaphysis Dynamic Cancellous Histomorphometry Results for Exp. 2.

	Day	AC	HU	HU+VJE
MS/BS (%)	28	5.19 ± 1.21	-	6.55 ± 1.51 †
	56	3.62 ± 1.43	2.00 ± 0.69 †	2.33 ± 1.16
	112	5.51 ± 0.97	3.97 ± 2.47	4.20 ± 1.06
MAR (μm/day)	28	0.92 ± 0.14	-	1.01 ± 0.16
	56	0.81 ± 0.28	0.57 ± 0.46	0.51 ± 0.38
	112	0.88 ± 0.13	0.79 ± 0.23	0.81 ± 0.16
BFR/BS ($\mu m^3/\mu m^2$/day)	28	0.048 ± 0.013	-	0.066 ± 0.020 †
	56	0.028 ± 0.011	0.013 ± 0.013	0.013 ± 0.012
	112	0.049 ± 0.014	0.033 ± 0.026	0.035 ± 0.014

Data presented as mean ± SD.
† indicates significant difference from AC at same time point, $p < 0.05$.

5. DISCUSSION

The purpose of this study was twofold. The first purpose was to evaluate the skeletal effects of a single period of bisphosphonate treatment, either alendronate (ALN) or zoledronate (ZOL), at multiple bone sites in adult rats following multiple periods of hindlimb unloading (HU). This was investigated in Experiment 1. The purpose of Experiment 2 was to develop and validate a positive reinforcement based model of voluntary jumping exercise (VJE) as a countermeasure to HU-induced bone loss in skeletally mature male rats.

5.1. Experiment 1

Our hypothesis that the protective effects of bisphosphonate treatment would continue to prevent bone loss through two 28-day periods of HU and an intervening 56 days of recovery was supported by the results of this study. ALN treatment administered by three subcutaneous injections (2.4 μg/kg body mass) three times per week starting one week before the initiation of HU was protective against bone mass and density losses, as well as against changes to the trabecular microarchitecture in the proximal tibia metaphysis (PTM), throughout the study period. ZOL treatment administered in one 60 μg/kg body mass injection seven days prior to the first HU was overprotective against these same changes during the course of the study. Treatment by both bisphosphonates resulted in bone mass and density values that were not significantly different or were significantly higher compared to the aging control (AC) animals at the end of the first

HU period, throughout the 56-day recovery period, and at the end of the second bout of HU.

Our hypothesis that ZOL treatment would be more successful at preventing the detrimental effects of disuse on bone strength and quality compared to ALN treatment was also supported by the results of this study. The HU+ZOL group had significantly higher bone densitometric and geometric values compared to both the AC and HU+ALN groups throughout the study. Bone strength as assessed by femoral neck mechanical testing and reduced platen compression (RPC) of the proximal tibia metaphysis also trended higher for the HU+ZOL group compared to both the AC and HU+ALN groups, but differences were not statistically significant.

5.1.1. Densitometry and Morphology

The densitometric, morphological, and microarchitectural findings of Experiment 1 were threefold. First, 28 days of HU without countermeasure induced significant changes in proximal tibia bone density and morphology that were partially recovered during the 56 days following HU. Second, the magnitude of bone densitometric and morphologic changes resulting from a subsequent HU period following recovery was reduced compared to that of the first HU period. Third, treatment with both ALN and ZOL was successful as a countermeasure to densitometric and morphologic changes, preventing bone loss and geometric changes through both HU periods. Table 5.1 summarizes the densitometric and morphologic results from Experiment 1.

Table 5.1 Summary of Experiment 1 Densitometric and Morphologic Results.
Trend directionality is noted by up or down arrows where statistically significant. Greater magnitude of change is indicated by double-arrows.

Bone Site	Group	*Ex vivo* pQCT (d112)	*In vivo* pQCT				µCT (d112)
			d28	d56	d84	d112	
PTM Cancellous	AC	-	-	↓	↓↓	↓↓	-
	HU	-	↓	↓	↓↓	↓↓	-
	HU+ALN	-	-	-	-	-	↑↑
	HU+ZOL	↑↑	-	-	-	-	↑↑
PTM Cortical	AC	-	-	↑	↑	↑	-
	HU	-	-	-	↑	↑	-
	HU+ALN	-	↑	↑	↑	↑	-
	HU+ZOL	↑↑	↑↑	↑↑	↑↑	↑↑	-
TD	AC	↑	↑	↑	↑	↑	
	HU	↑	-	-	-	↑	
	HU+ALN	↑	↑	↑	↑	↑	
	HU+ZOL	↑	↑	↑	↑	↑	
DFM	AC	-	HU		HU		
	HU	-					
	HU+ALN	-					
	HU+ZOL	↑↑					
FD	AC	↑					
	HU	↑					
	HU+ALN	↑					
	HU+ZOL	↑↑					
FN	AC	-					
	HU	-					
	HU+ALN	↑					
	HU+ZOL	↑					

During the first HU period, results from *in vivo* peripheral quantitative computed tomography (pQCT) of the proximal tibia metaphysis indicate that total BMC, total vBMD, and cortical thickness suffered HU-induced changes, as the HU group had significantly lower values for these three outcomes at day 28 (end of first HU) compared to baseline and the AC group. The HU group also had significantly decreased cancellous vBMD compared to baseline, while the AC group did not. For the second HU period, cancellous vBMD was significantly different pre- to post-HU for the HU group, and the HU group also had significantly lower total BMC compared to baseline at day 112 (end of second HU), but did not at day 84 (end of recovery, start of second HU). Additionally, the soleus wet masses for the HU, HU+ALN, and HU+ZOL groups were significantly lower compared to both the BC and AC groups at day 112. The soleus is a postural muscle in the hindlimb composed mainly of slow-twitch muscle fibers. Reduction in soleus wet mass has previously been found to be a good indicator of successful unloading (Shirazi-Fard et al., 2013a, Shirazi-Fard et al., 2013b). Taken together, these results indicate that during both the first and second HU periods, rats in the HU, HU+ALN, and HU+ZOL group were successfully unloaded, and rats that did not receive a countermeasure (HU group) suffered HU-induced bone loss.

The milder negative response of the bone density and morphology of the proximal tibia metaphysis to the second HU period is consistent with previous work (Gupta et al., 2013, Gupta et al., 2012). In 4-month-old male mice exposed for one, two, or three cycles of 2 weeks of HU plus 4 weeks of recovery, the degree of loss of trabecular bone volume (% BV/TV) and trabecular thickness was reduced for each

successive period of HU. The cumulative impact of multiple HU periods also resulted in compounded negative effects on trabecular microarchitecture suggesting that the 4 week recovery periods did not result in a return to baseline values (Gupta et al., 2013, Gupta et al., 2012). Later studies showed that increasing the recovery time between HU periods to 9 weeks did not promote recovery (Manske et al., 2015).

Previous work in our laboratory with 6-month-old male rats demonstrated reduced mechanosensitivity during a second HU period, but did not support the hypothesis of cumulative negative bone effects from multiple HU exposures (Shirazi-Fard et al., 2013a). Rats were exposed to 28 days of HU, followed by 56 days of recovery, followed by a second 28 days of HU, and then another 56 days of recovery. *In vivo* pQCT of the proximal tibia metaphysis revealed that total bone mineral content (BMC) decreased more during the first HU (-8.77%) than during the second HU (-2.80%), as did total volumetric bone mineral density (vBMD,-7.23%, -1.87% for first and second HU, respectively) and cortical thickness (-10.5%, -1.48% for first and second HU respectively). The present study had similar results for total BMC (-7.1%, -1.81%), total vBMD (-5.04%, -0.247%), and cortical thickness (-1.72%, 0.0%) losses during the first and second HU periods. Shirazi-Fard et al. (2013a) also failed to find any significant differences between pQCT bone density and geometry values or μCT trabecular microarchitecture values for the twice unloaded rats compared to age-matched rats that were exposed only to one (the second) HU period (Shirazi-Fard et al., 2013a).

Astronaut crewmembers experience more rapid bone loss than earth-bound elderly or osteoporotic populations (Lang et al., 2004, Lang et al., 2006). Additionally,

cancellous bone compartments, in particular, suffer more significant losses in density and microarchitecture in both human spaceflight (Carpenter et al., 2010, Vico et al., 2000) and ground-based rodent studies (Bloomfield et al., 2002),. Astronauts suffered significant losses in cancellous vBMD of the femoral neck as assessed by quantitative computed tomography (QCT); this measure of cancellous bone density never recovered to baseline values following return to normal weight-bearing activities on Earth, even after 2 – 4.5 years (Carpenter et al., 2010). Vico et al. (2017) monitored astronauts before and up to 1 year after their missions with high-resolution peripheral QCT (HR-pQCT), and found that total vBMD, cancellous vBMD, and cancellous BV/TV of the distal tibia suffered significant losses in many individuals during spaceflight that never recovered (Vico et al., 2017). As such, results for the cancellous compartment are of special interest in the present study.

Previous findings in our laboratory demonstrated significant age-related declines in pQCT-assessed cancellous vBMD of the proximal tibia metaphysis in aging control (AC) male rats from 6 to 10 months of age, such that cancellous vBMD losses due to multiple HU exposures were not significantly different from the losses in the AC group after the end of the second HU period (Shirazi-Fard et al., 2013a). Additionally, proximal tibia metaphysis % BV/TV and trabecular thickness values assessed by μCT were not significantly different for the HU group compared to the AC at the end of the second HU (Shirazi-Fard et al., 2013a). Findings in the present study are consistent with these results. Both the HU and AC groups suffered significant losses in cancellous vBMD over the course of the study, and were not significantly different from each other

at any point in the study, though values for the HU group compared to those for the AC group trended lower at the end of the first (-12.7%) and second (-3.31%) HU periods. The HU group also did not have significantly different BV/TV or trabecular thickness compared to the AC group at the end of the second HU period (day 112). However, contrary to previous findings, trabecular number (Tb.N.) for the AC and HU groups was significantly lower at day 112 (end of second HU) compared to baseline controls (BC) and the AC and HU group trabecular thickness values were not significantly different from BC. Previously, rats exposed to multiple HU periods suffered loss in proximal tibia metaphysis % BV/TV through trabecular thinning while trabecular number remained constant for both AC and HU groups (Shirazi-Fard et al., 2013a). Data from time points other than day 112 (end of second HU) of the present study would be necessary to fully elucidate why this difference occurred.

Data from the present study confirm the cortical thinning in the proximal tibia found in previous work in our laboratory (Shirazi-Fard et al., 2013a, Shirazi-Fard et al., 2013b). Cortical thickness was significantly lower at day 28 (end of first HU) for the HU group compared to the AC group. However, constant total bone area over the period between day 0 and day 28 suggests that this cortical thinning occurred due to bone resorption at the endocortical surface. Periosteal perimeter by μCT for the HU group was not significantly different from either the AC or BC groups, supporting this conclusion. Previously, total bone area decreased alongside cortical thickness during the first HU period, suggesting periosteal resorption (Shirazi-Fard et al., 2013a, Shirazi-Fard et al., 2013b).

Bisphosphonates are one of the most common clinical treatments for osteoporosis and other conditions with elevated bone resorption. An overwhelming number of studies have found that bisphosphonates excel at reducing osteoclast activity, bone loss, and fracture risk (Black et al., 2007, Cavanagh et al., 2005). The most recent NASA Bone Research and Clinical Advisory Panel meeting in 2016 resulted in a recommendation that all astronauts participating in missions longer than 6 months receive an intravenous infusion of zoledronate (ZOL) prior to launch as a countermeasure against microgravity induced bone density and strength losses (Sibonga et al., 2017). There are a wide variety of bisphosphonates available, with different hydroxyapatite binding affinities and anti-resorptive potencies (Russell et al., 2008). Bisphosphonates are very effective anti-resorptive agents, and bone quality gains resulting from their use are not just a result of reduced of bone resorption, but also an increase in secondary mineralization and continued formation in extant resorption cavities (Gasser, 2006).

Alendronate (ALN), one of the most regularly used bisphosphonates in the treatment of osteoporosis, was used in the only astronaut study to date investigating the efficacy of bisphosphonate treatment to prevent microgravity-induced bone loss (Sibonga et al., 2019). ALN has been shown to reduce the incidence of spine and hip fractures in patients with prior vertebral fractures or osteoporosis (Black et al., 1996, Black et al., 2000). However, 20% of astronaut participants (two astronauts out of a total of 10) were forced to drop out of the study due to negative gastrointestinal side effects resulting from ALN. Even when in normal gravity, oral administration of ALN can be

difficult, as the best way to avoid gastrointestinal side effects requires overnight fasting, taking without food, and remaining upright for 30 minutes after taking the pill. These strict requirements are a serious factor in reducing patient compliance with ALN treatment (Cramer et al., 2007) and are either impractical, or impossible, for most long-duration spaceflight scenarios.

ZOL is the most powerful bisphosphonate, with high binding affinity to hydroxyapatite, lengthy duration of effectiveness, and high anti-resorptive potency (Grey et al., 2012, Russell et al., 2008). ZOL is also significantly easier to administer than ALN and many other bisphosphonates, as only a single 5 mg intravenous infusion per year is necessary (Green et al., 1994). Zoledronate has been shown to reduce the incidence of vertebral fractures by 70% and hip fractures by 41% over 3 years in patients with prior vertebral fractures or osteoporosis (Black et al., 2007). Intravenous infusion prior to spaceflight would have the added benefit of allowing flight surgeons to monitor for adverse side effects prior to takeoff. ZOL would also eliminate any need for astronauts to take oral doses during flight, and the beneficial skeletal effects would last for a number of years, which could be the length of future exploration class missions.

Few studies have examined the effectiveness of ALN treatment in rats exposed to disuse. Our dose of 2.4 μg/kg body mass via subcutaneous injection three times per week is equivalent to 1.0 mg/kg body mass of oral ALN in a 60 kg human, given a bioavailability of 0.6% for the oral dose (Allen et al., 2011). Mosekilde et al. (2000) used a model of unilateral hindlimb immobilization in 4-month-old female rats treated with a dose of 1.0 mg/kg body mass per day of oral ALN. After 28 days of hindlimb

immobilization, ALN treatment protected against whole tibia and proximal tibia metaphysis losses assessed by dual-energy x-ray absorptiometry (DXA) areal BMD (Mosekilde et al., 2000). Previous work in our laboratory and results from the present study confirmed these findings with total vBMD from pQCT (Swift et al., 2011).

In a study by Siu et al. (2013), 3-month-old male rats were given 1.0 mg/kg body mass per day of oral ALN during 28 days of hindlimb unloading. ALN treatment protected against the pQCT total and cancellous vBMD loss experienced by the HU control group at the distal femur, but not at the proximal tibia (Siu et al., 2013). In contrast, results from the present study demonstrated that ALN treatment did protect against total and cancellous vBMD losses in the proximal tibia metaphysis due to the first 28-day HU, and there were no significant losses from the second HU period for the HU group compared to AC. The HU group also had significantly lower distal femur metaphysis (DFM) cancellous vBMD compared to the BC group that was protected against by ALN treatment.

Our lab previously demonstrated that subcutaneous injections of 30 μg/kg body mass ALN per week protected against losses in pQCT-assessed total BMC, total and cancellous vBMD, but not total bone area at the proximal tibia metaphysis (Swift et al., 2011). Additionally, cortical BMC, cortical area, and polar area moment of inertia (MOI) at the tibia mid-diaphysis (TD) did not experience normal growth gains in either the HU control or ALN-treated groups (Macias et al., 2012). Results from the present study confirm that a lower, more clinically relevant dose of 2.4 μg/kg body mass ALN given via subcutaneous injections three times per week also protect against reductions in

these bone density values at the proximal tibia metaphysis. However, we did not see any change in total bone area due to HU in the present study. The lower dose of ALN in the present study also allowed normal growth gains in the tibia diaphysis for cortical BMC and cortical area, as well as cortical vBMD and cortical thickness. Polar area MOI did not experience any increases during the study period for any group.

We are not currently aware of any previous study in the literature on the efficacy of ZOL treatment in rats exposed to HU. However, a single study by Brouwers et al. (2008) of 35-week-old ovariectomized (OVX) female rats given 20 μg/kg body mass of ZOL via subcutaneous injection demonstrated that ZOL treatment completely prevented changes in the trabecular microarchitecture of the lumbar vertebrae. μCT demonstrated that % BV/TV and trabecular thickness reductions due to HU were protected against by ZOL treatment (Brouwers et al., 2008). In the present study, μCT was performed only at day 112 (end of the second HU), but the HU+ZOL and HU+ALN groups both had significantly higher BV/TV and trabecular thickness, and significantly lower trabecular separation (Tb.Sp.) compared to the AC and HU groups at the proximal tibia metaphysis.

In another study by Lloyd et al. (2008), 12-week-old mice were administered a single dose of 45 μg/kg body mass ZOL followed by 14 days of HU. ZOL treatment mitigated the proximal tibia metaphysis % BV/TV and trabecular connectivity reductions due to HU as assessed by μCT (Lloyd et al., 2008). As reported above for the present study, % BV/TV and trabecular thickness were significantly higher in the HU+ZOL group compared to both the AC and HU groups at day 112 (end of second

HU). Previous work in our laboratory showed similar results in male rats administered a single dose of 60 μg/kg body mass ZOL before 28 days of HU. Proximal tibia metaphysis total BMC, total vBMD, and cortical thickness were overprotected, and proximal tibia metaphysis trabecular microarchitecture as assessed by μCT was protected from HU-related loss by ZOL treatment (Boudreaux, 2014). The present study confirms these findings, as ZOL treatment was overprotective of pQCT total BMC, total vBMD, cancellous vBMD, and cortical thickness at the proximal tibia metaphysis, as well as % BV/TV, trabecular separation, and trabecular number at day 112 (end of second HU) via μCT of the proximal tibia metaphysis.

Ex vivo pQCT results from the present study were limited to day 112 (end of second HU). As the magnitude of bone density and morphology changes were smaller for the second HU compared to the first HU, it is not surprising that there were very few HU-induced changes in the femur or tibia at day 112. Total and cancellous vBMD were significantly lower for the HU group compared to the BC group at the proximal tibia metaphysis, and proximal tibia metaphysis HU group cortical thickness was significantly lower compared to both the AC and BC groups. ALN treatment was protective against reduced cancellous vBMD, but only ZOL treatment was overprotective against reductions in all three variables. Cancellous vBMD at the distal femur metaphysis was significantly lower for HU animals compared to BC animals, and ZOL treatment was overprotective against these changes as well. In the tibia diaphysis and femur mid-diaphysis, all groups experienced normal growth-related increases in all densitometric and geometric variables. At the femoral neck, HU group cancellous vBMD was

significantly reduced compared to the BC group, and the HU+ALN and HU+ZOL groups both had significantly higher values compared to the HU group.

5.1.2. Biomechanical Properties

Biomechanical data were obtained only at day 112 (end of the second HU) in the present study, and as such, no longitudinal comparisons throughout the study period are possible. The major biomechanical finding in Experiment 1 was that the mechanical properties of mid-diaphysis tibiae and femora were not significantly affected by two 28-day periods of HU separated by 56 days of recovery when compared to the aging controls. Additionally, neither ALN nor ZOL treatment resulted in any significant alteration to mechanical properties for the mean values of the HU+ALN and HU+ZOL groups compared to those for the AC and HU groups at the end of the study.

Bone strength and fracture resistance are determined by both bone quantity and bone quality (NIH Consensus Development Panel on Osteoporosis Prevention, 2001). Bone quality is a general term encompassing the various factors that influence bone strength, including structural properties (geometry, microarchitecture) and material properties (density, mineral content, microdamage accumulation, etc.), as well as the rate of bone turnover (Felsenberg and Boonen, 2005). As a result, predictions of mechanical strength based solely on densitometric changes tend to be inaccurate. Reductions in mechanical strength tend to be much larger than corresponding changes in vBMD (Marshall et al., 1996, Seeman and Delmas, 2006, Stone et al., 2003). Reductions in cancellous bone mass and density place a larger share of stress on cortical bone, which contributes to fracture but does not fully predict fracture risk (Marshall et al., 1996).

Similarly, changes in densitometric outcomes alone do not fully characterize the effects of bisphosphonate treatment (Benhamou, 2007). In spaceflight, reduction in finite element analysis based proximal femoral strength (0.6% - 3.9% per month) was notably higher than DXA aBMD losses (0.4% - 1.8% per month) (Keyak et al., 2009).

Fracture risk is of special importance in the case of astronauts, as the occurrence of a fracture during an exploration class mission could jeopardize the success of the mission and the safety of the crew. The "stabilize and transport" protocol currently in place for missions to the ISS, which would quickly return to Earth any astronaut suffering a fracture or other serious medical condition, would not be feasible for any mission passing beyond low Earth orbit (Hamilton et al., 2008). Procedural practices that reduce fracture risk, such as design safety specifications for ladders and codified limits on the weight astronauts may safely carry based on their to-date duration in microgravity have been captured by the Bone Fracture Risk Module established by researchers at NASA's Glenn Research Center (Lewandowski et al., 2007). Countermeasures such as pharmaceuticals that can further reduce fracture risk without impacting mission activities are therefore greatly desirable.

However, pharmaceutical countermeasures can introduce their own additional risks. Atypical femoral fracture (AFF), defined as an oblique fracture of the subtrochanteric or shaft regions of the femur, has been associated with long-term bisphosphonate use. Age-adjusted relative risk (RR, where values greater than 1 suggest the risk of an event is increased by exposure to a treatment) of AFF associated with bisphosphonate use was 55 in women and 54 in men in a group of 172 patients over age

55 with atypical femoral shaft fractures. Absolute risk was 11 in 10,000 for patients who used bisphosphonates for greater than 4 years; this risk decreased by 70% per year following discontinuation of bisphosphonate treatment (Schilcher et al., 2015). A systematic review of 25 studies found 3.0 - 9.8 AFF per 100,000 person-years, with RR increasing with length of bisphosphonate use (Khow et al., 2017).

The pathophysiology of AFF remains unclear, but a promising hypothesis is that increased matrix mineralization as a result of extended reduction of bone resorption can lead to reduced bone toughness and increased rate of crack initiation, which in turn increases the risk of crack propagation and fracture (Lloyd et al., 2017, Silverman et al., 2018). Another possibility is an accumulation of bone microdamage, also as a result of extended reduction of bone resorption. One year of ALN treatment in dogs increased the microdamage accumulation in the 9^{th} rib by 322% and three-point bending toughness was reduced significantly by 20% (Mashiba et al., 2000).

It is important to note that these risks are still relatively low in populations using bisphosphonates for an extended period of time and tend to occur in the elderly and/or those suffering from chronic disease. AFF is exceedingly rare in healthy, middle-aged populations. Astronauts are all healthy compared to the average population, and most are middle-aged at the time of their missions. Additionally, the longest exploration class mission currently in discussion would only last three years, and astronauts would likely only receive a single bisphosphonate dose during that time. It can be argued that the very low risk of AFF is thus seemingly outweighed by the risk of fracture associated with microgravity induced bone loss.

Of the studies that previously investigated the use of bisphosphonate treatment as a countermeasure to OVX or HU, only a handful collected biomechanical data, and all those data were collected at the end of a single HU period. Treatment with oral doses of 1.0 mg/kg body mass ALN per day mitigated reductions in femoral neck ultimate force due to 28 days hindlimb immobilization in 4-month-old female rats (Mosekilde et al., 2000). In the study by Siu et al. (2013), 3-month-old male rats exposed to 28 days of HU also showed significant reductions in femur three-point bending ultimate force and stiffness. Oral treatment with 1.0 mg/kg body per day (with bioavailability equal to 0.6%, this dose is equal to 7.0 μg/kg body mass per week ALN via subcutaneous injection) protected against the loss in stiffness, but not the loss in ultimate force (Siu et al., 2013).

Only a single previous study in the literature investigating ZOL treatment in rodents reported biomechanical results (Lloyd et al., 2008). ZOL treatment (single 45 μg/kg body mass injection) in 12-week-old female mice exposed to 14 days of HU mitigated femur three-point bending ultimate and yield force reductions due to HU (Lloyd et al., 2008). Previous work in our laboratory demonstrated that ZOL treatment (single 60 μg/kg body mass injection) protected against HU-induced reductions in ultimate force and energy to ultimate force for the femoral neck mechanical test. Tibia three-point bending ultimate stress was also significantly lower for HU animals compared to AC animals, and ZOL treatment similarly protected against this change (Boudreaux, 2014).

In the present study, femoral neck mechanical test and three-point bending data were collected only at day 112 (end of the second HU period). As reported above, changes in bone densitometric and geometric properties were greatly reduced for the second HU period compared to the first HU period. As such, it is not surprising that very few changes in mechanical properties were observed at the end of the second HU period. No significant differences between groups were found in femoral neck mechanical test outcome variables; tibia three-point bending results revealed significantly higher mean stiffness values for all groups compared to the BC group; and femur three-point bending results demonstrated significantly higher mean values for ultimate and yield force for all groups compared to the BC group, as well as significantly higher mean stiffness values for the HU+ZOL group compared to the BC group.

The results in the present study for tibia and femur three-point bending correspond very well to the *in vivo* and *ex vivo* densitometric values at day 112 (end of second HU). *In vivo* pQCT of the tibia diaphysis did not show significant differences between groups for any outcome variables at day 112. Similarly, *ex vivo* pQCT of the tibia diaphysis and femur diaphysis showed only significantly higher outcome variables compared to BC animals and no differences between groups at day 112. Mechanical outcome variables for tibia and femur three-point bending showed no differences between groups at day 112, matching perfectly with the trends from pQCT.

In the present study, we examined the femoral neck because it is an important clinical site in humans, as osteoporotic fracture most commonly occurs in the femoral neck and intertrochanteric hip. In the year following a hip fracture, patients older than 50

suffer 8% - 36% excess mortality and 60% of hip fracture patients do not fully regain their pre-fracture level of independence (Abrahamsen et al., 2009, Cosman et al., 2014). Rat and human femoral necks differ in that rats have a thicker cortical shell compared to the human femur, but the clinical importance of the site maintains our interest (Bagi et al., 1997). Another important difference is that humans are bipedal and rats are quadrupedal, so the precise mechanical loading differs appreciably. Nevertheless, the rat femoral neck is another site in the hindlimbs with a mix of both cortical and cancellous bone. Despite these differences, previously published work has documented HU-induced losses in femoral neck bone strength in rats. 5- to 6-month-old female rats exposed to 21 days of HU demonstrated significantly reduced femoral neck stiffness and energy to ultimate force compared to control animals (Peres-Ueno et al., 2017).

In the present study, no significant differences between groups were found for any of the extrinsic outcome variables reported for the femoral neck mechanical test. This corresponds with the very few number of significant differences found in *ex vivo* pQCT of the femoral neck. Ultimate force did trend slightly lower for HU animals, and trended comparatively higher for HU+ALN and HU+ZOL animals, which could reflect the significantly lower femoral neck cancellous vBMD for the HU group compared to the BC group and the significantly higher cancellous vBMD for the HU+ALN and HU+ZOL groups compared to the HU group. Previous work in our laboratory has shown that mechanical test outcome variables generally have higher variability compared to densitometric outcome variables, and this higher variability could be masking relatively small changes in mechanical outcomes produced by the few significant differences

between groups observed in *ex vivo* femoral neck pQCT (Shirazi-Fard et al., 2013a, Shirazi-Fard et al., 2013b, Swift et al., 2013).

Similarly, no significant differences between groups for any proximal tibia metaphysis RPC outcome variables were observed at day 112 (end of the second HU period). The only significant differences between groups for *in vivo* pQCT of the proximal tibia metaphysis were significantly higher values for HU+ZOL animals compared to AC and HU animals in total BMC, total and cancellous vBMD, cortical vBMD, and cortical thickness at day 112. The HU+ALN group also had significantly higher cancellous vBMD compared to the HU and AC groups at day 112, as ALN treatment prevented age-related losses in cancellous bone density. *Ex vivo* pQCT at the proximal tibia metaphysis similarly revealed higher total BMC, total, cancellous, and cortical vBMD, and cortical thickness for HU+ZOL animals compared to AC and HU animals at day 112, while HU+ALN rats had significantly higher cancellous vBMD compared to HU rats at day 112. The HU+ZOL and HU+ALN groups both had significantly higher proximal tibia metaphysis % BV/TV and trabecular number and significantly lower trabecular separation compared to the AC and HU groups at day 112 as assessed by *ex vivo* μCT. HU+ZOL values for all four reported proximal tibia metaphysis RPC intrinsic mechanical outcomes trended higher than AC and HU values, which corresponds strongly with the relationships among groups for *in vivo* and *ex vivo* densitometric values at the proximal tibia metaphysis on day 112. Additionally, ultimate stress, energy at ultimate stress, and strain at ultimate stress all trended higher for HU+ALN animals compared to HUanimals , though to a lesser degree than HU+ZOL

animals. This also corresponds well with the relatively fewer significant differences found between the HU+ALN and HU groups in the day 112 densitometric results.

I would speculate that more statistically significant differences in mechanical properties among groups would have been observed at time points earlier in the study, especially at the end of the first HU period (day 28). Specimens collected at the end of the study (day 112) have been through 56-days of recovery after the initial HU period. This could have allowed any HU-induced negative effects on bone strength to partially recover. As discussed above, the exposure to a second HU period results in reduced mechanosensitivity and consequently reduced magnitudes of loss in bone density, morphology, and strength. Recovery followed by the reduced bone loss during the second HU period could have prevented significant differences in mechanical properties from being observed at day 112.

5.1.3. Bone Turnover

The key histomorphometric findings in Experiment 1 were twofold. First, bisphosphonate treatment significantly reduced bone resorption, and HU significantly reduced bone formation following two 28-day periods of HU and an intervening 56-day recovery period. Second, the HU group had significantly increased bone formation after the recovery period, while the bisphosphonate-treated groups did not.

The rate at which bone turnover occurs dictates how much and how quickly bone changes in response to mechanical stimuli. Consistently, the rate of bone resorption increases and the rate of bone formation decreases in response to unloading, whether in rodents exposed to spaceflight or to ground-based HU. Bone formation in 10-week-old

mice flown on STS-108 for 12 days was 60% lower than ground controls, and serum tartrate resistant acid phosphatase isoform 5b (TRAcP5b) levels were significantly elevated for spaceflight mice compared to ground controls (Bateman and Countryman, 2002, Lloyd et al., 2015). TRAcp5b is a biomarker of osteoclast number that has been shown to predict bone fracture in elderly women (Gerdhem et al., 2004). In 3-month-old mice exposed to 21 days of HU, mineral apposition rate (MAR) was significantly lower compared to control animals, and sclerostin was significantly reduced in control animals compared to HU animals (Spatz et al., 2013). Sclerostin is a protein secreted by osteoclasts that inhibits Wnt signaling, resulting in increased osteoclast differentiation and activity.

Only one previous study in the literature investigating the effects of bisphosphonate treatment on HU reported histomorphometry results. Lloyd et al. exposed female 12-week-old mice to 14 days of HU. HU resulted in reduced total, periosteal, and endocortical bone formation rates (BFR) compared to loaded controls, but ZOL treatment (single 45 μg/kg body mass injection) even further significantly reduced total and endocortical BFR compared to HU animals not receiving ZOL (Lloyd et al., 2008). Previous work in our laboratory demonstrated that 30 μg/kg body mass of subcutaneously injected ALN per week did not prevent reductions in mineralizing surface to total bone surface ratio (MS/BS), MAR, and BFR at the proximal tibia metaphysis in 6-month-old male rats exposed to 28 days of HU (Swift et al., 2011). Similarly, tibia diaphysis MS/BS, MAR, and BFR at both the periosteal and endocortical surfaces was significantly lower for the ALN treated group compared to both the AC and

HU control groups (Macias et al., 2012). Additionally, proximal tibia metaphysis % BV/TV and trabecular thickness assessed by static histomorphometry were lower in the ALN treated group after HU compared to the AC group. Relative osteoid surface (OS/BS) and relative osteoblast surface (Ob.S/BS) were significantly lower for the ALN-treated group compared to both the AC and HU control groups (Swift et al., 2011).

In the present study, dynamic histomorphometry of the tibia diaphysis was performed in the middle (day 56) and at the end (day 84) of recovery. Previous studies in our laboratory have collected histomorphometric data at the end of HU periods, and results consistently demonstrated that bisphosphonate treatment did not improve reductions in MS/BS, MAR, and BFR due to HU, and potentially caused further reductions in bone formation (Boudreaux, 2014, Swift et al., 2011). Therefore, we decided to examine the impact of bisphosphonate treatment on the recovery of histomorphometric outcomes following a period of HU. Midway through recovery (day 56), significantly higher MAR was observed in the HU group compared to the AC group. At day 84 (end of recovery), MS/BS, MAR, and BFR were all significantly higher for the HU group compared to the AC group. No significant differences between the bisphosphonate-treated groups and the AC group were identified at either time point.

One plausible explanation for this discrepancy between the histomorphometric results for the HU group and the bisphosphonate-treated groups during recovery might be differing strain magnitudes or distributions following the first HU period. Results from pQCT of the tibia diaphysis did not demonstrate significant reductions in bone densitometric or geometric outcomes at the end of the first HU period. However, *in vivo*

pQCT of the proximal tibia metaphysis indicated that the HU group had significantly lower total BMC and vBMD compared to the AC group, and significantly reduced cancellous vBMD compared to the baseline HU value (day 0). Conversely, the ALN and ZOL treated groups did not incur any significant bone mass or density losses as a result of the first HU period. The significantly higher bone formation outcomes in the HU group after reambulation are potentially caused by the HU-induced bone mass and density loss resulting in higher strains when the mechanical load is instantaneously returned to normal once animals are removed from the suspension apparatus. The ALN and ZOL treated groups did not lose bone mass and density during HU, and therefore presumably did not suffer higher than normal strains that would necessitate compensatory rapid bone formation. Higher strain magnitudes at the proximal tibia metaphysis could result in higher histomorphometric outcomes for the whole bone, or strain distribution changes at the proximal tibia metaphysis could directly affect the strain distributions in the tibia diaphysis.

Static histomorphometry at the distal femur metaphysis was performed on bone samples collected at the end of the second HU period (day 112). HU resulted in lower relative osteoid surface, significant only in the HU+ALN group (vs. the HU group) and the HU+ZOL group (vs. the AC and HU groups), though the HU group trended lower. The more powerful bisphosphonate, ZOL, decreased relative osteoid surface even further than HU alone, while ALN did not. Relative osteoclast surface (Oc.S/BS) was significantly lower for the HU+ZOL group compared to the AC and HU groups, which is expected since bisphosphonate treatment functions by reducing osteoclast activity.

While not significant, the HU+ALN group also had reduced relative osteoclast surface. The effects of ALN treatment would be expected to begin wearing off sooner than those of ZOL treatment as a result of ALN's lower binding affinity and anti-resorptive potency, which likely explains the lack of significance. More data at time points throughout the study would be required for a definitive answer.

No significant differences between groups were found for % BV/TV, trabecular thickness, trabecular separation, or trabecular number at the distal femur metaphysis derived from static histomorphometry, though the trends of all four outcomes correspond to results from μCT of the proximal tibia metaphysis. μCT is able to cover a much larger bone volume for these measures, so it is possible that μCT of the distal femur metaphysis would produce observable significant differences.

5.2. Experiment 2

Our hypothesis that 28 days of VJE pre-treatment would preserve bone strength and quality during a subsequent 28 days of unloading was supported by the results from the present study. VJE consisting of 30 jumps/day, 5 days/week for 28 days increased bone density and geometry outcomes at day 28 (end of exercise) and resulted in significantly higher bone densitometric, geometric, and trabecular microarchitectural outcomes for HU+VJE animals at day 56 (end of HU) at the proximal tibia metaphysis, tibia diaphysis, distal femur metaphysis, and femoral neck compared to aging and HU controls. Direct measures of bone strength through mechanical testing of the proximal tibia metaphysis, tibia diaphysis, femur diaphysis, and femoral neck suggested higher femur diaphysis and femoral neck strength at day 28 (end of exercise) for HU+VJE

animals compared to aging controls and higher proximal tibia metaphysis, tibia diaphysis, femur diaphysis, and femoral neck strength at day 56 (end of HU) for HU+VJE animals compared to HU controls.

Support for our hypothesis that the beneficial effects of VJE pre-treatment would not extend to the recovery period following 28 days of unloading in the results from the present study was mixed and depended on bone site. Despite other work showing persistent benefits of exercise even a year after the conclusion of the exercise protocol in humans (Karinkata et al., 2009) and 14 weeks after exercise cessation in rats (Jarvinen et al., 2003), previous work in our laboratory found that a different form of jumping resistance exercise prior to HU did not reduce the rate of bone loss, but merely allowed bone measures to start at a higher point prior to unloading (Shirazi-Fard et al., 2014). Subsequent recovery after exercise and unloading was not previously studied, but we hypothesized that without further exercise, bone densitometric and strength outcomes would return to normal levels after significant loss during HU.

In the present study, values for bone density and geometry at the femur diaphysis and the cortical compartment of the proximal tibia metaphysis were largely found to be significantly lower for HU+VJE animals compared to aging and HU controls at day 112 (end of recovery). Additionally, densitometric outcomes at the tibia diaphysis and femoral neck were not found to be significantly different from other groups at day 112, and intrinsic bone strength outcomes were significantly lower for HU+VJE compared to HU. On the other hand, bone densitometric and geometric outcomes at the distal femur metaphysis and the cancellous compartment of the proximal tibia metaphysis were

generally found to be significantly higher for HU+VJE animals compared to aging and HU controls at day 112, and intrinsic bone strength outcomes for the cancellous proximal tibia metaphysis and femur diaphysis were largely significantly higher for HU+VJE animals compared to aging and HU controls at day 112. No differences in proximal tibia metaphysis trabecular microarchitecture were found at day 112. Taken together, these results suggest that 28 days of VJE pre-treatment can protect against HU-induced bone quality and strength loss and promote recovery at certain bone sites.

5.2.1. Densitometry and Morphology

The densitometric, morphological, and microarchitectural findings of Experiment 2 were fourfold. First, 28 days of VJE pre-treatment induced significant positive changes in bone density, especially in the cancellous compartment. Second, 28 days of HU without countermeasure induced significant changes in proximal tibia metaphysis, distal femur metaphysis, and femoral neck bone density and morphology. Third, 28 days of VJE pre-treatment resulted in significantly higher bone densitometric, geometric, and trabecular microarchitectural outcomes at the proximal tibia metaphysis, tibia diaphysis, distal femur metaphysis, and femoral neck at the end of a subsequent 28-day HU period compared to HU animals that received no countermeasure before the unloading period. Fourth, the ability of 28 days of VJE prior to 28 days of HU to promote recovery of bone quality was bone site dependent, and where it occurred, was achieved primarily through preventing negative changes in bone density and morphology as a result of HU that would otherwise need to recover. Table 5.2 summarizes the densitometric and morphologic results from Experiment 2.

Table 5.2 Summary of Experiment 2 Densitometric and Morphologic Results.
Trend directionality is noted by up or down arrows where statistically significant. Greater magnitude of change is indicated by double-arrows.

Bone Site	Group	*Ex vivo* pQCT (d112)			*In vivo* pQCT				µCT (d112)		
		d28	d56	d112	d28	d56	d84	d112	d28	d56	d112
PTM Cancellous	AC	-	-	-	-	-	-	-	-	-	-
	HU		↓	-	-	↓↓	↓↓	↓↓		-	-
	HU+VJE	-	↑↑	↑↑	-	-	↑↑	↑↑	-	↑	-
PTM Cortical	AC	-	-	-	-	-	↑	↑			
	HU		-	↓	-	-	↑	↑			
	HU+VJE	↑	-	-	-	-	↓	↓			
TD	AC	-	-	-	↑	↑	↑	↑			
	HU		-	-	↑	↑	↑	↑			
	HU+VJE	↑	↑↑	-	↑	↑	↑	↑			
DFM	AC	-	-	-	HU						
	HU		↓	-							
	HU+VJE	-	↑↑	↑↑							
FD	AC	-	-	-							
	HU		-	-							
	HU+VJE	↓	-	↓↓							
FN	AC	-	-	-							
	HU		↓	↓							
	HU+VJE	↑	↑	↑							

Mechanical loading is required for normal maintenance of skeletal health. Above a certain threshold of daily mechanical loading, bone quality is maintained through normal bone remodeling. Below that threshold, bone resorption is increased and bone mass and density are lost. Prior to the installation of the advanced resistive exercise device (ARED) aboard the ISS, astronauts were not able to reliably reach this mechanical threshold while exercising. The interim resistive exercise device (iRED), which was placed on board the ISS while the ARED was being designed and manufactured, was only able to produce maximum loads of 1337 N (300 lbf), and would often malfunction resulting in no opportunity for astronauts to engage in resistance exercise. The ARED is able to produce maximum loads up to 2675 N (601 lbf) and has a simpler design than the iRED, with fewer moving parts and a lower risk of malfunction. QCT results from the proximal femur in a study of astronauts on 4 – 6 month ISS missions showed significantly better protection from bone loss with ARED use (n = 10) compared to pre-ARED (n = 18). The 18 astronauts composing the pre-ARED group actually performed a mix of iRED resistance exercise and no resistance exercise when the iRED was not functioning. Additionally, finite element analysis based on the QCT images demonstrated significantly higher bone strength for the ARED group compared to the pre-ARED group (Leblanc et al., 2013, Sibonga et al., 2019). In addition to exercise, a focus on proper nutrition during spaceflight is integral to the preservation of bone in astronauts. Increased energy and protein intake during flight has been significantly correlated with increased pelvic BMC pre- to post-flight (Smith et al., 2012).

Various models of resistance exercise in rodents have been used previously. External loading involves the cyclical compression of a bone (usually the tibia or ulna) axially via an external device. The drawbacks of this model are that the rodent must be anesthetized for every loading session, and the mechanical loading taking place is non-physiological in both direction and strain characterization. Simulated resistance training (SRT) provides loading via electrical stimulation of intact muscle (Macias et al., 2012, Swift et al., 2010b). Though this model results in a loading paradigm that more closely resembles physiological conditions, the rodent must still be anesthetized for every SRT session, and the strain magnitudes are very likely supra-physiological. Anesthesia reduces cardiac output and mean arterial pressure (Janssen et al., 2004), which are serious circulatory effects that may introduce confounding factors that would be avoided with a resistance exercise model that does not require anesthetization. *In vivo*, the largest physiological loads, and therefore the largest strains applied to bone are a result of muscle contractions. These muscle-mediated forces have the largest impact on the mechanical environment of bone, and muscle mass and strength are highly correlated to bone mass and strength as a result (Turner, 2000). The direction these muscle-mediated forces act on the bones is based on the muscle attachment points and the muscle position relative to the bone. As such, the forces that affect bone the most are unlikely to be strictly axial in most cases.

The main alternative rat model of resistance exercise is voluntary "squat-like" exercise or voluntary jumping exercise trained via negative reinforcement. Squatting and jumping both involve the same muscle groups and similar movements, though jumping

is slightly more “explosive”, in that the motion takes place over a shorter period of time. It has been demonstrated that voluntary exercise in these rodent models increases muscle mass and muscle protein synthesis (Fluckey et al., 1995, Gasier et al., 2011, Westerlind et al., 1998). The squatting behavior consists of rats alternately pulling a low and high lever in a standing and squatting motion with both concentric and eccentric muscle contractions, resulting in a fair approximation of a human squat exercise (Westerlind et al., 1998). The jumping behavior grew out of the squatting procedure, and simply involves rats jumping to reach a target (the lever) on the wall of the cage (Shirazi-Fard et al., 2014, Swift et al., 2010a). Similar models of voluntary jumping exercise consist of rats jumping from a low position up to a higher ledge (Ju et al., 2013, Shimano et al., 2018, Umemura et al., 1995).

Jumping resistance exercise has been proven more effective at preventing bone loss and aiding recovery from HU than aerobic exercise. Treadmill running does increase bone mass and improve bone microarchitecture (Ju et al., 2012, Umemura et al., 1995), and adding weighted backpacks to 5-month-old female rats during treadmill running increases BMC compared to rats that ran longer without weight (van der Wiel et al., 1995). However, Umemura et al. (1995) showed that jumping exercise (100 jumps (40 cm)/day, 5 days/week for 8 weeks) significantly increased the fat-free weight of tibiae and femora in 27-week-old female rats while treadmill running (30 m/min, 1 hour/day, 5 days/week for 8 weeks) did not. The tibia diameter was also greater in jumping exercise rats compared to that in treadmill running rats (Umemura et al., 1995).

Results from a separate study conducted by Ju et al. (2012) in skeletally immature rats (5 weeks old) that performed jumping exercise (10 jumps (40 cm)/day, 5 days/week, for 5 weeks) after 14 days of HU demonstrated that jumping exercise promoted recovery in bone density and microarchitecture more than treadmill running. Dual-energy x-ray absorptiometry (DXA)-assessed areal BMD (aBMD) in the femur recovered in control animals after 5 weeks, but was significantly higher in animals that spent the 5-week recovery period performing either treadmill running or jumping resistance exercise, with no difference between the exercise protocols. *Ex vivo* μCT of the distal femur metaphysis, however, demonstrated that the trabecular microarchitecture of the control animals did not fully recover, as trabecular separation was significantly higher and trabecular number was significantly lower compared to animals that were not unloaded. Jumping exercise animals had significantly higher trabecular thickness compared to all other groups, and were not significantly different from non-HU controls in any measure of trabecular microarchitecture at the distal femur metaphysis, other than the significantly higher % BV/TV shared by treadmill runners (Ju et al., 2012).

Many studies investigating jumping exercise as a countermeasure to HU have been conducted, but direct comparisons with the present study are often complicated by either the use of young, skeletally immature animals or performance of jumping exercise during or after HU as opposed to a pre-treatment approach. Young animals are consistently found to have a more pronounced bone response to mechanical stimuli when compared to older animals, due to higher levels of bone turnover and growth of the bones themselves (Rubin et al., 1992, Steinberg and Trueta, 1981, Turner et al., 1995).

A study investigating jumping exercise as a countermeasure to OVX-induced bone loss was conducted in 10-week-old female rats (Okubo et al., 2017). Jumping exercise (20 jumps (40 cm)/day, 5 days/week for 12 weeks) started three days after OVX, before the onset of osteopenia. DXA aBMD of the femur and fifth lumbar (L5) vertebra was significantly higher in the OVX exercise group compared to the OVX sedentary group at the end of the 12 week jumping exercise program (Okubo et al., 2017). Results from the present study confirm these femoral findings, as VJE pre-treatment resulted in significantly higher distal femur metaphysis total BMC and total vBMD for the HU+VJE group compared to the HU group, and significantly higher cancellous vBMD for HU+VJE animals compared to both aging and HU controls at day 56 (end of HU). However, distal femur metaphysis cortical vBMD and cortical thickness were significantly lower for HU+VJE animals compared to aging controls at the same time point. No examination of the vertebrae was conducted in the present study.

In a study investigating various time courses of jumping exercise and HU, 8-week-old female rats performed VJE (20 jumps (40 cm)/day, 5 days/week) for 2 weeks prior to 3 weeks of HU, during 3 weeks of HU, or both before and during HU (Yanagihara et al., 2016). The jumping exercise prior to HU group had significantly lower DXA aBMD of the femur and tibia at the end of HU compared to the end of HU values for the jumping exercise during HU group. The jumping exercise during HU group also had significantly higher femur and tibia DXA aBMD compared to HU controls. Taken together, this suggests that jumping exercise during HU was significantly better at preventing HU-induced bone changes in aBMD than pre-treatment

jumping exercise. However, rats that performed jumping exercise during HU were reloaded for each jumping exercise session, while rats that performed jumping exercise before HU were not reloaded during HU, and jumping exercise prior to HU was conducted for only 2 weeks (Yanagihara et al., 2016). In the present study, 28 days of VJE prior to HU successfully protected against cancellous vBMD loss at the proximal tibia metaphysis assessed by *in vivo* pQCT, and protected against total BMC and total and cancellous vBMD loss at the proximal tibia metaphysis assessed by *ex vivo* pQCT. VJE prior to HU also prevented changes in the distal femur metaphysis as described above. Though continuing VJE during HU would undoubtedly better protect against HU-induced bone loss, pre-treatment VJE was still successful as a countermeasure to HU-induced densitometric and morphologic changes in the present study.

Resistance exercise consisting of 11 sessions of two sets of a maximum of 25 repetitions in 6-month-old male rats during 4 weeks of HU attenuated the loss of soleus wet mass and prevented loss in DXA aBMD at the distal femur metaphysis (Fluckey et al., 2002). In the present study, pre-treatment with VJE did not reduce soleus wet mass loss, but distal femur metaphysis changes due to HU were prevented as described above.

Previous work in our laboratory (Shirazi-Fard et al., 2014) demonstrated that rats performing an 8-week progressive jumping exercise program during a recovery period between two 28-day periods of HU significantly improved bone densitometric and morphologic outcomes more quickly and to higher values than in HU controls (animals exposed only to weight-bearing cage activity). The progressive jumping exercise program consisted of the addition of weight to vests worn by the rats during the first 6

weeks of exercise. Starting at 80g added weight and 50 jumps, weight was increased and jump number was decreased by 5% per week, resulting in 270g added weight and 11 jumps in the 18th session after 6 weeks of three sessions per week. Remaining sessions were all conducted with 270g and 11 jumps. At the end of the 56-day recovery-exercise period, proximal tibia metaphysis total BMC and vBMD were significantly higher in the resistance trained HU group compared to aging and HU controls. These benefits were maintained through the subsequent HU period, as total BMC and vBMD were still significantly higher for resistance-trained HU rats compared to HU controls. *Ex vivo* μCT of the proximal tibia metaphysis demonstrated similar results, as trabecular thickness and trabecular number were significantly higher for trained HU animals compared to both aging and HU controls at the end of the recovery-exercise period and also at the end of the second HU period (Shirazi-Fard et al., 2014).

Though this progressive jumping exercise program took place before a 28-day HU period, it also followed a previous HU period. The exercise involved progressively higher weights and lower repetitions, and the exercise period was also twice as long as in the present study. That being said, results of the present study also demonstrated that the beneficial effects of VJE before a HU period prevent or reduce losses in bone mass and density. At day 28 (end of exercise), HU+VJE animals exhibited significantly higher *in vivo* pQCT total vBMD compared to HU animals and significantly higher *ex vivo* pQCT total vBMD and cortical vBMD compared to aging controls at the proximal tibia metaphysis. At day 56 (end of HU), *in vivo* pQCT cancellous vBMD at the proximal tibia metaphysis for HU+VJE animals was not significantly different from aging

controls, and *ex vivo* pQCT total BMC and vBMD at the proximal tibia metaphysis for HU+VJE animals were significantly higher compared to HU controls. Cancellous vBMD at the proximal tibia metaphysis assessed by *ex vivo* pQCT was also significantly higher for HU+VJE animals compared to both aging and HU controls. Proximal tibia metaphysis trabecular microarchitecture also benefited significantly from VJE pre-treatment from day 28 (end of exercise) through day 56 (end of HU). Both % BV/TV and trabecular thickness were significantly higher, and trabecular separation significantly lower, for HU+VJE animals compared to AC animals at day 56, which is consistent with previous findings in our laboratory and the literature (Shirazi-Fard et al., 2014, Westerlind et al., 1998). However, all the values for trabecular microarchitectural outcomes were lower (not significant) for the HU+VJE group compared to the AC group at day 28, except for trabecular separation which was significantly higher for the HU+VJE group compared to the AC group at day 28. It is possible that VJE resulted in improvements to trabecular microarchitecture, but these improvements were not enough to overcome the body mass differences between HU+VJE animals and aging controls at day 28. Data from *in vivo* longitudinal μCT or baseline animals euthanized at day 0 (start of exercise) would be required to know for certain.

The beneficial skeletal effects of resistance exercise have been demonstrated to persist after cessation of exercise. Following an eight week exercise protocol starting with 11-week-old female rats, whole tibia BMC by DXA and bone strength remained elevated for 24 weeks (Umemura et al., 2008). These findings remained true for 44-week-old male rats 24 weeks after cessation of exercise (Honda et al., 2008). Previous

work in our laboratory showed that total vBMD of the proximal tibia metaphysis as well as trabecular thickness and % BV/TV (assessed by μCT) remained elevated compared to aging controls up to 28 days after cessation of exercise even with a period of HU interposed in 6-month-old male rats (Shirazi-Fard et al., 2014), but recovery beyond that time point was not studied.

In the present study, the effects of VJE pre-treatment on recovery after 28 days of HU depended heavily on bone site and compartment (cortical or cancellous). *In vivo* pQCT results at the proximal tibia metaphysis demonstrated that VJE pre-treatment prevented age-related cancellous bone density loss, as cancellous vBMD remained significantly elevated for HU+VJE animals compared to aging and HU controls at day 84 (midway through recovery) and day 112 (end of recovery). On the other hand, proximal tibia metaphysis cortical vBMD and cortical thickness for HU+VJE animals remained significantly depressed at the same time points, while total BMC steadily recovered throughout recovery. *Ex vivo* proximal tibia metaphysis pQCT confirmed these results, as total vBMD was significantly higher for HU+VJE animals compared to both aging and HU controls, while cortical area was significantly lower for HU+VJE animals compared to aging and HU controls at day 112. *Ex vivo* μCT at day 112, however, revealed no significant differences between groups for any trabecular microarchitectural outcomes.

Also in the present study, *in vivo* pQCT of the tibia diaphysis showed age-related bone density and morphology gains for all densitometric and geometric outcomes. *Ex vivo* pQCT of the same bone site confirmed these increasing trends, but significant

differences between groups were also observed. Cortical BMC, cortical area, cortical thickness, and polar area MOI were all significantly higher for HU+VJE animals compared to aging controls and untrained HU animals at day 56. The HU+VJE group also had significantly higher cortical vBMD at day 28 compared to the AC group. Though all outcome measures at the femur diaphysis had generally increasing trends over the three *ex vivo* time points, the differences between groups were opposite to those observed in the tibia. Cortical BMC, vBMD, area, thickness, and polar area MOI were all significantly lower for HU+VJE animals compared to aging controls at day 28. Additionally, cortical BMC, area, thickness, and polar area MOI were all significantly lower for HU+VJE animals compared to both aging and HU controls at day 112. It's possible the discrepancies in femur and tibia outcomes were caused by the different loading conditions placed on the tibia and femur during the performance of VJE. The muscles in the leg and hip that mediate the jumping motion create varying strain magnitudes and directions in the tibia and femur. The direction and magnitude of strains created by the impact forces experienced when jumping onto and dismounting the platform are also different for the tibia and femur. As such, it is not necessarily surprising that the tibia and femur would react differently to VJE.

Results from the present study also demonstrated that femoral neck total BMC at day 28 was significantly lower for HU+VJE animals compared to aging controls, while total vBMD was significantly higher. This is likely explained by the significantly smaller body mass for HU+VJE animals compared to aging controls at this time point. This is a perfect example of why vBMD is generally a better measure of bone quality than BMC.

BMC is very sensitive to changes in bone size, whereas vBMD is not as it is a volumetrically normalized parameter. The HU group had significantly lower total vBMD compared to the AC group at day 56 (end of HU) and day 112 (end of recovery), while the HU+VJE group was not significantly different from the AC group and was significantly higher compared to the HU group at these same time points. Total bone area was significantly lower for HU+VJE animals at day 28 compared to aging controls and at day 112 compared to HU controls, and these significant differences were mirrored in polar area MOI. This makes sense as the distance from the cross-section's center to the outer edge of the bone is a major factor in polar area MOI. HU+VJE animals had significantly higher cortical thickness at day 28 compared to aging controls, at day 56 compared to HU controls, and at day 112 compared to both aging and HU controls.

5.2.2. Biomechanical Properties

The major biomechanical finding of Experiment 2 was that VJE pre-treatment resulted in significantly higher mechanical properties for the femoral neck at the end of the exercise period and for the proximal tibia metaphysis and femur diaphysis at the end of the HU period and the end of recovery.

As discussed earlier, reductions in mechanical strength tend to be much larger than corresponding changes in vBMD, especially for cancellous bone (Marshall et al., 1996, Seeman and Delmas, 2006, Stone et al., 2003). In the present study, cancellous vBMD at day 56 was 20.2% higher for the HU+VJE group compared to the HU group as assessed by *in vivo* pQCT, and was 40.9% higher for the HU+VJE group compared to the HU group as assessed by *ex vivo* pQCT; μCT-assessed % BV/TV at the proximal

tibia metaphysis was 21.1% higher for the HU+VJE group compared to the HU group at day 56. By contrast, ultimate stress for HU+VJE rats was 240% higher compared to HU controls at day 56 as assessed by proximal tibia metaphysis reduced platen compression (RPC) testing, almost a six times greater difference than the highest percent difference in cancellous vBMD or % BV/TV.

Resistance exercise is also effective in improving bone mechanical properties in ovariectomized (OVX) rats, which lose bone mass and strength due to estrogen deficiency. In the study by Okubo et al. (2017), 10-week-old female rats had significantly higher femoral neck mechanical test stiffness (+35.0%), and had significantly higher L5 compression ultimate force (+55.8%) and stiffness (+30.3%) for the exercise OVX group compared to the sedentary OVX group after 12 weeks of jumping exercise (20 jumps (40 cm)/day, 5 days/week) starting three days after OVX surgery (Okubo et al., 2017). Results from the present study confirm these findings. Femoral neck mechanical test stiffness was significantly higher for HU+VJE rats compared to aging controls at both day 28 (+30.7%, end of exercise) and day 56 (+29.7%, end of HU), and trended higher compared to HU at day 56 (+14.4%, not significant) as well. Vertebral compression was not performed in the present study, but RPC testing is a fairly comparable test of cancellous bone material properties. RPC of the proximal tibia metaphysis demonstrated that the HU+VJE group had significantly higher ultimate stress, elastic modulus, and energy to ultimate stress at day 56 and day 112 (end of recovery) compared to the HU group. Additionally, trends for proximal tibia metaphysis RPC ultimate force (+50.9%) and stiffness (+32.2%) at day 56 for the

HU+VJE group compared to the AC group in the present study corresponded to those observed in the Okubo et al. (2017) study.

Our laboratory previously demonstrated that rats performing an 8-week progressive jumping exercise program during a recovery period between two 28-day periods of HU achieved significantly higher RPC-tested proximal tibia metaphysis elastic modulus and strain at ultimate stress compared to aging and HU controls at the end of the 56-day recovery and exercise period. Though not significant, ultimate stress trended higher than both the aging and HU control groups at the end of the recovery-exercise period, as did elastic modulus and ultimate stress at the end of the second HU period (Shirazi-Fard et al., 2014). Results from the present study confirm these findings, as HU+VJE animals had higher values for proximal tibia ultimate stress, elastic modulus, energy to ultimate stress, and strain at ultimate stress compared to aging controls at day 28 (end of exercise), though these differences were not significant. While the HU group had significantly lower proximal tibia metaphysis ultimate stress and energy to ultimate stress at day 56 (end of HU) compared to aging controls, the HU+VJE group had significantly higher ultimate stress, elastic modulus, and energy to ultimate stress compared to the HU group at day 56. The present study followed the rats through 56 days of recovery after the HU period, and HU+VJE animals exhibited significantly higher ultimate stress compared to both aging and HU controls, as well as significantly higher elastic modulus and energy to ultimate stress compared to HU controls. These results suggest that VJE pre-treatment is effective at preventing deterioration in the

mechanical properties of proximal tibia metaphysis cancellous bone due to HU, and that these benefits extend through 56 days of recovery following 28 days of unloading.

When mid-shaft tibiae were tested in three-point bending, ultimate force was significantly higher for HU+VJE rats compared to aging controls at day 56, while ultimate stress and elastic modulus for HU+VJE animals were significantly lower compared to HU controls at the same time point. Results from e*x vivo* pQCT of the tibia diaphysis revealed that polar area MOI had significantly higher values for the HU+VJE group compared to the HU group at day 56. These higher polar area MOI values explain the lower ultimate stress and elastic modulus values, since cross-sectional MOI (I) is derived from polar area MOI and cross-sectional MOI is in the denominator in both three-point bending equations for ultimate stress (Equation 1.3) and elastic modulus (Equation 1.5).

Similarly, smaller polar area MOI values at the femur diaphysis for the HU+VJE group at day 28 (significant compared to the AC group), day 56 (not significant), and day 112 (significant compared to the AC and HU groups) also helps explain the significantly higher ultimate stress and elastic modulus from femur three-point bending. Notably, ultimate force at day 28 was lower for HU+VJE animals compared to aging controls, but ultimate stress and elastic modulus were both significantly higher. This demonstrates the value of converting extrinsic, structure-level properties into intrinsic, tissue-level properties. Larger bones will always sustain greater applied force, but the size of the bone is not necessarily related to the quality of the bone tissue. Intrinsic

properties such as ultimate stress and elastic modulus are better representations of bone quality and bone's ability to resist fracture, independent of size and shape.

At day 28, HU+VJE animals had significantly higher total vBMD and cortical thickness compared to aging controls (assessed by *ex vivo* pQCT) and significantly higher femoral neck mechanical test ultimate force and stiffness. Slightly higher values of cortical vBMD and thickness for HU+VJE animals compared to aging controls (not significant) likely contributed to the significantly higher femoral neck mechanical test stiffness compared to aging controls.

Densitometric outcomes and RPC outcomes at the proximal tibia metaphysis similarly correspond. At day 56, HU+VJE group cancellous vBMD (*in vivo* pQCT) was significantly higher compared to the HU group, cancellous vBMD (*ex vivo* pQCT) was significantly higher compared to the AC and HU groups. Also at d56, % BV/TV and trabecular thickness (assessed by μCT) were both significantly higher and trabecular separation lower for the HU+VJE group compared to the AC group and trended higher (trabecular separation lower) compared to the HU group. At the same time point, the HU group had significantly lower cancellous vBMD (assessed by *in vivo* pQCT) compared to the AC group, and significantly lower total BMC and vBMD, as well as lower trending cancellous vBMD (*ex vivo* pQCT) compared to the AC group. RPC results reflect this, as ultimate stress, elastic modulus, and energy to ultimate stress were all significantly higher for HU+VJE compared to HU at day 56. Similarly, at day 112, HU+VJE animals had significantly higher proximal tibia metaphysis cancellous vBMD (*in vivo* pQCT) compared to HU controls and significantly higher proximal tibia

metaphysis total and cortical vBMD and trending higher cancellous vBMD (assessed by *ex vivo* pQCT) compared to HU controls that correspond to significantly higher ultimate stress (vs. aging and HU controls), elastic modulus (vs. HU controls), and energy to ultimate stress (vs. HU controls). Changes in densitometric values in the present study were good indicators of mechanical property changes, though the magnitude of change in mechanical properties was often underpredicted by the magnitude of change in densitometric properties.

5.2.3. Bone Turnover

The primary histomorphometric findings in Experiment 2 were twofold. First, as demonstrated many times before, 28 days of HU significantly increased bone resorption and decreased bone formation. Second, 28 days of VJE pre-treatment significantly increased bone formation and reduced osteoclast activity.

As previously discussed, activity of bone resorbing and bone forming cells, coordinated by osteocytes is the sole mechanism through which bone adapts to its mechanical environment. Resistance exercise increases the mechanical load on bone, which in turn increases the rate of bone formation. Moderate amounts of resistance exercise can produce a net increase in bone formation activity, and can protect against microgravity and osteoporosis induced bone loss (Cosman et al., 2014, Sibonga et al., 2019).

In an external loading model, normal or bending forces are applied to a single long bone via an external mechanical device in an anesthetized animal, with no involved muscle contractions. External loading of rodent bone can result in decreased relative

lining cell surface and increased relative osteoblast surface after just one loading session (Boppart et al., 1998). Similarly, bone formation increased and bone resorption decreased in the vertebrae of 13-week-old rats after a single period of external loading (Chow et al., 1993). Externally loading the tibia of female rats using a four-point bending device created a unique strain distribution that resulted in a very rapid bone formation response. Woven (non-lamellar) bone formation was increased by 40% after just a single external loading session (Forwood and Turner, 1994). Direct conversion from a quiescent bone surface to bone formation without resorption or any osteoclast activity has also been documented in response to a single external loading session (Pead et al., 1988).

In 10-week-old female rats performing jumping exercise (20 jumps (40 cm)/day, 5 days/week for 12 weeks) starting 3 days after OVX, before the onset of osteopenia, relative osteoclast surface in proximal tibia metaphysis cancellous bone was significantly lower for the exercised OVX group compared to the sedentary OVX group at the end of the exercise period (Okubo et al., 2017). However, jumping exercise did not prevent significantly lower relative osteoid surface in the OVX rats. Jumping exercise protected from OVX-induced reductions in cancellous BV/TV, and mitigated the OVX-induced reduction in trabecular number and OVX-induced growth in trabecular separation at the proximal tibia metaphysis (Okubo et al., 2017).

Previous work in our laboratory investigated the effects of a progressive jumping exercise program performed by rats during a recovery period between two 28-day periods of HU (Shirazi-Fard et al., 2014). Serum carboxy-terminal crosslinking

telopeptide of collagen 1 (CTX-1) is a crosslink peptide released from Type 1 collagen during bone resorption, and is commonly used as a biomarker of osteoclast activity. In exercised HU rats, CTX-1 was significantly lower compared to baseline values at the end of the recovery and exercise period. Though CTX-1 levels were significantly higher for exercised HU rats at the end of the subsequent HU period compared to before the HU period, CTX-1 levels were not significantly higher compared to aging controls at the end of the second HU period. Procollagen type 1 N-terminal propeptide (P1NP), a serum biomarker of bone formation, was significantly lower for exercised HU animals compared to aging controls at the end of the second HU period (Shirazi-Fard et al., 2014).

In the present study, static histomorphometric analysis of proximal tibia metaphysis cancellous bone demonstrated that HU+VJE animals had significantly higher relative osteoid surface and significantly lower relative osteoclast surface compared to aging controls at day 28 (end of exercise). Similarly, animals undergoing VJE pre-treatment had significantly higher MS/BS and BFR at the mid-shaft tibia compared to aging controls at day 28. These results confirm previous findings in the literature and our laboratory. Resistance exercise increases bone formation and reduces resorption, which protects bone from subsequent HU-induced changes.

Histomorphometric results in the present study correspond with densitometric and mechanical testing results. The HU group had elevated relative osteoclast surface (not significant) and decreased MS/BS (significant compared to the AC group) at day 56, as HU increased bone resorption and reduced bone formation. The higher bone

formation levels (MS/BS, BFR, relative osteoid surface) and lower bone resorption levels (relative osteoclast surface) for the HU+VJE group at the start of HU (day 28) helped protect against loss of bone quality and strength. Bone formation fell significantly by the end of HU, as relative osteoid surface was significantly lower for HU+VJE animals compared to both aging and HU controls; further, MS/BS, MAR, and BFR values for the HU+VJE group were all lower (but not significantly so) than the AC group values at day 56. Relative osteoclast surface, however, was not greatly elevated at day 56, suggesting that the depression of bone resorption at the start of HU was a persistent effect.

5.3. Limitations

No study is without limitations, and this one is not an exception. Firstly, neither a bisphosphonate-treated non-HU (weight-bearing) group (Experiment 1) nor a VJE-treated non-HU group (Experiment 2) was included in the experimental design. This lack of a fully orthogonal design resulted in a situation where the options for statistical analysis of the data were limited. However, finite experimental resources inherently create constraints on experimental design features that result in trade-offs.

The experimental design of Experiment 1, due to its longitudinal nature, presented severely limited opportunities for tissue collection. Performing all of the *ex vivo* measurement (pQCT, μCT, mechanical testing, histomorphometry) at time points other than the end of the study, where bone turnover has been depressed by two successive exposures to HU, would be extremely beneficial and would help characterize the changes that occur throughout HU and recovery. Experiment 2 would also benefit

from additional time points for *ex vivo* analysis, including a baseline (day 0) time point for the HU+VJE group and a day 28 (start of HU) time point for the HU group. A mid-recovery (day 84) time point for all groups would further characterize the recovery from HU. The labor-intensive nature of these animal protocols would, however, result in extremely expensive experiments were animals terminated at all intermediate time points. The ability to perform *in vivo* pQCT imaging provides useful information that makes up for the lack of *ex vivo* time points, to a certain degree. Analysis of blood serum collected at each study time point would also provide useful longitudinal data without drastically increasing the labor-related costs of the experiment.

For Experiment 1, AC, HU, and HU+ZOL animals were not given vehicle injections to match the extra injections that HU+ALN rats received. Previous work in our laboratory without vehicle injections has demonstrated results consistent with studies that did use vehicle injections for control groups (Boudreaux, 2014, Gasser et al., 2008). Additionally, three subcutaneous injections per week was not deemed a harsh enough intervention to necessitate replicating it in control animals. Sham procedures for harsher interventions, such as OVX (anesthesia, major abdominal surgery, significant healing and inflammation processes, and pain medication) should absolutely be performed. Animals in the HU+ALN group, however, underwent very little additional distress compared to AC, HU, and HU+VJE rats. That being said, the lack of vehicle injections in non-ALN treated groups cannot be ruled out as a possible confounding factor in this study.

In Experiment 2, rats were assigned to AC, HU, and HU+VJE groups partially by jumping ability. Though ideally animals would be block assigned to groups based only on body mass, circumstances made this impossible. All 110 animals went through the acclimation and operant conditioning phases prior to the start of the study (day 0), but they did not all learn to perform the jumping behavior at the same rate. Only 35 to 40 of the 45 animals that were assigned to the HU+VJE group were fully trained (meaning they could perform 20 jumps up and down from a 10-inch platform in approximately 10 minutes or less) when the exercise phase began (day 0). The individuals that were not fully trained merely performed jumps to the best of their ability while we encouraged them to improve and reach the eventual goal of 30 jumps/day onto and off of a 10 inch platform in 10 minutes or less. The concept of a shy-bold continuum for the personalities of humans and other animals is widely accepted as a useful model (APA, 2018, Franks et al., 2014, Oswald et al., 2013, Wilson et al., 1993). Individuals with shy natures are more likely to be cautious around novel stimuli, while bold natures lead individuals to exhibit curious and exploratory behavior. As a result, shy individuals are at less risk of being preyed upon, but do not use unfamiliar resources as readily. In VJE, rats with bold natures will more quickly adjust to the custom jumping cage, novel food rewards, and concept of performing a behavior in order to receive a reward, allowing them to proceed more quickly through training. There is no way to tell how many shy or bold animals you will receive, or if the shy ones will adequately adjust within the training period so that they can perform the desired behavior reliably. Therefore, it was necessary to assign

rats to groups partly based on jumping ability, which prevented a randomized block assignment, in order to fairly test the efficacy of this training mode on bone outcomes.

Also in Experiment 2, the HU+VJE group had significantly lower body masses compared to the AC and HU groups throughout the study. Though there were control animals present in each cohort of the experiment, logistical complications caused there to be more AC and HU animals present in earlier cohorts, while the HU+VJE animals were concentrated in later cohorts. These earlier cohorts were simply made up of larger rats, which likely caused most of the difference between the average body masses among groups. However, because we assigned animals to groups partially by jumping ability, we cannot rule out that smaller rats were better at performing the jumping exercise for some reason, potentially confounding our results.

A limitation of RPC mechanical testing is the possibility that RPC could underestimate trabecular mechanical properties, especially for HU animals. The central portion of the proximal tibia metaphysis tends to lose more bone, based on visual observations of RPC samples and μCT images (Ju et al., 2012). The strength of cancellous bone depends on a number of factors including trabecular number and trabecular thickness, but it also depends on the orientation and distribution of trabeculae. The platen diameter in RPC testing is equal to 70% of the diameter of the largest circle that can fit within the endocortical perimeter, so only the central portion of the cancellous bone specimen is tested. Fewer trabeculae in the center of the cancellous compartment almost certainly reduces the strength of the entire proximal tibia metaphysis, so focusing the mechanical test on the portion of the compartment that most

suffers from bone loss, as RPC does, could over-estimate strength losses that are suffered *in vivo* by the entire cancellous bone compartment of the tibia metaphysis.

A limitation common to all animal models is the differences between the animal and the human. There are two major differences between rats and humans in terms of bone. Rats do not have osteons in their cortical bone microstructure, which can affect mechanical properties and other outcomes dependent on intra-cortical bone remodeling. However, rodents provide an excellent model of properties of human cancellous bone; the ovariectomized rat is one of the standard models used by the pharmaceutical industry in evaluating therapies to treat osteoporosis. Additionally, rats are quadrupedal, and the loading conditions at their various bone sites are significantly different when compared to bipedal humans. Nevertheless, useful information is gained from animals studies that provide important and meaningful contributions to basic knowledge and understanding when results are interpreted responsibly by taking relevant differences into account.

Finally, this study included only male rats. Women make up an increasingly large proportion of members of the astronauts corps (Foster, 2004, Seag, 2017). Women also make up the largest portion of osteoporosis patients (French and Emanuele, 2019). As such, including female rats in studies of this nature would benefit human space exploration and improve generalizability of findings to osteoporosis.

5.4. Future Work

Blood serum was collected at all intermediate and euthanasia time points in both experiments of this study. Serum analysis for biomarkers of bone resorption and formation at the end of Experiment 1 and throughout Experiment 2 would provide

valuable insight into intermediate changes in bone turnover caused by HU and the various countermeasures. *Ex vivo* μCT of the distal femur metaphysis followed by RPC could also be performed with already collected sampled from the present study, adding useful information about an additional bone site. Finite element analysis using μCT images of RPC samples would create a more granular picture of the stress and strain patterns in the sample, and how stress and strain are shared between the cortical and cancellous compartment.

For Experiment 1, extending the recovery after one or two HU periods for a year or more would allow for the investigation of matrix mineralization, microdamage accumulation, and reduced toughness potentially caused by bisphosphonate treatment. The risk of AFF increases with increasing duration of bisphosphonate treatment, so it would be interesting to examine whether ZOL treatment similar to that recommended for use in astronauts (one dose in a three year span) might contribute to increased mineralization or microdamage accumulation.

For Experiment 2, ground reaction forces generated during the voluntary jumping exercise protocol would further validate the efficacy of jumping resistance exercise. Using a force plate would allow for a better understanding of the loading conditions the long bones of the fore- and hindlimbs are subjected to when jumping onto and dismounting from the platform. Measuring the strain at various bone sites with strain gauges applied directly to the bones is a more invasive option that could better elucidate the physiological loading conditions the bone is placed under.

Future studies should look at VJE in combination with other factors. A combination of VJE and bisphosphonate treatment as countermeasures to HU-induced skeletal changes would be interesting. The combination of anabolic exercise and anti-catabolic pharmaceuticals could produce important results, given previous evidence that bisphosphonates blunt the positive effects of resistance exercise and simulated resistance training (Boudreaux, 2014, Swift et al., 2011). In addition, combining VJE, HU, and radiation would fully simulate the space environment astronauts will be exposed to beyond low Earth orbit. Galactic cosmic radiation consists of protons and heavier ions emitted by stars and other celestial bodies traveling at a significant percentage of the speed of light. Beyond low Earth orbit and the Earth's magnetic field, nothing protects astronauts from this radiation, and it has been shown to have serious negative effects on numerous body systems including the circulatory system, the nervous system, cognition and behavior, and bone (Chancellor et al., 2014, Delp et al., 2016, Macias et al., 2016, Nelson, 2016). Microgravity and radiation are simple realities of the space environment, and astronauts will certainly be exercising in order to preserve health and performance no matter their mission or what vehicle they use. Combining VJE, HU, and radiation exposure would match this environment in a rodent model.

6. CONCLUSIONS

Astronauts undergo significant bone loss at weight-bearing sites during spaceflight. On 4-6 month missions to the International Space Station (ISS), astronauts can lose up to 1.5% of integral bone mineral density per month in the hip, which is nearly 10-fold greater than the bone loss rate in postmenopausal Caucasian women, the population most at-risk for osteoporosis.

The purpose of the current study was to investigate the effects of a single period of bisphosphonate treatment on bone loss resulting from multiple periods of simulated microgravity. We hypothesized that the protective effects of bisphosphonate treatment would extend through two periods of HU and an intervening recovery period, and that zoledronate (ZOL) would outperform alendronate (ALN) at preserving bone strength and quality due to the higher binding affinity and anti-resorptive potency of ZOL. The first and second HU periods resulted in significant declines in total (-5.05%, -0.25%) and cancellous (-18.4%, -9.98%) vBMD at the proximal tibia metaphysis. The second HU resulted in a lower magnitude of bone mass and density loss compared to the loss during the first HU. ALN treatment protected from these losses in bone mass and density for both HU periods. ZOL treatment was overprotective against bone mass, density, and microarchitecture losses for both HU periods. These results indicate that bisphosphonate treatment may be a successful countermeasure against spaceflight bone loss, and the extended beneficial skeletal effects of a single dose of ZOL could be very useful as a countermeasure for astronauts on long-duration exploration class missions.

Additionally, we aimed to develop a model of voluntary jumping exercise (VJE) that employs positive reinforcement-based training methods and to validate the efficacy of this VJE model as a countermeasure to simulated microgravity-induced bone strength and quality loss. We hypothesized that VJE pre-treatment would effectively preserve bone strength and quality during a subsequent HU period, and that these beneficial effects would not extend to the recovery period following unloading. HU+VJE animals had significantly higher total vBMD at the proximal tibia metaphysis (+8.95%), distal femur metaphysis (+7.57%), and femoral neck (+6.03%) compared to aging controls at day 28 (end of exercise). At day 56 (end of HU), HU+VJE animals also had significantly higher bone densitometric and morphologic outcomes at the proximal tibia metaphysis, tibia diaphysis and distal femur metaphysis compared to HU controls. RPC results demonstrated that the proximal tibia metaphysis cancellous bone of animals that performed VJE prior to HU had significantly higher ultimate stress (+240%, +108%), elastic modulus (+208%, +57.9%), and energy to ultimate stress (+209%, +119%) at day 56 (end of HU) and day 112 (end of recovery) compared to HU controls. These results indicate that positive reinforcement based VJE pre-treatment is a valid model of resistance exercise that can be used to counter HU-induced bone loss and aid subsequent recovery at certain bone sites, and offer a useful exercise model for future work investigating long-term exposure to microgravity with the rodent HU model.

REFERENCES

Abrahamsen, B., T. van Staa, R. Ariely, M. Olson, and C. Cooper, *Excess mortality following hip fracutre: a systematic epidemiological review.* Osteoporos Int, 2009. **10**: p. 1633-50.

Allen, M.R. and D.B. Burr, *Bisphosphonate effects on bone turnover, microdamage, and mechanical properties: what we think we know and what we know that we don't know.* Bone, 2011. **49**(1): p. 56-65.

Allen, M.R., H.A. Hogan, and S.A. Bloomfield, *Differential bone and muscle recovery following hindlimb unloading in skeletally mature male rats.* J Musculoskelet Neuronal Interact, 2006. **6**(3): p. 217-225.

Allen, M.R., J.J. Turek, R.J. Phipps, and D.B. Burr, *Greater magnitude of turnover suppression occurs earlier after treatment initiation with risedronate than alendronate.* Bone, 2011. **49**: p. 128-132.

APA. *Shy-bold Continuum*. American Psychology Association Dictionary of Psychology 2018 [cited 2020 February 15]; Available from: https://dictionary.apa.org/shy-bold-continuum.

Apseloff, G., B. Girten, M. Walker, D.R. Shepard, M.E. Krecic, L.S. Stern, and N. Gerber, *Aminohydroxybutane Bisphosphonate and Clenbuterol Prevent Bone Changes and Retard Muscle Atrophy Respectively in Tail-Suspended Rats.* The Journal of Pharmacology and Experimental Therapeutics, 1993a. **264**(3): p. 1071-1078.

Apseloff, G., B. Girten, S.E. Weisbrode, M. Walker, L.S. Stern, M.E. Krecic, and N. Gerber, *Effects of Aminohydroxybutane Bisphosphonate on Bone Growth when Administered after Hind-Limb Bone Loss in Tail-Suspended Rats.* The Journal of Pharmacology and Experimental Therapeutics, 1993b. **267**(1): p. 515-521.

Bagi, C.M., D. Wilkie, K. Georgelos, D. Williams, and D. Bertolini, *Morphological and structural characteristics of the proximal femur in human and rat.* Bone, 1997. **21**(3): p. 261-7.

Bartel, D.L., D.T. Davy, and T.M. Keaveny, *Orthopaedic Biomechanics*. 2006, Upper Saddle River, New Jersey: Pearson Prentice Hall.

Bass, S.L., G. Naughton, L. Saxon, S. Iuliano-Burns, R.M. Daly, E.M. Briganti, C. Hume, and C. Nowson, *Exercise and calcium combined results in a greater osteogenic effect than either factor alone: a blinded randomized placebocontrolled trial in boys.* J Bone Miner Res, 2007. **22**(3): p. 458-64.

Bateman, T.A. and S. Countryman, *Osteoprotegerin and bone loss associated with spaceflight.* Drug Discov Today, 2002. **7**(8): p. 456-7.

Bauer, J.S., S. Kohlmann, F. Eckstein, D. Mueller, E.M. Lochmuller, and T.M. Link, *Structural analysis of trabecular bone of the proximal femur using multislice computed tomography: a comparison with dual X-ray absorptiometry for predicting biomechanical strength in vitro.* Calcif Tissue Int, 2006. **78**: p. 78-89.

Benhamou, C.L., *Effects of osteoporosis medications on bone quality.* Joint Bone Spine, 2007. **74**(1): p. 39-47.

Bikle, D.D., E.R. Morey-Holton, S.B. Doty, P.A. Currier, S.J. Tanner, and B.P. Halloran, *Alendronate increases skeletal mass of growing rats during unloading by inhibiting resorption of calcified cartilage.* J Bone Miner Res, 1994. **9**(11): p. 1777-87.

Black, D.M., M.L. Bouxsein, L.M. Marshall, S.R. Cummings, T.F. Lang, and J.A. Cauley, *Proximal femoral structure and the prediction of hip fracture in men: a large prospective study using QCT.* J Bone Miner Res, 2008. **23**: p. 1326-33.

Black, D.M., S.R. Cummings, D.B. Karpf, J.A. Cauley, D.E. Thompson, M.C. Nevitt, D.C. Bauer, H.K. Genant, W.L. Haskell, R. Marcus, S.M. Ott, J.C. Torner, S.A. Quandt, T.F. Reiss, and K.E. Ensrud, *Randomised trial of effect of alendronate on risk of fracture in women with existing vertebral fractures. Fracture Intervention Trial Research Group.* The Lancet, 1996. **348**(9041): p. 1535-41.

Black, D.M., P.D. Delmas, R. Eastell, I.R. Reid, S. Boonen, J.A. Cauley, F. Cosman, P. Lakatos, P.C. Leung, Z. Man, C. Mautalen, P. Mesenbrink, H. Hu, J. Caminis, K. Tong, T. Rosario-Jansen, J. Krasnow, T.F. Hue, D. Sellmeyer, E.F. Eriksen, and S.R. Cummings, *Once-Yearly Zoledronic Acid for Treatment of Postmenopausal Osteoporosis.* N Engl J Med, 2007. **356**(18): p. 1809-1822.

Black, D.M., D.E. Thompson, D.C. Bauer, K.E. Ensrud, T. Musliner, M. Hochberg, M.C. Nevitt, S. Suryawanshi, and S.R. Cummings, *Fracture risk reduction with alendronate in women with osteoporosis: the Fracture Intervention Trial. FIT Research Group.* J Clin Endocrinol Metab, 2000. **85**(11): p. 4118-24.

Bloomfield, S.A., M.R. Allen, H.A. Hogan, and M.D. Delp, *Site- and Compartment-specific Changes in Bone With Hindlimb Unloading in Mature Adult Rats.* Bone, 2002. **31**(1): p. 149-157.

Bloomfield, S.A., D.A. Martinez, R.D. Boudreaux, and A.V. Mantri, *Microgravity Stress: Bone and Connective Tissue.* Comp Physiol, 2016. **6**: p. 645-686.

Boppart, M.D., D.B. Kimmel, J.A. Yee, and D.M. Cullen, *Time Course of Osteoblast Appearance After In Vivo Mechanical Loading.* Bone, 1998. **23**(5): p. 409-415.

Boudreaux, R.D., *Sequential High-Impact, Free-Fall Loading and Zoledronic Acid as a Novel Pre-Treatment for Disuse-induced Bone Loss*, in *Department of Biomedical Engineering*. 2014, Texas A&M University.

Bousson, V., A. Le Bras, F. Roqueplan, Y. Kang, D. Mitton, and S. Kolta, *Volumetric quantitative computed tomography of the proximal femur: relationships linking geometric and densitometric variables to bone strength.* Osteoporos Int, 2006. **17**: p. 855-64.

Bouxsein, M.L., S.K. Boyd, B.A. Christiansen, R.E. Guldberg, K.J. Jepsen, and R. Muller, *Guidelines for assessment of bone microstructure in rodents using micro-computed tomography.* J Bone Miner Res, 2010. **25**(7): p. 1468-86.

Brouwers, J.E., B. van Rietbergen, and M.L. Bouxsein, *Influence of early and late zoledronic acid administration on vertebral structure and strength in ovariectomized rats.* Calcif Tissue Int, 2008. **83**(3): p. 186-91.

Burr, D.B. and M.R. Allen, eds. *Basic and Applied Bone Biology*. 2014, Academic Press: Waltham, MA.

Carpenter, R.D., A. LeBlanc, H. Evans, J. Sibonga, and T.F. Lang, *Long-term changes in the density and structure of the human hip and spine after long-duration spaceflight.* Acta Astronautica, 2010. **67**: p. 71-81.

Cauley, J.A., L. Lui, K.L. Stone, T.A. Hillier, J.M. Zmuda, M. Hochberg, T.J. Beck, and K.E. Ensrud, *Longitudinal Study of Changes in Hip Bone Mineral Density in Caucasian and African-American Women.* JAGS, 2005. **53**: p. 183-189.

Cavanagh, P.R., A.A. Licata, and A.J. Rice, *Exercise and Pharmacological Countermeasures for Bone Loss DUring Long-Duration Space Flight.* Gravitational and Space Biology, 2005. **18**(2): p. 39-58.

Chancellor, J.C., G.B.I. Scott, and J.P. Sutton, *Space Radiation: The Number One Risk to Astronaut Health beyond Low Earth Orbit.* Life, 2014. **4**: p. 491-510.

Chappard, D., A.S. Palle, L. Vico, B.V. Morukov, S.S. Rodionova, P. Minaire, and G. Riffat, *Effects of a Bisphosphonate (1-Hydroxy Ethylidene-1,1 Bisphosphonic Acid) on Osteoclast Number During Prolonged Bed Rest in Healthy Humans.* Metabolism, 1989. **38**(9): p. 822-825.

Chow, J.W., C.J. Jagger, and T.J. Chambers, *Characterization of osteogenic response to mechanical stimulation in cancellous bone of rat caudal vertebrae.* Am J Physiol, 1993. **265**(2 Pt 1): p. E340-7.

Colletti, L.A., J. Edwards, L. Gordon, J. Shary, and N.H. Bell, *The effects of muscle-building exercise on bone mineral density of the radius, spine, and hip in young men.* Calcif Tissue Int, 1989. **45**(1): p. 12-14.

Cooper, J.J., N. Cracknell, J. Hardiman, H. Wright, and D. Mills, *The welfare consequences and efficacy of training pet dogs with remote electronic training collars in comparison to reward based training.* PLoS One, 2014. **9**(9): p. e102722.

Cosman, F., S.J. de Beur, M.S. LeBoff, E.M. Lewiecki, B. Tanner, S. Randall, and R. Lindsay, *Clinician's Guide to Prevention and Treatment of Osteoporosis.* Osteoporos Int, 2014. **25**: p. 2359-2381.

Cowin, S.C., ed. *Bone Mechanics Handbook*. Second Edition ed. 2001, CRC Press: Boca Raton, FL.

Cramer, J.A., D.T. Gold, S.L. Silverman, and E.M. Lewiecki, *A systematic review of persistence and compliance with bisphosphonates for osteoporosis.* Osteoporos Int, 2007. **18**(8): p. 1023-31.

Currey, J.D., *Bones: Structure and Mechanics*. Second Edition ed. 2006, Princeton, NJ: Princeton University Press.

Daly, R.M., L. Saxon, C.H. Turner, A.G. Robling, and S.L. Bass, *The relationship between muscle size and bone geometry during growth and in response to exercise.* Bone, 2004. **34**(2): p. 281-7.

Damilakis, J., J.E. Adams, G. Guglielmi, and T.M. Link, *Radiation exposure in X-ray-based imaging techniques used in osteoporosis.* Eur Radiol, 2010. **20**: p. 2707-14.

Delp, M.D., J.M. Charvat, C.L. Limoli, R.K. Globus, and P. Ghosh, *Apollo Lunar Astronauts Show Higher Cardiovascular Disease Mortality: Possible Deep Space Radiation Effects on the Vascular Endothelium.* Sci Rep, 2016. **6**.

du Plessis, A., C. Broeckhoven, A. Guelpa, and S.G. le Roux, *Laboratory x-ray micro-computed tomography: a user guideling for biological samples.* Gigascience, 2017. **6**(6): p. 1-11.

Engelke, K., J.E. Adams, G. Armbrecht, P. Augat, C.E. Bogado, M.L. Bouxsein, D. Felsenberg, M. Ito, S. Prevrhal, D.B. Hans, and E.M. Lewiecki, *Clinical use of quantitative computed tomography and peripheral quantitative computed tomography in the management of osteoporosis in adults: the 2007 ISCD Official Positions.* J Clin Densitom, 2008. **11**(1): p. 123-62.

Engelke, K., W. Kemmler, D. Lauber, C. Beeskow, R. Pintag, and W.A. Kalendar, *Exercise maintains bone density at spine and hip EFOPS: a 3-year longitudinal study in early postmenopausal women.* Osteoporos Int, 2006. **17**(1): p. 133-42.

Farrell, P.A., M.J. Fedele, J. Hernandez, J.D. Fluckey, J.L. Miller, III, C.H. Lang, T.C. Vary, S.R. Kimball, and L.S. Jefferson, *Hypertrophy of skeletal muscle in diabetic rats in response to chronic resistance exercise.* J Appl Physiol, 1999. **87**(3): p. 1075-1082.

Farrell, P.A., M.J. Fedele, T.C. Vary, S.R. Kimball, and L.S. Jefferson, *Effects of intensity of acute-resistance exercise on rates of protein synthesis in moderately diabetic rats.* J Appl Physiol, 1998. **85**(6): p. 2291-2297.

Felsenberg, D. and S. Boonen, *The bone quality framework: determinants of bone strength and their interrelationships, and implications for osteoporosis management.* Clin Ther, 2005. **27**(1): p. 1-11.

Fluckey, J.D., E.E. Dupont-Versteegden, D.C. Montague, M. Knox, P. Tesch, C.A. Peterson, and D. Gaddy-Kurten, *A rat resistance exercise regimen attenuates losses of musculoskeletal mass during hindlimb suspension.* Acta Physiol Scand, 2002. **176**: p. 293-300.

Fluckey, J.D., W.J. Kraemer, and P.A. Farrell, *Pancreatic islet insulin secretion is increased after resistance exercise in rats.* J Appl Physiol, 1995. **79**(4): p. 1100-1105.

Fluckey, J.D., T.C. Vary, L.S. Jefferson, W.J. Evans, and P.A. Farrell, *Insulin Stimulation of Protein Synthesis in Rat Skeletal Muscle Following Resistance Exercise Is Maintained With Advancing Age.* Journal of Gerontology, 1996. **51A**(5): p. B323-B330.

Forwood, M.R. and C.H. Turner, *The response of rat tibiae to incremental bouts of mechanical loading: a quantum concept for bone formation.* Bone, 1994. **15**(6): p. 603-9.

Foster, A.E., *Integrating Women into the Astronaut Corps: Politics and Logistics at NASA, 1972-2004*. 2004, Baltimore, MD: JHU Press.

Franks, B., E.T. Higgins, and F.A. Champagne, *A Theoretically Based Model of Rat Personality with Implications for Welfare.* PLoS One, 2014. **9**(4).

Fratzl, P., ed. *Collagen: Structure and Mechanics*. 2008, Springer: Boston, MA.

French, K.D. and D. Emanuele, *Osteoporosis: Increasing Screening and Treatment for Postmenopausal Women.* The Journal for Nurse Practitioners, 2019. **15**(5): p. 347-50.

Frost, H.M., *The Laws of Bone Structure*. 1964, Springfield, MI: CC Thomas.

Fuchs, R.K., J.J. Bauer, and C.M. Snow, *Jumping improves hip and lumbar spine bone mass in prepubescent children: a randomized controlled trial.* J BONe Miner Res, 2001. **16**(1): p. 148-56.

Garland, D.E., C.A. Stewart, R.H. Adkins, S.S. Hu, C. Rosen, F.J. Liotta, and D.A. Weinstein, *Osteoporosis After Spinal Cord Injury.* Journal of Orthopaedic Research, 1992. **10**: p. 371-378.

Garner, R.P., L. Terracio, T.K. Borg, and J. Buggy, *Intracranial self-stimulation motivates weight-lifting exercise in rats.* J Appl Physiol, 1991. **71**(4): p. 1627-1631.

Gasier, H.G., S.E. Riechman, M.P. Wiggs, A. Buentello, S.F. Previs, and J.D. Fluckey, *Cumulative responses of muscle protein synthesis are augmented with chronic resistance exercise training.* Acta Physiol (Oxf), 2011. **201**(3): p. 381-9.

Gasser, J.A., *The relative merits of anabolics versus anti-resorptive compounds: where our tarets should be, and whether we are addressing them.* Curr Opin Pharmacol, 2006. **6**(3): p. 313-8.

Gasser, J.A., P. Ingold, A. Venturiere, V. Shen, and J.R. Green, *Long-term protective effects of zoledronic acid on cancellous and cortical bone in the ovariectomized rat.* J Bone Miner Res, 2008. **23**(4): p. 544-51.

Genant, H.K., K. Engelke, and S.F. Previs, *Advnced CT bone imaging in osteoporosis.* Rheumatology, 2008. **4**: p. 9-16.

Gerdhem, P., K.K. Ivaska, S.L. Alatalo, J.M. Halleen, J. Hellman, A. Isaksson, K. Pettersson, H.K. Vaananen, K. Akesson, and O.K. J., *Biochemical markers of bone metabolism and prediction of fracture in elderly women.* J Bone Miner Res, 2004. **19**(3): p. 386-93.

Giangregorio, L. and C.J.R. Blimkie, *Skeletal Adaptations to Alteration sin Weight-Bearing Activity: A Comparison of MOdels of Disuse Osteoporosis.* Sports Med, 2002. **32**(7): p. 459-476.

Globus, R.K. and E. Morey-Holton, *Hindlimb unloading: rodent analog for microgravity.* J Appl Physiol (1985), 2016. **120**(10): p. 1196-206.

Green, J.R., K. Muller, and K.A. Jeaeggi, *Preclinical pharmacology of CGP 42'446, a new, potent, heterocyclic bisphospohonate compound.* J Bone Miner Res, 1994. **9**(5): p. 745-51.

Grey, A., M.J. Bolland, A. Horne, D. Wattie, M. House, G. Gamble, and I.R. Reid, *Five years of anti-resorptive activity after a single dose of zoledronate--results from a randomized double-blind placebo-controlled trial.* Bone, 2012. **50**(6): p. 1389-93.

Gupta, S., S.L. Manske, and S. Judex, *Increasing the Number of Unloading/Reambulation Cycles does not Adversely Impact Body Composition and Lumbar Bone Mineral Density but Reduces Tissue Sensitivity.* Acta Astronaut, 2013. **92**(1): p. 89-96.

Gupta, S., S. vijayaraghavan, G. Uzer, and S. Judex, *Multiple exposures to unloading decrease bone's responsivity but compound skeletal losses in C57BL/6 mice.* Am J Physiol Regul Integr Comp Physiol, 2012. **303**(2): p. R159-R167.

Hamilton, D., K. Smart, S. Melton, J.D. Polk, and K. Johnson-Throop, *Autonomous medical care for exploration class space missions.* J Trauma, 2008. **64**(4 Suppl): p. S354-63.

Hogan, H.A., S.P. Ruhmann, and H.W. Sampson, *The mechanical properties of cancellous bone in the proximal tibia of ovariectomized rats.* J Bone Miner Res, 2000. **15**(2): p. 284-92.

Honda, A., N. Sogo, S. Nagasawa, T. Kato, and Y. Umemura, *Bones benefits gained by jump training are preserved after detraining in young and adult rats.* J Appl Physiol (1985), 2008. **105**(3): p. 849-53.

Hubal, M.J., C.P. Ingalls, M.R. Allen, J.C. Wenke, H.A. Hogan, and S.A. Bloomfield, *Effects of eccentric exercise training on cortical bone and muscle strength in the estrogen-deficient mouse.* J Appl Physiol (1985), 2005. **98**(5): p. 1674-81.

Janssen, B.J., T. De Cell, J.J. Debets, A.E. Brouns, M.F. Callahan, and T.L. Smith, *Effects of anesthetics on systemic hemodynamics in mice.* Am J Physiol Heart Circ Physiol, 2004. **287**(4): p. H1618-24.

Jarvinen, T.L., I. Pajamaki, H. Sievanen, T. Vuohelainen, J. Tuukkanen, M. Jarvinen, and P. Kannus, *Femoral neck response to exercise and subsequent deconditioning in young and adult rats.* J Bone Miner Res, 2003. **18**(7): p. 1292-9.

Ju, Y.I., T. Sone, K. Ohnaru, H.J. Choi, K.-A. Choi, and M. Fukunaga, *Jumpe exercise during hindlimb unloading protect against the deterioration of trabecular bone microarchitecture in growing young rats.* SpringerPlus, 2013. **2**(35).

Ju, Y.I., T. Sone, K. Ohnaru, H.J. Choi, and M. Fukunaga, *Differential effects of jump versus running exercise on trabecular architecture during remobilization after suspension-induced osteopenia in growing rats.* J Appl Physiol (1985), 2012. **112**(5): p. 766-72.

Karinkata, S., A. Heinonen, H. Sievanen, K. Uusi-Rasi, M. Fogelholm, and P. Kannus, *Maintenance of exercise-induced benefits in physical functioning and bone among elderly women.* Osteoporos Int, 2009. **20**(4): p. 665-74.

Keyak, J.H., A.K. Koyama, A. LeBlanc, Y. Lu, and T.F. Lang, *Reduction in proximal femoral strength due to long-duration spaceflight.* Bone, 2009. **44**(3): p. 449-53.

Khow, K.S.F., P. Shibu, S.C.Y. Yu, M.J. Chehade, and R. Visvanathan, *Epidemiology and postoperative outcomes of atypical femoral fractures in older adults: A systematic review.* J Nutr Health Aging, 2017. **21**: p. 83-91.

Kodama, Y., K. Nakayama, H. Fuse, S. Fukumoto, H. Kawahara, H. Takahashi, T. Kurokawa, C. Sekiguchi, T. Nakamura, and T. Matsumoto, *Inhibition of Bone Resorption by Pamidronate Cannot Restore Normal Gain in Cortical Bone Mass and Strength in Tail-Suspended Rapidly Growing Rats.* J Bone Miner Res, 1997. **12**(7): p. 1058-1067.

Kohrt, W.M., S.A. Bloomfield, K.D. Little, M.E. Nelson, and V.R. Yingling, *American College of Sports Medicine Position Stand: Physical Activity and Bone Health.* Med Sci Sports Exerc, 2004. **36**: p. 1985-1996.

Kubek, D.J., D.B. Burr, and M.R. Allen, *Ovariectomy stimulates and bisphosphonates inhibit intracortical remodeling in the mouse mandible.* Orthod Craniofac Res, 2010. **13**(4): p. 214-22.

Lang, T., A. LeBlanc, H. Evans, Y. Lu, H. Genant, and A. Yu, *Cortical and trabecular bone mineral loss from the spine and hip in long-duration spaceflight.* J Bone Miner Res, 2004. **19**(6): p. 1006-12.

Lang, T.F., J. Keyak, M.W. Heitz, P. Augat, Y. Lu, and A. Mathur, *Volumetric quantitative computed tomography of the proximal femur: recision and relation to bone strength.* Bone, 1997. **21**: p. 101-8.

Lang, T.F., A.D. Leblanc, H.J. Evans, and Y. Lu, *Adaptation of the proximal femur to skeletal reloading after long-duration spaceflight.* J Bone Miner Res, 2006. **21**(8): p. 1224-30.

Lawson, R. and L.S. Watson, Jr., *Learning in the Rat (Rattus Norvegicus) under Positive vs. Negative Reinforcement with Incentive Conditions Controlled.* Ohio Journal of Science, 1963. **63**(2): p. 87-91.

Leblanc, A., T. Matsumoto, J. Jones, J. Shapiro, T. Lang, L. Shackelford, S.M. Smith, H. Evans, E. Spector, R. Ploutz-Snyder, J. Sibonga, J. Keyak, T. Nakamura, K. Kohri, and H. Ohshima, *Bisphosphonates as a supplement to exercise to protect bone during long-duration spaceflight.* Osteoporos Int, 2013. **24**(7): p. 2105-14.

LeBlanc, A., V. Schneider, L. Shackelford, S. West, V.S. Oganov, A.V. Bakulin, and L. Voronin, *Bone mineral and lean tissue loss after long duration space flight.* J Musculoskelet Neuronal Interact, 2000. **1**(2): p. 157-160.

Leblanc, A.D., T.B. Driscol, L.C. Shackelford, H.J. Evans, N.J. Rianon, S.M. Smith, D.L. Feeback, and D. Lai, *Alendronate as an effective countermeasure to disuse induced bone loss.* J Musculoskelet Neuronal Interact, 2002. **2**(4): p. 335-343.

LeBlanc, A.D., E.R. Spector, H.J. Evans, and J.D. Sibonga, *Skeletal responses to space flight and the bed rest analog: A review.* J Musculoskelet Neuronal Interact, 2007. **7**(1): p. 33-47.

Lewandowski, B.E., J.G. Myers, E.S. Nelson, A. Licatta, and D. Griffin, *Risk assessment of bone fracture during space exploration missions to the moon and mars*, in *Space Systems Engineering and Risk Management Symposium*. 2007, NASA.gov: Los Angeles, CA.

Linden, C., H.G. Ahlborg, J. Besjakov, P. Gardsell, and M.K. Karlsson, *A school curriculum-based exercise program increases bone mineral accrual and bone size in prepubertal girls: two-year data from the pediatric osteoporosis prevention (POP) study.* J Bone Miner Res, 2006. **21**(6): p. 829-35.

Lloyd, A.A., B. Gludovatz, C. Riedel, E.A. Luengo, R. Saiyed, E. Marty, D.G. Lorich, J.M. Lane, R.O. Ritchie, B. Busse, and E. Donnelly, *Atypical fracture with long-term bisphosphonate therapy is associated with altered cortical composition and reduced fracture resistance.* PNAS, 2017. **114**(33): p. 8722-8727.

Lloyd, S.A., S.E. Morony, V.L. Ferguson, S.J. Simske, L.S. Stodieck, K.S. Warmington, E.W. Livingston, D.L. Lacey, P.J. Kostenuik, and T.A. Bateman, *Osteoprotegerin is an effective countermeasure for spaceflight-induced bone loss in mice.* Bone, 2015: p. 562-572.

Lloyd, S.A., N.D. Travis, T. Lu, and T.A. Bateman, *Development of a low-dose anti-resorptive drug regimen reveals synergistic suppression of bone formation when coupled with disuse.* J Appl Physiol (1985), 2008. **104**(3): p. 729-38.

Luan, H.-Q., L.-W. Sun, Y.-F. Huang, Y. Wang, C.J. McClean, and Y.-B. Fan, *The application of micro-CT in monitoring bone alterations in tail-suspended rats in vivo.* Advances in Space Research, 2014. **53**(11): p. 1567-1573.

Macias, B.R., F. Lima, J.M. Swift, Y. Shirazi-Fard, E.S. Green, M.R. Allen, J.D. Fluckey, H.A. Hogan, L. Braby, S. Wang, and S.A. Bloomfield, *Simulating the Lunar Environment: Partial Weightbearing and High-LET Radiation-Induce Bone Loss and Increase Sclerostin-Positive Osteocytes.* Rad Res, 2016. **186**: p. 254-63.

Macias, B.R., J.M. Swift, M.I. Nilsson, H.A. Hogan, S.D. Bouse, and S.A. Bloomfield, *Simulated resistance training, but not alendronate, increases cortical bone formation and suppresses sclerostin during disuse.* J Appl Physiol, 2012. **112**: p. 918-925.

Manske, S.L., S. Vijayaraghavan, A. Tuthill, O. Brutus, J. Yang, S. Gupta, and S. Judex, *Extending Rest between Unloading Cycles Does Not Enhance Bone's Long-Term Recovery.* Med Sci Sports Exerc, 2015. **47**(10).

Marshall, D., O. Johnell, and H. Wedel, *Meta-analysis of how well measures of bone mineral density predict occurrence of osteoporotic fractures.* Br Med J, 1996. **312**: p. 1254-9.

Mashiba, T., T. Hirano, C.H. Turner, M.R. Forwood, C.C. Johnston, and D.B. Burr, *Suppressed bone turnover by bisphosphonates increases microdamage accumulation and reduces some biomechanical properties in dog rib.* J Bone Miner Res, 2000. **15**(4): p. 613-20.

Morey-Holton, E., R.K. Globus, A. Kaplansky, and G. Durnova, *The Hindlimb Unloading Rat Model: Literature Overview, Technique Update and Comparison with Space Flight Data.* 2005. **10**: p. 7-40.

Morey-Holton, E.R. and R.K. Globus, *Hindlimb Unloading of Growing Rats: A Model for Predicting Skeletal Changes During Space Flight.* Bone, 1998. **22**(5): p. 83S-88S.

Morey-Holton, E.R. and R.K. Globus, *Hindlimb unloading rodent model: technical aspects.* J Appl Physiol (1985), 2002. **92**(4): p. 1367-77.

Morse, A., M.M. McDonald, N.H. Kelly, K.M. Melville, A. Schindeler, I. Kramer, M. Kneissel, M.C.H. van der Meulen, and D.G. Little, *Mechanical Load Increases in Bone Formation via a Sclerostin-Independent Pathway.* J Bone Miner Res, 2014. **29**(11): p. 2456-2467.

Mosekilde, L.I., J.S. Thomsen, M.S. Mackey, and R.J. Phipps, *Treatment With Risedronate or Alendronate Prevents Hind-Limb Imoobilization-induced Loss of Bone Density and Strenght in Adult Female Rats.* Bone, 2000. **27**(5): p. 639-645.

Nelson, G.A., *Space Radiation and Human Exposures, A Primer.* Rad Res, 2016. **185**: p. 349-58.

NIH Consensus Development Panel on Osteoporosis Prevention, D., and Therapy, *Osteoporosis prevention, diagnosis, and therapy.* JAMA, 2001. **285**(6): p. 785-95.

Okubo, R., L.S. Sanada, V.A. Castania, M.J. Louzada, F.J. de Paula, N. Maffulli, and A.C. Shimano, *Jumping exercise preserves bone mineral density and mechanical properties in osteopenic ovariectomized rats even following established osteopenia.* Osteoporos Int, 2017. **28**(4): p. 1461-1471.

Orwoll, E.S., R.A. Adler, S. Amin, N. Binkley, E.M. Lewiecki, S.M. Petak, S.A. Shapses, M. Sinaki, N.B. Watts, and J.D. Sibonga, *Skeletal health in long-duration astronauts:*

nature, assessment, and management recommendations from the NASA Bone Summit. J Bone Miner Res, 2013. **28**(6): p. 1243-55.

Oswald, M.E., M. Singer, and B.D. Robison, *The Quantitative Genetic Architecture of the Bold-Shy Continuum in Zebrafish, Danio rerio* PLoS One, 2013. **8**(7).

Papapoulos, S.E., *Bisphosphonates: how do they work?* Best Pract Res Clin Endocrinol Metab, 2008. **22**(5): p. 831-47.

Pead, M.J., T.M. Skerry, and L.E. Lanyon, *Direct transformation from quiescence to bone formation int he adult periosteum following a single brief period of bone loading.* J Bone Miner Res, 1988. **3**(6): p. 647-56.

Peres-Ueno, M.J., C.T. Stringhetta-Garcia, R.C. Castoldi, G.A.T. Ozaki, A.H. Chaves-Neto, R.C.M. Dornelles, and M.J.Q. Louzada, *Model of hindlimb unloading in adult female rats: Characterizing bone physicochemical, microstructural, and biomechanical properties.* PLoS One, 2017. **12**(12).

Rogers, M.J., *New Insights Into the Molecular Mechanisms of Action of Bisphosphonates.* Current Pharmaceutical Design, 2003. **9**: p. 2643-2658.

Rubin, C.T., S.D. Bain, and K.J. McLeod, *Suppression of the osteogenic response in the aging skeleton.* Calcif Tissue Int, 1992. **50**(4): p. 306-13.

Russell, R.G., N.B. Watts, F.H. Ebetino, and M.J. Rogers, *Mechanisms of action of bisphosphonates: similarities and differences and their potential influence on clinical efficacy.* Osteoporos Int, 2008. **19**(6): p. 733-59.

Schilcher, J., V. Koeppen, P. Aspenberg, and K. Michaelsson, *Risk of atypical femoral fracture during and after bisphosphonate use.* Acta Orthop, 2015. **86**(1): p. 100-7.

Seag, M., *Women need not apply: gendered institutional change in Antarctica and Outer Space.* The Polar Journal, 2017. **7**(2): p. 319-35.

Seeman, E. and P.D. Delmas, *Bone quality - the material and structural basis of bone strength and fragility.* N Engl J Med, 2006. **354**: p. 2250-61.

Shackelford, L.C., A.D. Leblanc, T.B. Driscoll, H.J. Evans, N.J. Rianon, S.M. Smith, E. Spector, D.L. Feeback, and D. Lai, *Resistance exercise as a countermeasure to disuse-induced bone loss.* J Appl Physiol, 2004. **97**: p. 119-129.

Shimano, R.C., G.R. Yanagihara, A.P. Macedo, J.S. Yamanaka, A.C. Shimano, J. Tavares, and J.P.M. Issa, *Effects of high-impact exercise on the physical properties of bones of ovariectomized rats fed to a high-protein diet.* Scand J Med Sci Sports, 2018. **28**(5): p. 1523-1531.

Shirazi-Fard, Y., R.A. Anthony, A.T. Kwaczala, S. Judex, S.A. Bloomfield, and H.A. Hogan, *Previous exposure to simulated microgravity does not exacerbate bone loss during subsequent exposure in the proximal tibia of adult rats.* Bone, 2013a. **56**(2): p. 461-73.

Shirazi-Fard, Y., J.S. Kupke, S.A. Bloomfield, and H.A. Hogan, *Discordant recovery of bone mass and mechanical properties during prolonged recovery from disuse.* Bone, 2013b. **52**(1): p. 433-43.

Shirazi-Fard, Y., C.E. Metzger, A.T. Kwaczala, S. Judex, S.A. Bloomfield, and H.A. Hogan, *Moderate intensity resistive exercise improves metaphyseal cancellous bone recovery following an initial disuse period, but does not mitigate decrements during a subsequent disuse period in adult rats.* Bone, 2014. **66**: p. 296-305.

Sibonga, J., T. Matsumoto, J. Jones, J. Shapiro, T. Lang, L. Shackelford, S.M. Smith, M. Young, J. Kevak, K. Kohri, H. Ohshima, E. Spector, and A. LeBlanc, *Resistive exercise in astronauts on prolonged spaceflights provides partial protection against spaceflight-induced bone loss.* Bone, 2019. **128**.

Sibonga, J.D., H.J. Evans, S.A. Smith, E.R. Spector, G. Yardley, and J. Alwood, *Risk of Early Onset Osteoporosis Due to Space Flight*. 2017, National Aeronautics and Space Administration Lyndon B. Johnson Space Center.

Silva, M.J., T.M. Keaveny, and W.C. Hayes, *Load sharing between the shell and centrum in the lumbar vertebral body.* Spine, 1997. **22**: p. 140-150.

Silverman, S., E. Kupperman, and S. Bukata, *Bisphospohonate-related atypical femoral fracture: Managing a rare but serious complication.* Cleve Clin J Med, 2018. **85**(11): p. 885-93.

Siu, W.S., C.H. Ko, L.K. Hung, C.P. Lau, C.B. Lau, K.P. Fung, and P.C. Leung, *Effect of anti-osteoporotic agents on the prevention of bone loss in unloaded bone.* Mol Med Rep, 2013. **8**(4): p. 1188-94.

Skinner, B.F., *Science and Human Behavior*. 1954, New York: MacMillan Co.

Smith, S.M., M. Heer, L.C. Shackelford, J.D. Sibonga, J. Spatz, R.A. Pietrzyk, E.K. Hudson, and S.R. Zwart, *Bone metabolism and renal stone risk during International Space Station missions.* Bone, 2015. **81**: p. 712-720.

Smith, S.M., M.A. Heer, L.C. Shackelford, J.D. Sibonga, L. Ploutz-Snyder, and S.R. Zwart, *Benefits for bone from resistance exercise and nutrition in long-duration spaceflight: Evidence from biochemistry and densitometry.* J Bone Miner Res, 2012. **27**(9): p. 1896-906.

Song, H., S. Cho, H. Lee, H. Lee, and W. Song, *The Effects of Progressive Resistance Exercise on Recovery Rate of Bone and Muscle in a Rodent Model of Hindlimb Suspension.* Frontiers in Psychology, 2018. **9**(1085).

Spatz, J.M., R. Ellman, A.M. Cloutier, L. Louis, M. van Vliet, L.J. Suva, D. Dwyer, M. Stolina, H.Z. Ke, and M.L. Bouxsein, *Sclerostin Antibody Inhibits Skeletal Deterioration Due to Reduced Mechanical Loading.* J Bone Miner Res, 2013. **28**(4): p. 865-74.

Steinberg, M.E. and J. Trueta, *Effects of activity on bone growth and development in the rat.* Clin Orthop Relat Res, 1981(156): p. 52-60.

Stone, K.L., D.G. Seeley, L.Y. Lui, J.A. Cauley, K.E. Ensrud, and W. Browner, *BMD at multiple sites and risk of fracture of multiple types: long-term results from the study of osteoporotic fractures.* J Bone Miner Res, 2003. **18**: p. 1947-54.

Swift, J.M., H.G. Gasier, S.N. Swift, M.P. Wiggs, H.A. Hogan, J.D. Fluckey, and S.A. Bloomfield, *Increased training loads do not magnify cancellous bone gains with rodent jump resistance exercise.* J Appl Physiol, 2010a. **109**: p. 1600-1607.

Swift, J.M., F. Lima, B.R. Macias, M.R. Allen, E.S. Greene, Y. Shirazi-Fard, J.S. Kupke, H.A. Hogan, and S.A. Bloomfield, *Partial Weight Bearing Does Not Prevent Musculoskeletal Losses Associated with Disuse.* Med Sci Sports Exerc, 2013. **45**(11): p. 2052-60.

Swift, J.M., M.I. Nilsson, H.A. Hogan, L.R. Sumner, and S.A. Bloomfield, *Simulated resistance training during hindlimb unloading abolishes disuse bone loss and maintains muscle strength.* J Bone Miner Res, 2010b. **25**(3): p. 564-74.

Swift, J.M., S.N. Swift, M.I. Nilsson, H.A. Hogan, S.D. Bouse, and S.A. Bloomfield, *Cancellous bone formation response to simulated resistance training during disuse is blunted by concurrent alendronate treatment.* J Bone Miner Res, 2011. **26**(9): p. 2140-50.

Turner, C.H., *Muscle-Bone Interactions, Revisited.* Bone, 2000. **27**(3): p. 339-340.

Turner, C.H. and D.B. Burr, *Basic biomechanical measurements of bone: a tutorial.* Bone, 1993. **14**(4): p. 595-608.

Turner, C.H., Y. Takano, and I. Owan, *Aging changes mechanical loading thresholds for bone formation in rats.* J Bone Miner Res, 1995. **10**(10): p. 1544-9.

Umemura, Y., T. Ishiko, H. Tsujimoto, H. Miura, N. Mokushi, and H. Suzuki, *Effects of jump training on bone hypertrophy in young and old rats.* Int J Sports Med, 1995. **16**(6): p. 364-7.

Umemura, Y., T. Ishiko, T. Yamauchi, M. Kurono, and S. Mashiko, *Five Jumps per Day Increase Bone Mass and Breaking Force in Rats.* J BOne Miner Res, 1997. **12**(9): p. 1480-1485.

Umemura, Y., S. Nagasawa, N. Sogo, and A. Honda, *Effects of jump training on bone are preserved after detraining, regardless of estrogen secretion state in rats.* J Appl Physiol, 2008. **104**(4): p. 1116-20.

van der Wiel, H.E., P. Lips, W.C. Graafmans, C.C. Danielsen, J. Nauta, A. van Lingen, and L. Mosekilde, *Additional weight-bearing during exercise is more important than duration of exercise for anabolic stimulus of bone: a study of running exercise in female rats.* Bone, 1995. **16**(1): p. 73-80.

Vico, L., D. Chappard, C. Alexandre, S. Palle, P. Minaire, G. Riffat, B.V. Morukov, and S. Rakhmanov, *Effects of a 120 day period of bed-rest on bone mass and bone cell activities in man: attempts at countermeasure.* J Bone Miner Res, 1987. **2**(5): p. 383-94.

Vico, L., P. Collet, A. Guignandon, M.-H. Lafage-Proust, T. Thomas, M. Rehailia, and C. Alexandre, *Effects of long-term microgravity exposure on cancellous and cortical weight-bearing bones of cosmonauts.* Lancet, 2000. **355**(9215): p. 1607-1611.

Vico, L., B. Rietbergen, N. Vilayphious, M. Linossier, H. Locrelle, M. Normand, M. Zouch, M. Gerbaix, N. Bonnet, V. Novikov, T. Thomas, and G. Vassilieva, *Cortical and Trabecular Bone Microstructure Did Not Recover at Weight-Bearing Skeletal Sites and Progressively Deteriorated at Non-Weight-Bearing Sites During the Year Following International Space Station Missions.* J Bone Miner Res, 2017. **32**(10): p. 2010-2021.

Watanabe, Y., H. Ohshima, K. Mizuno, C. Sekiguchi, M. Fukunaga, K. Kohri, J. Rittweger, D. Felsenberg, T. Matsumoto, and T. Nakamura, *Intravenous pamidronate prevents femoral bone loss and renal stone formation during 90-day bed rest.* J Bone Miner Res, 2004. **19**(11): p. 1771-8.

Westerlind, K.C., J.D. Fluckey, S.E. Gordon, W.J. Kraemer, P.A. Farrell, and R.T. Turner, *Effect of resistance exercise training on cortical and cancellous bone in mature male rats.* J Appl Physiol, 1998. **84**(2): p. 459.

Wilson, D.S., K. Coleman, A.B. Clark, and L. LBiederman, *Shy-bold continuum in pumpkinseed sunfish (Lepomis gibbosus)): AN ecological study of apsychological trait.* Journal of Comparative Psychology, 1993. **107**(3): p. 250-260.

Wolff, J., *Das Gesetz der Transformation der Knochen.* 1892.

Yanagihara, G.R., A.G. Paiva, G.A. Gasparini, A.P. Macedo, P.D. Frighetto, J.B. Volpon, and A.C. Shimano, *High-impact exercise in rats prior to and during suspension can prevent bone loss.* Braz J Med Biol Res, 2016. **49**(3).

Zerwekh, J.R., L.A. Ruml, F. Gottschalk, and C.Y.C. Pack, *The Effects of Twelve Weeks of Bed Rest n Bone Histology, Biochemical Markers of Bone TUrnover, and Calcium Homeostasis in Eleven Normal Subjects.* J Bone Miner Res, 1998. **13**(10): p. 1594-1601.

APPENDIX A

EXPERIMENT 1 FULL NUMERICAL RESULTS

This appendix contains full numerical results for all Experiment 2 outcome variables, organized by type of analysis. Data are presented as mean ± standard deviation.

A.1. Animals

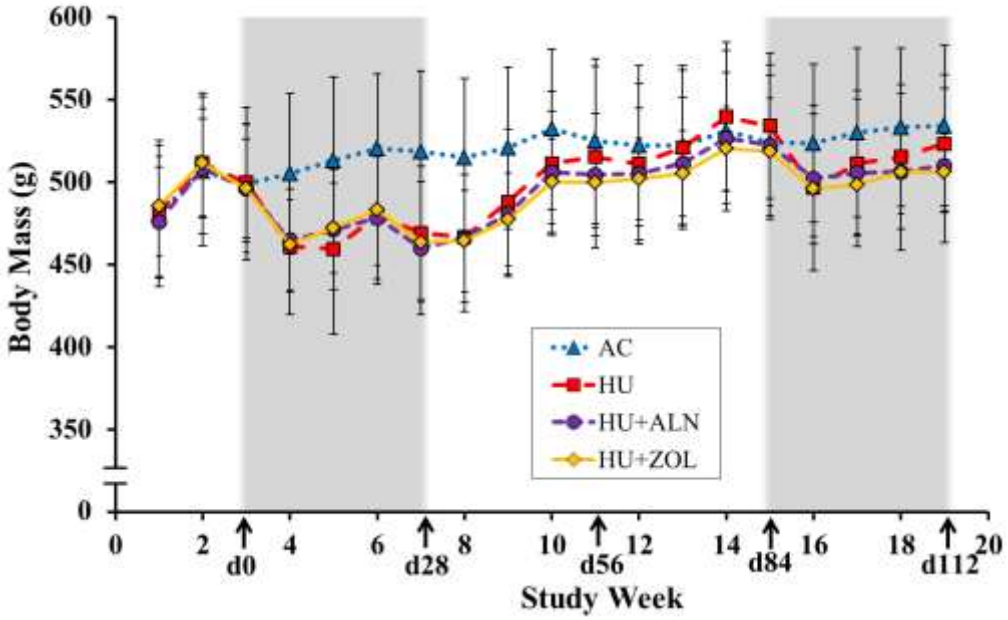

Figure A.1 Weekly Body Mass for Exp. 1.

Table A.1 Soleus Wet Mass Numerical Data for Exp. 1.

Group	d0		d112	
	Left	Right	Left	Right
BC	0.173 ± 0.019	0.169 ± 0.023	-	-
AC	-	-	0.181 ± 0.032	0.181 ± 0.022
HU	-	-	0.083 ± 0.006	0.082 ± 0.010
HU+ALN	-	-	0.097 ± 0.028	0.094 ± 0.030
HU+ZOL	-	-	0.100 ± 0.045	0.092 ± 0.043

A.2 *In Vivo* Longitudinal Peripheral Quantitative Computed Tomography

Table A.2 Proximal Tibia Metaphysis Densitometry Numerical Data for Exp. 1.

	Day	AC	HU	HU+ALN	HU+ZOL
Total BMC (mg/mm)	0	11.3 ± 0.78	11.2 ± 0.69	11.3 ± 0.76	11.7 ± 0.67
	28	11.3 ± 0.68	10.4 ± 0.71	10.7 ± 0.63	12.6 ± 0.92
	56	11.1 ± 0.83	10.6 ± 0.78	11.1 ± 0.74	12.8 ± 0.76
	84	11.2 ± 1.02	11.0 ± 0.99	11.2 ± 1.00	13.1 ± 0.91
	112	11.1 ± 0.88	10.8 ± 0.82	10.8 ± 0.94	13.1 ± 0.87
Total vBMD (mg/cm^3)	0	593.8 ± 35.4	580.7 ± 17.4	586.5 ± 27.4	596.7 ± 21.2
	28	592.6 ± 33.5	551.4 ± 29.1	597.3 ± 28.6	646.4 ± 19.8
	56	594.7 ± 43.6	555.0 ± 31.6	597.1 ± 21.7	657.2 ± 26.6
	84	589.7 ± 36.1	567.7 ± 26.8	605.7 ± 48.6	672.3 ± 18.3
	112	591.9 ± 31.9	566.3 ± 41.4	605.8 ± 26.2	682.4 ± 20.4
Cancellous BMC (mg/mm)	0	2.79 ± 0.58	2.80 ± 0.44	2.82 ± 0.50	2.86 ± 0.48
	28	2.54 ± 0.44	2.29 ± 0.45	2.27 ± 0.37	2.77 ± 0.49
	56	2.10 ± 0.54	2.15 ± 0.41	2.61 ± 0.55	2.65 ± 0.48
	84	2.06 ± 0.56	2.09 ± 0.43	2.52 ± 0.73	2.79 ± 0.58
	112	1.81 ± 0.47	1.85 ± 0.42	2.18 ± 0.63	2.53 ± 0.47
Cancellous vBMD (mg/cm^3)	0	250.9 ± 48.9	245.6 ± 29.0	247.4 ± 33.5	251.0 ± 33.0
	28	229.8 ± 39.7	200.5 ± 29.2	221.5 ± 33.7	257.3 ± 34.1
	56	197.9 ± 38.6	190.7 ± 25.5	239.5 ± 38.5	252.7 ± 38.9
	84	189.7 ± 41.1	185.9 ± 25.5	231.9 ± 42.7	267.1 ± 43.0
	112	173.0 ± 35.7	167.3 ± 26.4	211.0 ± 42.4	252.8 ± 40.3
Cortical BMC (mg/mm)	0	8.55 ± 0.59	8.36 ± 0.57	8.46 ± 0.51	8.78 ± 0.45
	28	8.79 ± 0.67	8.14 ± 0.86	8.40 ± 0.73	9.82 ± 0.60
	56	9.00 ± 0.75	8.43 ± 0.81	8.49 ± 0.51	10.1 ± 0.68
	84	9.15 ± 0.86	8.86 ± 0.86	8.64 ± 0.53	10.3 ± 0.63
	112	9.24 ± 0.85	8.91 ± 0.99	8.64 ± 0.61	10.5 ± 0.83
Cortical vBMD (mg/cm^3)	0	1049 ± 22.7	1043 ± 14.7	1047 ± 19.2	1054 ± 15.9
	28	1063 ± 24.0	1053 ± 36.2	1079 ± 22.9	1100 ± 16.2
	56	1076 ± 34.0	1053 ± 31.1	1068 ± 22.1	1110 ± 15.5
	84	1080 ± 27.3	1067 ± 27.2	1074 ± 37.2	1117 ± 37.2
	112	1092 ± 22.8	1081 ± 36.6	1096 ± 31.2	1132 ± 16.6

Table A.3 Proximal Tibia Metaphysis Geometry Numerical Data for Exp. 1.

	Day	AC	HU	HU+ALN	HU+ZOL
Total Bone Area (mm^2)	0	19.2 ± 1.93	19.3 ± 1.35	19.3 ± 1.25	19.6 ± 1.33
	28	19.2 ± 1.87	19.0 ± 1.18	17.9 ± 0.88	19.5 ± 1.51
	56	18.9 ± 2.34	19.1 ± 1.19	18.6 ± 1.32	19.5 ± 0.95
	84	19.2 ± 2.46	19.4 ± 1.73	18.6 ± 2.21	19.5 ± 1.08
	112	18.8 ± 2.07	19.1 ± 1.25	18.0 ± 1.71	19.2 ± 1.12
Cancellous Bone Area (mm^2)	0	11.1 ± 1.47	11.3 ± 1.01	11.2 ± 1.02	11.2 ± 1.01
	28	11.0 ± 1.40	11.3 ± 1.02	10.1 ± 0.68	10.6 ± 0.98
	56	10.5 ± 1.87	11.1 ± 1.01	10.7 ± 1.00	10.3 ± 0.69
	84	10.7 ± 1.81	11.0 ± 1.19	10.5 ± 1.81	10.3 ± 0.71
	112	10.3 ± 1.53	10.8 ± 1.18	10.1 ± 1.31	9.86 ± 0.64
Cortical Bone Area (mm^2)	0	8.15 ± 0.56	8.02 ± 0.50	8.08 ± 0.45	8.34 ± 0.44
	28	8.27 ± 0.60	7.72 ± 0.62	7.79 ± 0.57	8.94 ± 0.61
	56	8.37 ± 0.67	8.00 ± 0.60	7.95 ± 0.46	9.13 ± 0.54
	84	8.47 ± 0.81	8.32 ± 0.78	8.05 ± 0.53	9.25 ± 0.55
	112	8.47 ± 0.77	8.24 ± 0.69	7.89 ± 0.57	9.30 ± 0.69
Cortical Thickness (mm)	0	0.60 ± 0.023	0.58 ± 0.026	0.59 ± 0.029	0.61 ± 0.022
	28	0.61 ± 0.028	0.57 ± 0.044	0.59 ± 0.041	0.66 ± 0.025
	56	0.63 ± 0.039	0.59 ± 0.044	0.59 ± 0.025	0.68 ± 0.035
	84	0.63 ± 0.036	0.61 ± 0.042	0.60 ± 0.035	0.68 ± 0.031
	112	0.63 ± 0.040	0.61 ± 0.055	0.60 ± 0.032	0.70 ± 0.040

Table A.4 Tibia Mid-Diaphysis Densitometry and Geometry Numerical Data for Exp. 1.

	Day	AC	HU	HU+ALN	HU+ZOL
Cortical BMC (mg/mm)	0	8.68 ± 0.41	8.64 ± 0.54	8.71 ± 0.61	8.73 ± 0.49
	28	8.94 ± 0.40	8.77 ± 0.62	8.83 ± 0.50	8.96 ± 0.48
	56	8.68 ± 0.41	8.64 ± 0.54	8.71 ± 0.61	8.73 ± 0.49
	84	9.23 ± 0.51	9.00 ± 0.58	9.07 ± 0.71	9.22 ± 0.43
	112	9.43 ± 0.49	9.12 ± 0.52	9.19 ± 0.68	9.25 ± 0.43
Cortical vBMD (mg/cm^3)	0	1326 ± 12.4	1321 ± 13.3	1324 ± 12.4	1327 ± 16.1
	28	1345 ± 6.8	1340 ± 10.5	1331 ± 32.3	1343 ± 13.7
	56	1358 ± 8.13	1340 ± 18.0	1343 ± 10.2	1349 ± 14.3
	84	1355 ± 12.0	1343 ± 11.4	1347 ± 27.7	1348 ± 13.4
	112	1364 ± 12.5	1369 ± 9.5	1372 ± 17.7	1367 ± 24.2
Cortical Area (mm^2)	0	6.55 ± 0.30	6.54 ± 0.43	6.58 ± 0.48	6.58 ± 0.35
	28	6.64 ± 0.30	6.55 ± 0.46	6.63 ± 0.34	6.67 ± 0.36
	56	6.81 ± 0.43	6.64 ± 0.39	6.59 ± 0.55	6.73 ± 0.39
	84	6.82 ± 0.39	6.70 ± 0.44	6.73 ± 0.52	6.83 ± 0.30
	112	6.91 ± 0.35	6.66 ± 0.37	6.70 ± 0.48	6.77 ± 0.36
Cortical Thickness (mm)	0	0.77 ± 0.025	0.76 ± 0.025	0.77 ± 0.035	0.76 ± 0.034
	28	0.78 ± 0.023	0.76 ± 0.024	0.78 ± 0.036	0.78 ± 0.037
	56	0.80 ± 0.023	0.77 ± 0.019	0.78 ± 0.036	0.78 ± 0.039
	84	0.79 ± 0.027	0.77 ± 0.018	0.80 ± 0.050	0.79 ± 0.040
	112	0.80 ± 0.023	0.77 ± 0.027	0.80 ± 0.048	0.80 ± 0.037
Polar Area MOI (mm^4)	0	14.2 ± 1.77	14.9 ± 2.49	14.6 ± 2.52	14.7 ± 2.04
	28	14.5 ± 1.65	14.4 ± 2.86	14.5 ± 1.87	14.9 ± 1.99
	56	15.2 ± 2.98	14.9 ± 2.31	14.2 ± 2.71	15.0 ± 2.04
	84	15.2 ± 2.09	15.3 ± 2.83	14.5 ± 2.51	15.3 ± 1.42
	112	15.4 ± 2.22	14.7 ± 1.86	13.8 ± 1.93	14.3 ± 1.94

A.3. *Ex Vivo* Peripheral Quantitative Computed Tomography

Table A.5 Proximal Tibia Metaphysis and Tibia Mid-Diaphysis Densitometry and Geometry Numerical Data for Exp. 1.

	BC	AC	HU	HU+ALN	HU+ZOL
Proximal Tibia Metaphysis					
Total BMC (mg/mm)	11.5 ± 1.49	11.7 ± 0.90	10.9 ± 0.97	11.1 ± 0.79	13.7 ± 1.43
Total vBMD (mg/cm^3)	615.6 ± 30.3	586.3 ± 30.8	551.0 ± 23.1	580.3 ± 30.4	682.8 ± 22.1
Cancellous BMC (mg/mm)	2.62 ± 1.09	2.32 ± 0.57	2.12 ± 0.35	2.76 ±0.65	3.11 ± 0.74
Cancellous vBMD (mg/cm^3)	236.5 ± 45.3	200.1 ± 40.0	181.1 ± 26.7	237.5 ± 37.6	285.4 ± 48.9
Cortical BMC (mg/mm)	8.92 ± 0.55	9.38 ± 0.71	8.74 ± 0.78	8.37 ± 0.48	10.6 ± 0.95
Cortical vBMD (mg/cm^3)	1086 ± 41.1	1088 ± 24.0	1073 ± 10.9	1072 ± 30.7	1132 ± 21.2
Total Bone Area (mm^2)	18.9 ± 3.00	20.1 ± 2.19	19.7 ± 1.51	19.3 ± 1.70	20.1 ± 1.98
Cancellous Bone Area (mm^2)	10.6 ± 2.29	11.4 ± 1.63	11.6 ± 0.91	11.5 ± 1.39	10.7 ± 1.18
Cortical Bone Area (mm^2)	8.24 ± 0.76	8.63 ± 0.69	8.15 ± 0.70	7.82 ±0.45	9.38 ± 0.92
Cortical Thickness (mm)	0.61 ± 0.019	0.62 ± 0.030	0.59 ± 0.033	0.57 ± 0.025	0.68 ± 0.040
Tibia Diaphysis					
Cortical BMC (mg/mm)	8.62 ± 0.52	9.66 ± 0.54	9.48 ± 0.48	9.52 ± 0.65	9.54 ± 0.39
Cortical vBMD (mg/cm^3)	1368 ± 16.7	1400 ± 9.26	1389 ± 5.96	1392 ± 15.5	1394 ± 10.8
Cortical Area (mm^2)	6.31 ± 0.39	6.89 ± 0.38	6.83 ± 0.34	6.84 ± 0.46	6.85 ± 0.27
Cortical Thickness (mm)	0.75 ± 0.032	0.79 ± 0.024	0.78 ± 0.030	0.79 ± 0.038	0.78 ± 0.028
Polar Area MOI (mm^4)	13.3 ± 2.09	15.8 ± 2.19	15.6 ± 1.69	15.4 ± 1.96	15.7 ± 1.43

Table A.6 Distal Femur Metaphysis and Femur Mid-Diaphysis Densitometry and Geometry Numerical Data for Exp. 1.

	BC	AC	HU	HU+ALN	HU+ZOL
Distal Femur Metaphysis					
Total BMC (mg/mm)	12.0 ± 1.33	12.0 ± 1.22	10.8 ± 1.40	11.7 ± 1.00	13.8 ± 2.06
Total vBMD (mg/cm^3)	630.7 ± 71.2	589.1 ± 85.2	599.5 ± 106.2	612.2 ± 87.0	674.2 ± 51.5
Cancellous BMC (mg/mm)	6.18 ± 1.30	5.86 ± 1.75	5.43 ± 1.03	6.36 ± 1.17	7.12 ± 1.93
Cancellous vBMD (mg/cm^3)	391.4 ± 39.9	335.6 ± 59.2	317.5 ± 85.7	399.6 ± 100.7	440.2 ± 78.9
Cortical BMC (mg/mm)	5.84 ± 0.65	6.09 ± 1.21	5.33 ± 1.04	5.33 ± 1.12	6.67 ± 0.55
Cortical vBMD (mg/cm^3)	1366 ± 36.7	1378 ± 54.7	1358 ± 51.2	1350 ± 80.8	1406 ± 64.0
Total Bone Area (mm^2)	19.6 ± 2.88	21.1 ± 3.45	20.6 ± 3.11	20.4 ± 2.08	20.5 ± 2.39
Cancellous Bone Area (mm^2)	15.3 ± 2.91	16.7 ± 3.76	16.7 ± 2.72	16.5 ± 1.95	15.8 ± 2.31
Cortical Bone Area (mm^2)	4.26 ± 0.40	4.40 ± 0.73	3.91 ± 0.68	3.91 ± 0.62	4.70 ± 0.34
Cortical Thickness (mm)	0.30 ± 0.047	0.30 ± 0.084	0.31 ± 0.061	0.28 ± 0.038	0.32 ± 0.027
Femur Diaphysis					
Cortical BMC (mg/mm)	12.8 ± 0.82	15.0 ± 1.01	15.1 ± 1.21	15.0 ± 1.11	15.5 ± 0.64
Cortical vBMD (mg/cm^3)	1423 ± 11.9	1449 ± 5.51	1445 ± 9.22	1455 ± 4.56	1450 ± 10.7
Cortical Area (mm^2)	9.02 ± 0.57	10.4 ± 0.70	10.4 ± 0.79	10.3 ± 0.78	10.7 ± 0.45
Cortical Thickness (mm)	0.84 ± 0.031	0.91 ± 0.044	0.91 ± 0.048	0.93 ± 0.048	0.96 ± 0.041
Polar Area MOI (mm^4)	28.7 ± 4.07	37.1 ± 5.67	37.7 ± 5.55	34.3 ± 5.02	37.2 ± 3.46

Table A.7 Femoral Neck Densitometry and Geometry Numerical Data for Exp. 1.

	BC	AC	HU	HU+ALN	HU+ZOL
Total BMC (mg/mm)	5.47 ± 0.64	5.40 ± 0.64	5.34 ± 0.68	5.81 ± 0.97	6.32 ± 0.76
Total vBMD (mg/cm^3)	1089 ± 53.1	1109 ± 45.8	1070 ± 55.3	1099 ± 55.3	1130 ± 37.7
Cancellous BMC (mg/mm)	1.90 ± 0.49	1.65 ± 0.36	1.57 ± 0.53	2.02 ± 0.78	2.13 ± 0.52
Cancellous vBMD (mg/cm^3)	746.7 ± 63.6	715.5 ± 65.2	628.9 ± 68.7	731.6 ± 69.0	776.6 ± 56.3
Cortical BMC (mg/mm)	3.58 ± 0.32	3.75 ± 0.51	3.76 ± 0.31	3.79 ± 0.43	4.20 ± 0.41
Cortical vBMD (mg/cm^3)	1424 ± 28.4	1456 ± 52.8	1478 ± 28.6	1456 ± 38.2	1457 ± 22.4
Total Bone Area (mm^2)	5.05 ± 0.71	4.86 ± 0.53	5.03 ± 0.89	5.33 ± 1.10	5.61 ± 0.74
Cancellous Bone Area (mm^2)	2.53 ± 0.59	2.30 ± 0.34	2.48 ± 0.74	2.72 ± 0.90	2.72 ± 0.57
Cortical Bone Area (mm^2)	2.52 ± 0.23	2.56 ± 0.33	2.55 ± 0.23	2.61 ± 0.32	2.89 ± 0.32
Cortical Thickness (mm)	0.37 ± 0.033	0.39 ± 0.044	0.38 ± 0.032	0.38 ± 0.042	0.41 ± 0.040
Polar Area MOI (mm^4)	4.37 ± 0.77	4.57 ± 0.70	4.48 ± 1.26	4.85 ± 1.51	5.51 ± 1.15

A.4 *Ex Vivo* Micro-computed Tomography

Table A.8 Proximal Tibia Metaphysis Densitometry and Geometry Numerical Data for Exp. 1.

	BC	AC	HU	HU+ALN	HU+ZOL
Cancellous Compartment					
BV/TV (%)	15.5 ± 4.08	12.3 ± 4.15	11.6 ± 2.56	16.3 ± 3.52	24.0 ± 5.90
Trabecular Thickness (mm)	0.093 ± 0.005	0.094 ± 0.00	0.091 ± 0.005	0.089 ± 0.004	0.100 ± 0.010
Trabecular Separation (mm)	0.31 ± 0.050	0.34 ± 0.058	0.32 ± 0.037	0.28 ± 0.049	0.25 ± 0.043
Trabecular Number (#/mm)	1.65 ± 0.39	1.29 ± 0.39	1.27 ± 0.26	1.83 ± 0.39	2.40 ± 0.48
Cortical Compartment					
Cortical Thickness (mm)	0.39 ± 0.042	0.36 ± 0.017	0.38 ± 0.032	0.38 ± 0.029	0.36 ± 0.027
Porosity (%)	0.42 ± 0.34	0.51 ± 0.41	0.32 ± 0.30	0.59 ± 0.49	0.22 ± 0.17
Total Bone Area (mm^2)	7.39 ± 0.91	7.26 ± 0.67	7.24 ± 0.38	7.83 ± 1.14	6.98 ± 0.79
Marrow Area (mm^2)	11.9 ± 1.23	12.5 ± 1.44	12.4 ± 1.71	12.8 ± 1.86	13.1 ± 1.08
Endocortical Perimeter (mm)	16.6 ± 1.63	19.3 ± 1.98	16.8 ± 1.81	16.5 ± 2.82	17.5 ± 1.45
Periosteal Perimeter (mm)	19.5 ± 1.38	19.7 ± 1.18	20.1 ± 0.87	22.5 ± 4.37	20.0 ± 1.44

A.5 Mechanical Testing

Table A.9 Tibia Mid-Diaphysis Three-Point Bending Numerical Data for Exp. 1.

	BC	AC	HU	HU+ALN	HU+ZOL
Extrinsic Properties					
Stiffness (N/mm)	393.0 ± 44.0	469.0 ± 45.9	461.6 ± 40.8	439.7 ± 42.3	465.4 ± 33.6
Ultimate Force (N)	128.4 ± 15.5	135.1 ± 24.2	140.6 ± 16.7	144.7 ± 11.3	147.1 ± 11.1
Yield Force (N)	100.2 ± 9.72	101.2 ± 23.1	103.8 ± 10.2	108.7 ± 14.3	108.1 ± 8.90
Post-Yield Displacement (mm)	0.45 ± 0.22	0.40 ± 0.29	0.31 ± 0.22	0.52 ± 0.17	0.38 ± 0.19
Intrinsic Properties					
Energy to Ultimate Stress (mJ)	36.1 ± 10.5	36.5 ± 18.8	38.5 ± 13.8	45.4 ± 14.1	41.3 ± 11.1
Ultimate Stress (MPa)	154.9 ± 30.9	139.2 ± 32.5	151.3 ± 21.6	149.3 ± 25.0	150.4 ± 13.6
Elastic Modulus (GPa)	3.59 ± 0.31	3.62 ± 0.35	3.62 ± 0.31	3.51 ± 0.44	3.61 ± 0.24

Table A.10 Proximal Tibia Metaphysis Reduced Platen Compression Numerical Data for Exp. 1.

	BC	AC	HU	HU+ALN	HU+ZOL
Ultimate Stress (MPa)	2.13 ± 2.02	1.21 ± 0.76	0.98 ± 0.50	1.23 ± 0.94	2.40 ± 1.45
Elastic Modulus (MPa)	35.4 ± 28.9	22.0 ± 19.1	21.1 ± 14.0	13.3 ± 5.80	37.9 ± 23.7
Energy to Ultimate Stress (mJ)	1.00 ± 0.83	0.63 ± 0.87	0.65 ± 0.65	0.98 ± 1.20	3.59 ± 4.45
Strain at Ultimate Stress (%)	0.12 ± 0.074	0.18 ± 0.13	0.13 ± 0.093	0.18 ± 0.13	0.21 ± 0.17

Table A.11 Femur Mid-Diaphysis Three-Point Bending Numerical Data for Exp. 1.

	BC	AC	HU	HU+ALN	HU+ZOL
Extrinsic Properties					
Stiffness (N/mm)	478.2 ± 57.4	522.4 ± 30.5	515.1 ± 53.5	547.4 ± 52.8	552.9 ± 44.4
Ultimate Force (N)	248.2 ± 20.7	289.7 ± 28.0	296.0 ± 32.9	292.3 ± 26.4	305.1 ± 20.7
Yield Force (N)	127.8 ± 14.9	155.5 ± 35.5	157.5 ± 22.1	148.0 ± 13.3	148.6 ± 11.7
Post-Yield Displacement (mm)	0.61 ± 0.15	0.50 ± 0.13	0.55 ± 0.14	0.61 ± 0.16	0.67 ± 0.22
Intrinsic Properties					
Energy to Ultimate Stress (mJ)	119.2 ± 25.2	128.2 ± 26.6	138.5 ± 16.3	136.7 ± 17.1	142.3 ± 23.6
Ultimate Stress (MPa)	127.9 ± 7.64	124.4 ± 14.8	124.4 ± 9.22	132.8 ± 12.0	129.0 ± 12.3
Elastic Modulus (GPa)	1.19 ± 0.19	1.00 ± 0.15	0.97 ± 0.14	1.13 ± 0.15	1.05 ± 0.09

Table A.12 Femoral Neck Mechanical Test Numerical Data for Exp. 1.

	BC	AC	HU	HU+ALN	HU+ZOL
Stiffness (N/mm)	168.6 ± 25.3	170.1 ± 10.0	136.9 ± 54.1	177.5 ± 32.3	169.5 ± 41.4
Ultimate Force (N)	115.0 ± 22.8	115.7 ± 3.44	109.8 ± 18.2	114.8 ± 17.3	128.7 ± 16.7
Energy to Ultimate Force (mJ)	44.0 ± 14.9	42.7 ± 2.62	50.5 ± 23.2	40.6 ± 12.6	56.0 ± 16.6

A.6 Histomorphometry

Table A.13 Distal Femur Metaphysis Static Cancellous Histomorphometry Numerical Data for Exp. 1.

	AC	HU	HU+ALN	HU+ZOL
Oc.S/BS (%)	3.20 ± 2.06	3.28 ± 1.53	2.21 ± 0.84	0.79 ± 0.74
OS/BS (%)	3.04 ± 1.84	1.29 ± 0.84	0.73 ± 0.81	0.11 ± 0.16
BV/TV (%)	12.3 ± 3.23	14.0 ± 4.42	13.8 ± 4.66	19.2 ± 7.04
Trabecular Thickness (mm)	0.064 ± 0.0068	0.063 ± 0.014	0.054 ± 0.0068	0.073 ± 0.0116
Trabecular Separation (mm)	0.48 ± 0.13	0.41 ± 0.12	0.37 ± 0.12	0.33 ± 0.10
Trabecular Number (#/mm)	1.90 ± 0.36	2.20 ± 0.47	2.52 ± 0.69	2.63 ± 0.74

Table A.14 Tibia Mid-Diaphysis Cortical Histomorphometry Numerical Data for Exp. 1.

	AC	HU	HU+ALN	HU+ZOL
Mid-Recovery (d56)				
MS/BS (%)	32.8 ± 14.4	50.5 ± 23.8	33.9 ± 16.0	33.1 ± 7.07
MAR (μm/day)	0.59 ± 0.26	1.07 ± 0.39 †	0.79 ± 0.36	0.77 ± 0.16
BFR/BS ($\mu m^3/\mu m^2$/day)	0.21 ± 0.13	0.54 ± 0.34	0.30 ± 0.21	0.26 ± 0.097
End of Recovery (d84)				
MS/BS (%)	29.2 ± 17.8	56.8 ± 12.8 †	45.5 ± 10.2	44.2 ± 10.2
MAR (μm/day)	0.65 ± 0.19	0.87 ± 0.12 †	0.96 ± 0.37	0.73 ± 0.10
BFR/BS ($\mu m^3/\mu m^2$/day)	0.22 ± 0.17	0.51 ± 0.17 †	0.45 ± 0.25	0.33 ± 0.11

APPENDIX B

EXPERIMENT 2 FULL NUMERICAL RESULTS

This appendix contains full numerical results for all Experiment 2 outcome variables, organized by type of analysis. Data are presented as mean ± standard deviation.

B.1 Animals

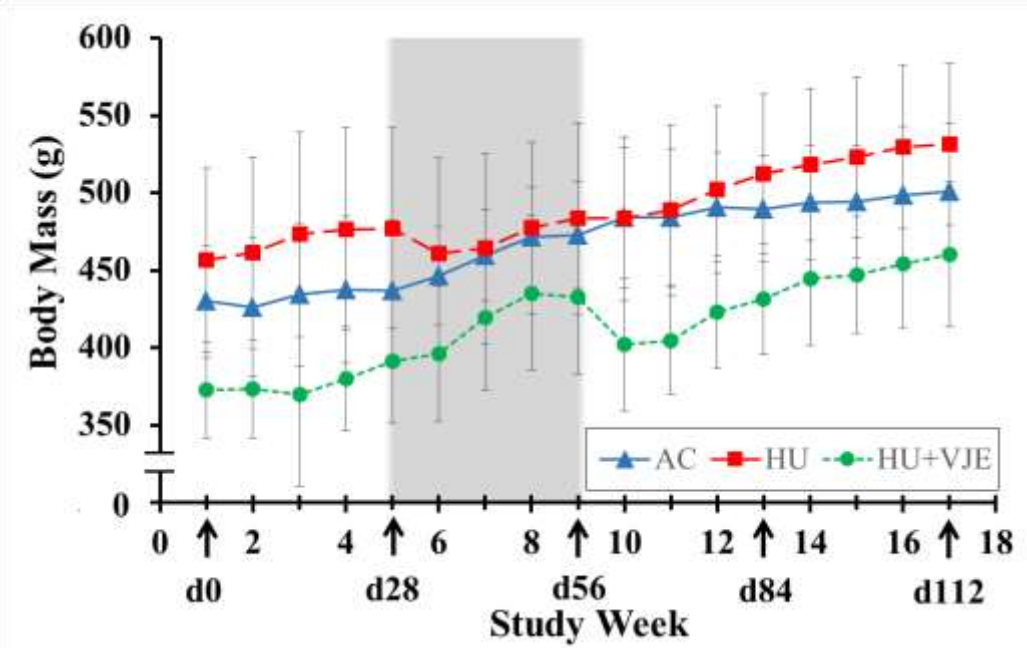

Figure B.1 Weekly Body Mass for Exp. 2.

Table B.1 Soleus Wet Mass Numerical Data for Exp. 2.

Group	d0	d28	d56	d112
AC	0.192 ± 0.044	0.183 ± 0.038	0.179 ± 0.037	0.188 ± 0.047
HU	-	-	0.099 ± 0.015	0.210 ± 0.035
HU+VJE	-	0.149 ± 0.012	0.079 ± 0.012	0.161 ± 0.025

B.2 *In Vivo* Longitudinal Peripheral Quantitative Computed Tomography

Table B.2 Proximal Tibia Metaphysis Densitometry Numerical Data for Exp. 2.
Animals euthanized at all time points included.

	Day	AC	HU	HU+VJE
Total BMC (mg/mm)	0	10.3 ± 1.00	10.8 ± 0.92	10.1 ± 1.08
	28	10.5 ± 1.01	11.1 ± 0.87	10.9 ± 1.15
	56	10.7 ± 0.99	10.3 ± 0.83	10.5 ± 1.26
	84	10.7 ± 1.09	10.6 ± 0.64	10.0 ± 0.81
	112	10.7 ± 1.08	11.1 ± 0.95	10.2 ± 0.91
Total vBMD (mg/cm^3)	0	614.5± 34.9	611.7 ± 31.2	624.5 ± 36.3
	28	627.0 ± 36.1	626.2 ± 33.6	660.7 ± 34.3
	56	630.0 ± 40.2	598.7 ± 34.3	638.2 ± 36.5
	84	630.2 ± 43.2	623.2 ± 46.1	606.4 ± 45.3
	112	627.4 ± 43.9	615.8 ± 46.3	606.0 ± 20.2
Cancellous BMC (mg/mm)	0	1.85 ± 0.43	1.95 ± 0.65	2.12 ± 0.56
	28	1.78 ± 0.40	1.85 ± 0.57	1.89 ± 0.52
	56	1.83 ± 0.50	1.64 ± 0.48	1.85 ± 0.49
	84	1.73 ± 0.57	1.53 ± 0.47	2.21 ± 0.64
	112	1.66 ± 0.37	1.67 ± 0.56	2.18 ± 0.48
Cancellous vBMD (mg/cm^3)	0	201.2 ± 30.5	199.4 ± 41.0	213.3 ± 34.8
	28	195.5 ± 27.5	190.5 ± 35.4	217.8 ± 36.8
	56	197.1 ± 35.7	170.2 ± 27.2	204.6 ± 32.5
	84	186.4 ± 38.7	164.4 ± 28.1	224.7 ± 45.2
	112	180.6 ± 32.1	167.8 ± 29.4	224.2 ± 31.8
Cortical BMC (mg/mm)	0	8.44 ± 0.91	8.83 ± 0.85	8.82 ± 0.60
	28	8.74 ± 0.92	9.27 ± 0.62	8.96 ± 0.89
	56	8.90 ± 0.90	8.64 ± 0.73	8.70 ± 1.06
	84	8.96 ± 1.09	9.04 ± 0.37	7.83 ± 0.99
	112	9.08 ± 1.23	9.42 ± 0.63	8.04 ± 0.64
Cortical vBMD (mg/cm^3)	0	1083 ± 27.6	1079 ± 31.8	1088 ± 27.7
	28	1100 ± 25.1	1098 ± 27.5	1114 ± 21.9
	56	1105 ± 28.4	1098 ± 29.4	1114 ± 27.6
	84	1109 ± 36.5	1114 ± 31.2	1074 ± 45.4
	112	1113 ± 30.1	1108 ± 32.5	1080 ± 19.3

Table B.3 Proximal Tibia Metaphysis Geometry Numerical Data for Exp. 2.
Animals euthanized at all time points included.

	Day	AC	HU	HU+VJE
Total Bone Area (mm^2)	0	16.8 ± 1.78	17.7 ± 1.81	16.2 ± 2.20
	28	16.9 ± 1.89	17.9 ± 1.89	16.5 ± 1.96
	56	17.1 ± 1.82	17.3 ± 1.75	16.6 ± 1.99
	84	17.1 ± 1.91	17.1 ± 1.94	16.7 ± 1.34
	112	18.2 ± 1.48	18.2 ± 2.29	16.9 ± 1.69
Cancellous Bone Area (mm^2)	0	9.01 ± 1.25	9.53 ± 1.45	8.72 ± 1.63
	28	8.92 ± 1.32	9.42 ± 1.51	8.45 ± 1.37
	56	9.08 ± 1.37	9.42 ± 1.40	8.79 ± 1.35
	84	8.99 ± 1.49	9.01 ± 1.65	9.46 ± 1.15
	112	9.04 ± 1.03	9.65 ± 1.87	9.47 ± 1.21
Cortical Bone Area (mm^2)	0	7.80 ± 0.79	8.18 ± 0.71	7.50 ± 0.69
	28	7.95 ± 0.83	8.46 ± 0.56	8.05 ± 0.79
	56	8.06 ± 0.77	7.87 ± 0.61	7.80 ± 0.88
	84	8.07 ± 0.87	8.13 ± 0.40	7.28 ± 0.70
	112	8.15 ± 0.97	8.51 ± 0.63	7.46 ± 0.59
Cortical Thickness (mm)	0	0.62 ± 0.047	0.63 ± 0.048	0.61 ± 0.033
	28	0.63 ± 0.049	0.66 ± 0.035	0.65 ± 0.044
	56	0.64 ± 0.050	0.62 ± 0.041	0.63 ± 0.050
	84	0.64 ± 0.061	0.65 ± 0.034	0.57 ± 0.053
	112	0.64 ± 0.069	0.65 ± 0.053	0.59 ± 0.029

Table B.4 Tibia Mid-Diaphysis Densitometry and Geometry Numerical Data for Exp. 2. Animals euthanized at all time points included.

	Day	AC	HU	HU+VJE
Cortical BMC (mg/mm)	0	7.81 ± 0.54	7.92 ± 0.49	7.66 ± 0.72
	28	8.03 ± 0.53	8.16 ± 0.54	8.29 ± 0.74
	56	8.25 ± 0.60	8.34 ± 0.53	8.60 ± 0.90
	84	8.54 ± 0.53	8.60 ± 0.56	8.42 ± 0.73
	112	8.76 ± 0.57	8.92 ± 0.55	8.49 ± 0.69
Cortical vBMD (mg/cm^3)	0	1338 ± 15.3	1336 ± 12.6	1342 ± 12.9
	28	1351 ± 11.8	1348 ± 12.3	1357 ± 11.7
	56	1358 ± 15.2	1364 ± 10.3	1370 ± 13.9
	84	1362 ± 14.1	1367 ± 13.2	1360 ± 19.4
	112	1371 ± 8.93	1369 ± 12.3	1369 ± 16.9
Cortical Area (mm^2)	0	5.84 ± 0.41	5.93 ± 0.38	5.71 ± 0.55
	28	5.94 ± 0.39	6.05 ± 0.39	6.11 ± 0.53
	56	6.08 ± 0.44	6.11 ± 0.40	6.28 ± 0.64
	84	6.27 ± 0.38	6.29 ± 0.44	6.19 ± 0.52
	112	6.39 ± 0.41	6.51 ± 0.40	6.20 ± 0.49
Cortical Thickness (mm)	0	0.74 ± 0.034	0.74 ± 0.035	0.74 ± 0.035
	28	0.75 ± 0.032	0.75 ± 0.037	0.78 ± 0.037
	56	0.76 ± 0.033	0.76 ± 0.035	0.80 ± 0.040
	84	0.77 ± 0.035	0.77 ± 0.036	0.77 ± 0.035
	112	0.78 ± 0.039	0.78 ± 0.040	0.78 ± 0.029
Polar Area MOI (mm^4)	0	10.8 ± 1.69	11.3 ± 1.75	10.2 ± 2.45
	28	11.1 ± 1.58	11.6 ± 1.78	11.5 ± 2.20
	56	11.8 ± 1.94	11.7 ± 1.84	11.9 ± 2.70
	84	12.5 ± 2.10	12.4 ± 2.24	12.1 ± 2.42
	112	12.9 ± 1.79	13.6 ± 2.18	12.0 ± 2.39

B.3 *Ex Vivo* Peripheral Quantitative Computed Tomography

Table B.5 Proximal Tibia Metaphysis Densitometry and Geometry Numerical Data for Exp. 2.

	Day	AC	HU	HU+VJE
Total BMC (mg/mm)	28	11.7 ± 1.45	-	10.9 ± 0.99
	56	11.8 ± 1.56	10.5 ± 0.88	12.2 ± 1.40
	112	11.6 ± 1.32	12.2 ± 1.25	11.0 ± 1.09
Total vBMD (mg/cm^3)	28	614.2 ± 40.9	-	669.1 ± 35.4
	56	622.7 ± 37.5	565.6 ± 51.9	630.4 ± 29.8
	112	600.9 ± 33.1	589.3 ± 43.7	640.4 ± 39.7
Cancellous BMC (mg/mm)	28	2.51 ± 0.90	-	2.00 ± 0.59
	56	2.41 ± 0.90	2.11 ± 0.73	3.05 ± 1.19
	112	2.41 ± 0.77	2.57 ± 0.92	2.15 ± 0.50
Cancellous vBMD (mg/cm^3)	28	225.1 ± 31.2	-	229.0 ± 39.1
	56	218.6 ± 34.0	185.5 ± 37.6	261.4 ± 49.2
	112	213.5 ± 40.3	207.0 ± 44.7	225.1 ± 27.0
Cortical BMC (mg/mm)	28	9.17 ± 0.85	-	8.91 ± 0.84
	56	9.42 ± 0.85	8.38 ± 0.69	9.16 ± 0.69
	112	9.17 ± 0.91	9.60 ± 0.57	8.83 ± 0.74
Cortical vBMD (mg/cm^3)	28	1079 ± 51.3	-	1073 ± 10.9
	56	1093 ± 44.6	1067 ± 54.2	1063 ± 39.0
	112	1126 ± 32.8	1092 ± 43.9	1110 ± 24.5
Total Bone Area (mm^2)	28	19.3 ± 3.37	-	16.4 ± 1.51
	56	19.2 ± 3.34	18.8 ± 2.38	19.5 ± 2.82
	112	19.4 ± 2.55	21.0 ± 2.83	17.2 ± 2.02
Cancellous Bone Area (mm^2)	28	10.7 ± 2.51	-	8.44 ± 1.20
	56	10.5 ± 2.45	10.9 ± 2.12	11.1 ± 2.34
	112	10.9 ± 1.84	11.9 ± 2.32	9.27 ± 1.48
Cortical Bone Area (mm^2)	28	8.54 ± 1.03	-	7.92 ± 0.67
	56	8.67 ± 1.04	7.86 ± 0.52	8.40 ± 0.66
	112	8.47 ± 0.90	9.07 ± 0.70	7.97 ± 0.69
Cortical Thickness (mm)	28	0.63 ± 0.037	-	0.65 ± 0.049
	56	0.65 ± 0.038	0.59 ± 0.044	0.62 ± 0.037
	112	0.62 ± 0.042	0.64 ± 0.035	0.63 ± 0.036

Table B.6 Tibia Mid-Diaphysis Densitometry and Geometry Numerical Data for Exp. 2.

	Day	AC	HU	HU+VJE
Cortical BMC (mg/mm)	28	8.33 ± 0.51	-	8.30 ± 0.48
	56	8.44 ± 0.57	8.55 ± 0.63	9.40 ± 0.85
	112	8.93 ± 0.68	9.03 ± 0.72	8.73 ± 0.78
Cortical vBMD (mg/cm^3)	28	1383 ± 14.1	-	1393 ± 18.9
	56	1396 ± 11.3	1391 ± 14.7	1395 ± 13.6
	112	1406 ± 12.5	1396 ± 5.84	1400 ± 13.6
Cortical Area (mm^2)	28	6.03 ± 0.35	-	5.96 ± 0.34
	56	6.04 ± 0.42	6.15 ± 0.46	6.74 ± 0.62
	112	6.35 ± 0.50	6.47 ± 0.50	6.24 ± 0.52
Cortical Thickness (mm)	28	0.76 ± 0.036	-	0.76 ± 0.036
	56	0.75 ± 0.029	0.76 ± 0.038	0.81 ± 0.037
	112	0.77 ± 0.036	0.78 ± 0.036	0.78 ± 0.032
Polar Area MOI (mm^4)	28	11.4 ± 1.68	-	11.0 ± 1.16
	56	11.8 ± 1.99	11.8 ± 2.32	14.5 ± 3.09
	112	13.0 ± 2.66	13.2 ± 2.70	12.0 ± 2.34

Table B.7 Distal Femur Metaphysis Densitometry and Geometry Numerical Data for Exp. 2.

	Day	AC	HU	HU+VJE
Total BMC (mg/mm)	28	13.0 ± 0.94	-	12.9 ± 1.25
	56	12.9 ± 1.14	11.4 ± 0.92	13.4 ± 1.51
	112	12.5 ± 1.22	12.8 ± 1.24	12.3 ± 1.19
Total vBMD (mg/cm^3)	28	611.6 ± 35.9	-	657.9 ± 42.4
	56	599.0 ± 27.2	524.0 ± 32.8	591.2 ± 27.8
	112	595.6 ± 54.9	557.6 ± 32.5	620.3 ± 56.4
Cancellous BMC (mg/mm)	28	5.01 ± 0.57	-	4.57 ± 0.47
	56	4.90 ± 1.19	4.54 ± 0.85	6.18 ± 1.37
	112	4.44 ± 1.16	4.72 ± 1.09	4.69 ± 0.71
Cancellous vBMD (mg/cm^3)	28	369.6 ± 39.4	-	396.4 ± 38.4
	56	350.7 ± 54.2	303.7 ± 46.2	403.4 ± 49.0
	112	329.0 ± 57.6	309.9 ± 48.2	375.8 ± 31.2
Cortical BMC (mg/mm)	28	8.04 ± 0.58	-	8.31 ± 1.04
	56	7.96 ± 0.59	6.90 ± 0.99	7.25 ± 0.68
	112	8.02 ± 1.43	8.06 ± 0.84	7.66 ± 0.86
Cortical vBMD (mg/cm^3)	28	1016 ± 26.0	-	1028 ± 21.3
	56	1020 ± 50.0	968.6 ± 74.4	948.8 ± 58.5
	112	1030 ± 60.1	1013 ± 52.2	1011 ± 47.4
Total Bone Area (mm^2)	28	21.4 ± 1.35	-	19.6 ± 1.14
	56	21.5 ± 1.78	22.0 ± 1.61	22.8 ± 2.43
	112	21.0 ± 2.10	23.0 ± 2.37	20.0 ± 2.15
Cancellous Bone Area (mm^2)	28	13.5 ± 1.10	-	11.5 ± 0.93
	56	13.7 ± 1.62	14.9 ± 1.47	15.1 ± 1.98
	112	13.3 ± 2.12	15.0 ± 2.02	12.4 ± 1.94
Cortical Bone Area (mm^2)	28	7.90 ± 0.48	-	8.10 ± 0.99
	56	7.81 ± 0.37	7.09 ± 0.61	7.65 ± 0.68
	112	7.75 ± 0.99	7.95 ± 0.61	7.57 ± 0.67
Cortical Thickness (mm)	28	0.54 ± 0.028	-	0.59 ± 0.070
	56	0.53 ± 0.029	0.47 ± 0.040	0.50 ± 0.033
	112	0.54 ± 0.085	0.52 ± 0.034	0.54 ± 0.051

Table B.8 Femur Mid-Diaphysis Densitometry and Geometry Numerical Data for Exp. 2.

	Day	AC	HU	HU+VJE
Cortical BMC (mg/mm)	28	12.8 ± 1.17	-	11.5 ± 0.70
	56	12.8 ± 1.16	13.1 ± 0.76	12.9 ± 1.03
	112	13.9 ± 1.48	14.7 ± 1.44	12.5 ± 1.54
Cortical vBMD (mg/cm^3)	28	1441 ± 18.2	-	1426 ± 15.5
	56	1438 ± 15.8	1437 ± 21.4	1429 ± 16.8
	112	1457 ± 15.9	1451 ± 21.4	1448 ± 14.5
Cortical Area (mm^2)	28	8.91 ± 0.80	-	8.02 ± 0.45
	56	8.91 ± 0.81	9.14 ± 0.49	9.04 ± 0.75
	112	9.56 ± 1.01	10.2 ± 0.95	8.64 ± 1.00
Cortical Thickness (mm)	28	0.85 ± 0.048	-	0.81 ± 0.034
	56	0.85 ± 0.050	0.86 ± 0.039	0.85 ± 0.029
	112	0.90 ± 0.047	0.92 ± 0.065	0.85 ± 0.050
Polar Area MOI (mm^4)	28	27.3 ± 4.82	-	22.0 ± 2.15
	56	27.3 ± 4.66	28.8 ± 3.79	28.4 ± 5.28
	112	30.4 ± 6.58	34.4 ± 6.03	25.2 ± 6.20

Table B.9 Femoral Neck Densitometry and Geometry Numerical Data for Exp. 2.

	Day	AC	HU	HU+VJE
Total BMC (mg/mm)	28	5.29 ± 0.71	-	4.63 ± 0.43
	56	5.11 ± 0.26	4.96 ± 0.45	5.26 ± 0.66
	112	5.08 ± 0.71	5.58 ± 0.66	4.65 ± 0.52
Total vBMD (mg/cm^3)	28	1115 ± 38.8	-	1182 ± 65.1
	56	1137 ± 57.5	1056 ± 61.2	1129 ± 67.1
	112	1160 ± 63.4	1102 ± 69.6	1202 ± 71.7
Cancellous BMC (mg/mm)	28	1.74 ± 0.52	-	1.19 ± 0.29
	56	1.57 ± 0.42	1.70 ± 0.44	1.51 ± 0.53
	112	1.51 ± 0.52	1.83 ± 0.46	1.09 ± 0.32
Cancellous vBMD (mg/cm^3)	28	741.0 ± 55.7	-	752.3 ± 82.4
	56	736.0 ± 71.1	670.3 ± 37.9	697.1 ± 75.9
	112	753.2 ± 67.4	719.1 ± 71.0	737.7 ± 78.2
Cortical BMC (mg/mm)	28	3.55 ± 0.28	-	3.43 ± 0.24
	56	3.53 ± 0.30	3.26 ± 0.34	3.75 ± 0.46
	112	3.57 ± 0.33	3.74 ± 0.37	3.56 ± 0.31
Cortical vBMD (mg/cm^3)	28	1452 ± 31.5	-	1470 ± 21.9
	56	1477 ± 26.3	1469 ± 27.7	1481 ± 24.1
	112	1481 ± 23.8	1473 ± 22.8	1479 ± 22.2
Total Bone Area (mm^2)	28	4.76 ± 0.73	-	3.93 ± 0.48
	56	4.51 ± 0.37	4.73 ± 0.63	4.68 ± 0.69
	112	4.41 ± 0.77	5.09 ± 0.76	3.90 ± 0.59
Cancellous Bone Area (mm^2)	28	2.32 ± 0.56	-	1.60 ± 0.40
	56	2.12 ± 0.46	2.51 ± 0.62	2.15 ± 0.63
	112	2.00 ± 0.63	2.55 ± 0.65	1.49 ± 0.47
Cortical Bone Area (mm^2)	28	2.45 ± 0.22	-	2.34 ± 0.14
	56	2.39 ± 0.18	2.22 ± 0.21	2.53 ± 0.32
	112	2.41 ± 0.23	2.55 ± 0.27	2.41 ± 0.20
Cortical Thickness (mm)	28	0.38 ± 0.026	-	0.41 ± 0.035
	56	0.38 ± 0.045	0.34 ± 0.045	0.40 ± 0.056
	112	0.39 ± 0.039	0.38 ± 0.040	0.43 ± 0.040
Polar Area MOI (mm^4)	28	4.05 ± 0.86	-	3.16 ± 0.61
	56	3.74 ± 0.42	3.71 ± 0.70	4.12 ± 0.91
	112	3.74 ± 0.99	4.57 ± 1.07	3.12 ± 0.75

B.4 *Ex Vivo* Micro-Computed Tomography

Table B.10 Proximal Tibia Metaphysis Cancellous Densitometry and Geometry Numerical Data for Exp. 2.

	Day	AC	HU	HU+VJE
BV/TV (%)	28	13.2 ± 4.47	-	11.6 ± 1.98
	56	10.0 ± 3.45	12.3 ± 5.46	14.9 ± 6.46
	112	10.6 ± 4.13	11.3 ± 5.78	11.1 ± 1.80
Trabecular Thickness (mm)	28	0.098 ± 0.065	-	0.081 ± 0.011
	56	0.075 ± 0.010	0.079 ± 0.013	0.085 ± 0.014
	112	0.079 ± 0.011	0.086 ± 0.014	0.080 ± 0.0064
Trabecular Separation (mm)	28	0.34 ± 0.079	-	0.36 ± 0.038
	56	0.34 ± 0.034	0.32 ± 0.052	0.30 ± 0.049
	112	0.35 ± 0.049	0.36 ± 0.076	0.33 ± 0.042
Trabecular Number (#/mm)	28	1.49 ± 0.46	-	1.44 ± 0.24
	56	1.32 ± 0.31	1.50 ± 0.49	1.71 ± 0.48
	112	1.31 ± 0.32	1.26 ± 0.42	1.39 ± 0.24

B.5 Mechanical Testing

Table B.11 Tibia Mid-Diaphysis Three-Point Bending Numerical Data for Exp. 2.

	Day	AC	HU	HU+VJE
Extrinsic Properties				
Stiffness (N/mm)	28	354.7 ± 50.4	-	354.0 ± 42.2
	56	352.2 ± 53.5	386.9 ± 44.5	385.3 ± 63.1
	112	387.2 ± 47.3	400.7 ± 32.8	380.8 ± 56.3
Ultimate Force (N)	28	123.0 ± 19.5	-	128.2 ± 16.8
	56	124.9 ± 15.6	138.8 ± 13.5	140.0 ± 20.2
	112	126.6 ± 23.5	124.2 ± 20.5	134.3 ± 16.2
Yield Force (N)	28	89.8 ± 13.4	-	96.5 ± 11.8
	56	92.2 ± 17.0	102.4 ± 12.0	102.5 ± 17.0
	112	96.7 ± 12.1	96.9 ± 16.2	103.0 ± 12.6
Post-Yield Displacement (mm)	28	0.43 ± 0.26	-	0.64 ± 0.16
	56	0.36 ± 0.19	0.43 ± 0.17	0.53 ± 0.24
	112	0.31 ± 0.21	0.26 ± 0.19	0.57 ± 0.18
Intrinsic Properties				
Energy to Ultimate Stress (mJ)	28	40.8 ± 17.7	-	39.7 ± 8.73
	56	36.3 ± 11.9	43.1 ± 6.18	42.5 ± 14.3
	112	33.3 ± 15.0	34.8 ± 17.5	40.6 ± 10.5
Ultimate Stress (MPa)	28	142.4 ± 22.5	-	154.4 ± 24.6
	56	140.4 ± 20.2	158.3 ± 23.4	134.5 ± 18.6
	112	139.4 ± 29.7	139.0 ± 24.0	152.2 ± 20.2
Elastic Modulus (GPa)	28	3.83 ± 0.50	-	3.94 ± 0.38
	56	3.71 ± 0.67	4.07 ± 0.62	3.34 ± 0.72
	112	3.70 ± 0.49	3.77 ± 0.63	3.95 ± 0.32

Table B.12 Proximal Tibia Metaphysis Reduced Platen Compression Numerical Data for Exp. 2.

	Day	AC	HU	HU+VJE
Ultimate Stress (MPa)	28	1.95 ± 1.14	-	2.83 ± 0.1.70
	56	1.60 ± 0.76	0.62 ± 0.48	2.11 ± 0.73
	112	1.77 ± 1.27	1.37 ± 1.20	2.85 ± 0.1.60
Elastic Modulus (MPa)	28	30.5 ± 16.4	-	40.0 ± 33.2
	56	28.1 ± 21.6	10.4 ± 6.30	32.0 ± 17.1
	112	27.7 ± 23.3	23.3 ± 22.1	36.8 ± 23.6
Energy to Ultimate Stress (mJ)	28	1.82 ± 1.77	-	3.00 ± 2.62
	56	1.57 ± 1.01	0.56 ± 0.61	1.73 ± 1.05
	112	1.43 ±1.11	1.39 ± 1.50	3.05 ± 2.74
Strain at Ultimate Stress (%)	28	0.19 ± 0.12	-	0.21 ± 0.12
	56	0.19 ± 0.11	0.18 ± 0.094	0.15 ± 0.10
	112	0.16 ± 0.067	0.18 ± 0.11	0.22 ± 0.13

Table B.13 Femur Mid-Diaphysis Three-Point Bending Numerical Data for Exp. 2.

	Day	AC	HU	HU+VJE
Extrinsic Properties				
Stiffness (N/mm)	28	576.7 ± 93.6	-	559.3 ± 57.0
	56	613.4 ± 91.9	588.6 ± 108.6	593.4 ± 111.8
	112	609.3 ± 135.4	537.4 ± 138.4	659.2 ± 127.7
Ultimate Force (N)	28	261.5 ± 22.9	-	240.8 ± 22.7
	56	262.3 ± 27.4	262.7 ± 19.6	275.3 ± 27.1
	112	270.7 ± 41.7	283.6 ± 26.8	269.5 ± 38.2
Yield Force (N)	28	160.0 ± 34.3	-	174.3 ± 14.9
	56	164.7 ± 43.7	156.7 ± 29.5	169.1 ± 31.4
	112	186.0 ± 38.4	194.7 ± 61.6	185.3 ± 26.2
Post-Yield Displacement (mm)	28	0.51 ± 0.15	-	0.46 ± 0.09
	56	0.50 ± 0.13	0.49 ± 0.19	0.52 ± 0.13
	112	0.41 ± 0.18	0.44 ± 0.16	0.44 ± 0.07
Intrinsic Properties				
Energy to Ultimate Stress (mJ)	28	125.4 ± 22.7	-	112.5 ± 21.6
	56	123.8 ± 25.8	121.7 ± 38.8	134.7 ± 39.0
	112	128.7 ± 43.8	141.3 ± 27.1	113.7 ± 20.9
Ultimate Stress (MPa)	28	144.1 ± 24.8	-	151.7 ± 10.6
	56	142.5 ± 17.4	133.3 ± 15.3	148.0 ± 24.0
	112	138.3 ± 27.2	135.6 ± 16.1	157.7 ± 10.0
Elastic Modulus (GPa)	28	1.51 ± 0.26	-	1.81 ± 0.24
	56	1.63 ± 0.39	1.43 ± 0.28	1.49 ± 0.28
	112	1.46 ± 0.42	1.16 ± 0.35	1.89 ± 0.26

Table B.14 Femoral Neck Mechanical Test Numerical Data for Exp. 2.

	Day	AC	HU	HU+VJE
Stiffness (N/mm)	28	128.1 ± 29.8	-	167.4 ± 51.0
	56	134.7 ± 36.3	173.1 ± 41.7	166.0 ± 38.2
	112	162.9 ± 63.0	174.8 ± 45.8	138.3 ± 42.7
Ultimate Force (N)	28	97.0 ± 25.1	-	100.6 ± 8.67
	56	95.0 ± 12.6	107.6 ± 21.9	102.8 ± 15.8
	112	106.6 ± 19.6	118.7 ± 29.2	99.6 ± 10.4
Energy to Ultimate Force (mJ)	28	43.3 ± 22.6	-	36.6 ± 9.36
	56	38.6 ± 12.5	45.9 ± 30.1	36.2 ± 11.8
	112	40.7 ± 16.7	45.8 ± 23.5	40.6 ± 9.38

B.6 Histomorphometry

Table B.15 Proximal Tibia Metaphysis Static Cancellous Histomorphometry Numerical Data for Exp. 2.

	Day	AC	HU	HU+VJE
Oc.S/BS (%)	28	3.48 ± 1.69	-	1.52 ± 0.51
	56	1.56 ± 0.81	3.76 ± 1.86	2.00 ± 0.49
	112	1.37 ± 0.32	1.81 ± 0.55	1.01 ± 0.42
OS/BS (%)	28	1.39 ± 1.03	-	3.70 ± 1.77
	56	1.54 ± 0.73	0.95 ± 0.76	0.25 ± 0.12
	112	1.01 ± 0.48	0.88 ± 0.65	0.83 ± 0.25

Table B.16 Proximal Tibia Metaphysis Dynamic Cortical Histomorphometry Numerical Data for Exp. 2.

	Day	AC	HU	HU+VJE
MS/BS (%)	28	5.19 ± 1.21	-	6.55 ± 1.51
	56	3.62 ± 1.43	2.00 ± 0.69	2.33 ± 1.16
	112	5.51 ± 0.97	3.97 ± 2.47	4.20 ± 1.06
MAR (μm/day)	28	0.92 ± 0.14	-	1.01 ± 0.16
	56	0.81 ± 0.28	0.57 ± 0.46	0.51 ± 0.38
	112	0.88 ± 0.13	0.79 ± 0.23	0.81 ± 0.16
BFR/BS ($\mu m^3/\mu m^2$/day)	28	4.82 ± 1.31	-	6.62 ± 2.04
	56	2.81 ± 1.10	1.32 ± 1.33	1.33 ± 1.19
	112	4.88 ± 1.36	3.28 ± 2.60	3.53 ± 1.39